Astronomy & Astrophysics manuscript no. 11550aph
February 26, 2009

© ESO 2009

arXiv:0902.4694v1 [astro-ph.GA] 26 Feb 2009

Increased complexity in interstellar chemistry: Detection and chemical modeling of ethyl formate and *n*-propyl cyanide in Sgr B2(N) ⋆

A. Belloche[1], R. T. Garrod[2,1], H. S. P. Müller[3,1], K. M. Menten[1], C. Comito[1], and P. Schilke[1]

[1] Max-Planck Institut für Radioastronomie, Auf dem Hügel 69, 53121 Bonn, Germany
e-mail: `[belloche;kmenten;ccomito;schilke]@mpifr-bonn.mpg.de`
[2] Department of Astronomy, Cornell University, 106 Space Sciences Building, Ithaca, NY 14853, USA
e-mail: `rgarrod@astro.cornell.edu`
[3] I. Physikalisches Institut, Universität zu Köln, Zülpicher Str. 77, 50937 Köln, Germany
e-mail: `hspm@ph1.uni-koeln.de`

Received 19 December 2008; accepted 17 February 2009

ABSTRACT

Context. In recent years, organic molecules of increasing complexity have been found toward the prolific Galactic center source Sagittarius B2.
Aims. We wish to explore the degree of complexity that the interstellar chemistry can reach in star-forming regions.
Methods. We carried out a complete line survey of the hot cores Sgr B2(N) and (M) with the IRAM 30 m telescope in the 3 mm range, plus partial surveys at 2 and 1.3 mm. We analyzed this spectral survey in the local thermodynamical equilibrium approximation. We modeled the emission of all known molecules simultaneously, which allows us to search for less abundant, more complex molecules. We compared the derived column densities with the predictions of a coupled gas-phase and grain-surface chemical code.
Results. We report the first detection in space of ethyl formate (C_2H_5OCHO) and *n*-propyl cyanide (C_3H_7CN) toward Sgr B2(N). The detection of *n*-propyl cyanide is based on refined spectroscopic parameters derived from combined analyses of available laboratory spectroscopic data. For each molecule, we identified spectral features at the predicted frequencies having intensities compatible with a unique rotation temperature. For an assumed source size of 3″, our modeling yields a column density of 5.4×10^{16} cm^{-2}, a temperature of 100 K, and a linewidth of 7 km s^{-1} for ethyl formate. *n*-Propyl cyanide is detected with two velocity components having column densities of 1.5×10^{16} cm^{-2} and 6.6×10^{15} cm^{-2}, respectively, for a source size of 3″, a temperature of 150 K, and a linewidth of 7 km s^{-1}. The abundances of ethyl formate and *n*-propyl cyanide relative to H_2 are estimated to be 3.6×10^{-9} and 1.0×10^{-9}, respectively. We derived column density ratios of 0.8 / 15 / 1 for the related species *t*-HCOOH / CH_3OCHO / C_2H_5OCHO and 108 / 80 / 1 for CH_3CN / C_2H_5CN / C_3H_7CN. Our chemical modeling reproduces these ratios reasonably well. It suggests that the sequential, piecewise construction of ethyl and *n*-propyl cyanide from their constituent functional groups on the grain surfaces is their most likely formation route. Ethyl formate is primarily formed on the grains by adding CH_3 to functional-group radicals derived from methyl formate, although ethanol may also be a precursor.
Conclusions. The detection in Sgr B2(N) of the next stage of complexity in two classes of complex molecule, esters and alkyl cyanides, suggests that greater complexity in other classes of molecule may be present in the interstellar medium.

Key words. astrobiology – astrochemistry – line: identification – stars: formation – ISM: individual objects: Sagittarius B2 – ISM: molecules

1. Introduction

More than 150 molecules have been discovered in the interstellar medium or in circumstellar envelopes over the past four decades (see, e.g., Müller et al. 2005[1]). Among them, "complex" organic molecules with up to 13 atoms have been found, showing that the interstellar chemistry in some regions is efficient enough to achieve a relatively high degree of chemical complexity[2]. In addition, much larger molecules have been found in meteorites discovered on Earth, including more than 80 distinct amino acids. The non-terrestrial isotopic ratios of these amino acids, as well as their racemic distributions[3], suggest that they, or at least their direct precursors, have an interstellar origin (see, e.g., Ehrenfreund et al. 2001; Bernstein et al. 2002; Elsila et al. 2007, and references therein). Interstellar chemistry is therefore very likely capable of producing more complex organic molecules than those discovered in the interstellar medium so far. However, the degree of complexity that may be reached is still an open question; the partition functions of larger molecules are large, making it much more difficult to detect such species, even if they are present in reasonably large quantities.

Grain-surface chemistry is frequently invoked as the formation mechanism of many complex species, particularly following recent determinations of some key gas-phase reaction rates. Gas-

---

⋆ Based on observations carried out with the IRAM 30 m telescope. IRAM is supported by INSU/CNRS (France), MPG (Germany) and IGN (Spain).

[1] Visit the Cologne Database for Molecular Spectroscopy (CDMS) at http://www.cdms.de for an updated list.

[2] These molecules are "complex" for astronomers, not for biologists!

[3] A racemic distribution means equal amounts of left- and right-handed enantiomers. Enantiomers are stereoisomers that are mirror images of each other and non-superposable.

phase production of methyl formate, a molecule ubiquitous in hot-core spectra, appears prohibitively slow (Horn et al. 2004), pointing to an efficient alternative. Additionally, the dissociative recombination of large organic molecular ions with electrons, which is typically the final step in the gas-phase synthesis of complex molecules, appears strongly to favor the fragmentation of complex structure (Geppert et al. 2006).

In the case of hot cores, the granular ice mantles built up during prior phases of evolution present a rich source of simple saturated molecules from which more complex species may form, as has long been realized (Millar et al. 1991). However, while the efficiency of complex molecule formation in the gas phase is limited (not exclusively) by the need to stabilize the energized complex, often resulting in fragmentation, adhesion to a grain surface allows an adduct to quickly thermalize. Thus, molecular radicals derived from the ice mantles may combine *in situ* on the grain surfaces to build up complex structures efficiently, if dust temperatures are sufficient for the reactants to meet by thermal diffusion. The hot-core models of Garrod & Herbst (2006) and Garrod et al. (2008) have demonstrated the plausibility of such mechanisms in reproducing observed abundances of many complex organic species.

The detection of new complex molecules places valuable constraints on the chemical models. In the context of the model employed, e.g., by Garrod et al. (2008), obtaining abundances of structurally-related molecules allows one to isolate the chemical behavior of the functional groups from which they are constructed, and to relate these back to more fundamental model parameters such as photodissociation rates, binding energies, and initial ice composition. Such an approach then allows further observational predictions to be made.

One of the current best sources to search for new molecules in the interstellar medium is the hot dense core Sagittarius B2(N) – hereafter Sgr B2(N) for short. This source, dubbed the "Large Molecule Heimat" by Snyder et al. (1994), is extraordinary for its rich molecular content: most complex organic molecules such as, e.g., acetic acid (CH_3COOH, Mehringer et al. 1997), glycolaldehyde ($CH_2(OH)CHO$, Hollis et al. 2000), acetamide (CH_3CONH_2, Hollis et al. 2006), and aminoacetonitrile (NH_2CH_2CN, Belloche et al. 2008a,b), were first discovered in Sgr B2(N). This hot core is located in the very massive and extremely active region of high-mass star formation Sagittarius B2, at a projected distance of ∼ 100 pc from the Galactic center, whose distance is 8.0 ± 0.5 kpc from the Sun (Reid 1993). A second major and somewhat more evolved center of star formation activity, Sgr B2(M), is situated in its vicinity (∼ 2 pc). A more detailed introduction on these two sources and their environment can be found in, e.g., Belloche et al. (2008a).

Here, we report the detection of warm compact emission from ethyl formate (C_2H_5OCHO) and *n*-propyl cyanide (C_3H_7CN) in Sgr B2(N) with the IRAM 30 m telescope. Section 2 summarizes the observational details. The detections of ethyl formate and *n*-propyl cyanide are presented in Sects. 3 and 4, respectively. Implications in terms of interstellar chemistry are discussed in Sect. 5 based on a coupled gas-phase and grain-surface chemical code. Our conclusions are summarized in Sect. 6.

2. Observations and data analysis

2.1. Observations

We observed the two hot core regions Sgr B2(N) and Sgr B2(M) in January 2004, September 2004, and January 2005 with the IRAM 30 m telescope on Pico Veleta, Spain. We carried out a complete spectral survey toward both sources in the 3 mm atmospheric window between 80 and 116 GHz. A complete survey was performed in parallel in the 1.3 mm window between 201.8 and 204.6 GHz and between 205.0 and 217.7 GHz. Additional selected spectra were also obtained in the 2 mm window and between 219 and 268 GHz. The coordinates of the observed positions are $\alpha_{J2000}=17^h47^m20\overset{s}{.}0$, $\delta_{J2000}=-28°22'19.0''$ for Sgr B2(N) with a systemic velocity V_{lsr} = 64 km s^{-1} and $\alpha_{J2000}=17^h47^m20\overset{s}{.}4$, $\delta_{J2000}=-28°23'07.0''$ for Sgr B2(M) with V_{lsr} = 62 km s^{-1}. More details about the observational setup and the data reduction can be found in Belloche et al. (2008a). An rms noise level of 15–20 mK on the $T_a^\star$ scale was achieved below 100 GHz, 20–30 mK between 100 and 114.5 GHz, about 50 mK between 114.5 and 116 GHz, and 25–60 mK in the 2 mm window. At 1.3 mm, the confusion limit was reached for most of the spectra obtained toward Sgr B2(N).

2.2. Modeling of the spectral survey

The overall goal of our survey was to characterize the molecular content of Sgr B2(N) and (M). It also allows searches for new species once lines emitted by known molecules have been identified, including vibrationally and torsionally excited states, as well as less abundant isotopologues containing, e.g., ^{13}C, ^{18}O, ^{17}O, ^{34}S, ^{33}S, or ^{15}N. We detected about 3700 and 950 lines above 3σ over the whole 3 mm band toward Sgr B2(N) and (M), respectively. These numbers correspond to an average line density of about 100 and 25 features per GHz. Given this high line density, the assignment of a line to a given molecule can be trusted only if all lines emitted by this molecule in our frequency coverage are detected with the right intensity predicted by a model (see below) and no predicted line is missing in the observed spectrum.

We used the XCLASS software (see Comito et al. 2005) to model the emission of all known molecules in the local thermodynamical equilibrium approximation (LTE for short). Each molecule is modeled separately and assumed to be emitted by a uniform region. For each molecule, the free parameters are: source size, temperature, column density, velocity linewidth, velocity offset with respect to the systemic velocity of the source, and a flag indicating if its transitions are in emission or in absorption. For some of the molecules, it was necessary to include several velocity components to reproduce the observed spectra. The velocity components in emission are supposed to be non-interacting, i.e. the intensities add up linearly. This approximation is valid for two distinct, non-overlapping sources smaller than the beam of the telescope, but it is *a priori* less good for, e.g., a source that consists of a hot, compact region surrounded by a cold, extended envelope or two overlapping sources of spectrally overlapping optically thick emission. More details about the entire analysis are given in Belloche et al. (2008a) and the detailed results of this modeling will be published in a forthcoming article describing the complete survey (Belloche et al., in prep.). So far, we have identified 49 different molecules, 60 rare isotopologues, and lines arising from within 42 vibrationally or torsionally excited states apart from the gound state in Sgr B2(N). This represents about 60% of the lines detected above the 3σ level. In Sgr B2(M), the corresponding numbers are 42, 53, 23, and 50%, respectively.

3. Identification of ethyl formate

3.1. Ethyl formate frequencies

Ethyl formate, C_2H_5OCHO, is also known as formic acid ethyl ester, or, according to the International Union of Pure and Applied Chemistry (IUPAC), as ethyl methanoate. Its rotational spectrum was studied in the microwave (Riveros & Bright Wilson 1967) and in the millimeter wave regions up to 241 GHz (Demaison et al. 1984). The molecule occurs in two conformers. The heavy atoms C-C-O-C=O form a planar zigzag chain in the lowest *anti*-conformer which occasionally is also called the *trans*-conformer. The two conformers are depicted schematically in Medvedev et al. (2009). The terminal methyl group is rotated by $\sim$ 95° to the left or to the right in the *gauche*-conformer. Because of these two options, the *gauche*-conformer would be twice as abundant as the *anti*-conformer if the energy difference between the two were zero. However, the *gauche*-conformer is 0.78 ± 0.25 kJ mol^{-1} or 65 ± 21 cm^{-1} or 94 ± 30 K higher in energy (Riveros & Bright Wilson 1967). Therefore, the abundance of the *gauche*-conformer is less than twice that of the *anti*-conformer, in particular at lower temperatures. Since the energy difference has been estimated at room temperature only from relative intensities in the ground state spectra and since excited vibrational states have not been taken into consideration the error in the energy difference may well be larger.

Anti-ethyl formate is a strongly prolate molecule ($A \gg B \approx C$) with electric dipole moments for *a*- and *b*-type transitions, μ_a and μ_b, of 1.85 and 0.70 D, respectively. The *gauche*-conformer is more asymmetric, *A* is smaller by approximately one third and *B* and *C* are larger by about one third. The dipole moment components are $\mu_a = 1.45$, $\mu_b = 1.05$, and $\mu_c = 0.25$ D (Riveros & Bright Wilson 1967). Internal rotation of the terminal methyl group can be neglected. Tunneling between the two *gauche*-conformers has not been observed (Riveros & Bright Wilson 1967).

In the early stages of the current study we received additional ethyl formate data from E. Herbst (Medvedev et al. 2009) based on spectra taken at the Ohio State University (OSU) and covering the frequency range 106 – 378 GHz. The predictions used for the current analysis are based on this data set. An entry for ethyl formate will be available in the catalog section of the Cologne Database for Molecular Spectroscopy (CDMS[4], see Müller et al. 2001, 2005). The partition function of ethyl formate is 5.690×10^4 and 1.518×10^4 at 150 and 75 K, respectively. In the course of the analysis, the two conformers have been treated separately on occasion to evaluate if the abundance of either conformer is lower than would be expected under LTE conditions.

3.2. Detection of ethyl formate in Sgr B2(N)

For us to claim a reliable detection of a new molecule, it is essential that many lines of this molecule be detected in our spectral survey *and* that all the other expected lines, as predicted by our LTE model, either be blended with lines of other species or be below our detection limit (see Belloche et al. 2008a). Therefore, in the following, we inspect all transitions of ethyl formate in our frequency range. We list in Tables 1 and 2 (*online material*) only the transitions that our LTE modeling predicts to be stronger than 20 mK in the main-beam brightness temperature scale. 711 transitions of the *anti*-conformer and 478 transitions of the *gauche*-conformer are above this threshold that is conservative since it is below 1.5 times the rms noise level of the *best* part of our survey (and even below the rms noise level of *most* parts of our survey). To save some space, when two transitions have a frequency difference smaller than 0.1 MHz that cannot be resolved, we list only the first one. We number the transitions in Col. 1 and give their quantum numbers in Col. 2. The frequencies, the frequency uncertainties, the energies of the lower levels in temperature units, and the $S\mu^2$ values are listed in Col. 3, 4, 5, and 6, respectively. Since the spectra are in most cases close to the line confusion limit and it is difficult to measure the noise level, we give in Col. 7 the rms sensitivity computed from the system temperature and the integration time: $\sigma = \frac{F_{\rm eff}}{B_{\rm eff}} \times \frac{2\,T_{\rm sys}}{\sqrt{\delta f\, t}}$, with $F_{\rm eff}$ and $B_{\rm eff}$ the forward and beam efficiencies, $T_{\rm sys}$ the system temperature, δf the spectral resolution, and t the total integration time (on-source plus off-source).

We list in Col. 8 of Tables 1 and 2 comments about the blends affecting the transitions of the *anti*- and *gauche*-conformers of ethyl formate. As can be seen in these tables, most of the ethyl formate lines covered by our survey of Sgr B2(N) are heavily blended with lines of other molecules and therefore cannot be identified in this source based on our single-dish data. Only 46 of the 711 transitions of the *anti*-conformer are relatively free of contamination from other molecules, known or still unidentified according to our modeling. They are marked "Detected" or "Group detected" in Col. 8 of Table 1, and are listed with more information in Table 3. We stress that all transitions of sufficient strength predicted in the frequency range of our spectral survey are either detected or blended, i.e. no predicted transition is missing in the observed spectrum. The 46 detected transitions correspond to 24 observed features that are shown in Fig. 1 (*online material*) and labeled in Col. 8 of Table 3. For reference, we show the spectrum observed toward Sgr B2(M) in these figures also. We identified the ethyl formate lines and the blends affecting them with the LTE model of this molecule and the LTE model including all molecules (see Sect. 2.2). The parameters of our best-fit LTE model of ethyl formate are listed in Table 4, and the model is overlaid in red on the spectrum observed toward Sgr B2(N) in Fig. 1. The best-fit LTE model including all molecules is shown in green in the same figures.

For the frequency range corresponding to each detected ethyl formate feature, we list in Table 3 the integrated intensities of the observed spectrum (Col. 10), of the best-fit model of ethyl formate (Col. 11), and of the best-fit model including all molecules (Col. 12). In these columns, the dash symbol indicates transitions belonging to the same feature. Columns 1 to 7 of Table 3 are the same as in Table 1. The 1σ uncertainty given for the integrated intensity in Col. 10 was computed using the estimated noise level of Col. 7.

The measurements of the *anti*-conformer of ethyl formate are plotted in the form of a population diagram in Fig. 2a, which plots upper level column density divided by statistical weight, N_u/g_u, versus the upper level energy in Kelvins (see Goldsmith & Langer 1999). The data are shown in black and our best-fit model of ethyl formate in red. Out of 12 features encompassing several transitions, one contains transitions with different energy levels and was ignored in the population diagram (feature 17). We used equation A5 of Snyder et al. (2005) to compute the ordinate values:

$$\ln\left(\frac{N_u}{g_u}\right) = \ln\left(\frac{1.67 W_T \times 10^{14}}{S\mu^2 B\nu}\right) = -\frac{E_u}{T_{rot}} + \ln\left(\frac{N_T}{Z}\right), \quad (1)$$

where W_T is the integrated intensity in K km s^{-1} in main-beam brightness temperature scale, $S\mu^2$ the line strength times the

---

[4] http://www.cdms.de

Table 3. Transitions of the *anti*-conformer of ethyl formate detected toward Sgr B2(N) with the IRAM 30 m telescope.

N^a (1)	Transition (2)	Frequency (MHz) (3)	Unc.^{b} (kHz) (4)	$E_l{}^c$ (K) (5)	$S\mu^2$ (D^2) (6)	σ^d (mK) (7)	F^e (8)	τ^f (9)	$I_{obs}{}^g$ (K km s^{-1}) (10)	$I_{mod}{}^g$ (K km s^{-1}) (11)	$I_{all}{}^g$ (12)	Comments (13)
1	$15_{2,14}-14_{2,13}$	81779.567	4	30	51	13	1	0.05	0.52(06)	0.32	0.44	blend with U-line
16	$15_{6,10}-14_{6,9}$	82351.854	4	54	43	19	2	0.07	1.02(08)	0.44	0.55	partial blend with C_2H_5CN, υ_{13}=1/υ_{21}=1 and U-line
17	$15_{6,9}-14_{6,8}$	82351.858	4	54	43	19	2	–	–	–	–	–
26	$15_{2,13}-14_{2,12}$	84081.357	4	31	51	19	3	0.05	0.53(08)	0.35	0.42	partial blend with CH_3CH_3CO, υ_t=1
28	$16_{0,16}-15_{0,15}$	85065.106	4	31	55	22	4	0.06	0.73(10)	0.39	0.57	partial blend with c-C_2H_4O
44	$16_{8,8}-15_{8,7}$	87810.372	4	78	41	17	5	0.05	1.28(07)	0.40	1.22	partial blend with $CH_2(OH)CHO$ and C_2H_5CN
45	$16_{8,9}-15_{8,8}$	87810.372	4	78	41	17	5	–	–	–	–	–
46	$16_{7,9}-15_{7,8}$	87826.665	4	67	44	17	6	0.06	0.99(07)	0.48	0.86	partial blend with HNCO, υ_5=1
47	$16_{7,10}-15_{7,9}$	87826.665	4	67	44	17	6	–	–	–	–	–
53	$16_{3,14}-15_{3,13}$	87993.944	4	38	53	19	7	0.05	1.01(08)	0.39	0.64	partial blend with CH_3CH_3CO and U-line
54	$16_{4,12}-15_{4,11}$	88001.562	4	43	51	19	8	0.05	0.66(08)	0.35	0.62	blend with C_2H_5CN, υ_{13}=1/υ_{21}=1
73	$17_{10,7}-16_{10,6}$	93284.077	4	108	38	22	9	0.04	0.07(09)	0.33	0.35	uncertain baseline
74	$17_{10,8}-16_{10,7}$	93284.077	4	108	38	22	9	–	–	–	–	–
75	$17_{9,8}-16_{9,7}$	93292.297	4	94	42	22	10	0.05	0.56(09)	0.42	0.50	uncertain baseline
76	$17_{9,9}-16_{9,8}$	93292.297	4	94	42	22	10	–	–	–	–	–
77	$17_{8,9}-16_{8,8}$	93304.955	4	82	45	22	11	0.06	0.96(09)	0.51	0.67	partial blend with U-line
78	$17_{8,10}-16_{8,9}$	93304.955	4	82	45	22	11	–	–	–	–	–
79	$17_{7,11}-16_{7,10}$	93324.728	4	71	48	22	12	0.07	1.32(09)	0.60	0.74	partial blend with U-lines
80	$17_{7,10}-16_{7,9}$	93324.728	4	71	48	22	12	–	–	–	–	–
81	$17_{6,12}-16_{6,11}$	93356.821	4	62	51	22	13	0.08	1.68(10)	0.70	1.24	blend with CH_3CH_3CO and U-line?
82	$17_{6,11}-16_{6,10}$	93356.838	4	62	51	22	13	–	–	–	–	–
83	$17_{5,13}-16_{5,12}$	93412.160	4	54	53	22	14	0.08	1.12(10)	0.79	0.85	partial blend with U-line?
84	$17_{5,12}-16_{5,11}$	93413.168	4	54	53	22	14	–	–	–	–	–
86	$17_{4,14}-16_{4,13}$	93504.972	4	47	55	24	15	0.05	1.47(10)	0.44	0.87	blend with $CH_3{}^{18}OH$
87	$17_{4,13}-16_{4,12}$	93539.303	4	47	55	24	16	0.05	0.84(10)	0.44	0.45	no blend
94	$18_{15,3}-17_{15,2}$	98760.931	5	202	19	18	17	0.04	0.87(09)	0.68	0.78	blend with U-line
95	$18_{15,4}-17_{15,3}$	98760.931	5	202	19	18	17	–	–	–	–	–
96	$18_{14,4}-17_{14,3}$	98761.079	5	181	24	18	17	–	–	–	–	–
97	$18_{14,5}-17_{14,4}$	98761.079	5	181	24	18	17	–	–	–	–	–
98	$18_{16,2}-17_{16,1}$	98761.555	5	224	13	18	17	–	–	–	–	–
99	$18_{16,3}-17_{16,2}$	98761.555	5	224	13	18	17	–	–	–	–	–
100	$18_{13,5}-17_{13,4}$	98762.218	5	162	30	18	17	–	–	–	–	–
101	$18_{13,6}-17_{13,5}$	98762.218	5	162	30	18	17	–	–	–	–	–
102	$18_{17,1}-17_{17,0}$	98762.790	5	248	7	18	17	–	–	–	–	–
103	$18_{17,2}-17_{17,1}$	98762.790	5	248	7	18	17	–	–	–	–	–
104	$18_{12,6}-17_{12,5}$	98764.650	5	144	34	18	17	–	–	–	–	–
105	$18_{12,7}-17_{12,6}$	98764.650	5	144	34	18	17	–	–	–	–	–
118	$18_{5,14}-17_{5,13}$	98928.453	4	58	57	18	18	0.07	2.37(09)	0.96	2.23	blend with C_2H_5CN, υ_{13}=1/υ_{21}=1
119	$18_{5,13}-17_{5,12}$	98930.153	4	58	57	18	18	–	–	–	–	–
160	$20_{1,20}-19_{1,19}$	105234.713	5	49	68	28	19	0.07	1.66(11)	0.76	1.27	blend with C_2H_5OH and CH_3OCHO
161	$19_{1,18}-18_{1,17}$	105272.047	5	47	65	28	20	0.07	2.07(11)	0.73	0.81	blend with U-lines
162	$19_{3,16}-18_{3,15}$	105447.141	5	52	64	37	21	0.06	1.07(15)	0.69	1.07	no blend
165	$20_{2,19}-19_{2,18}$	108552.378	100	53	68	20	22	0.07	2.05(08)	0.79	1.24	partial blend with C_2H_3CN, υ_{15}=1 and U-lines
233	$21_{6,16}-20_{6,15}$	115395.797	5	81	66	60	23	0.11	2.94(23)	1.37	1.37	partial blend with U-line
234	$21_{6,15}-20_{6,14}$	115395.986	5	81	66	60	23	–	–	–	–	–
238	$22_{1,22}-21_{1,21}$	115595.764	5	59	75	79	24	0.08	-0.05(30)	0.99	2.22	blend with CH_3CH_3CO, υ_t=1, uncertain baseline

Notes: [a] Numbering of the observed transitions associated with a modeled line stronger than 20 mK (see Table 1). [b] Frequency uncertainty. [c] Lower energy level in temperature units (E_l/k_B). [d] Calculated rms noise level in T_{mb} scale. [e] Numbering of the observed features. [f] Peak opacity of the modeled feature. [g] Integrated intensity in T_{mb} scale for the observed spectrum (Col. 10), the ethyl formate model (Col. 11), and the model including all molecules (Col. 12). The uncertainty in Col. 10 is given in parentheses in units of the last digit.

dipole moment squared in D^2, B the beam filling factor, ν the frequency in GHz, T_{rot} the rotation temperature in K, N_T the molecular column density in cm^{-2}, and Z the partition function. This equation assumes optically thin emission. To estimate by how much line opacities affect this diagram, we applied the opacity correction factor $C_\tau = \frac{\tau}{1-e^{-\tau}}$ (see Goldsmith & Langer 1999; Snyder et al. 2005) to the modeled intensities, using the opacities from our radiative transfer calculations (Col. 9 of Table 3); the result is shown in green in Fig. 2a. The population diagram derived from the modeled spectrum is slightly shifted upwards but its shape, in particular its slope (the inverse of which *approximately* determines the rotation temperature), is not significantly changed, since $ln\, C_\tau$ does not vary much (from 0.019 to 0.053). The populations derived from the *observed* spectrum in the opti-

Table 4. Parameters of our best-fit LTE model of ethyl formate.

Size^a ($''$) (1)	$T_{\rm rot}$^{b} (K) (2)	N^c (cm^{-2}) (3)	ΔV^d (km s^{-1}) (4)	$V_{\rm off}$^{e} (km s^{-1}) (5)
3.0	100	5.40×10^{16}	7.0	0.0

Notes: ^{a} Source diameter (*FWHM*). ^{b} Temperature. ^{c} Column density. ^{d} Linewidth (*FWHM*). ^{e} Velocity offset with respect to the systemic velocity of Sgr B2(N) $V_{\rm lsr}$ = 64 km s^{-1}.

cally thin approximation are therefore not significantly affected by the optical depth of the ethyl formate transitions[5]. The scatter of the black crosses in Fig. 2a is therefore dominated by the blends with other molecules and uncertainties in the baseline removal (indicated by the downwards and upwards blue arrows, respectively).

The population diagram derived from the modeled spectrum in Fig. 2a is systematically below the measurements. Since most of the detected features of the *anti*-conformer of ethyl formate are partially blended with lines from other molecules (see Col. 13 of Table 3), we can use our model including all identified molecules (shown in green in Fig. 1) to remove the expected contribution from the contaminating molecules. Instead of computing N_u/g_u with the integrated intensities $I_{\rm obs}$ listed in Col. 10 of Table 3, we can use the value $I_{\rm obs} - (I_{\rm all} - I_{\rm mod})$ derived from Col. 10, 11, and 12. The corrected population diagram is shown in Fig. 2b. The predicted (red) and measured (black) points are much closer to each other. A close inspection of Fig. 1 shows however that the wings of most detected features of ethyl formate are still contaminated by U-lines, which explains why the measured points are still above the predicted ones in the population diagram (our fitting method with XCLASS is mainly focused on the peak intensity, not on the integrated intensity). The only exception is feature 9 for which the level of the baseline was obviously overestimated (see panel 7 of Fig. 1).

Given the remaining uncertainties due to the contamination from U-lines, it is difficult to derive the temperature with high accuracy. However, feature 17, which can unfortunately not be shown in the population diagram since it is a blend of several transitions with different energy levels (from 149 to 253 K), is significantly detected in panel 13 of Fig. 1. This is a strong indication that the temperature cannot be much lower than 100 K. Overall, we estimate the resulting uncertainty on the derived column density to be on the order of 25%. Finally, since all detected transitions are optically thin and the region emitting in ethyl formate is most likely compact given its high temperature, column density and source size are degenerate. We fixed the source size to 3$''$. This is approximately the size of the region emitting in the chemically related molecule methyl formate (CH_3OCHO) that we measured with the IRAM Plateau de Bure interferometer (see Table 5 of Belloche et al. 2008b).

From this analysis, we conclude that our best-fit model for the *anti*-conformer of ethyl formate is fully consistent with our 30 m data of Sgr B2(N). This detection of ethyl formate is, to our knowledge, the first one in space[6].

No feature of the *gauche*-conformer of ethyl formate is clearly detected in our spectral survey of Sgr B2(N). Only one feature at 213.6 GHz is possibly detected, but the baseline in this frequency range is very uncertain and the feature is blended with a transition of $H^{13}CCCN$ (see Table 2). If we consider this feature as a detection, then it implies a column density a factor 2 smaller than for the *anti*-conformer. This may suggest that the distribution of ethyl formate molecules in the two conformers is not in thermodynamical equilibrium. However, we first have to evaluate the uncertainty on the ratio of the *anti*- and *gauche*-conformer populations coming from the uncertainty on the energy difference between the two conformers (ΔE = 65±21 cm^{-1}, see Sect. 3.1). With $\Delta E = 0$, the ratio would be 1/2. For the preferred energy difference of 65 cm^{-1}, we have a ratio of about 0.56/0.44 at 100 K. If we assume an energy difference of 86 cm^{-1} this ratio would change to 0.62/0.38, i.e. a variation of $\sim$ 30%. This is not enough to compensate for the factor 2 mentioned above, but can have a significant contribution. In addition, a model of the emission spectrum of the *gauche*-conformer with the same parameters as for the *anti*-conformer is not excluded because of the large uncertainty on the baseline at 213.6 GHz. Therefore, given the large densities characterizing the hot core in Sgr B2(N) (see, e.g., Belloche et al. 2008a,b), it seems unlikely that the population in the *gauche*-conformer is subthermal compared to the *anti*-conformer.

3.3. Upper limit in Sgr B2(M)

We do not detect ethyl formate in our spectral survey toward Sgr B2(M). Using the same source size, linewidth, and temperature as for Srg B2(N) (see Table 4), we find $\sim 3\sigma$ column density upper limits of 2.0×10^{16} cm^{-2} and 4.0×10^{16} cm^{-2} in the LTE approximation for the *anti*- and *gauche*-conformers, respectively. The column density of ethyl formate is thus at least a factor $\sim$ 3 lower toward Sgr B2(M) than toward Sgr B2(N). This is not surprising since, e.g., Nummelin et al. (2000) found that hot-core-type molecules are more abundant in Sgr B2(N) by factors 3–8 as compared to Sgr B2(M).

3.4. Comparison to related species

We easily detect the already known molecules formic acid in the *trans* form (*t*-HCOOH or *t*-HOCHO), methyl formate (CH_3OCHO), ethanol (C_2H_5OH), and dimethyl ether (CH_3OCH_3) in our survey toward Sgr B2(N) (see also, e.g.,

---

[5] Note that our modeled spectrum is anyway calculated with the full LTE radiative transfer that takes into account the optical depth effects (see Sect. 2.2).

[6] Jones et al. (2007) tentatively identified three lines detected with the Australia Telescope Compact Array at ~86.2738, ~86.9784, and ~86.9787 GHz as two transitions of the *anti*-conformer of ethyl formate, the second one with two velocity components. However, our model predicts a peak temperature of the ethyl formate transition at 86.977087 GHz on the order of 2 mK whereas the two lines detected with the 30 m telescope close to this frequency have peak temperatures of 0.38 and 0.65 K, respectively! We identified these two lines with two velocity components of a transition of the vibrationally excited $\upsilon_{13}{=}1/\upsilon_{21}{=}1$ state of ethyl cyanide, and our modeled spectrum matches the observed lines very well. The tentative identification of Jones et al. (2007) at this frequency is therefore not confirmed. On the other hand, the line detected at ~86.2738 GHz in our survey is still unidentified. The frequency of the $45_{5,41}$–$44_{6,38}$ transition of ethyl formate mentioned by Jones et al. (2007) comes from the JPL catalog (Pickett et al. 1998, see http://spec.jpl.nasa.gov/). Our catalog contains a significantly different frequency for this transition (86256.5339 ± 0.0114 MHz instead of 86273.7945 ± 0.2103 MHz), and our model anyway predicts a very low peak temperature on the order of 0.3 mK for this transition. Our catalog contains two other overlapping transitions closer to 86.2738 GHz ($35_{10,26}$–$36_{9,27}$ and $35_{10,25}$–$36_{9,28}$ at 86.2703101 and 86.2703225 GHz, respectively). However, our model predicts a very low peak temperature of 0.6 mK for these transitions as well. Therefore, this tentative identification of Jones et al. (2007) is not confirmed either.

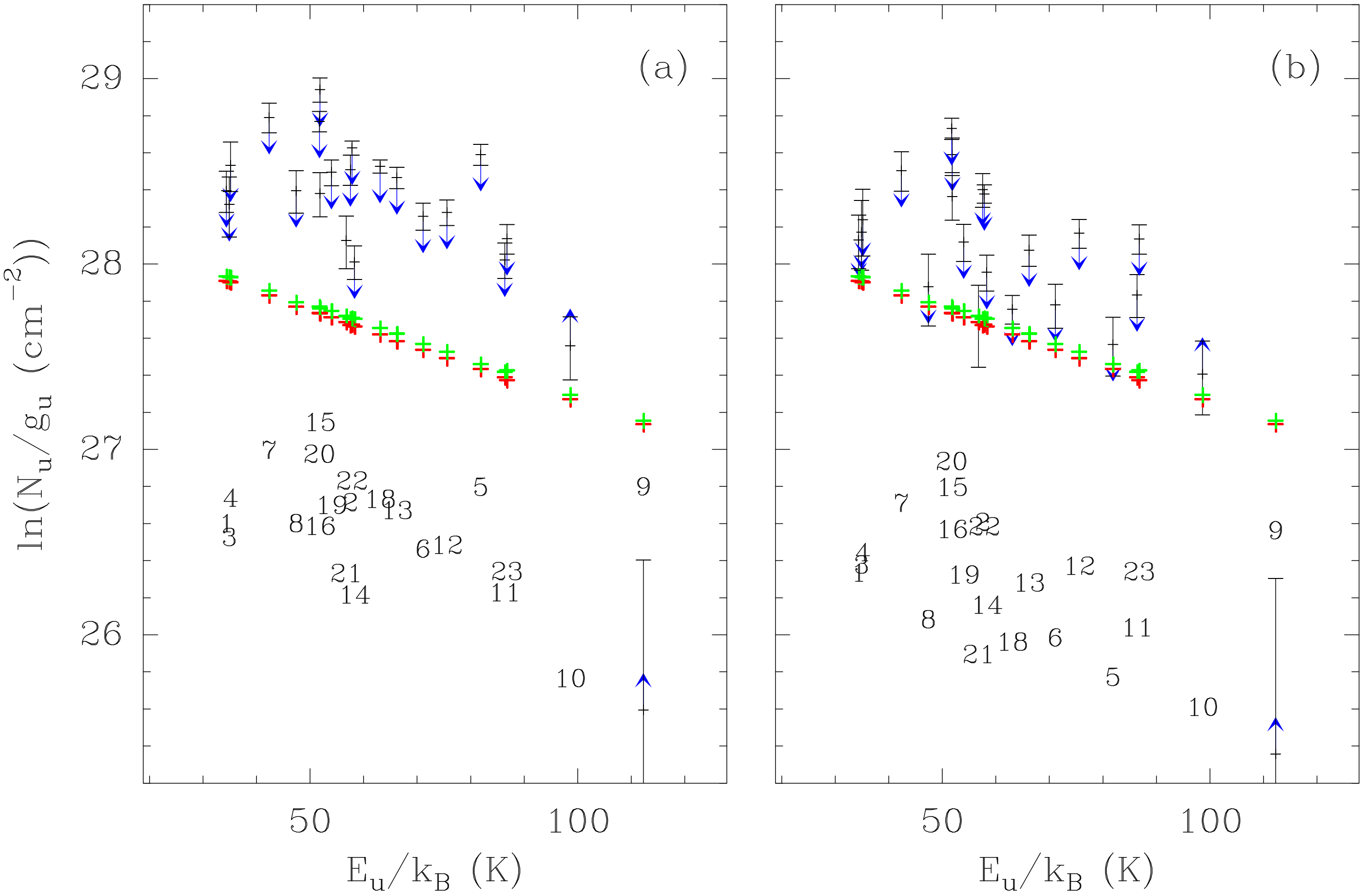

Fig. 2. a) Population diagram of the *anti*-conformer of ethyl formate in Sgr B2(N). The red points were computed in the optically thin approximation using the integrated intensities of our best-fit *model* of ethyl formate, while the green points were corrected for the opacity. The black points were computed in the optically thin approximation using the integrated intensities of the spectrum *observed* with the IRAM 30 m telescope. The error bars are 1σ uncertainties on N_u/g_u. Blue arrows pointing downwards mark the transitions blended with transitions from other molecules, while blue arrows pointing upwards indicate that the baseline removed in the observed spectrum is uncertain. The arrow length is arbitrary. The feature labels are shown in black shifted by -1.8 along the Y-axis for clarity, except for feature 9 for which it is shifted by +1.2. The measurement corresponding to feature 24 (at E_u/k_B = 65 K) is not shown since the integrated intensity measured toward Sgr B2(N) is negative, most likely because the level of the baseline was overestimated. Feature 17 is a blend of several transitions with different energy levels and was therefore also omitted. **b)** Same as **a)** but with the expected contribution from the contaminating molecules removed from the integrated intensities of the observed spectrum.

Nummelin et al. 2000; Liu et al. 2001). The parameters of our current best fit models of these molecules are listed in Table 5. All species have two velocity components that correspond to the two hot cores embedded in Sgr B2(N) (see, e.g., Belloche et al. 2008a for a discussion about these two sources). Ethyl formate may have a second velocity component too, but our survey is not sensitive enough to detect it with a significant signal-to-noise ratio. Using the same parameters as for the first velocity component but a velocity shift of 10 km s^{-1}, we estimate a 3σ upper limit of $\sim 2.4 \times 10^{16}$ cm^{-2} for the column density of a second velocity component of ethyl formate.

The lines of formic acid are optically thin in our model, so the size of the emitting region cannot be measured with our single-dish data. It was here fixed to 5″, assuming that a more extended region would have a lower temperature. Nummelin et al. (2000) derived a temperature of 74^{+82}_{-30} K and a beam-averaged column density of $\sim 4.2^{+2.0}_{-1.0} \times 10^{14}$ cm^{-2} in the LTE approximation with the SEST telescope (*HPBW* ~ 23″ at 1.3 mm). They used a linewidth of 13 km s^{-1} (*FWHM*), which more or less corresponds to the combination of the two velocity components we identified. Their column density translates into a column density of $\sim 9.3^{+4.4}_{-2.1}\times 10^{15}$ cm^{-2} for a source size of 5″, i.e. about a factor 2 smaller than the sum of the column densities of both velocity components in Table 5. At least two reasons may explain this discrepancy. First of all, as we noticed in our own partial survey at 1.3 mm, the level of the baseline in this wavelength range is very uncertain for Sgr B2(N) because of the line confusion and it may easily be overestimated. Second, at these high frequencies in Sgr B2(N), the dust is partially optically thick and should partially absorb the line emission[7]. We estimate that the combina-

---

[7] Lis et al. (1993) measured a peak flux of 20 Jy/4.5″ × 3.7″-beam at 227 GHz toward Sgr B2(N), i.e. 28 K in temperature unit. For a temperature of ~ 100 K, this yields a dust optical depth of ~ 0.34. On larger scales (~ 10″), Gordon et al. (1993) estimated that the dust opacity toward Sgr B2(N) reaches a value of 1 at 850 μm, which implies an opacity of ~0.43–0.53 at 1.3 mm. As a result, if not taken into account, these significant opacities imply an underestimate of the line intensities by a factor ~ 1.4–1.7.

Table 5. Parameters of our best-fit LTE models of formic acid, methyl formate, ethanol, and dimethyl ether.

Molecule[a] (1)	Size[b] (″) (2)	$T_{\rm rot}$[c] (K) (3)	N[d] (cm^{-2}) (4)	ΔV[e] (km s^{-1}) (5)	$V_{\rm off}$[f] (km s^{-1}) (6)
t-HCOOH	5.0	70	1.50×10^{16}	8.0	-1.0
	5.0	70	7.50×10^{15}	8.0	9.0
CH_3OCHO	4.0	80	4.50×10^{17}	7.2	0.0
	4.0	80	1.50×10^{17}	7.2	10.0
C_2H_5OH	3.0	100	8.40×10^{17}	8.0	0.0
	3.0	100	3.00×10^{17}	7.0	10.0
CH_3OCH_3	2.5	130	2.30×10^{18}	6.0	0.0
	2.5	130	1.10×10^{18}	6.0	10.0

Notes: [a] We used the CDMS entry for *t*-HCOOH (version 1), and the JPL entries for CH_3OCHO (ver. 1), C_2H_5OH (ver. 4), and CH_3OCH_3 (ver. 1). See references to the laboratory data therein. [b] Source diameter (*FWHM*). [c] Temperature. [d] Column density. [e] Linewidth (*FWHM*). [f] Velocity offset with respect to the systemic velocity of Sgr B2(N) $V_{\rm lsr}$ = 64 km s^{-1}.

tion of these two effects can lead to underestimating the true line intensities by about a factor 2 or 3. In addition, assuming a temperature of 200 K, Liu et al. (2001) measured a beam-averaged column density of $1.1 \pm 0.3 \times 10^{16}$ cm^{-2} with the BIMA interferometer at 86–90 GHz (*HPBW* ∼ 14″ × 4″). This translates into a column density of $\sim 6.3 \pm 1.5 \times 10^{15}$ cm^{-2} for a source size of 5″ and a temperature of 70 K. The interferometric detection of Liu et al. (2001) is somewhat uncertain but suggests that about half of the 30 m flux may be emitted by an extended region filtered out by the interferometer. The formic acid column density of the compact sources listed in Table 5 may therefore be overestimated by up to a factor 2.

The lines of methyl formate have opacities of up to about 1 in our model of the 3 mm spectrum, which puts only weak constraints on the source size that we fixed to 4″. Assuming a temperature of 200 K, Nummelin et al. (2000) derived a beam-averaged column density of $\sim 5.6^{+0.3}_{-0.1} \times 10^{15}$ cm^{-2} with the SEST telescope for the *a*-type lines and, assuming a temperature of 500 K, $\sim 4.0^{+0.3}_{-0.4} \times 10^{16}$ cm^{-2} for the *b*-type lines. For a temperature of 80 K and a source size of 4″, the column density of the *a*-type lines translates into a column density of $\sim 1.2 \times 10^{17}$ cm^{-2}, which is about a factor 5 smaller than the one we derived here for the sum of the two velocity components. Again, the uncertainty on the level of the baseline and the partial dust absorption at 1.3 mm may explain part of this discrepancy. In addition, we note that our model at 3 mm reproduces quite well both the *a*- and *b*-type lines with the same temperature and column density (see Appendix A, *online material*), while Nummelin et al. (2000) found an order of magnitude difference between the column densities of the two types. We believe that this discrepancy results from the fact that they did not properly take into account the line blending, which is large in Sgr B2(N) and should affect the (weak) *b*-type lines the most, and that they underestimated the line opacities of the (strong) *a*-type lines that our model predicts to be on the order of 1–3 in the 1.3 mm range. Using the BIMA interferometer at 90.15 GHz with a beam size of 14″ × 4″, Liu et al. (2001) found a beam-averaged column density of 1.1×10^{17} cm^{-2} for an assumed temperature of 200 K in the optically thin approximation. This translates into a column density of 1.5×10^{17} cm^{-2} for a source size of 4″ and a temperature of 80 K. However, our model predicts an opacity of ∼ 0.6 for this transition, which implies a higher column density of 2.0×10^{17} cm^{-2}. This is still about a factor 2 times lower than our estimate and suggests that, like in the case of formic acid, half of the single-dish flux may actually come from a region more extended than the size of our model and may be filtered out by the interferometer. This conclusion is further supported by the flux ratio of 1.7 between the 12 m telescope (*HPBW* = 71″) and BIMA (*HPBW* = 25.2″ × 6.3″) measurements of Friedel et al. (2004) at 86–90 GHz, and the flux ratio of 2.3 we found between the measurements done with the 30 m telescope and the Plateau de Bure interferometer at 82.2 GHz (see Table 5 of Belloche et al. 2008b). As a result, the methyl formate column density of the compact sources listed in Table 5 may be overestimated by up to a factor 2.

Most lines of ethanol are optically thin at 3 mm ($\tau < 0.7$), except for three lines that are marginally optically thick ($\tau \sim 1 - 1.2$). As a result, the source size is not well contrained and we fixed it to 3″. Nummelin et al. (2000) derived a beam-averaged column density of $4.2 \pm 0.2 \times 10^{15}$ cm^{-2} for a temperature of 73^{+5}_{-4} K with the SEST telescope. This translates into a column density of 2.5×10^{17} cm^{-2} for a source size of 3″, which is significantly lower than our measurement. However, Nummelin et al. (2000) used an earlier version of the JPL entry for ethanol that turned out to be inaccurate (J. Pearson, *private communication*). With this older version, we determined column densities of 2.8×10^{17} and 8.9×10^{16} cm^{-2} for both velocity components, which was consistent with the result of Nummelin et al. (2000). The column densities given in Table 5 were obtained with the latest JPL entry for ethanol (Pearson et al. 2008). The high-energy lines ($E_{\rm l}/k_{\rm B} \sim 40 - 80$ K) detected by Friedel et al. (2004) with the NRAO 12 m telescope and the BIMA interferometer have the same fluxes with both instruments, implying that they are emitted by a compact region. Only the $4_{1,4} - 3_{0,3}$ line with $E_{\rm l}/k_{\rm B} = 5.0$ K has an interferometric flux significantly lower than the single-dish flux. Our LTE model is also too weak for this transition compared to the spectrum obtained with the 30 m telescope. However, it fits well the low-energy transitions at 84.595868 GHz ($E_{\rm l}/k_{\rm B} = 9.4$ K) and 112.807174 GHz ($E_{\rm l}/k_{\rm B} = 2.1$ K) detected in our survey. Therefore, it is unclear whether the BIMA missing flux of the $4_{1,4} - 3_{0,3}$ transition suggests an additional cold, extended component, or this line is heavily blended with a transition of another molecule.

Our model of dimethyl ether predicts line opacities up to 2. The size of the emitting region is thus reasonably well constrained for this molecule. Nummelin et al. (2000) derived a beam-averaged column density of $7.9^{+0.8}_{-0.7} \times 10^{15}$ cm^{-2} for a temperature of 197^{+31}_{-22} K with the SEST telescope. This translates into a column density of 6.8×10^{17} cm^{-2} for a source size of 2.5″, which is a factor 4 lower than derived here. The discrepancy most likely comes from the beam filling factor of unity assumed by Nummelin et al. (2000) that leads to underestimating the line opacities. Our LTE model indeed predicts line optical depths up to 9 in the 1.3 mm window.

After rescaling to the same size of 3″, the relative column densities of the three related molecules *t*-HCOOH / CH_3OCHO / C_2H_5OCHO are about 0.8 / 15 / 1 for the first velocity component, and 0.9 / 11 / 1 for the second velocity component using the upper limit found for ethyl formate. We discuss these ratios and the implications for the interstellar chemistry in Sect. 5.

4. Identification of *n*-propyl cyanide

4.1. *n*-Propyl cyanide frequencies

n-Butanenitrile, C_3H_7CN, is more commonly known as *n*-propyl cyanide or *n*-butyronitrile. Its rotational spectrum has been investigated in the microwave (Hirota 1962; Demaison & Dreizler 1982; Vormann & Dreizler 1988) and in the millimeter wave regions up to 284 GHz (Włodarczak et al. 1988). The *n* indicates the *normal* isomer with the carbon atoms forming a chain, in contrast to the *iso* isomer which has a branched structure. This isomer has been studied to a lesser extent. However, its rotational spectrum is currently under investigation in Cologne.

n-Propyl cyanide exists in two conformers, *anti* and *gauche*, just as does ethyl formate. Again, the *anti*-conformer is the lower energy form, is strongly prolate, and has a large *a*-dipole moment component of 3.60 D and a still sizable *b*-dipole moment component of 0.98 D. The *gauche*-conformer is 1.1 ± 0.3 kJ mol^{-1} or 92 ± 25 cm^{-1} or 132 ± 36 K higher in energy, more asymmetric, and has $\mu_a = 3.27$ and $\mu_b = 2.14$ D (Włodarczak et al. 1988). The energy difference has been estimated at room temperature and at 233 K from relative intensities in the ground state spectra. Since excited vibrational states have not been taken into consideration the error in the energy difference may well be slightly larger than mentioned above. The residuals quoted in the most recent study (Vormann & Dreizler 1988) for their measurements are frequently much larger than the suggested uncertainties of about 5 kHz suggesting an insufficient set of spectroscopic parameters was used. Moreover, only newly determined rotational and centrifugal distortion parameters were given for the *gauche*-conformer. Therefore, new sets of rotational and centrifugal distortion parameters were determined for both conformers in the present study.

In the initial fits transition frequencies were taken from all four studies (Hirota 1962; Demaison & Dreizler 1982; Włodarczak et al. 1988; Vormann & Dreizler 1988). Two *b*-type transitions from Włodarczak et al. (1988) were omitted from the fits as suggested in the erratum to this paper (Włodarczak et al. 1991). On the other hand, transition frequencies not given in Vormann & Dreizler (1988), but deposited at the library of the University of Kiel were obtained from there and included in the fits. Uncertainties of 200, 10, 50, and 5 kHz were assigned to the transitions from Hirota (1962), Demaison & Dreizler (1982), Włodarczak et al. (1988), and Vormann & Dreizler (1988), respectively. Demaison & Dreizler (1982) and Vormann & Dreizler (1988) resolved in part internal rotation of the methyl group or quadrupole splitting of the ^{14}N nucleus in their laboratory measurements. The methyl internal rotation is unlikely to be resolved in astronomical observations. The quadrupole splitting may be resolvable for some low energy transitions, but these will be generally too weak. Therefore, only the unsplit frequencies were used from these two studies. In the unlikely event of detecting *n*-propyl cyanide in cold sources, quadrupole parameters published in Vormann & Dreizler (1988) would be adequate.

There were comparatively few transitions reported in Hirota (1962), and their uncertainties were fairly large. Trial fits with these transitions omitted from the fits caused essentially no change in the values and in the uncertainties of the spectroscopic parameters. Therefore, these transitions were omitted from the final fits. Two transitions, $36_{1,36} - 35_{0,35}$ of the *anti*-conformer and $31_{5,27}-30_{5,26}$ of the *gauche*-conformer, had residuals between observed and calculated frequencies larger than four times the experimental uncertainties. Therefore, these transitions were omitted from the data sets. The final line list for the *anti*-conformer contained 4, 93, and 50 different transition frequencies from Demaison & Dreizler (1982), Włodarczak et al. (1988), and Vormann & Dreizler (1988), respectively. The total number of transitions is larger by 62 because of unresolved asymmetry splitting. The corresponding numbers of different transition frequencies for the *gauche*-conformer are 4, 119, and 46. Unresolved asymmetry splitting causes the total number of transitions to be larger by 46. The final line lists for both conformers are given in Tables 6 and 7 (*online material*).

Table 8. Spectroscopic parameters[a] (MHz) of *n*-propyl cyanide.

Parameter	*anti*	*gauche*
A	23 668.319 31 (143)	10 060.416 49 (108)
B	2 268.146 892 (147)	3 267.662 408 (301)
C	2 152.963 946 (168)	2 705.459 572 (290)
$D_K \times 10^3$	240.653 (29)	60.235 (6)
$D_{JK} \times 10^3$	−10.826 31 (92)	−18.264 70 (117)
$D_J \times 10^6$	398.674 (69)	3 195.064 (207)
$d_1 \times 10^6$	−46.637 (42)	−1 037.470 (55)
$d_2 \times 10^6$	−0.590 1 (59)	−77.186 4 (183)
$H_K \times 10^6$	2.5	1.806 (18)
$H_{KJ} \times 10^9$	372.4 (24)	−517.3 (35)
$H_{JK} \times 10^9$	−20.67 (20)	9.92 (68)
$H_J \times 10^9$	0.353 (11)	4.486 (56)
$h_1 \times 10^9$	0.117 (14)	2.505 (29)
$h_2 \times 10^{12}$	–	524.6 (135)
$h_3 \times 10^{12}$	–	111.3 (31)
$L_{KKJ} \times 10^{12}$	–	30.6 (31)
$L_{JK} \times 10^{12}$	–	−4.11 (78)

[a] Watson's S-reduction was used in the representation I^r. Numbers in parentheses are one standard deviation in units of the least significant figures. Parameter values with no uncertainties given were estimated. A long dash indicates parameters that are determinable in theory, but could not be determined with significance here.

The asymmetry parameter $\kappa = (2B - A - C)/(A - C)$ is -0.9893 for *anti*-*n*-propyl cyanide, rather close to the symmetric prolate limit of –1. In such cases it is advisable to avoid using Watson's A-reduction and use the S-reduction instead. In the case of the *gauche*-conformer one finds $\kappa = -0.8471$. In this case both reductions may be used. In the present work the S-reduction was used throughout for consistency reason. The sextic distortion parameter H_K of the *anti*-conformer was initially estimated to be smaller than D_K by the same factor that that parameter is smaller than A. This is certainly only a crude estimate. Trial fits with H_K released suggested its value to be slightly larger than this estimate. But since the uncertainty was more than a third of its value and since the difference was smaller than the uncertainty, H_K was finally fixed to the estimated value. The final spectroscopic parameters are given in Table 8. Overall, the transition frequencies have been reproduced within experimental uncertainties as the dimensionless rms errors are 0.75 and 0.66 for the *anti* and *gauche*-conformer, respectively. The values for the individual data sets do not differ very much from these values. Moreover, this is reasonably close to 1.0 and suggests the ascribed uncertainties are quite appropriate.

The *gauche*-conformer is considerably more asymmetric than the *anti*-conformer. Therefore, it is probably not surprising that the distortion parameters describing the asymmetry splitting (the off-diagonal d_i and the h_i) are not only larger in magnitude for the former conformer, but also more of these terms are required in the fits. In addition, two octic centrifugal distortion parameters L were needed in the fit of the *gauche*-conformer resulting in an overall much larger parameter set and thus a much slower converging Hamiltonian compared with the *anti*-conformer. A similar situation occured in the recent investigation of ethyl formate (Medvedev et al. 2009) where also a much larger set of spectroscopic parameters was needed to fit the data of the *gauche*-conformer compared to the *anti*-conformer.

The predictions used for the current analysis will be made available in the CDMS (Müller et al. 2001, 2005, see footnote 4). The partition function of *n*-propyl cyanide is 5.608×10^4 at 150 K. In the course of the analysis, the two conformers again have been treated separately on occasion to evaluate if the abundance of either conformer is lower than would be expected under LTE conditions.

4.2. Detection of n-propyl cyanide in Sgr B2(N)

To identify *n*-propyl cyanide, we used the same method as for ethyl formate (see Sect. 3.2). In our spectral survey, 636 transitions of the *anti*-conformer and 706 transitions of the *gauche*-conformer are predicted above the threshold of 20 mK defined in Sect. 3.2. They are listed in Tables 9 and 10 (*online material*), respectively, which are presented in the same way as Tables 1 and 2. Again, as can be seen in these tables, most of the *n*-propyl cyanide lines covered by our survey of Sgr B2(N) are heavily blended with lines of other molecules and therefore cannot be identified in this source. Only 50 of the 636 transitions of the *anti*-conformer are relatively free of contamination from other molecules, known or still unidentified according to our modeling. They are marked "Detected" or "Group detected" in Col. 8 of Table 9, and are listed with more information in Table 11. We stress that all transitions of sufficient strength predicted in the frequency range of our spectral survey are either detected or blended, i.e. no predicted transition is missing in the observed spectrum. The 50 detected transitions correspond to 12 observed features that are shown in Fig. 3 (*online material*) and labeled in Col. 8 of Table 11. For reference, we show the spectrum observed toward Sgr B2(M) in these figures also. We identified the *n*-propyl cyanide lines and the blends affecting them with the LTE model of this molecule and the LTE model including all molecules (see Sect. 2.2). The parameters of our best-fit LTE model of *n*-propyl cyanide are listed in Table 12, and the model is overlaid in red on the spectrum observed toward Sgr B2(N) in Fig. 3. The best-fit LTE model including all molecules is shown in green in the same figures.

For the frequency range corresponding to each detected *n*-propyl cyanide feature, we list in Table 11 the integrated intensities of the observed spectrum (Col. 10), of the best-fit model of *n*-propyl cyanide (Col. 11), and of the best-fit model including all molecules (Col. 12). In these columns, the dash symbol indicates transitions belonging to the same feature. Columns 1 to 7 of Table 11 are the same as in Table 9. The 1σ uncertainty given for the integrated intensity in Col. 10 was computed using the estimated noise level of Col. 7.

As we did for ethyl formate, we show in Fig. 4a a population diagram derived from the integrated intensities of the detected features of the *anti*-conformer of *n*-propyl cyanide. Figure 4b displays the corresponding diagram after removing the expected contribution from contaminating molecules (see Sect. 3.2 for details). This figure is less helpful than in the case of ethyl formate because all features containing several transitions (6 out of 12) have transitions with different energy levels and cannot be shown in a population diagram. Therefore, this diagram does not help much for the determination of the temperature. Feature 3, which is a blend of transitions with upper energy levels from 61 to 147 K, is however reasonably well fitted by our 150 K model (see panel 2 of Fig. 3) and gives us some confidence in this high temperature. This is further confirmed by the high temperatures measured in our survey for chemically related molecules (see Sect. 4.4 below).

Table 12. Parameters of our best-fit LTE model of *n*-propyl cyanide with two velocity components.

Size^a (″) (1)	$T_{\rm rot}{}^b$ (K) (2)	N^c (cm^{-2}) (3)	ΔV^d (km s^{-1}) (4)	$V_{\rm off}{}^e$ (km s^{-1}) (5)
3.0	150	1.50×10^{16}	7.0	-1.0
3.0	150	6.60×10^{15}	7.0	9.0

Notes: ^{a} Source diameter (*FWHM*). ^{b} Temperature. ^{c} Column density. ^{d} Linewidth (*FWHM*). ^{e} Velocity offset with respect to the systemic velocity of Sgr B2(N) $V_{\rm lsr}$ = 64 km s^{-1}.

Our model for the *anti*-conformer of *n*-propyl cyanide consists of two components with different velocities. The need for a second component mainly comes from the shape of features 2, 9, and 12. Its velocity is consistent with the velocity of the second component we find for many other, more abundant molecules in our survey toward Sgr B2(N). It was shown interferometrically that this second velocity component is a physically distinct source located $\sim 5''$ to the North of the main hot core in Sgr B2(N) (see, e.g., Sect. 3.4 of Belloche et al. 2008a). Our data are consistent with a second component about half as strong in *n*-propyl cyanide as the first component (Table 12). This is also the ratio we found for the two components of ethyl cyanide (C_2H_5CN) with the IRAM Plateau de Bure interferometer and the 30 m telescope (see Table 5 of Belloche et al. 2008b). Finally, since all detected transitions are optically thin and the two regions emitting in *n*-propyl cyanide are most likely compact given their high temperature, column density and source size are degenerated. We fixed the source size to 3″. This is approximately the size of the region emitting in the chemically related molecule ethyl cyanide that we measured with the IRAM Plateau de Bure interferometer (see Table 5 of Belloche et al. 2008b).

From this analysis, we conclude that our best-fit model for the *anti*-conformer of *n*-propyl cyanide is fully consistent with our 30 m data of Sgr B2(N). This is, to our knowledge, the first clear detection of this molecule in space[8].

No feature of the *gauche*-conformer of *n*-propyl cyanide is clearly detected in our spectral survey of Sgr B2(N). Only one feature at 211.4 GHz is possibly detected but the baseline in this frequency range is very uncertain and this feature is blended with a transition of acetone. If we consider this feature as a detection, it implies a column density a factor 2 smaller than for the

---

[8] Jones et al. (2007) tentatively identified two lines detected with the Australia Telescope Compact Array at ~86.9556 and ~90.0560 GHz as transitions of the *gauche*-conformer of *n*-propyl cyanide. However, our model predicts a peak temperature of the *n*-propyl cyanide transition at 86.955466 GHz 15 times smaller than the peak temperature (0.13 K) of the line detected with the 30 m telescope at this frequency. The tentative identification of Jones et al. (2007) at this frequency is therefore not confirmed. The origin of this line in our survey is still unknown. As far as the other transition is concerned, our model of *n*-propyl cyanide predicts a peak intensity equal to only one quarter of the peak intensity (0.07 K) of the line detected with the 30 m telescope at ~90.0560 GHz. Since this line is blended with a transition of $^{13}CH_3CH_2CN$ that has a stronger contribution according to our modeling, the tentative identification of Jones et al. (2007) should be viewed with caution too.

Table 11. Transitions of the *anti*-conformer of *n*-propyl cyanide detected toward Sgr B2(N) with the IRAM 30 m telescope.

N^a	Transition	Frequency	Unc.^{b}	$E_l{}^c$	$S\mu^2$	σ^d	F^e	τ^f	$I_{\rm obs}{}^g$	$I_{\rm mod}{}^g$	$I_{\rm all}{}^g$	Comments
		(MHz)	(kHz)	(K)	(D^2)	(mK)			(K km s^{-1})	(K km s^{-1})		
(1)	(2)	(3)	(4)	(5)	(6)	(7)	(8)	(9)	(10)	(11)	(12)	(13)
5	$19_{6,14} - 18_{6,13}$	84021.555	4	73	221	19	1	0.06	3.27(13)	1.90	2.68	partial blend with C_2H_5CN
6	$19_{6,13} - 18_{6,12}$	84021.556	4	73	221	19	1	–	–	–	–	–
7	$19_{7,12} - 18_{7,11}$	84022.819	5	87	212	19	1	–	–	–	–	–
8	$19_{7,13} - 18_{7,12}$	84022.819	5	87	212	19	1	–	–	–	–	–
9	$19_{5,15} - 18_{5,14}$	84023.956	4	62	229	19	1	–	–	–	–	–
10	$19_{5,14} - 18_{5,13}$	84023.960	4	62	229	19	1	–	–	–	–	–
11	$19_{8,11} - 18_{8,10}$	84026.382	5	102	202	19	1	–	–	–	–	–
12	$19_{8,12} - 18_{8,11}$	84026.382	5	102	202	19	1	–	–	–	–	–
32	$20_{6,14} - 19_{6,13}$	88444.212	5	77	235	17	2	0.06	4.30(11)	2.31	3.28	partial blend with CH_3CH_3CO, C_2H_5OH, and U-line?
33	$20_{6,15} - 19_{6,14}$	88444.212	5	77	235	17	2	–	–	–	–	–
34	$20_{7,13} - 19_{7,12}$	88445.075	5	91	227	17	2	–	–	–	–	–
35	$20_{7,14} - 19_{7,13}$	88445.075	5	91	227	17	2	–	–	–	–	–
36	$20_{5,16} - 19_{5,15}$	88447.526	5	66	243	17	2	–	–	–	–	–
37	$20_{5,15} - 19_{5,14}$	88447.532	5	66	243	17	2	–	–	–	–	–
38	$20_{8,12} - 19_{8,11}$	88448.528	5	106	217	17	2	–	–	–	–	–
39	$20_{8,13} - 19_{8,12}$	88448.528	5	106	217	17	2	–	–	–	–	–
40	$20_{9,11} - 19_{9,10}$	88453.836	5	124	206	17	3	0.05	1.90(11)	1.40	2.42	partial blend with $C_2H_5{}^{13}CN$, $^{13}CH_3CH_2CN$, and $CH_2(OH)CHO$
41	$20_{9,12} - 19_{9,11}$	88453.836	5	124	206	17	3	–	–	–	–	–
42	$20_{4,17} - 19_{4,16}$	88458.794	5	57	248	17	3	–	–	–	–	–
43	$20_{4,16} - 19_{4,15}$	88459.387	5	57	248	17	3	–	–	–	–	–
44	$20_{10,10} - 19_{10,9}$	88460.625	5	143	194	17	3	–	–	–	–	–
45	$20_{10,11} - 19_{10,10}$	88460.625	5	143	194	17	3	–	–	–	–	–
53	$20_{1,19} - 19_{1,18}$	89391.938	5	42	258	16	4	0.03	0.65(08)	0.44	0.62	blend with CH_3OCHO, υ_t=1
55	$21_{0,21} - 20_{0,20}$	92164.912	5	44	272	27	5	0.03	1.15(14)	0.49	0.66	blend with $CH_3{}^{13}CN$, υ_8=1 and U-line?
57	$21_{6,16} - 20_{6,15}$	92866.939	5	82	250	28	6	0.07	1.54(21)	3.17	3.21	uncertain baseline
58	$21_{6,15} - 20_{6,14}$	92866.939	5	82	250	28	6	–	–	–	–	–
59	$21_{7,14} - 20_{7,13}$	92867.332	5	95	242	28	6	–	–	–	–	–
60	$21_{7,15} - 20_{7,14}$	92867.332	5	95	242	28	6	–	–	–	–	–
61	$21_{8,13} - 20_{8,12}$	92870.627	5	110	232	28	6	–	–	–	–	–
62	$21_{8,14} - 20_{8,13}$	92870.627	5	110	232	28	6	–	–	–	–	–
63	$21_{5,17} - 20_{5,16}$	92871.289	5	70	256	28	6	–	–	–	–	–
64	$21_{5,16} - 20_{5,15}$	92871.298	5	70	256	28	6	–	–	–	–	–
65	$21_{9,12} - 20_{9,11}$	92875.977	5	128	222	28	6	–	–	–	–	–
66	$21_{9,13} - 20_{9,12}$	92875.977	5	128	222	28	6	–	–	–	–	–
77	$21_{2,19} - 20_{2,18}$	93376.934	5	49	269	22	7	0.03	0.52(11)	0.49	0.51	no blend
104	$22_{2,20} - 21_{2,19}$	97867.394	5	53	282	20	8	0.03	0.61(10)	0.58	0.63	uncertain baseline
108	$10_{4,6} - 11_{3,9}$	101512.348	5	23	1	16	9	0.03	0.67(08)	0.66	0.96	small blend with CH_3CH_3CO, υ_t=1
109	$23_{2,22} - 22_{2,21}$	101515.201	5	58	295	16	9	–	–	–	–	–
110	$23_{7,16} - 22_{7,15}$	101711.846	5	104	270	16	10	0.08	5.74(11)	4.35	6.38	partial blend with $^{13}CH_2CHCN$, uncertain baseline
111	$23_{7,17} - 22_{7,16}$	101711.846	5	104	270	16	10	–	–	–	–	–
112	$23_{6,18} - 22_{6,17}$	101712.624	5	91	277	16	10	–	–	–	–	–
113	$23_{6,17} - 22_{6,16}$	101712.624	5	91	277	16	10	–	–	–	–	–
114	$23_{8,15} - 22_{8,14}$	101714.680	5	120	262	16	10	–	–	–	–	–
115	$23_{8,16} - 22_{8,15}$	101714.680	5	120	262	16	10	–	–	–	–	–
116	$23_{5,19} - 22_{5,18}$	101719.429	5	79	283	16	10	–	–	–	–	–
117	$23_{5,18} - 22_{5,17}$	101719.450	5	79	283	16	10	–	–	–	–	–
118	$23_{9,14} - 22_{9,13}$	101720.011	5	137	252	16	10	–	–	–	–	–
119	$23_{9,15} - 22_{9,14}$	101720.011	5	137	252	16	10	–	–	–	–	–
161	$24_{3,22} - 23_{3,21}$	106188.197	5	68	306	25	11	0.03	0.97(11)	0.76	0.82	noisy
205	$25_{1,24} - 24_{1,23}$	111593.662	5	65	323	29	12	0.03	1.48(14)	0.90	1.08	no blend

Notes: [a] Numbering of the observed transitions associated with a modeled line stronger than 20 mK (see Table 9). [b] Frequency uncertainty. [c] Lower energy level in temperature units (E_l/k_B). [d] Calculated rms noise level in $T_{\rm mb}$ scale. [e] Numbering of the observed features. [f] Peak opacity of the modeled feature. [g] Integrated intensity in $T_{\rm mb}$ scale for the observed spectrum (Col. 10), the *n*-propyl cyanide model (Col. 11), and the model including all molecules (Col. 12). The uncertainty in Col. 10 is given in parentheses in units of the last digit.

model of the *anti*-conformer, which may suggest a non-thermal distribution of the molecules in the two conformers. However, we first have to evaluate the uncertainty on the ratio of the *anti*- and *gauche*-conformer populations coming from the uncertainty on their energy difference ($\Delta E = 92\pm25$ cm^{-1}, see Sect. 4.1). For $\Delta E = 92$ cm^{-1}, the *anti* to *gauche* ratio is 0.51/0.49 at 150 K, and increases to 0.57/0.43 for $\Delta E = 117$ cm^{-1}, i.e. a variation of $\sim$ 30%. This is not enough to explain the factor 2 mentioned

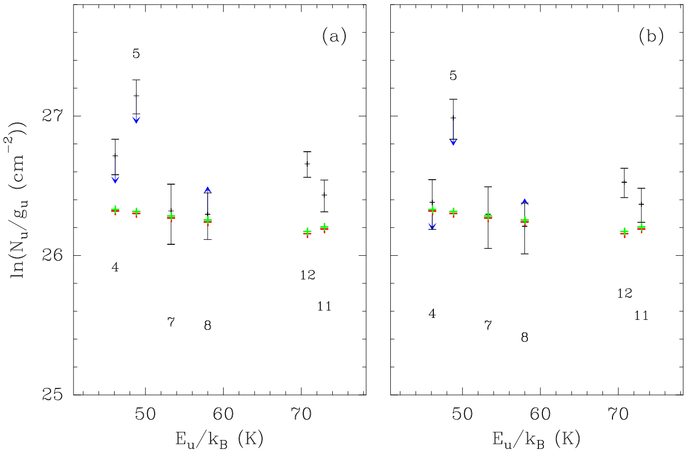

Fig. 4. Population diagram of the *anti*-conformer of *n*-propyl cyanide presented in the same way as for ethyl formate in Fig. 2 (see the caption of that figure for details). Panel **a)** shows the population diagram derived from the measured integrated intensities while panel **b)** presents the population diagram after correction for the expected contribution from contaminating molecules. Features 1, 2, 3, 6, 9, and 10 are blends of several transitions with different energy levels and were therefore omitted.

above, but it can have a significant contribution. Above all, the uncertainty on the baseline level at 211.4 GHz is quite large and the data are still consistent with a thermal distribution of the *gauche*- and *anti*-conformers.

4.3. Upper limit in Sgr B2(M)

We do not detect *n*-propyl cyanide in our spectral survey toward Sgr B2(M). Using the same source size, linewidth, and temperature as for Srg B2(N) (see Table 12), we find a $\sim 3\sigma$ column density upper limit of 6×10^{15} cm^{-2} in the LTE approximation for both conformers. The column density of *n*-propyl cyanide is thus at least a factor $\sim$ 2 lower toward Sgr B2(M) than toward Sgr B2(N), which is again consistent with the results of, e.g., Nummelin et al. (2000) for other molecules.

4.4. Comparison to related species

We easily detect the already known molecules methyl cyanide (CH_3CN) and ethyl cyanide (C_2H_5CN) in our survey toward Sgr B2(N) (see also, e.g., Miao et al. 1995; Liu & Snyder 1999; Nummelin et al. 2000). The parameters of our current best fit models of these two molecules are listed in Table 13. Our models use also constraints from the weaker isotopologues containing ^{13}C (see, e.g., Müller et al. 2008). The source size is constrained by the optically thick transitions, once the temperature has been fitted. For ethyl cyanide, we used in addition the constraints on the source size derived from our high angular resolution observations with the IRAM Plateau de Bure interferometer (see Table 5 of Belloche et al. 2008b). The first two velocity components detected in methyl cyanide and ethyl cyanide correspond to the two hot cores embedded in Sgr B2(N) (see, e.g., Hollis et al. 2003; Belloche et al. 2008a). They are also seen in *n*-propyl cyanide. In addition, methyl cyanide and ethyl cyanide show a third component that may arise from the blueshifted lobe of an outflow (see the cyanoacetylene $v_7 = 1$ emission in Fig.5k to m of Belloche et al. 2008a). The redshifted counterpart is blended with the northern component in the single-dish beam (see Fig. 3 of Hollis et al. 2003). The third velocity component is too faint to be detected in *n*-propyl cyanide.

Table 13. Parameters of our best-fit LTE models of methyl cyanide, ethyl cyanide, vinyl cyanide, and aminoacetonitrile, and column density upper limit for cyanomethylidyne.

Molecule^a (1)	Size^b ($''$) (2)	T_{rot}^{c} (K) (3)	N^d (cm^{-2}) (4)	ΔV^e (km s^{-1}) (5)	V_{off}^{f} (km s^{-1}) (6)
CH_3CN	2.7	200	2.00×10^{18}	6.5	-1.0
	2.7	200	8.00×10^{17}	6.5	9.0
	2.7	200	1.00×10^{17}	8.0	-11.0
C_2H_5CN	3.0	170	1.20×10^{18}	6.5	-1.0
	2.3	170	1.40×10^{18}	6.5	9.0
	1.7	170	9.00×10^{17}	8.0	-11.0
C_2H_3CN	2.3	170	8.00×10^{17}	7.0	-1.0
	2.3	170	2.40×10^{17}	7.0	9.0
	2.3	170	1.00×10^{17}	10.0	-9.0
NH_2CH_2CN	2.0	100	2.80×10^{16}	7.0	0.0
CCN^g	3.0	200	$< 1.20 \times 10^{17}$	6.5	-1.0
	3.0	200	$< 1.20 \times 10^{17}$	6.5	9.0

Notes: ^{a} We used the JPL entry for CH_3CN (version 3), and the CDMS entries for C_2H_5CN (ver. 1), C_2H_3CN (ver. 1), NH_2CH_2CN (ver. 1), and CCN (ver. 1). See references to the laboratory data therein. ^{b} Source diameter (*FWHM*). ^{c} Temperature. ^{d} Column density. ^{e} Linewidth (*FWHM*). ^{f} Velocity offset with respect to the systemic velocity of Sgr B2(N) V_{lsr} = 64 km s^{-1}. ^{g} The column density upper limit is $\sim 3\sigma$. The other parameters were fixed.

The model parameters for the compact sources listed for methyl cyanide in Table 13 are mostly based on the ^{13}C isotopologues with a $^{12}C/^{13}C$ isotopic ratio of 20 because the transitions of the ^{12}C main isotopologue are very optically thick and most likely dominated by large scale emission (see maps of, e.g., de Vicente et al. 1997; Jones et al. 2008). de Vicente et al. (1997) analysed their maps of methyl cyanide emission in the Large Velocity Gradient approximation. They found that the emission consists of several components (hot core, warm envelope, diffuse and hot envelope), and mentioned that their modeling toward Sgr B2(N) is uncertain because of the large opacities. However, their figure 5 suggests that the temperature and column density of methyl cyanide are strongly centrally peaked toward Sgr B2(N). Therefore, the emission of the optically thin ^{13}C isotopologues should be dominated by the compact hot cores which gives us some confidence (within a factor of 2) in the column densities listed in Table 13. Friedel et al. (2004) measured similar intensities for $CH_3{}^{13}CN$ with the NRAO 12 m telescope and the BIMA interferometer toward Sgr B2(N), an additional evidence that the compact hot cores dominate the emission of the ^{13}C isotopologues we detected with the 30 m telescope. For a source size of 2.7$''$, Nummelin et al. (2000) found column densities of $0.7 - 1.1 \times 10^{17}$ cm^{-2} for the ^{13}C isotopologues, which translates into a column density of $1.4 - 2.2 \times 10^{18}$ cm^{-2} for the main isotopologue assuming a $^{12}C/^{13}C$ isotopic ratio of 20. This is in very good agreement with our result (see Table 13).

Assuming a temperature of 200 K and optically thin emission, Liu et al. (2001) obtained a beam-averaged column density of $4.63 \pm 0.14 \times 10^{16}$ cm^{-2} for ethyl cyanide with BIMA at 89.6 GHz ($HPBW = 14'' \times 4''$). For a source size of 3$''$, this translates into a column density of 2.9×10^{17} cm^{-2}, which is a factor 4 smaller than the column density we derive for the main velocity component. However, our model predicts peak line opacities of 4–6 for these transitions, which is supported by our simultaneous modeling of the ^{13}C isotopologues of ethyl cyanide (see Müller et al. 2008). As a result, Liu et al. (2001) most likely underestimated the column densities of ethyl cyanide by a factor of a few, which reconciles the single-dish and interferometric measurements and confirms that the source of ethyl cyanide emission is compact. This is also confirmed by the reasonable agreement between the 30 m and Plateau de Bure Interferometer fluxes published by Belloche et al. (2008b) at 81.7 GHz (see their Table 5). The compactness of the source of ethyl cyanide emission most likely explains the discrepancy with the column density found by Nummelin et al. (2000) with SEST in the 1.3 mm wavelength range ($HPBW \sim 23''$). These authors derived temperatures of 175^{+25}_{-20} K and 210^{+30}_{-30} K and beam-averaged column densities of $1.6^{+0.2}_{-0.1} \times 10^{15}$ cm^{-2} and $1.5^{+0.4}_{-0.3} \times 10^{16}$ cm^{-2} for the ethyl cyanide *a*- and *b*-type lines, respectively. While they find an order of magnitude difference between the column densities of the *a*- and *b*-type lines, we successfully reproduce the ethyl cyanide emission in our 3 mm survey with a single model for the two types of lines, the former being optically thick while the latter are optically thin. Our model with a small source size predicts line opacities on the order of 10–30 for the *a*-type lines in the 1.3 mm range. Hence, we believe that the column density derived by Nummelin et al. (2000) for these lines at 1.3 mm is underestimated by a large factor because they assumed a beam filling factor of 1, yielding opacities for these lines that were too low. On the other hand, since our model predicts opacities $\lesssim 1$ for the *b*-type lines at 1.3 mm, we would expect the column density derived by these authors to match ours. For a source size of 3″, their column density of the *b*-type lines translates into a column density of 9.0×10^{17} cm^{-2}, which is about a factor 2 smaller than the sum of the column densities of the two main velocity components in Table 13 (after rescaling the second one to a source size of 3″). As in Sect. 3.4, we think that the discrepancy arises from the uncertain baseline level and the partial dust absorption in the 1.3 mm wavelength range. Our current model, which suffers from the same problems, also over-predicts intensities for the lines detected in our partial 1.3 mm survey.

After rescaling to the same size of 3″, the relative column densities of the three related molecules CH_3CN / C_2H_5CN / C_3H_7CN are 108 / 80 / 1 for the first velocity component and 98 / 125 / 1 for the second velocity component. We discuss these ratios and the implications for the interstellar chemistry in Sect. 5.

In addition, we list in Table 13 the best-fit parameters we found for vinyl cyanide (Müller et al. 2008) and aminoacetonitrile (Belloche et al. 2008a), as well as an upper limit for the column density of cyanomethylidyne (CCN) for which the other parameters were fixed.

5. Chemical modeling and discussion

To better understand the observational results, we model the chemistry of Sgr B2(N) using a coupled gas-phase and grain-surface chemical code. Garrod et al. (2008) constructed a reaction network to account for the grain-surface formation of many complex molecules observed in hot cores. Surface formation was assumed to occur primarily by the addition of functional-group radicals derived from molecular ices or from other molecules formed in this way. Such reactions are viable when larger radicals become mobile at intermediate grain temperatures ($T_d \gtrsim$ 20 K), achieved during the warm-up to typical hot-core temperatures (> 100 K). The network also includes destruction mechanisms for all complex species, consisting of neutral–neutral reactions on the grain surfaces, ion–molecule reactions with simple ions in the gas phase, and cosmic ray-induced photodissociation both in the gas phase and on the grains. To this network we have added appropriate formation and destruction mechanisms for ethyl formate, ethyl and *n*-propyl cyanide, and also the recently identified aminoacetonitrile (NH_2CH_2CN, Belloche et al. 2008a,b), whose surface formation routes may be similar to the other cyanides. In addition, surface hydrogenation routes have been added to allow for the full hydrogenation of the carbon chains C_3 and C_4, which was not previously considered, as well as the associated hydrogenated species and their destruction channels. The techniques used to construct the new reaction set are presented in detail by Garrod et al. (2008); the current model may be regarded as a consistent extension to that network.

We employ the single-point physical model used by Garrod & Herbst (2006), in which the isothermal collapse of a diffuse medium, to a density $n_H = 10^7$ cm^{-3}, is followed by a warm-up from 10 to 200 K. Their T_2 warm-up profile is assumed, in which the hot-core temperature has a t^2 dependence on the time, *t*, elapsed in the warm-up phase. Dust and gas temperatures are assumed to be well coupled, hence we let $T = T_K = T_{dust}$. The warm-up timescale is representative of the time required for a parcel of gas to achieve a temperature of 200 K, as the hot core forms; it therefore does not relate directly to the *current* infall timescale.

This model traces the evolution of the chemistry up to a temperature of 200 K, associated with the central hot-core region. However, these time-dependent results may also be considered to represent differing spatial extents from the hot-core center, with the innermost regions being the most evolved and achieving the highest temperatures. As such, the time-dependent abundance profiles presented below also indicate a snapshot of the chemistry through the hot core.

Since we are interested mainly in specific features of the model, we choose not to fix the ice composition prior to the warm-up phase, but use the unadulterated composition computed in the collapse-phase.

Other details of the model may be found in Garrod et al. (2008). One important difference is the removal, in keeping with prior chemical networks, of the activation energy barrier for the surface reaction $OH + H_2CO \rightarrow HCO + H_2O$. Garrod et al. employed an activation energy merely for consistency with other hydrogen-abstraction reactions of OH. The available evidence, however, suggests there is no barrier[9]. This change makes HCO radicals somewhat more abundant on the grains, tending to increase the final abundances of species such as methyl formate, which is consistent with our observational results.

5.1. Surface Chemistry

Surface chemical routes for the formation of methyl cyanide, CH_3CN, were already present in the Garrod et al. (2008) network, including direct addition of methyl and nitrile groups, and repetitive surface hydrogenation of gas phase-produced C_2N. Formation of ethyl cyanide, C_2H_5CN, was limited to repetitive surface hydrogenation of cyanoacetylene HC_3N and vinyl cyanide, C_2H_3CN, both of which may be formed in the gas phase. *n*-Propyl cyanide and aminoacetonitrile were not present at all.

---

[9] See the chemical kinetics database of the National Institute of Standards and Technology (NIST), *http://kinetics.nist.gov/kinetics*.

Table 14 shows the full set of surface reactions employed in the current model to form methyl cyanide, ethyl cyanide, *n*-propyl cyanide, aminoacetonitrile, and ethylformate, as well as a selection of significant cosmic ray-induced photodissociation processes that may occur on grain surfaces. (The same CR-induced processes are assumed also to occur in the gas phase, at the same rates). A cosmic-ray ionization rate of $\zeta_0 = 1.3 \times 10^{-17}$ s^{-1} is assumed.

The new reactions allow each cyanide to be constructed by sequential formation of its carbon backbone by the addition of CH_2, CH_3, or yet larger hydrocarbon radicals; however, photodissociation also allows the break-down of these structures. The resultant radicals may further react with another functional-group radical, to extend the backbone, or with a hydrogen atom, to terminate this sequence. Similarly, aminoacetonitrile may be formed by the addition of NH or NH_2 groups, or by direct addition of CN to CH_2NH_2, or CH_2NH (followed by hydrogenation). Different routes will dominate according to the relative mobilities of competing radicals, and their availabilities. Hence, the net direction of inter-conversion between cyanides may change with temperature, or as the abundances of molecular precursors vary.

Ethyl formate may be formed on grain surfaces by the addition of a CH_3 or HCO radical to a CH_2OCHO or C_2H_5O radical, respectively. These latter species are formed directly by cosmic ray-induced photodissociation of methyl formate or ethanol on the grains; hence, methyl formate need not be the only precursor for ethyl formate, nor the most important one. We do not consider other routes to the formation of CH_2OCHO and C_2H_5O; radical addition to formaldehyde, H_2CO, would almost certainly be mediated by a substantial activation energy barrier. Alternatively, addition of an oxygen atom to C_2H_5 is unlikely to be important, due to the relative scarcity of atomic oxygen, which is mainly bound in the ice mantles as H_2O; however, this route cannot be entirely ruled out.

When the grain surface-produced molecules evaporate, they are subject to gas-phase destruction mechanisms. Whilst cosmic ray-induced photodissociation in the gas phase is also included for consistency, the gas-phase destruction of these molecules is dominated by reaction with the ions C^+, He^+, $H_3{}^+$, H_3O^+ and HCO^+ (followed by dissociative recombination, if a protonated molecule results). Ion-molecule and dissociative recombination reaction rates are of a similar order for all new species; see Garrod et al. (2008).

5.2. Results

We analyse the model results for ethyl formate and the cyanides in the context of a selection of complex molecules to which they are chemically or observationally related. We consider first the results of the basic model described above (called hereafter *Basic* model), using an intermediate warm-up timescale of 2×10^5 yr. This timescale was found by Garrod et al. (2008) to be most appropriate to match the abundances of Sgr B2(N).

5.2.1. Ethyl formate and related species

Table 15 presents peak fractional abundances, and the temperatures at which they are achieved, derived from the chemical model. Model abundances are converted to values per mean particle with a mean molecular weight, μ, of 2.33, for comparison to the observations. Also listed are the observed rotational temperatures and abundances (Cols. 7 and 8, respectively). The latter were derived from the column densities given in Tables 4, 5, 12,

Table 14. Surface reactions and cosmic-ray induced surface photodissociation processes related to the formation of cyanides, and ethyl formate.

Reaction	Garrod et al. (2008)	*Basic* model	*Select* model
$C_2N + H \rightarrow HCCN$	●	●	●
$HCCN + H \rightarrow CH_2CN$	●	●	●
$CH_2CN + H \rightarrow CH_3CN$	●	●	●
$HC_3N + H \rightarrow C_2H_2CN$ (1210 K)	●	●	
$C_2H_2CN + H \rightarrow C_2H_3CN$	●	●	
$C_2H_3CN + H \rightarrow C_2H_4CN$ (750 K)	●	●	
$C_2H_4CN + H \rightarrow C_2H_5CN$	●	●	●
$C_3H_6CN + H \rightarrow C_3H_7CN$		●	●
$CH_2 + CN \rightarrow CH_2CN$	●	●	●
$CH_3 + CN \rightarrow CH_3CN$	●	●	●
$CH_2 + CH_2CN \rightarrow C_2H_4CN$		●	●
$CH_3 + CH_2CN \rightarrow C_2H_5CN$		●	●
$CH_2 + C_2H_4CN \rightarrow C_3H_6CN$		●	●
$CH_3 + C_2H_4CN \rightarrow C_3H_7CN$		●	●
$C_2H_5 + CN \rightarrow C_2H_5CN$		●	
$C_3H_7 + CN \rightarrow C_3H_7CN$		●	
$NH + CH_2CN \rightarrow NHCH_2CN$		●	●
$NH_2 + CH_2CN \rightarrow NH_2CH_2CN$		●	●
$H + NHCH_2CN \rightarrow NH_2CH_2CN$		●	●
$CH_2NH + CN \rightarrow NHCH_2CN$		●	
$CH_2NH_2 + CN \rightarrow NH_2CH_2CN$		●	
$CH_3CN + h\nu \rightarrow CH_2CN + H$		●	●
$CH_3CN + h\nu \rightarrow CH_3 + CN$	●	●	●
$C_2H_5CN + h\nu \rightarrow C_2H_4CN + H$		●	●
$C_2H_5CN + h\nu \rightarrow CH_3 + CH_2CN$		●	●
$C_2H_5CN + h\nu \rightarrow C_2H_5 + CN$	●	●	●
$C_3H_7CN + h\nu \rightarrow CH_3 + C_2H_4CN$		●	●
$C_3H_7CN + h\nu \rightarrow C_2H_5 + CH_2CN$		●	●
$C_3H_7CN + h\nu \rightarrow C_3H_7 + CN$		●	●
$NH_2CH_2CN + h\nu \rightarrow NH_2 + CH_2CN$		●	●
$NH_2CH_2CN + h\nu \rightarrow NH_2CH_2 + CN$		●	●
$CH_3 + CH_2OCHO \rightarrow C_2H_5OCHO$		●	●
$H + CH_2OCHO \rightarrow CH_3OCHO$		●	●
$HCO + C_2H_5O \rightarrow C_2H_5OCHO$		●	●
$H + C_2H_5O \rightarrow C_2H_5OH$		●	●
$CH_3OCHO + h\nu \rightarrow CH_2OCHO + H$		●	●
$C_2H_5OH + h\nu \rightarrow C_2H_5O + H$		●	●
$C_2H_5OCHO + h\nu \rightarrow CH_2OCHO + CH_3$		●	●
$C_2H_5OCHO + h\nu \rightarrow C_2H_5O + HCO$		●	●

Notes: Reactions that were present in the hot core model of Garrod et al. (2008) are indicated. Activation energies required for reaction are shown in brackets, where applicable.

and 13, assuming an H_2 column density of 1.8×10^{25} cm^{-2} for a source size of 2″ (see Belloche et al. 2008b), and an H_2 column density profile proportional to $r^{-0.5}$ that corresponds to an H_2 density profile proportional to $r^{-1.5}$ in spherical symmetry[10]. Given that the dust properties are uncertain by a factor ∼ 2 at least and that the contribution of the vibrationally or torsionally excited states of some molecules studied here (e.g. ethanol, see Pearson et al. 2008) to their partition function was not included, we estimate these observed abundances to be accurate within a factor ∼ 3.

Ethyl formate is clearly formed most significantly at late times (see Fig. 5a), and its grain-surface abundance (*dotted* red lines) scales well with that of methyl formate. Grain-surface methyl formate is, in fact, the primary source of precursor radicals (via photodissociation) for the formation of ethyl formate. When methyl formate evaporates, and ethanol is left as the dominant source of precursor radicals, ethyl formate production becomes dependent on the addition of HCO to C_2H_5O. The post-evaporation gas-phase abundance of ethyl formate relative to methyl formate and formic acid appears to match observational abundances and rotational temperatures reasonably well.

The gas-phase methyl formate peak abundance is also relatively close to the observed abundance (within a factor 5), and the model temperature at this peak is in very good agreement with the observed rotational temperature (see Table 5). However, the abundance quickly falls, and the ratio of gas phase CH_3OCHO to HCOOH, C_2H_5OH and CH_3OCH_3 at the higher temperatures most appropriate to the densest regions of the hot core is low compared to the observed values.

The *Basic* model uses the same binding energies for methyl formate and dimethyl ether as were employed by Garrod et al. (2008), appropriate to binding on amorphous water ice. These values cause relatively early evaporation of those species, resulting in significant destruction in the gas-phase, and low fractional abundances in comparison to observed values in the case of methyl formate. The binding energies of those molecules were obtained by simple interpolation of measured values obtained for other species. Laboratory data for methyl formate and dimethyl ether evaporation from appropriate ice surfaces are not currently available.

For species comprising at least one -OH functional group, binding-energy estimates take account of hydrogen-bonding interactions with the ice surface. Such species may act as both hydrogen-bond donors and acceptors, raising their binding strengths. However, both methyl formate and dimethyl ether have at least one unbonded electron pair attached to a strongly electro-negative atom (oxygen), allowing them to be hydrogen-bond acceptors. This may give them a somewhat stronger bond to the predominantly water-ice surface than has been assumed.

Here, the binding energy of methyl formate is raised beyond that of the *Basic* model, such that it falls approximately half way between its old value and that of ethanol, its most closely-matched counterpart with a single, fully hydrogen-bonding functional group. This augmentation constitutes an increase of approximately 1000 K, giving $E_D = 5200$ K. The binding energy of dimethyl ether is similarly raised by 1000 K.

Augmentation of methyl formate binding energy allows it to remain on grains for longer, reducing the time available for gas-phase destruction, before the majority of other species evaporate, damping the effect of ion-molecule destruction pathways (see Fig. 5b). This allows gas-phase methyl formate fractional abundances to remain high for longer, although the resulting peak-abundance temperature is somewhat greater, at 112 K.

Dimethyl ether does have a viable gas-phase formation mechanism, and is largely produced in the gas phase, due to the large abundance of methanol ($\sim 10^{-5} n_H$); hence, the peak abundance is not strongly affected by the augmentation of its binding energy. Its gas-phase abundance in the model is consistent with the observed value (within a factor 2, see Table 15). The peak-abundance temperature of the model is somewhat higher than that derived observationally. A slightly lower grain-surface methanol abundance would remedy this, as post-evaporation gas-phase methanol abundances should diminish more rapidly, reducing the rate of dimethyl ether formation. A slower warm-up subsequent to methanol evaporation would also produce a similar effect. Nevertheless, the observed rotational temperature of dimethyl ether seems consistent with gas-phase formation.

Surface formation rates of ethyl formate, methyl formate and ethanol are not strictly dependent on methanol abundance in the ices, but rather on the rate of formation of its photodissociation products, CH_3O, CH_2OH, and CH_3. These rates are not well constrained; however, they seem appropriate for this model. A lower grain-surface methanol abundance, as suggested above, would therefore necessitate slightly greater methanol photodissociation rates, in order to achieve appropriate abundances for methyl formate and other surface-formed species. Gas-phase and grain-surface ethyl formate abundances are largely unaffected by the changes in methyl formate binding energy. Both the gas-phase and grain-surface abundances of formic acid are strongly dependent on gas-phase processes (see Garrod et al. 2008). As a result, there appears to be no simple correlation with ethyl or methyl formate abundances. However, the low rotational temperature reported in Sect. 3.4 is qualitatively consistent with the low-temperature gas-phase formic acid peak at 40 – 60 K, a point noted by Garrod et al. (2008) in comparison to other hot-core observations. This "cold" peak presents a fractional abundance very close to the observed value (within a factor 4, see Table 15). In Sect 3.4, we modeled the spectrum of formic acid using a single temperature component; however, a two-component model with rotational temperatures (and inferred spatial extents) appropriate to the chemical models is not noticeably worse than the single-component fit. As discussed in Sect. 3.4, the existence of both hot, compact and cold, extended components would be consistent with the lower flux measured with the BIMA interferometer by Liu et al. (2001) compared to our lower-resolution single-dish measurement.

5.2.2. Cyanides

The *Basic* model is capable of producing cyanide species in appropriate absolute quantities (see Fig. 6a), however, their relative abundances are not well matched to the observationally determined values. In order to understand the behavior of the cyanide network, the different grain-surface formation mechanisms, and combinations, were isolated by artificially de-activating particular reaction routes. In fact, all combinations that include either the hydrogenation of the cyanopolyyne HC_3N and of vinyl cyanide, C_2H_3CN, or the addition of large, pre-formed hydrocarbons directly to the CN radical, produce wildly inaccurate ratios. In some such cases, *n*-propyl cyanide is the most abundant of all, often with methyl cyanide abundances deeply depressed. The only combination in which the correct proportion is reproduced is that in which only the sequential addition of

---

[10] Osorio et al. (1999) expect a density profile proportional to r^{-p} with $p = 1.5$ for the central region of a hot core. On larger scales in Sgr B2 (20–200″), Lis & Goldsmith (1989) derived a density profile $p \sim 2$–2.5 while de Vicente et al. (1997) found $p \sim 0.9$.

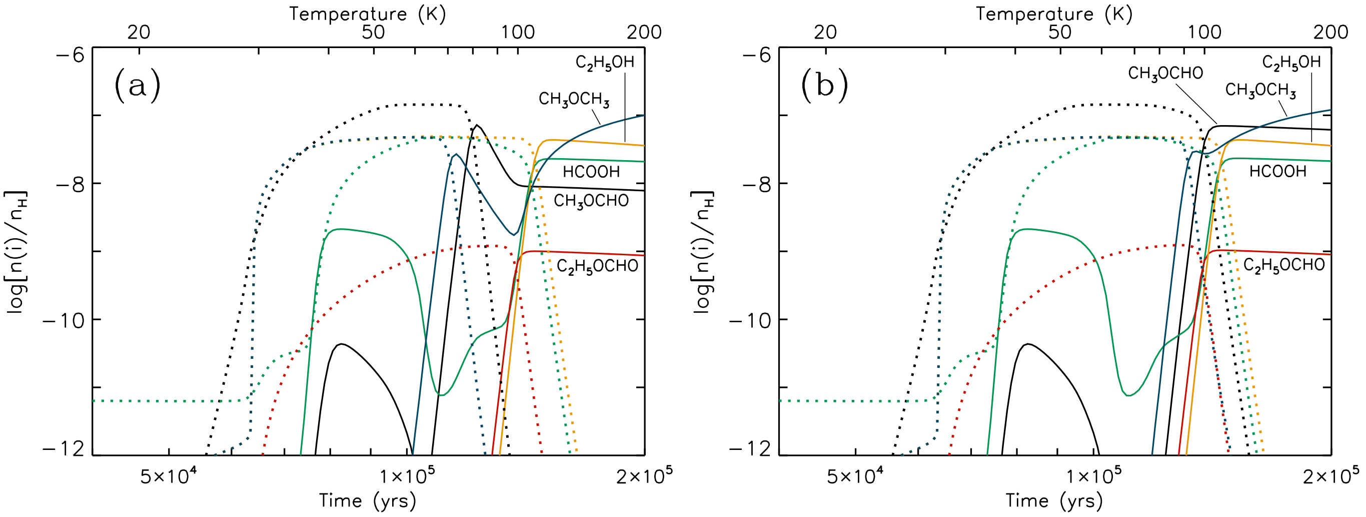

Fig. 5. a) *Basic* model, showing methyl formate, ethyl formate, formic acid, and related species. **b)** The same species, following augmentation of methyl formate and dimethyl ether binding energies. Solid lines indicate gas-phase species; dotted lines of the same color indicate the same species on the grain surfaces.

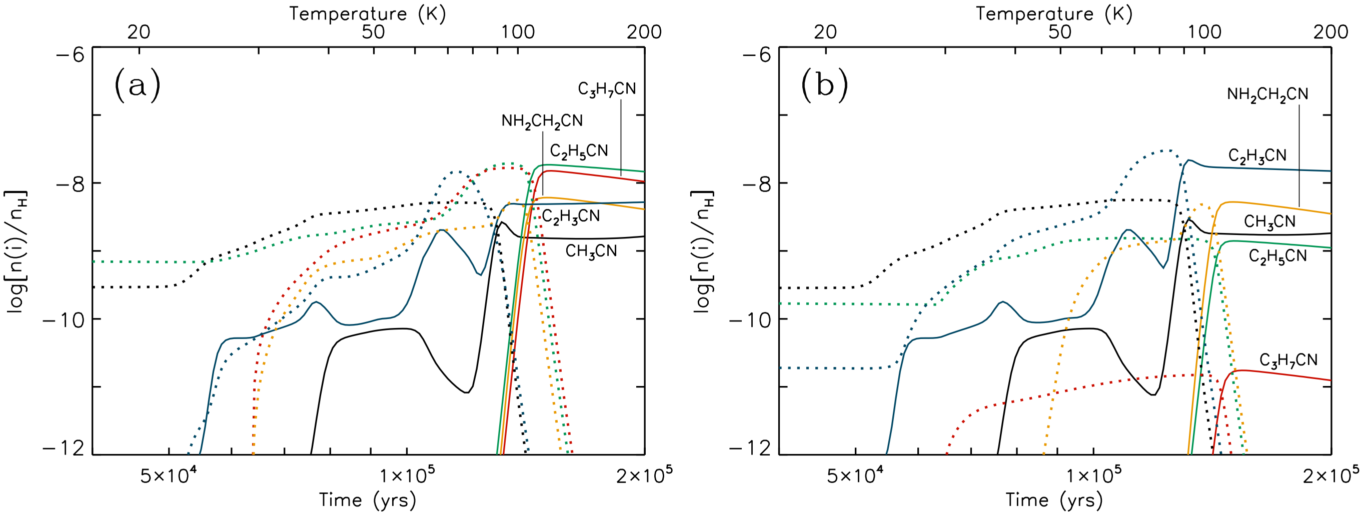

Fig. 6. a) *Basic* model, showing cyanides. **b)** The same species, using the *Select* model, in which selected grain-surface reactions are de-activated (see Table 14). Solid lines indicate gas-phase species; dotted lines of the same color indicate the same species on the grain surfaces.

grain-surface CH_2 and CH_3 functional groups is allowed (see Fig. 6b). We label this model, combined with the augmented binding energies of methyl formate and dimethyl ether, as the *Select* model. In this scheme, formation of the larger cyanides begins with cosmic ray-induced photodissociation of a smaller grain-surface alkyl cyanide molecule (resulting in the ejection of a hydrogen atom), or with the accretion of CH_2CN (which may be formed in the gas-phase following the evaporation of HCN). A methyl-group radical is then added to produce a larger alkyl cyanide molecule.

Methyl cyanide itself is mainly formed on the grains by addition of CH_3 and CN radicals, but it may also be formed by gas-phase processes fuelled by the evaporation of HCN. Methyl cyanide evaporates from the dust grains around 90 K, producing its greatest gas-phase abundance; however, the subsequent evaporation of all molecular material from the grains promotes rapid gas-phase formation, maintaining methyl cyanide abundances for longer, and providing qualitative agreement with the large rotational temperature derived from the observational data.

The abundance obtained for aminoacetonitrile is in reasonable agreement with that obtained observationally (within a factor 8), suggesting that the addition of NH or NH_2 to CH_2CN on grain surfaces, similar to the suggested mechanism for ethyl cyanide, is a plausible route to its formation. There may therefore be some degree of correlation between these two species, which should be investigated in future. The removal of the other formation routes for aminoacetonitrile, comprising the addition of grain-surface CN to either CH_2NH or CH_2NH_2, makes little difference to the results, mainly due to limited availability of the latter two radicals.

Vinyl cyanide, C_2H_3CN, a potential precursor of ethyl cyanide and *n*-propyl cyanide, is formed predominantly in the gas-phase in both the *Basic* and *Select* models. This occurs through the reaction of CN with ethylene (C_2H_4), which has been shown experimentally to be rapid over a range of temper-

Table 15. Peak gas-phase abundances from each model, with corresponding model temperatures, as well as source sizes, rotation temperatures, and gas-phase abundances derived from the observations of the main source in Sgr B2(N).

Species	*Basic* model		*Select* model		Observations			Abundance ratio
	$n[i]/n_{H_2}$	T^a (K)	$n[i]/n_{H_2}$	T^a (K)	Size ($''$)	T_{rot} (K)	$n[i]/n_{H_2}$	*Select* model over observation
(1)	(2)	(3)	(4)	(5)	(6)	(7)	(8)	(9)
HCOOH (hot)	5.4e-08	120	5.4e-08	120	5.0	70	1.3e-09	42
HCOOH (cold)	4.9e-09	42	4.9e-09	42	5.0	70	1.3e-09	3.8
CH_3OCHO	1.7e-07	81	1.6e-07	112	4.0	80	3.5e-08	4.6
C_2H_5OCHO	2.3e-09	110	2.3e-09	110	3.0	100	3.6e-09	0.6
C_2H_5OH	1.0e-07	120	1.0e-07	120	3.0	100	5.7e-08	1.8
CH_3OCH_3	2.3e-07	200	2.8e-07	200	2.5	130	1.4e-07	2.0
CH_3CN	6.3e-09	92	6.8e-09	92	2.7	200	1.3e-07	0.05
C_2H_5CN	4.4e-08	117	3.3e-09	117	3.0	170	8.1e-08	0.04
C_3H_7CN	3.5e-08	120	4.0e-11	123	3.0	150	1.0e-09	0.04
NH_2CH_2CN	1.4e-08	117	1.2e-08	117	2.0	100	1.5e-09	8.0
C_2H_3CN	1.2e-08	200	5.1e-08	92	2.3	170	4.7e-08	1.1

Notes: [a] The model temperatures are the temperatures at which the peak gas-phase abundances are achieved.

atures (Carty et al. 2001). The resultant gas-phase vinyl cyanide then accretes onto the grains until greater temperatures are achieved. Following evaporation of the ice mantles at $T >$ 100 K, vinyl cyanide is again formed rapidly in the gas-phase by the same mechanism, allowing it, like methyl cyanide, to retain large fractional abundances longer than the other cyanides. This effect is also in qualititative agreement with its relatively high rotational temperature. Both models show good agreement with the observational abundance of this molecule, but the *Select* model produces an excellent match (see Table 15).

For the *Basic* model, ratios of peak abundance values are HCOOH / CH_3OCHO / C_2H_5OCHO = 23 / 72 / 1 and CH_3CN / C_2H_5CN / C_3H_7CN = 0.18 / 1.3 / 1. For the *Select* model, these ratios are HCOOH / CH_3OCHO / C_2H_5OCHO = 23 / 70 / 1 and CH_3CN / C_2H_5CN / C_3H_7CN = 171 / 82 / 1. These seem a fair match to the observed values of Sects. 3.4 and 4.4 (0.8 / 15 / 1 and 108 / 80 / 1, respectively). Consideration of only the low temperature formic acid peak in the models further improves its ratio with ethyl formate abundances.

The warm-up timescale of $t_{max} = 2 \times 10^5$ yr appears to yield the most appropriate reproduction of observed cyanide ratios, although longer timescales are also plausible; the *Select* model, with $t_{max} = 10^6$ yr, produces peak abundance ratios of HCOOH / CH_3OCHO / C_2H_5OCHO = 4.2 / 3.3 / 1 and CH_3CN / C_2H_5CN / C_3H_7CN = 258 / 106 / 1.

5.3. Discussion

Based on the abundance ratios of the model, the dominant formation mechanism for alkyl cyanides is probably the sequential addition of CH_2 or CH_3 radicals to CN, CH_2CN and C_2H_4CN on the grain surfaces. Both the alternative routes – the grain-surface hydrogenation of gas phase-formed HC_3N and C_2H_3CN, or the direct grain-surface addition of pre-formed large hydrocarbon radicals like C_2H_5 or C_3H_7 to a CN radical – appear to be very much too fast, resulting in excessive quantities of the two largest alkyl cyanides.

To achieve the appropriate ratios, those two formation routes must be artificially disabled within the model. Why should these mechanisms be less efficient in reality than they would appear from the model? Firstly, gas-phase HC_3N and C_2H_3CN may be less abundant than the model suggests. The evaporation, and subsequent reaction, of HCN from the grains is a primary cause of gas-phase formation for each of these molecules. Variation in the evaporation characteristics or the composition/structure of the ices may weaken such mechanisms. However, the agreement between observed and modeled abundances of vinyl cyanide is very good. Indeed, the *Select* model shows excellent agreement, providing further justification for the omission of its hydrogenation reactions.

Alternatively, surface hydrogenation of HC_3N and C_2H_3CN, once they have accreted onto the grains, may be less efficient than has been assumed here. Importantly, activation energies are required for hydrogenation of both these species, whose values are poorly constrained. The fact that it is these very reactions that must be disabled suggests strongly that their activation energies should be significantly higher than has been assumed here. Additionally, our use of a "deterministic" gas-grain model may also produce somewhat more efficient hydrogenation than is really the case (although a test-run using the rate-modification method of Garrod (2008) shows no great difference in this respect).

In the case of the addition of large hydrocarbon radicals to CN, the over-dominance of these channels is probably due to the incompleteness of the hydrocarbon chemistry as a whole, particularly on the grains. Whilst up to 10 carbon atoms in a chain are considered in this model, the hydrogenation states of the larger chains are typically limited to 4 hydrogen atoms. Crucially, hydrogenation is the only type of reaction included in the network for most hydrocarbons, aside from the newly-added CN addition reactions. The hydrocarbon reaction set was largely devised with cold dark clouds in mind, where hydrogenation dominates. By including only a single new reaction (addition to CN) for any particular hydrocarbon, that reaction can easily become the dominant channel. The completion of the hydrocarbon network to include reactions with all major reactants would be beneficial, although this is not a trivial task.

The small hydrocarbons CH_2 and CH_3, on the other hand, as well as CN itself, have a much more comprehensive reaction network, making sequential addition and its apparent degree of efficiency more credible.

Ethyl formate and aminoacetonitrile also seem to be well reproduced with a similar addition scheme to that of the alkyl cyanides. Ethyl formate abundance may be dependent on ethanol as well as methyl formate, depending on the specific conditions.

The *Select* model reproduces well the abundance ratios for alkyl cyanides, but their absolute abundances are an order of magnitude lower than observational values. This also results in a poor match to abundance ratios relative to methyl formate and other methanol-related species. In fact, the chemistries of the cyanides and the methanol-related species do not strongly influence one another in the model. The overall abundances of each category of molecule are mainly influenced by different, independent parameters: the formation rate of the products of methanol photodissociation (i.e. the product of the photodissociation rate and absolute grain-surface abundance of methanol), and the quantity of HCN or related nitrile-group species in the ice mantles, respectively. Similarly, the modeled abundance of aminoacetonitrile relative to the alkyl cyanides is very high. The formation rate of this molecule is strongly dependent on the product of the abundance of NH_3 in the ices, and its rate of photodissociation. This indicates that one or both of these values may be too large, by at least an order of magnitude. A parameter search should yield the optimal values for all such quantities, but such is not the focus of this paper.

The augmentation of methyl formate binding energy allows its abundance to remain high at temperatures appropriate to the densest parts of the hot core. However, the low observed rotational temperatures suggest that methyl formate should still have a binding energy less than that of H_2O, which is indeed the case here, even with the highest value we use. A value somewhat lower than our maximum would also achieve quite acceptable results. Clearly, an experimental value for binding to astrophysically appropriate surfaces would be highly valuable for the chemical modeling of hot cores.

While certain crucial steps in the formation of these complex molecules occur only in the gas-phase or on the grain surfaces, processes in each phase are inter-dependent and cannot be understood in isolation.

6. Conclusions

We used the complete 3 mm and partial 2 and 1.3 mm line surveys obtained with the IRAM 30 m telescope toward the hot cores Sgr B2(N) and (M) to search for emission from the organic molecules ethyl formate and *n*-propyl cyanide. We report the detection of both molecules toward the hot core Sgr B2(N), which are the first detections of these molecules in the interstellar medium. Our main results and conclusions are the following:

1. New entries for the CDMS catalog have been created for *n*-propyl cyanide and ethyl formate.
2. 46 of the 711 significant transitions of the *anti*-conformer of ethyl formate covered by our 30 m line survey are relatively free of contamination from other molecules and are detected in the form of 24 observed features toward Sgr B2(N). The emission of the *gauche*-conformer is too weak to be clearly detected in our survey.
3. 50 of the 636 significant transitions of the *anti*-conformer of *n*-propyl cyanide covered by our 30 m line survey are relatively free of contamination from other molecules and are detected in the form of 12 observed features toward Sgr B2(N) with two velocity components. The emission of the *gauche*-conformer is too weak to be clearly detected in our survey.
4. With a source size of 3″, we derive an ethyl formate column density of 5.4×10^{16} cm^{-2} for a temperature of 100 K and a linewidth of 7 km s^{-1} in the LTE approximation. The abundance of ethyl formate relative to H_2 is estimated to be 3.6×10^{-9}.
5. The two velocity components detected in *n*-propyl cyanide have LTE column densities of 1.5×10^{16} and 6.6×10^{15} cm^{-2}, respectively, with a temperature of 150 K, a linewidth of 7 km s^{-1}, and a source size of 3″. The fractional abundance of *n*-propyl cyanide in the main source is estimated to be 1.0×10^{-9}.
6. We detected neither ethyl formate nor *n*-propyl cyanide toward the more evolved source Sgr B2(M) and derived column density upper limits of 2×10^{16} and 6×10^{15} cm^{-2}, respectively, for a source size of 3″.
7. We modeled the emission of chemically related species also detected in our survey of Sgr B2(N) and derived column density ratios of 0.8 / 15 / 1 for *t*-HCOOH / CH_3OCHO / C_2H_5OCHO and 108 / 80 / 1 for CH_3CN / C_2H_5CN / C_3H_7CN in the main hot core of Sgr B2(N).
8. The chemical models suggest that the sequential, piece-wise construction of ethyl and *n*-propyl cyanide from their constituent functional groups on the grain surfaces is their most likely formation route. Aminoacetonitrile formation proceeds similarly, suggesting a possible correlation with ethyl cyanide abundance. Vinyl cyanide is formed predominantly in the gas-phase.
9. Comparison of the observational and model results suggests that the production of alkyl cyanides by the hydrogenation of less saturated species is much less efficient than functional-group addition.
10. Ethyl formate can be formed on the grains by addition of HCO or CH_3 to functional-group radicals derived from methyl formate and ethanol; however, methyl formate appears to be the dominant precursor.
11. Understanding of the complex interactions between gas-phase and grain-surface processes may be necessary to fully explain the observational features displayed by many complex molecules, including formic acid and methyl formate.
12. The detection in Sgr B2(N) of the next stage of complexity in two classes of complex molecule, esters and alkyl cyanides, suggests that greater complexity also may be present in other classes of molecule in the interstellar medium.

Our results have demonstrated the power of the ”complete spectrum fitting” approach used by us as a technique that is mandatory today for the identification of new complex molecules by their generally weak signals. Ideally, one would want to verify identifications with interferometric observations as done for the case of aminoacetonitrile (Belloche et al. 2008a,b). However, given the limited collecting area, bandwidth and spatial resolution of today’s interferometer arrays, this would be very time consuming or even prohibitive. It will, however, be a trivial exercise for the Atacama Large Millimeter Array (ALMA) once it is fully operational.

Acknowledgements. We thank the anonymous referee and the editor for their careful reading of the manuscript and for their suggestions that helped improve the clarity of this article. H.S.P.M. thanks Dr. Jürgen Aschenbach from the library of the University of Kiel for providing the supplementary material to Vormann & Dreizler (1988). We are grateful to Eric Herbst for providing the ethyl formate spectroscopic line list as well as a preprint of the manuscript prior to publication. H.S.P.M. thanks the Deutsche Forschungsgemeinschaft (DFG) for initial support through the collaborative research grant SFB 494. He is grateful to the Bundesministerium für Bildung und Forschung (BMBF) for recent support which was administered through Deutsches Zentrum für Luft- und Raumfahrt (DLR). R.T.G thanks the Alexander von Humboldt Foundation for a Research Fellowship.

References

Belloche, A., Menten, K. M., Comito, C., Müller, H. S. P., Schilke, P., Ott, J., Thorwirth, S., & Hieret, C. 2008a, A&A, 482, 179

Belloche, A., Menten, K. M., Comito, C., Müller, H. S. P., Schilke, P., Ott, J., Thorwirth, S., & Hieret, C. 2008b, A&A, 492, 769

Bernstein, M. P., Dworkin, J. P., Sandford, S. A., Cooper, G. W., & Allamandola, L. J. 2002, Nature, 416, 401

Carty, D., Le Page, V., Sims, I. R., & Sims, I. W. M. 2001, Chem. Phys. Lett., 344, 310

Comito, C., Schilke, P., Phillips, T. G., Lis, D. C., Motte, F., & Mehringer, D. 2005, ApJS, 156, 127

Demaison, J., & Dreizler, H. 1982, Z. Naturforsch. A, 37, 199

Demaison, J., Boucher, D., Burie, J., & Dubrulle, A. 1984, Z. Naturforsch. A, 39, 560

de Vicente, P., Martin-Pintado, J., & Wilson, T. L. 1997, A&A, 320, 957

Ehrenfreund, P., Glavin, D. P., Botta, O., Cooper, G., & Bada, J. L. 2001, Proceedings of the National Academy of Science, 98, 2138

Elsila, J. E., Dworkin, J. P., Bernstein, M. P., Martin, M. P., & Sandford, S. A. 2007, ApJ, 660, 911

Friedel, D. N., Snyder, L. E., Turner, B. E., & Remijan, A. 2004, ApJ, 600, 234

Garrod, R. T., & Herbst, E. 2006, A&A, 457, 927

Garrod, R. T., Widicus Weaver, S. L., & Herbst, E. 2008, ApJ, 682, 283

Garrod, R. T. 2008, A&A, 491, 239

Geppert, W. D., Hamberg, M., Thomas, R. D., Österdahl, F., et al. 2006, Faraday Discuss. 133, 177

Goldsmith, P. F., & Langer, W. D. 1999, ApJ, 517, 209

Gordon, M. A., Berkermann, U., Mezger, P. G., Zylka, R., Haslam, C. G. T., Kreysa, E., Sievers, A., & Lemke, R. 1993, A&A, 280, 208

Hirota, E. 1962, J. Chem. Phys., 37, 2918

Hollis, J. M., Lovas, F. J., & Jewell, P. R. 2000, ApJ, 540, L107

Hollis, J. M., Pedelty, J. A., Boboltz, D. A., Liu, S.-Y., Snyder, L. E., Palmer, P., Lovas, F. J., & Jewell, P. R. 2003, ApJ, 596, L235

Hollis, J. M., Lovas, F. J., Remijan, A. J., Jewell, P. R., Ilyushin, V. V., & Kleiner, I. 2006, ApJ, 643, L25

Horn, A., Møllendal, H., Sekiguchi, O., Uggerud, E., Roberts, H., Herbst, E., Viggiano, A. A., & Fridgen, T. D. 2004, ApJ, 611, 605

Jones, P. A., Cunningham, M. R., Godfrey, P. D., & Cragg, D. M. 2007, MNRAS, 374, 579

Jones, P. A., Burton, M. G., Cunningham, M. R., Menten, K. M., Schilke, P., Belloche, A., Leurini, S., Ott, J., Walsh, A. J. 2008, MNRAS, 386, 117

Lis, D. C., & Goldsmith, P. F. 1989, ApJ, 337, 704

Lis, D. C., Goldsmith, P. F., Carlstrom, J. E., & Scoville, N. Z. 1993, ApJ, 402, 238

Liu, S.-Y., & Snyder, L. E. 1999, ApJ, 523, 683

Liu, S.-Y., Mehringer, D. M., & Snyder, L. E. 2001, ApJ, 552, 654

Medvedev, I. R., De Lucia, F. C., & Herbst, E. 2009, ApJS, in press

Mehringer, D. M., Snyder, L. E., Miao, Y., & Lovas, F. J. 1997, ApJ, 480, L71

Miao, Y., Mehringer, D. M., Kuan, Y.-J., & Snyder, L. E. 1995, ApJ, 445, L59

Millar, T. J., Herbst, E., & Charnley, S. B. 1991, ApJ, 369, 147

Müller, H. S. P., Thorwirth, S., Roth, D. A., & Winnewisser, G. 2001, A&A, 370, L49

Müller, H. S. P., Schlöder, F., Stutzki, J., & Winnewisser, G. 2005, J. Mol. Struct, 742, 215

Müller, H. S. P., Belloche, A., Menten, K. M., Comito, C., & Schilke, P. 2008, J. Mol. Spectrosc., 251, 319

Nummelin, A., Bergman, P., Hjalmarson, Å., Friberg, P., Irvine, W. M., Millar, T. J., Ohishi, M., & Saito, S. 2000, ApJS, 128, 213

Osorio, M., Lizano, S., & D'Alessio, P. 1999, ApJ, 525, 808

Pearson, J. C., Brauer, C. S., Drouin, B. J. 2008, J. Mol. Spectrosc., 251, 394

Pickett, H. M., Poynter, I. R. L., Cohen, E. A., Delitsky, M. L., Pearson, J. C., & Müller, H. S. P. 1998, J. Quant. Spectrosc. Radiat. Transfer, 60, 883

Reid, M. J. 1993, ARA&A, 31, 345

Riveros, J. M., & Bright Wilson, E., Jr. 1967, J. Chem. Phys., 46, 4605

Snyder, L. E., Kuan, Y.-J., & Miao, Y. 1994, The Structure and Content of Molecular Clouds, ed. T. L. Wilson & K. J. Johnston (Springer-Verlag), Lecture Notes in Physics, 439, 187

Snyder, L. E., Lovas, F. J., Hollis, J. M., Friedel, D. N., et al. 2005, ApJ, 619, 914

Vormann, K., & Dreizler, H. 1988, Z. Naturforsch. A, 43, 338

Włodarczak, G., Martinache, L., Demaison, J., Marstokk, K.-M., & Møllendal, H. 1988, J. Mol. Spectrosc., 127, 178

Włodarczak, G., Martinache, L., Demaison, J., Marstokk, K.-M., & Møllendal, H. 1991, J. Mol. Spectrosc., 146, 224

Appendix A: *a*-Type and *b*-type lines of methyl formate

Both *A* and *E* symmetry species of methyl formate (CH_3OCHO) are easily detected in our spectral survey of Sgr B2(N) at 3 mm. Sixty four lines of the *A* species are detected in the form of 57 features in our 3 mm survey and 48 lines of the *E* species in the form of 43 features. We followed the same procedure as described in Sect. 3.2 for ethyl formate to compute the population diagrams shown in Fig. A.1. In these diagrams, the *a*-type lines of methyl formate (with ΔK_a= 0 [2] and ΔK_c = 1 [2]) are marked with an additional circle. As mentioned in Sect. 3.4, both *a*- and *b*-type lines are well fitted with the same physical model (see Table 5). Although many *a*-type transitions with $E_u/k_B < 50$ K look systematically too low in the population diagrams after removal of the contribution of contaminating lines (Fig. A.1b and d), this can be explained by the limitations of our radiative transfer modeling: these *a*-type transitions (of the *A* or *E* species) have optical depths on the order of unity, as indicated by the significant shift between the red and green crosses in the lower energy range, and overlap with *a*-type lines of the other symmetry species (*E* or *A*, respectively) that have significant optical depths too. Since our current complete model treats the two symmetry species as independent and our radiative transfer program computes the contributions of overlapping transitions of different species independently, the sum of the overlapping *A* and *E* transitions with significant optical depths is systematically overestimated. For a transition of, e.g., the *A* species, the “contamination” by the *E* species is overestimated and its removal in Fig. A.1b yields an underestimated residual flux. Our model could be improved by treating both symmetry species as a single molecule but this would not significantly change the physical parameters found for methyl formate and is beyond the scope of this article focused on ethyl formate and *n*-propyl cyanide.

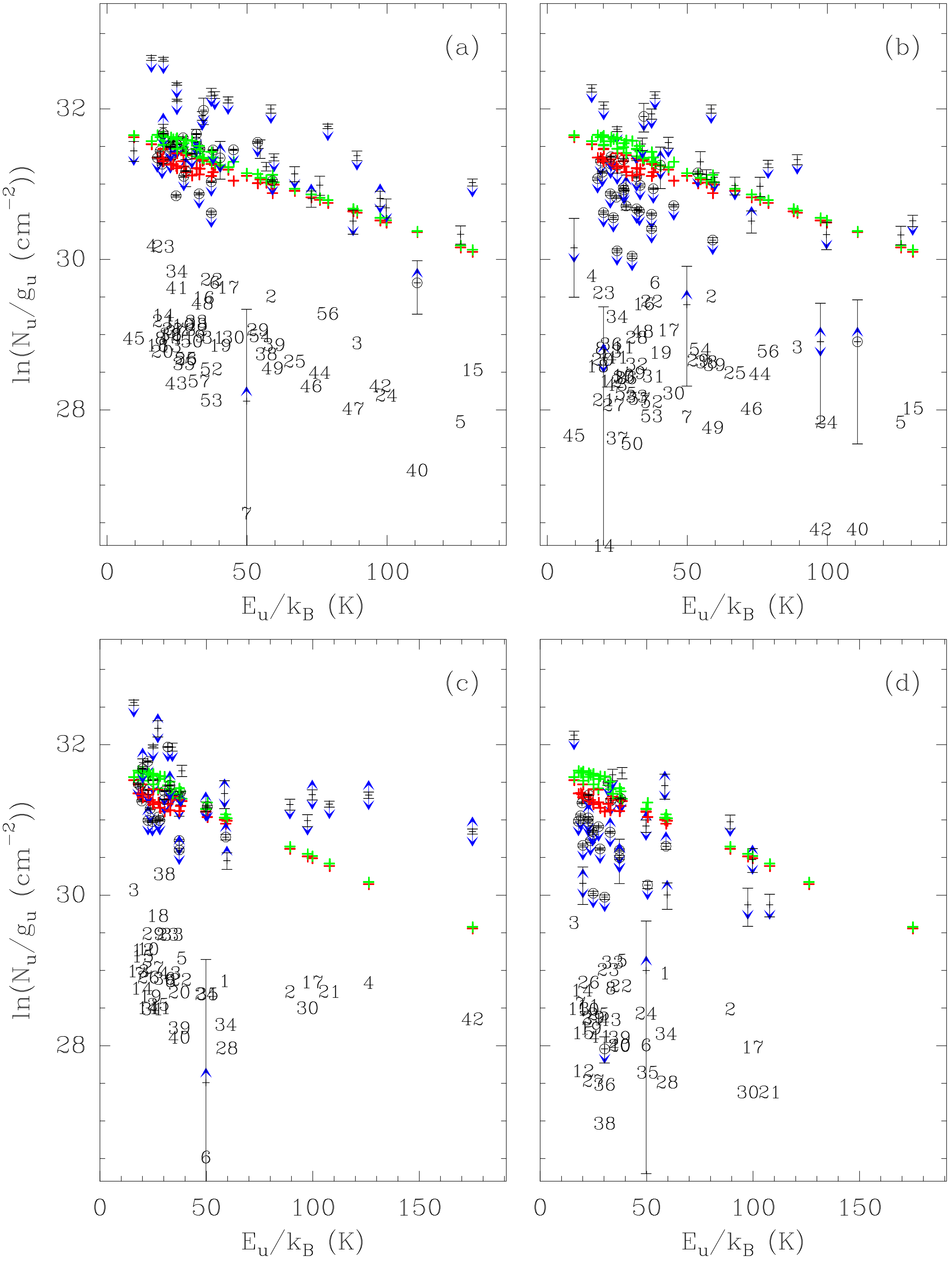

Fig. A.1. Population diagrams of the *A* and *E* symmetry species of methyl formate presented in the same way as for ethyl formate in Fig. 2 (see the caption of that figure for details). The *a*-type lines are marked with a circle. Panel **a** and **c** show the population diagrams derived from the measured integrated intensities for the *A* and *E* species, respectively, while panels **b** and **d** present the respective population diagrams after removing the expected contribution from contaminating molecules. Features 4 and 42 with $E_u/k_B > 120$ K (see panel **c**) are missing in panel **d** because the removal of the contaminating lines yields negative residuals. This is due to the uncertain level of the baseline that looks overestimated for both features in the observed spectrum.

Table 1. Transitions of the *anti*-conformer of ethyl formate observed with the IRAM 30 m telescope toward Sgr B2(N). The horizontal lines mark discontinuities in the observed frequency coverage. Only the transitions associated with a modeled line stronger than 20 mK are listed.

N^a (1)	Transition^b (2)	Frequency (MHz) (3)	Unc.^{c} (kHz) (4)	$E_l{}^d$ (K) (5)	$S\mu^2$ (D^2) (6)	σ^e (mK) (7)	Comments (8)
1	$15_{2,14}-14_{2,13}$	81779.567	4	30	50.5	13	**Detected**, blend with U-line
2	$15_{13,2}-14_{13,1}{}^\star$	82297.815	4	149	12.8	19	Blend with C_2H_5CN, υ_{13}=1/υ_{21}=1 and absorption line of c-$HC^{13}CCH$
4	$15_{14,1}-14_{14,0}{}^\star$	82297.944	4	169	6.6	19	Blend with C_2H_5CN, υ_{13}=1/υ_{21}=1 and absorption line of c-$HC^{13}CCH$
6	$15_{12,3}-14_{12,2}{}^\star$	82298.480	4	131	18.5	19	Blend with C_2H_5CN, υ_{13}=1/υ_{21}=1 and absorption line of c-$HC^{13}CCH$
8	$15_{10,5}-14_{10,4}{}^\star$	82303.360	4	100	28.6	19	Blend with HC_3N, υ_6=υ_7=1 and absorption line of c-$HC^{13}CCH$
10	$15_{9,6}-14_{9,5}{}^\star$	82308.580	4	86	32.9	19	Strong HC_3N, υ_6=υ_7=1
12	$15_{8,7}-14_{8,6}{}^\star$	82316.890	4	74	36.8	19	Strong HC_3N, υ_6=υ_7=1
14	$15_{7,8}-14_{7,7}{}^\star$	82330.125	4	63	40.2	19	Blend with CH_3CHO and $CH_3{}^{18}OH$
16	$15_{6,10}-14_{6,9}{}^\star$	82351.854	4	54	43.2	19	**Detected**, partial blend with C_2H_5CN, υ_{13}=1/υ_{21}=1 and U-line
18	$19_{3,17}-19_{2,18}$	82389.204	9	53	4.8	18	Blend with $^{13}CH_3OH$
19	$15_{5,11}-14_{5,10}$	82389.698	4	46	45.7	18	Blend with $^{13}CH_3OH$
20	$15_{5,10}-14_{5,9}$	82390.016	4	46	45.7	18	Blend with $^{13}CH_3OH$
21	$15_{4,12}-14_{4,11}$	82457.126	4	39	47.8	18	Strong CH_3OCH_3
22	$15_{4,11}-14_{4,10}$	82471.367	4	39	47.8	18	Blend with $CH_2(OH)CHO$ and U-line
23	$15_{3,13}-14_{3,12}$	82485.618	4	34	49.4	18	Blend with U-lines
24	$15_{3,12}-14_{3,11}$	82802.132	4	34	49.4	17	Blend with C_2H_5CN
25	$15_{1,14}-14_{1,13}$	83792.699	4	29	51.1	16	Blend with CH_3OH and U-lines
26	$15_{2,13}-14_{2,12}$	84081.357	4	31	50.5	19	**Detected**, partial blend with CH_3CH_3CO, υ_t=1
27	$16_{1,16}-15_{1,15}$	84444.095	4	31	54.6	19	Blend with $^{13}CH_3OH$ and C_2H_5CN, υ_{13}=1/υ_{21}=1
28	$16_{0,16}-15_{0,15}$	85065.106	4	31	54.7	22	**Detected**, partial blend with c-C_2H_4O
29	$16_{2,15}-15_{2,14}$	87160.417	4	34	54.0	17	Strong CH_3OCHO
30	$16_{14,2}-15_{14,1}{}^\star$	87785.462	4	173	12.9	17	Blend with C_2H_5CN, υ_{13}=1/υ_{21}=1, problem with baseline?
32	$16_{13,3}-15_{13,2}{}^\star$	87785.683	4	153	18.7	17	Blend with C_2H_5CN, υ_{13}=1/υ_{21}=1, problem with baseline?
34	$16_{15,1}-15_{15,0}{}^\star$	87785.966	4	193	6.6	17	Blend with C_2H_5CN, υ_{13}=1/υ_{21}=1, problem with baseline?
36	$16_{12,4}-15_{12,3}{}^\star$	87786.848	4	135	24.0	17	Blend with C_2H_5CN, υ_{13}=1/υ_{21}=1, problem with baseline?
38	$16_{11,5}-15_{11,4}{}^\star$	87789.267	4	119	28.9	17	Blend with U-line, uncertain baseline
40	$16_{10,6}-15_{10,5}{}^\star$	87793.413	4	104	33.4	17	Blend with $CH_3{}^{13}CH_2CN$ and U-line
42	$16_{9,7}-15_{9,6}{}^\star$	87800.031	4	90	37.5	17	Blend with $CH_3{}^{13}CH_2CN$ and HNCO, υ_4=1
44	$16_{8,8}-15_{8,7}{}^\star$	87810.372	4	78	41.2	17	**Group detected**, partial blend with $CH_2(OH)CHO$ and C_2H_5CN
46	$16_{7,9}-15_{7,8}{}^\star$	87826.665	4	67	44.4	17	**Group detected**, partial blend with HNCO, υ_5=1
48	$16_{6,11}-15_{6,10}{}^\star$	87853.244	4	58	47.2	17	Blend with NH_2CHO, problem with baseline?
50	$16_{5,12}-15_{5,11}$	87899.302	4	50	49.5	17	Strong $C_2H_5{}^{13}CN$, HNCO, and $HN^{13}CO$
51	$16_{5,11}-15_{5,10}$	87899.879	4	50	49.5	17	Strong $C_2H_5{}^{13}CN$, HNCO, and $HN^{13}CO$
52	$16_{4,13}-15_{4,12}$	87979.119	4	43	51.4	19	Blend with U-lines
53	$16_{3,14}-15_{3,13}$	87993.944	4	38	52.9	19	**Detected**, partial blend with CH_3CH_3CO and U-line
54	$16_{4,12}-15_{4,11}$	88001.562	4	43	51.4	19	**Detected**, blend with C_2H_5CN, υ_{13}=1/υ_{21}=1
55	$16_{3,13}-15_{3,12}$	88425.192	4	38	52.9	17	Blend with $CH_2(OH)CHO$
56	$16_{1,15}-15_{1,14}$	89218.355	4	33	54.6	16	Strong HCO^+ in absorption
57	$17_{1,17}-16_{1,16}$	89651.925	4	35	58.0	18	Blend with C_2H_5CN, υ_{13}=1/υ_{21}=1, CH_3OH, υ_t=2, and C_2H_5CN, υ_{20}=1
58	$16_{2,14}-15_{2,13}$	89804.728	4	35	54.0	18	Blend with CH_3CH_3CO
59	$17_{0,17}-16_{0,16}$	90190.497	5	35	58.1	17	Blend with $CH_2(OH)CHO$, C_2H_5CN, υ_{13}=1/υ_{21}=1, and U-line
60	$17_{2,16}-16_{2,15}$	92528.452	4	39	57.4	22	Blend with CH_3CN, υ_8=2
61	$17_{14,3}-16_{14,2}{}^\star$	93273.169	4	177	18.8	22	Blend with U-lines
63	$17_{15,2}-16_{15,1}{}^\star$	93273.377	5	198	12.9	22	Blend with U-lines
65	$17_{13,4}-16_{13,3}{}^\star$	93273.813	4	157	24.2	22	Blend with U-lines
67	$17_{16,1}-16_{16,0}{}^\star$	93274.251	5	220	6.7	22	Blend with U-lines
69	$17_{12,5}-16_{12,4}{}^\star$	93275.564	4	139	29.3	22	Blend with U-lines
71	$17_{11,6}-16_{11,5}{}^\star$	93278.797	4	123	33.9	22	Blend with U-lines
73	$17_{10,7}-16_{10,6}{}^\star$	93284.077	4	108	38.1	22	**Group detected**, uncertain baseline
75	$17_{9,8}-16_{9,7}{}^\star$	93292.297	4	94	42.0	22	**Group detected**, uncertain baseline
77	$17_{8,9}-16_{8,8}{}^\star$	93304.955	4	82	45.4	22	**Group detected**, partial blend with U-line
79	$17_{7,11}-16_{7,10}{}^\star$	93324.728	4	71	48.4	22	**Group detected**, partial blend with U-lines
81	$17_{6,12}-16_{6,11}{}^\star$	93356.821	4	62	51.0	22	**Group detected**, blend with CH_3CH_3CO and U-line?
83	$17_{5,13}-16_{5,12}$	93412.160	4	54	53.3	22	**Group detected**, partial blend with U-line?
84	$17_{5,12}-16_{5,11}$	93413.168	4	54	53.3	22	**Group detected**, partial blend with U-line?
85	$17_{3,15}-16_{3,14}$	93499.096	4	42	56.5	24	Blend with C_2H_5OH and U-line
86	$17_{4,14}-16_{4,13}$	93504.972	4	47	55.1	24	**Detected**, blend with $CH_3{}^{18}OH$
87	$17_{4,13}-16_{4,12}$	93539.303	4	47	55.1	24	**Detected**
88	$17_{3,14}-16_{3,13}$	94072.891	4	42	56.5	31	Blend with CH_3CH_3CO, υ_t=1 and $^{13}CH_3OH$, υ_t=1
89	$17_{1,16}-16_{1,15}$	94608.131	4	37	58.0	26	Blend with $^{13}CH_3CH_2CN$ and U-line
90	$18_{1,18}-17_{1,17}$	94852.542	5	40	61.5	28	Weak
91	$18_{0,18}-17_{0,17}$	95313.428	5	39	61.5	28	Weak, partial blend with C_2H_3CN, υ_{11}=1/υ_{15}=1, uncertain baseline
92	$17_{2,15}-16_{2,14}$	95517.316	4	39	57.5	23	Blend with C_2H_3CN, υ_{11}=2

Table 1. continued.

N^a (1)	Transition^b (2)	Frequency (MHz) (3)	Unc.^{c} (kHz) (4)	$E_l{}^d$ (K) (5)	$S\mu^2$ (D^2) (6)	σ^e (mK) (7)	Comments (8)
93	$18_{2,17} - 17_{2,16}$	97883.281	4	43	60.9	20	Blend with CH_3OCHO, υ_t=1 and NH_2CHO
94	$18_{15,3} - 17_{15,2}{}^\star$	98760.931	5	202	18.9	18	**Group detected**, blend with U-line
96	$18_{14,4} - 17_{14,3}{}^\star$	98761.079	5	181	24.4	18	**Group detected**, blend with U-line
98	$18_{16,2} - 17_{16,1}{}^\star$	98761.555	5	224	13.0	18	**Group detected**, blend with U-line
100	$18_{13,5} - 17_{13,4}{}^\star$	98762.218	5	162	29.5	18	**Group detected**, blend with U-line
102	$18_{17,1} - 17_{17,0}{}^\star$	98762.790	5	248	6.7	18	**Group detected**, blend with U-line
104	$18_{12,6} - 17_{12,5}{}^\star$	98764.650	5	144	34.3	18	**Group detected**
106	$18_{11,7} - 17_{11,6}{}^\star$	98768.818	5	127	38.7	18	Blend with U-line
108	$18_{10,8} - 17_{10,7}{}^\star$	98775.390	5	112	42.7	18	Blend with C_2H_5CN, υ_{20}=1
110	$18_{9,9} - 17_{9,8}{}^\star$	98785.427	5	99	46.3	18	Blend with U-line, CH_3OCHO, and C_2H_5CN, υ_{13}=1/υ_{21}=1
112	$18_{8,10} - 17_{8,9}{}^\star$	98800.707	5	86	49.6	18	Blend with CH_3CH_3CO
114	$18_{7,12} - 17_{7,11}{}^\star$	98824.411	4	76	52.4	18	Blend with C_2H_5OH
116	$18_{6,13} - 17_{6,12}{}^\star$	98862.724	4	66	54.9	18	Blend with strong U-line
118	$18_{5,14} - 17_{5,13}$	98928.453	4	58	57.0	18	**Group detected**, blend with C_2H_5CN, υ_{13}=1/υ_{21}=1
119	$18_{5,13} - 17_{5,12}$	98930.153	4	58	57.0	18	**Group detected**, blend with C_2H_5CN, υ_{13}=1/υ_{21}=1
120	$18_{3,16} - 17_{3,15}$	98999.806	4	47	60.0	18	Blend with U-lines
121	$18_{4,15} - 17_{4,14}$	99034.515	4	52	58.7	19	Blend with $^{13}CH_3CH_2CN$, CH_3CH_3CO, υ_t=1, and U-lines
122	$18_{4,14} - 17_{4,13}$	99085.662	4	52	58.7	19	Blend with a$(CH_2OH)_2$ and CH_3OCHO, υ_t=1
123	$18_{3,15} - 17_{3,14}$	99746.684	5	47	60.0	14	Blend with NH_2CN and C_2H_5CN, υ_{20}=1
124	$18_{1,17} - 17_{1,16}$	99959.814	4	42	61.4	14	Blend with NH_2CN and CH_3CH_3CO
125	$19_{1,19} - 18_{1,18}$	100046.587	5	44	64.9	14	Blend with $HCC^{13}CN$, υ_7=1 and U-line
126	$19_{0,19} - 18_{0,18}$	100436.418	5	44	64.9	24	Blend with CH_3OCH_3 and C_2H_5OH
127	$18_{2,16} - 17_{2,15}$	101213.969	5	44	61.0	21	Blend with U-line
128	$19_{2,18} - 18_{2,17}$	103224.624	5	48	64.4	25	Blend with c-C_2H_4O, CH_3OCHO, and U-line
129	$19_{15,4} - 18_{15,3}{}^\star$	104248.635	5	207	24.6	48	Blend with SO_2 and U-line?
131	$19_{16,3} - 18_{16,2}{}^\star$	104248.958	5	229	19.0	48	Blend with SO_2 and U-line?
133	$19_{14,5} - 18_{14,4}{}^\star$	104249.203	5	186	29.8	48	Blend with SO_2 and U-line?
135	$19_{17,2} - 18_{17,1}{}^\star$	104249.983	5	253	13.0	48	Blend with SO_2 and U-line?
137	$19_{13,6} - 18_{13,5}{}^\star$	104250.916	5	167	34.7	48	Blend with SO_2 and U-line?
139	$19_{18,1} - 18_{18,0}{}^\star$	104251.566	5	278	6.7	48	Blend with SO_2 and U-line?
141	$19_{12,7} - 18_{12,6}{}^\star$	104254.128	5	149	39.2	48	Blend with CH_3OCHO
143	$19_{11,8} - 18_{11,7}{}^\star$	104259.358	5	132	43.3	48	Weak, baseline problem?
145	$19_{10,9} - 18_{10,8}{}^\star$	104267.390	5	117	47.1	48	Weak
147	$19_{9,10} - 18_{9,9}{}^\star$	104279.474	5	103	50.6	48	Blend with C_2H_5CN, υ_{13}=1/υ_{21}=1 and C_2H_5OH
149	$19_{8,11} - 18_{8,10}{}^\star$	104297.698	5	91	53.6	48	Strong $^{13}CH_3OH$, CH_3OCHO, and CH_3OH
151	$19_{7,13} - 18_{7,12}{}^\star$	104325.811	5	80	56.3	48	Blend with C_2H_3CN, υ_{11}=3, $CH_3{}^{18}OH$, and U-lines
153	$19_{6,14} - 18_{6,13}{}^\star$	104371.094	5	71	58.7	48	Blend with U-lines
155	$19_{5,15} - 18_{5,14}$	104448.349	5	63	60.7	48	Blend with C_2H_5CN, υ_{13}=1/υ_{21}=1 and $^{13}CH_3CH_2CN$
156	$19_{5,14} - 18_{5,13}$	104451.132	5	63	60.7	48	Blend with $^{13}CH_3CH_2CN$, C_2H_3CN, and $^{13}CH_3OH$
157	$19_{3,17} - 18_{3,16}$	104494.782	5	52	63.5	25	Blend with C_2H_3CN and C_2H_3CN, υ_{15}=2
158	$19_{4,16} - 18_{4,15}$	104567.468	5	57	62.3	25	Blend with C_2H_3CN, υ_{15}=1
159	$19_{4,15} - 18_{4,14}$	104641.877	5	57	62.3	25	Blend with C_2H_3CN, υ_{15}=1, C_2H_3CN, υ_{11}=1/υ_{15}=1, and U-line
160	$20_{1,20} - 19_{1,19}$	105234.713	5	49	68.4	28	**Detected**, blend with C_2H_5OH and CH_3OCHO
161	$19_{1,18} - 18_{1,17}$	105272.047	5	47	64.8	28	**Detected**, blend with U-lines
162	$19_{3,16} - 18_{3,15}$	105447.141	5	52	63.5	37	**Detected**
163	$20_{0,20} - 19_{0,19}$	105561.113	5	49	68.4	37	Blend with CH_3OCH_3 and CH_3CH_3CO
164	$19_{2,17} - 18_{2,16}$	106890.388	100	49	64.5	24	Blend with C_2H_5CN, υ_{13}=1/υ_{21}=1 and U-lines
165	$20_{2,19} - 19_{2,18}$	108552.378	100	53	67.8	20	**Detected**, partial blend with C_2H_3CN, υ_{15}=1 and U-lines
166	$20_{16,4} - 19_{16,3}{}^\star$	109736.466	5	234	24.7	41	Strong HC_3N, υ_6=υ_7=1 and $HCC^{13}CN$, υ_5=1/υ_7=3
168	$20_{15,5} - 19_{15,4}{}^\star$	109736.499	5	212	30.0	41	Strong HC_3N, υ_6=υ_7=1 and $HCC^{13}CN$, υ_5=1/υ_7=3
170	$20_{17,3} - 19_{17,2}{}^\star$	109737.236	5	258	19.0	41	Strong HC_3N, υ_6=υ_7=1 and $HCC^{13}CN$, υ_5=1/υ_7=3
172	$20_{14,6} - 19_{14,5}{}^\star$	109737.553	5	191	35.0	41	Strong HC_3N, υ_6=υ_7=1 and $HCC^{13}CN$, υ_5=1/υ_7=3
174	$20_{18,2} - 19_{18,1}{}^\star$	109738.645	5	283	13.0	41	Strong HC_3N, υ_6=υ_7=1 and $HCC^{13}CN$, υ_5=1/υ_7=3
176	$20_{13,7} - 19_{13,6}{}^\star$	109739.922	5	172	39.6	41	Strong HC_3N, υ_6=υ_7=1 and $HCC^{13}CN$, υ_5=1/υ_7=3
178	$20_{19,1} - 19_{19,0}{}^\star$	109740.558	6	310	6.7	41	Strong HC_3N, υ_6=υ_7=1 and $HCC^{13}CN$, υ_5=1/υ_7=3
180	$20_{12,8} - 19_{12,7}{}^\star$	109744.026	100	154	43.9	41	Strong HC_3N, υ_6=υ_7=1 and $HCC^{13}CN$, υ_5=1/υ_7=3
182	$20_{11,9} - 19_{11,8}{}^\star$	109750.509	100	137	47.9	41	Strong HC_3N, υ_6=υ_7=1 and NH_2CHO
184	$20_{10,10} - 19_{10,9}{}^\star$	109760.033	100	122	51.4	41	Strong SO_2 and CH_3OCHO, υ_t=1
186	$20_{9,11} - 19_{9,10}{}^\star$	109774.484	100	108	54.7	41	Strong CH_3OCHO, υ_t=1 and $C^{18}O$
188	$20_{8,12} - 19_{8,11}{}^\star$	109796.006	100	96	57.6	41	Blend with CH_3CN, υ_4=1, $C^{18}O$? and U-line?, uncertain baseline
190	$20_{7,13} - 19_{7,12}{}^\star$	109829.206	100	85	60.2	41	Blend with CH_3CN, υ_4=1 and HNCO
192	$20_{6,15} - 19_{6,14}$	109882.071	5	76	62.4	41	Blend with C_2H_5CN
193	$20_{6,14} - 19_{6,13}$	109882.180	5	76	62.4	41	Blend with C_2H_5CN
194	$20_{5,16} - 19_{5,15}$	109971.950	100	68	64.3	41	Blend with U-lines

Table 1. continued.

N^a (1)	Transition^b (2)	Frequency (MHz) (3)	Unc.^{c} (kHz) (4)	$E_l{}^d$ (K) (5)	$S\mu^2$ (D^2) (6)	σ^e (mK) (7)	Comments (8)
195	$20_{5,15} - 19_{5,14}$	109976.496	100	68	64.3	41	Blend with U-lines
196	$20_{3,18} - 19_{3,17}$	109982.754	100	57	67.0	41	Blend with U-lines
197	$20_{4,17} - 19_{4,16}$	110103.554	100	62	65.8	24	Blend with HNCO, υ_5=1
198	$20_{4,16} - 19_{4,15}$	110209.376	5	62	65.8	24	Blend with ^{13}CO and HC$_3$N, υ_5=1/υ_7=3
199	$21_{1,21} - 20_{1,20}$	110417.565	5	54	71.8	24	Blend with HNCO, υ_5=1
200	$20_{1,19} - 19_{1,18}$	110544.656	100	52	68.2	32	Blend with CH$_3$^{13}CN, υ_8=1, C$_2$H$_5$OH, CH$_3$OCHO, and U-line
201	$21_{0,21} - 20_{0,20}$	110688.469	100	54	71.8	32	Blend with CH$_3$CN, υ_8=1
202	$20_{3,17} - 19_{3,16}$	111173.805	100	57	67.1	25	Blend with CH$_3$OCHO
203	$20_{2,18} - 19_{2,17}$	112542.864	100	54	67.9	31	Blend with U-lines
204	$21_{2,20} - 20_{2,19}$	113866.412	100	58	71.3	34	Blend with C$_2$H$_5$OH and U-lines
205	$21_{16,5} - 20_{16,4}{}^\star$	115224.084	5	239	30.2	60	Strong CO
207	$21_{15,6} - 20_{15,5}{}^\star$	115224.530	5	217	35.3	60	Strong CO
209	$21_{17,4} - 20_{17,3}{}^\star$	115224.552	5	263	24.8	60	Strong CO
211	$21_{18,3} - 20_{18,2}{}^\star$	115225.746	5	288	19.1	60	Strong CO
213	$21_{14,7} - 20_{14,6}{}^\star$	115226.140	5	196	40.0	60	Strong CO
215	$21_{19,2} - 20_{19,1}{}^\star$	115227.514	6	315	13.1	60	Strong CO
217	$21_{13,8} - 20_{13,7}{}^\star$	115229.252	5	177	44.4	60	Strong CO
219	$21_{20,1} - 20_{20,0}{}^\star$	115229.733	7	343	6.7	60	Strong CO
221	$21_{12,9} - 20_{12,8}{}^\star$	115234.500	100	159	48.5	60	Strong CO
223	$21_{11,10} - 20_{11,9}{}^\star$	115242.178	100	142	52.3	60	Strong CO
225	$21_{10,11} - 20_{10,10}{}^\star$	115253.747	100	127	55.7	60	Strong CO
227	$21_{9,12} - 20_{9,11}{}^\star$	115270.652	100	114	58.8	60	Strong CO
229	$21_{8,13} - 20_{8,12}{}^\star$	115295.734	100	101	61.6	60	Strong CO
231	$21_{7,14} - 20_{7,13}{}^\star$	115334.205	100	91	64.0	60	Strong CO
233	$21_{6,16} - 20_{6,15}$	115395.797	5	81	66.2	60	**Group detected**, partial blend with U-line
234	$21_{6,15} - 20_{6,14}$	115395.986	5	81	66.2	60	**Group detected**, partial blend with U-line
235	$21_{3,19} - 20_{3,18}{}^\star$	115462.453	100	62	70.5	60	Weak
237	$21_{5,16} - 20_{5,15}$	115506.424	100	73	68.0	60	Weak
238	$22_{1,22} - 21_{1,21}$	115595.764	5	59	75.2	79	**Detected**, blend with CH$_3$CH$_3$CO, υ_t=1, uncertain baseline
239	$21_{4,18} - 20_{4,17}$	115641.781	100	67	69.4	79	Blend with U-line
240	$21_{1,20} - 20_{1,19}$	115778.715	100	57	71.6	79	Blend with CH$_3$OCH$_3$
241	$21_{4,17} - 20_{4,16}$	115789.775	5	67	69.4	79	Weak
242	$22_{0,22} - 21_{0,21}$	115819.018	100	59	75.2	79	Weak
243	$26_{1,26} - 25_{1,25}$	136272.994	100	83	88.9	28	Blend with HC$_3$N, υ_4=1 and CH$_3$OCHO
244	$26_{0,26} - 25_{0,25}$	136369.733	100	83	88.9	28	Blend with U-line
245	$25_{1,24} - 24_{1,23}$	136400.164	100	81	85.2	28	Blend with HC^{13}CCN, υ_7=1 and C$_2$H$_3$CN, υ_{11}=2
246	$27_{2,26} - 26_{2,25}$	145476.697	100	94	91.9	25	Blend with C$_2$H$_5$CN, υ_{13}=1/υ_{21}=1 and O^{13}CS
247	$28_{5,24} - 27_{5,23}$	154303.763	50	118	93.0	112	Blend with C$_2$H$_5$OH and CH$_3$OCH$_3$
248	$28_{5,23} - 27_{5,22}$	154393.012	50	118	93.0	112	Blend with HCC^{13}CN, υ_7=1
249	$28_{4,25} - 27_{4,24}$	154410.681	50	111	94.1	112	Strong HNCO and CH$_3$OH
250	$31_{1,30} - 30_{2,29}$	163397.978	100	124	9.6	38	Blend with C$_2$H$_5$CN and CH$_3$COOH
251	$31_{2,30} - 30_{2,29}$	166330.213	100	124	105.7	66	Blend with ^{13}CH$_3$CH$_2$CN and U-lines
252	$33_{1,33} - 32_{0,32}$	172468.973	100	134	14.3	44	Strong C$_2$H$_5$CN and CH$_3$OCHO, υ_t=1
253	$31_{4,27} - 30_{4,26}$	172707.869	100	135	104.6	44	Blend with H^{13}CN in absorption and C$_2$H$_5$CN, υ_{13}=1/υ_{21}=1
254	$32_{7,26} - 31_{7,25}$	176045.797	4	166	104.5	365	Noisy
255	$32_{7,25} - 31_{7,24}$	176046.676	4	166	104.5	365	Noisy
256	$32_{6,27} - 31_{6,26}$	176266.224	100	157	105.9	365	Noisy
257	$32_{6,26} - 31_{6,25}$	176285.887	100	157	105.9	365	Noisy
258	$38_{1,37} - 37_{2,36}$	201872.699	100	185	13.2	138	Strong ^{13}CH$_3$CH$_2$CN
259	$53_{2,51} - 53_{1,52}$	201925.976	100	370	6.7	138	Strong CH$_2$CO
260	$36_{4,32} - 35_{4,31}$	201931.928	100	179	122.0	138	Strong CH$_2$CO
261	$36_{3,33} - 35_{3,32}$	202388.460	100	175	122.6	108	Blend with C$_2$H$_3$CN, υ_{11}=1
262	$53_{3,51} - 53_{2,52}$	202394.525	28	370	6.7	108	Blend with C$_2$H$_3$CN, υ_{11}=1
263	$62_{5,58} - 62_{3,59}$	202561.279	17	524	1.4	108	Strong C$_2$H$_3$CN, υ_{15}=1
264	$38_{2,37} - 37_{2,36}$	202563.884	100	185	129.7	108	Strong C$_2$H$_3$CN, υ_{15}=1
265	$38_{1,37} - 37_{1,36}$	202730.394	100	185	129.7	108	Blend with CH$_3$OCH$_3$ and C$_2$H$_3$CN, υ_{15}=1
266	$37_{23,14} - 36_{23,13}{}^\star$	203008.778	28	556	77.9	138	Blend with U-line
268	$37_{22,15} - 36_{22,14}{}^\star$	203008.823	19	523	82.0	138	Blend with U-line
270	$37_{24,13} - 36_{24,12}{}^\star$	203009.542	40	589	73.5	138	Blend with U-line
272	$37_{21,16} - 36_{21,15}{}^\star$	203009.945	13	492	86.0	138	Blend with U-line
274	$37_{25,12} - 36_{25,11}{}^\star$	203010.874	56	624	69.0	138	Blend with U-line
276	$37_{20,17} - 36_{20,16}{}^\star$	203012.456	9	463	89.8	138	Blend with U-line
278	$37_{26,11} - 36_{26,10}{}^\star$	203012.555	77	661	64.2	138	Blend with U-line
280	$37_{27,10} - 36_{27,9}{}^\star$	203014.377	104	699	59.3	138	Blend with U-line

Table 1. continued.

N^a (1)	Transition^b (2)	Frequency (MHz) (3)	Unc.^{c} (kHz) (4)	$E_l{}^d$ (K) (5)	$S\mu^2$ (D^2) (6)	σ^e (mK) (7)	Comments (8)
282	$37_{28,9}-36_{28,8}{}^{\star}$	203016.140	138	738	54.2	138	Blend with U-line
284	$37_{19,18}-36_{19,17}{}^{\star}$	203016.766	100	435	93.4	138	Blend with U-line
286	$37_{29,8}-36_{29,7}{}^{\star}$	203017.650	181	779	48.9	138	Blend with U-line
288	$37_{18,19}-36_{18,18}{}^{\star}$	203023.193	6	408	96.9	138	Blend with CH_3OCH_3
290	$37_{17,20}-36_{17,19}{}^{\star}$	203032.356	100	383	100.1	138	Blend with CH_3OCH_3 and $CH_3{}^{13}CN$, $v_8=1$
292	$37_{16,21}-36_{16,20}{}^{\star}$	203045.040	100	360	103.2	138	Blend with $CH_3{}^{13}CH_2CN$ and U-line
294	$37_{15,22}-36_{15,21}{}^{\star}$	203062.173	100	337	106.1	138	Blend with $^{13}CH_3CH_2CN$
296	$37_{14,23}-36_{14,22}{}^{\star}$	203085.040	100	316	108.7	138	Blend with $CH_3{}^{13}CH_2CN$
298	$37_{2,35}-36_{2,34}$	203093.256	100	181	126.0	138	Blend with $H^{13}CCCN$, $v_6=1$
299	$37_{13,24}-36_{13,23}{}^{\star}$	203115.417	100	297	111.2	138	Blend with C_2H_3CN, $v_{11}=1/v_{15}=1$
301	$37_{12,25}-36_{12,24}{}^{\star}$	203155.887	100	279	113.6	138	Strong CH_3CN, $v_8=1$
303	$37_{11,26}-36_{11,25}{}^{\star}$	203210.265	100	263	115.7	138	Blend with U-line
305	$39_{0,39}-38_{1,38}$	203277.722	100	187	17.2	161	Blend with C_2H_3CN, $v_{11}=1$
306	$37_{10,27}-36_{10,26}{}^{\star}$	203284.465	100	247	117.6	161	Blend with C_2H_3CN, $v_{11}=1$ and U-line
308	$39_{1,39}-38_{1,38}$	203293.314	100	187	133.5	161	Blend with CH_3CN, $v_8=2$
309	$39_{0,39}-38_{0,38}$	203297.717	100	187	133.5	161	Blend with CH_3CN, $v_8=2$
310	$39_{1,39}-38_{0,38}$	203313.274	100	187	17.2	161	Blend with U-line
311	$37_{9,29}-36_{9,28}{}^{\star}$	203387.942	4	234	119.4	161	Strong C_2H_5CN, CH_3OCH_3, and SO_2
313	$7_{6,2}-6_{5,1}{}^{\star}$	203409.735	13	24	2.7	161	Strong C_2H_5CN, CH_3OCH_3, and $^{13}CH_2CHCN$
315	$38_{2,37}-37_{1,36}$	203421.857	4	185	13.2	161	Strong CH_3OCH_3 and $^{13}CH_2CHCN$
316	$37_{8,30}-36_{8,29}$	203536.955	4	222	121.0	161	Blend with CH_3CN, $v_8=2$ and $^{13}CH_2CHCN$
317	$37_{8,29}-36_{8,28}$	203537.200	4	222	121.0	161	Blend with CH_3CN, $v_8=2$ and $^{13}CH_2CHCN$
318	$37_{7,31}-36_{7,30}$	203760.083	100	211	122.4	364	Blend with U-line
319	$37_{7,30}-36_{7,29}$	203765.767	100	211	122.4	364	Blend with C_3H_7CN and $^{13}CH_2CHCN$
320	$37_{4,34}-36_{4,33}$	203781.525	4	188	125.4	364	Blend with $^{13}CH_2CHCN$ and U-line
321	$18_{4,14}-17_{3,15}$	203899.881	11	47	2.8	364	Blend with C_3H_7CN and U-line
322	$37_{6,32}-36_{6,31}$	204086.275	100	202	123.6	364	Blend with $H^{13}CCCN$, $v_7=2$ and U-line
323	$34_{3,32}-33_{2,31}$	204129.239	11	153	7.0	316	Blend with $^{34}SO_2$
324	$37_{6,31}-36_{6,30}$	204178.927	100	202	123.6	316	Blend with CH_3CH_3CO and U-line?
325	$37_{5,33}-36_{5,32}$	204364.928	4	194	124.6	316	Blend with CH_3CH_3CO
326	$82_{8,75}-81_{9,72}$	204369.553	82	938	5.1	316	Blend with CH_3CH_3CO and SO_2
327	$75_{8,67}-74_{9,66}$	205281.393	47	792	5.8	100	Blend with SO_2
328	$37_{5,32}-36_{5,31}$	205282.240	100	194	124.6	100	Blend with SO_2
329	$13_{5,9}-12_{4,8}$	206264.566	12	32	2.8	280	Strong C_2H_5CN and CH_3OCHO
330	$13_{5,8}-12_{4,9}$	206270.541	12	32	2.8	280	Strong C_2H_5CN and CH_3OCHO
331	$38_{3,36}-37_{3,35}$	206596.942	100	191	129.3	106	Strong C_2H_5CN, $v_{13}=1/v_{21}=1$
332	$19_{4,16}-18_{3,15}$	206607.866	11	52	2.9	106	Strong C_2H_5CN
333	$35_{3,33}-34_{2,32}$	207085.257	11	162	7.5	117	Strong C_2H_5CN
334	$39_{1,38}-38_{2,37}$	207168.207	4	195	13.7	117	Blend with CH_3CH_3CO and U-line
335	$39_{2,38}-38_{2,37}$	207723.987	100	195	133.1	282	Blend with U-line and C_2H_5CN, $v_{13}=1/v_{21}=1$
336	$37_{4,33}-36_{4,32}$	207774.900	4	189	125.5	282	Blend with C_2H_5OH
337	$37_{3,34}-36_{3,33}$	207820.202	100	185	126.0	173	Blend with C_3H_7CN and C_2H_5OH
338	$39_{1,38}-38_{1,37}$	207859.555	4	195	133.1	173	Blend with C_2H_5CN, $v_{13}=1/v_{21}=1$
339	$38_{2,36}-37_{2,35}$	208144.350	100	191	129.4	173	Blend with $CH_2CH^{13}CN$ and C_2H_3CN, $v_{11}=1$
340	$39_{2,38}-38_{1,37}$	208415.332	4	195	13.7	168	Strong C_2H_5CN
341	$40_{0,40}-39_{1,39}$	208431.560	5	197	17.7	168	Strong C_2H_5CN
342	$40_{1,40}-39_{1,39}$	208443.521	100	197	137.0	168	Strong C_2H_5CN
343	$40_{0,40}-39_{0,39}$	208447.014	100	197	137.0	168	Strong C_2H_5CN
344	$40_{1,40}-39_{0,39}$	208459.081	5	197	17.7	168	Strong C_2H_5CN
345	$38_{23,15}-37_{23,14}{}^{\star}$	208493.011	28	565	82.6	168	Strong C_2H_5CN
347	$38_{24,14}-37_{24,13}{}^{\star}$	208493.410	41	599	78.3	168	Strong C_2H_5CN
349	$38_{22,16}-37_{22,15}{}^{\star}$	208493.496	19	533	86.6	168	Strong C_2H_5CN
351	$38_{25,13}-37_{25,12}{}^{\star}$	208494.438	57	634	73.9	168	Strong C_2H_5CN
353	$38_{21,17}-37_{21,16}{}^{\star}$	208495.153	13	502	90.5	168	Strong C_2H_5CN
355	$38_{26,12}-37_{26,11}{}^{\star}$	208495.863	79	671	69.3	168	Strong C_2H_5CN
357	$38_{27,11}-37_{27,10}{}^{\star}$	208497.466	107	709	64.5	168	Strong C_2H_5CN
359	$38_{20,18}-37_{20,17}{}^{\star}$	208498.313	9	473	94.2	168	Strong C_2H_5CN
361	$38_{28,10}-37_{28,9}{}^{\star}$	208499.037	142	748	59.6	168	Strong C_2H_5CN
363	$38_{29,9}-37_{29,8}{}^{\star}$	208500.372	185	789	54.4	168	Strong C_2H_5CN
365	$38_{19,19}-37_{19,18}{}^{\star}$	208503.415	100	445	97.8	168	Strong C_2H_5CN, $v_{13}=1/v_{21}=1$
367	$38_{18,20}-37_{18,19}{}^{\star}$	208510.857	100	418	101.1	168	Blend with C_2H_5OH and C_2H_3CN
369	$38_{17,21}-37_{17,20}{}^{\star}$	208521.187	100	393	104.3	168	Blend with C_2H_5OH
371	$38_{16,22}-37_{16,21}{}^{\star}$	208535.402	100	369	107.2	168	Blend with C_2H_5OH
373	$38_{15,23}-37_{15,22}{}^{\star}$	208554.387	100	347	110.0	168	Blend with C_2H_5CN, $v_{13}=1/v_{21}=1$ and U-line

Table 1. continued.

N^a (1)	Transition^b (2)	Frequency (MHz) (3)	Unc.^{c} (kHz) (4)	$E_l{}^d$ (K) (5)	$S\mu^2$ (D^2) (6)	σ^e (mK) (7)	Comments (8)
375	$38_{14,24} - 37_{14,23}{}^\star$	208579.484	100	326	112.6	168	Blend with CH_3CH_3CO, v_t=1 and U-line
377	$38_{13,25} - 37_{13,24}{}^\star$	208612.841	4	307	115.1	168	Strong C_2H_5CN, v_{13}=1/v_{21}=1
379	$38_{12,26} - 37_{12,25}{}^\star$	208657.029	4	289	117.3	168	Blend with CH_3OCHO and CH_3CH_3CO
381	$38_{11,27} - 37_{11,26}{}^\star$	208716.183	100	272	119.4	160	Blend with CH_3OCHO
383	$38_{10,29} - 37_{10,28}{}^\star$	208796.910	4	257	121.3	160	Blend with $CH_2CH^{13}CN$ and CH_3OCHO
385	$8_{6,3} - 7_{5,2}{}^\star$	208895.157	13	25	2.8	160	Strong CH_3OCHO and C_2H_3CN
387	$38_{8,31} - 37_{8,30}$	209071.357	4	231	124.6	160	Strong C_2H_3CN
388	$38_{8,30} - 37_{8,29}$	209071.723	4	231	124.6	160	Strong C_2H_3CN
389	$38_{4,35} - 37_{4,34}$	209201.665	4	197	128.8	58	Strong H_2CS and C_2H_3CN, v_{15}=1
390	$38_{7,32} - 37_{7,31}$	209313.439	4	221	125.9	58	Strong C_2H_3CN, v_{15}=1
391	$38_{7,31} - 37_{7,30}$	209321.499	4	221	125.9	58	Strong C_2H_3CN, v_{15}=1
392	$19_{4,15} - 18_{3,16}$	209541.953	11	52	2.9	58	Blend with C_2H_3CN
393	$38_{6,33} - 37_{6,32}$	209660.931	4	212	127.1	45	Blend with C_2H_3CN, v_{11}=1, $HC^{13}CCN$, v_7=2, and $HCC^{13}CN$, v_7=2
394	$38_{6,32} - 37_{6,31}$	209783.452	100	212	127.1	45	Blend with C_2H_3CN, v_{11}=1/v_{15}=1
395	$38_{5,34} - 37_{5,33}$	209918.890	4	204	128.1	45	Strong CH_3OCHO
396	$36_{3,34} - 35_{2,33}$	210218.541	10	172	8.0	64	Blend with C_2H_3CN, v_{11}=2
397	$40_{2,38} - 39_{3,37}$	210705.222	6	211	10.0	37	Blend with C_2H_3CN, v_{11}=2 and U-line
398	$38_{5,33} - 37_{5,32}$	211044.215	100	204	128.1	33	Blend with C_2H_5CN
399	$20_{4,17} - 19_{3,16}$	211264.158	11	57	3.0	33	Strong CH_3OCHO
400	$14_{5,10} - 13_{4,9}$	211717.651	12	35	2.9	47	Strong C_2H_3CN
401	$14_{5,9} - 13_{4,10}$	211728.949	12	35	2.9	47	Strong C_2H_3CN
402	$39_{3,37} - 38_{3,36}$	211830.506	100	201	132.7	47	Blend with $NH_2{}^{13}CHO$, v_{12}=1
403	$51_{1,50} - 51_{0,51}$	211833.125	40	333	3.3	47	Blend with $NH_2{}^{13}CHO$, v_{12}=1
404	$40_{1,39} - 39_{2,38}$	212435.627	4	205	14.2	36	Strong NH_2CHO and CH_3OCHO
405	$40_{2,39} - 39_{2,38}$	212881.373	100	205	136.5	99	Blend with $H^{13}CCCN$, v_7=2
406	$40_{1,39} - 39_{1,38}$	212991.436	100	205	136.5	99	Blend with $^{34}SO_2$ and U-line?
407	$39_{2,37} - 38_{2,36}$	213191.655	100	201	132.8	48	Blend with $CH_2(OH)CHO$
408	$38_{3,35} - 37_{3,34}$	213203.256	100	195	129.4	48	Blend with $CH_2(OH)CHO$
409	$40_{2,39} - 39_{1,38}$	213437.154	5	205	14.2	48	Blend with C_2H_5OH and CH_3OCH_3
410	$37_{3,35} - 36_{2,34}$	213536.157	9	181	8.5	48	Blend with C_2H_3CN, v_{11}=2
411	$41_{0,41} - 40_{1,40}$	213584.046	5	207	18.2	48	Blend with $^{13}CH_2CHCN$
412	$41_{1,41} - 40_{1,40}$	213593.386	100	207	140.4	48	Partial blend with $H^{13}CCCN$, v_5=1/v_7=3, uncertain baseline
413	$41_{0,41} - 40_{0,40}$	213596.056	100	207	140.4	48	Partial blend with $H^{13}CCCN$, v_5=1/v_7=3, uncertain baseline
414	$38_{4,34} - 37_{4,33}$	213600.651	100	199	129.0	48	Partial blend with $H^{13}CCCN$, v_5=1/v_7=3, uncertain baseline
415	$41_{1,41} - 40_{0,40}$	213605.377	5	207	18.2	48	Partial blend with $H^{13}CCCN$, v_5=1/v_7=3, uncertain baseline
416	$39_{23,16} - 38_{23,15}{}^\star$	213977.041	29	575	87.2	48	Strong $C_2H_5{}^{13}CN$ and $CH_3{}^{13}CH_2CN$
418	$39_{24,15} - 38_{24,14}{}^\star$	213977.045	42	609	83.1	48	Strong $C_2H_5{}^{13}CN$ and $CH_3{}^{13}CH_2CN$
420	$39_{25,14} - 38_{25,13}{}^\star$	213977.743	59	644	78.8	48	Strong $C_2H_5{}^{13}CN$ and $CH_3{}^{13}CH_2CN$
422	$39_{22,17} - 38_{22,16}{}^\star$	213978.002	20	543	91.2	48	Strong $C_2H_5{}^{13}CN$ and $CH_3{}^{13}CH_2CN$
424	$39_{26,13} - 38_{26,12}{}^\star$	213978.888	81	681	74.3	48	Strong $C_2H_5{}^{13}CN$ and $CH_3{}^{13}CH_2CN$
426	$39_{21,18} - 38_{21,17}{}^\star$	213980.233	13	512	95.0	48	Strong $C_2H_5{}^{13}CN$ and $CH_3{}^{13}CH_2CN$
428	$39_{27,12} - 38_{27,11}{}^\star$	213980.250	109	719	69.7	48	Strong $C_2H_5{}^{13}CN$ and $CH_3{}^{13}CH_2CN$
430	$39_{28,11} - 38_{28,10}{}^\star$	213981.610	145	758	64.8	48	Strong $C_2H_5{}^{13}CN$ and $CH_3{}^{13}CH_2CN$
432	$39_{29,10} - 38_{29,9}{}^\star$	213982.754	190	799	59.8	48	Strong $C_2H_5{}^{13}CN$ and $CH_3{}^{13}CH_2CN$
434	$39_{20,19} - 38_{20,18}{}^\star$	213984.089	9	483	98.6	48	Strong $C_2H_5{}^{13}CN$ and $CH_3{}^{13}CH_2CN$
436	$39_{19,20} - 38_{19,19}{}^\star$	213989.994	7	455	102.0	48	Strong $C_2H_5{}^{13}CN$ and $CH_3{}^{13}CH_2CN$
438	$39_{18,21} - 38_{18,20}{}^\star$	213998.464	6	428	105.3	48	Strong $C_2H_5{}^{13}CN$ and $CH_3{}^{13}CH_2CN$
440	$39_{17,22} - 38_{17,21}{}^\star$	214010.151	5	403	108.3	48	Strong $C_2H_5{}^{13}CN$ and $CH_3{}^{13}CH_2CN$
442	$39_{16,24} - 38_{16,23}{}^\star$	214025.894	5	379	111.3	48	Strong $C_2H_5{}^{13}CN$ and $CH_3{}^{13}CH_2CN$
444	$39_{15,24} - 38_{15,23}{}^\star$	214046.781	100	357	114.0	48	Blend with $^{13}CH_3CN$
446	$39_{14,25} - 38_{14,24}{}^\star$	214074.316	100	336	116.5	75	Strong CH_3OCH_3 and $CH_3{}^{13}CH_2CN$
448	$39_{13,26} - 38_{13,25}{}^\star$	214110.717	4	317	118.9	75	Blend with $^{13}CH_3CN$
450	$39_{12,27} - 38_{12,26}{}^\star$	214158.803	100	299	121.1	75	Blend with $C_2H_5{}^{13}CN$
452	$39_{11,28} - 38_{11,27}{}^\star$	214223.159	100	282	123.1	75	Strong CH_2NH and $^{13}CH_3CN$
454	$39_{10,30} - 38_{10,29}{}^\star$	214310.764	4	267	125.0	75	Strong $^{13}CH_3CN$
456	$66_{4,62} - 66_{3,63}$	214317.063	27	591	13.5	75	Strong $^{13}CH_3CN$
457	$9_{6,4} - 8_{5,3}{}^\star$	214379.791	13	27	2.8	75	Strong $^{13}CH_3CN$
459	$39_{9,31} - 38_{9,30}{}^\star$	214432.762	4	254	126.6	75	Blend with $CH_3{}^{13}CH_2CN$ and C_2H_5OH
461	$22_{3,19} - 21_{2,20}$	214433.988	14	63	1.7	75	Blend with $CH_3{}^{13}CH_2CN$ and C_2H_5OH
462	$65_{5,61} - 65_{4,62}$	214600.532	23	574	13.4	75	Blend with CH_3CH_3CO
463	$39_{4,36} - 38_{4,35}$	214605.781	4	207	132.3	75	Blend with CH_3CH_3CO and $CH_3{}^{13}CH_2CN$
464	$56_{8,49} - 56_{7,50}$	214606.526	11	457	15.7	75	Blend with CH_3CH_3CO and $CH_3{}^{13}CH_2CN$

Table 1. continued.

N^a (1)	Transition^b (2)	Frequency (MHz) (3)	Unc.^{c} (kHz) (4)	$E_l{}^d$ (K) (5)	$S\mu^2$ (D^2) (6)	σ^e (mK) (7)	Comments (8)
465	$39_{8,32} - 38_{8,31}$	214608.530	4	241	128.1	75	Blend with $CH_3{}^{13}CH_2CN$
466	$39_{8,31} - 38_{8,30}$	214609.070	4	241	128.1	75	Blend with $CH_3{}^{13}CH_2CN$
467	$39_{7,33} - 38_{7,32}$	214870.593	100	231	129.5	75	Blend with $^{13}CH_3CN$, $\upsilon_8=1$
468	$39_{7,32} - 38_{7,31}$	214881.820	4	231	129.5	75	Blend with $^{13}CH_2CHCN$
469	$39_{6,34} - 38_{6,33}$	215238.445	100	222	130.6	74	Strong C_2H_5CN, $\upsilon_{13}=1/\upsilon_{21}=1$ and C_2H_5CN, $\upsilon_{20}=1$
470	$20_{4,16} - 19_{3,17}$	215256.547	11	57	2.9	74	Strong C_2H_5CN, $\upsilon_{13}=1/\upsilon_{21}=1$ and C_2H_5CN, $\upsilon_{20}=1$
471	$39_{6,33} - 38_{6,32}$	215399.020	100	222	130.6	74	Strong C_2H_5CN
472	$39_{5,35} - 38_{5,34}$	215467.027	4	214	131.6	74	Strong C_2H_5CN, $\upsilon_{13}=1/\upsilon_{21}=1$
473	$21_{4,18} - 20_{3,17}$	215732.383	12	62	3.0	74	Strong C_2H_5CN, $\upsilon_{13}=1/\upsilon_{21}=1$
474	$39_{5,34} - 38_{5,33}$	216832.944	100	214	131.6	50	Strong CH_3OCHO
475	$61_{3,58} - 61_{3,59}$	216833.377	28	498	1.2	50	Strong CH_3OCHO
476	$41_{2,39} - 40_{3,38}$	216942.926	5	222	10.6	50	Strong CH_3OH
477	$38_{3,36} - 37_{2,35}$	217039.712	8	191	9.0	50	Blend with $^{13}CH_3OH$ and ^{13}CN
478	$40_{3,38} - 39_{3,37}$	217052.822	100	211	136.1	50	Blend with $^{13}CH_3OH$, ^{13}CN, and U-line
479	$15_{5,11} - 14_{4,10}$	217159.548	12	39	3.0	50	Blend with CH_3OCH_3
480	$15_{5,10} - 14_{4,11}$	217179.901	12	39	3.0	50	Blend with CH_3OCH_3 and U-line
481	$41_{1,40} - 40_{2,39}$	217679.824	4	215	14.7	50	Blend with U-line
482	$39_{4,35} - 38_{4,34}$	219402.429	4	209	132.5	92	Strong C_2H_3CN
483	$40_{24,16} - 39_{24,15}{}^\star$	219460.441	43	619	87.8	92	Strong C_2H_5CN
485	$40_{25,15} - 39_{25,14}{}^\star$	219460.780	60	655	83.6	92	Strong C_2H_5CN
487	$40_{23,17} - 39_{23,16}{}^\star$	219460.864	30	586	91.8	92	Strong C_2H_5CN
489	$40_{26,14} - 39_{26,13}{}^\star$	219461.621	83	691	79.2	92	Strong C_2H_5CN
491	$40_{22,18} - 39_{22,17}{}^\star$	219462.336	20	553	95.7	92	Strong C_2H_5CN
493	$40_{27,13} - 39_{27,12}{}^\star$	219462.721	112	729	74.7	92	Strong C_2H_5CN
495	$40_{28,12} - 39_{28,11}{}^\star$	219463.851	149	768	70.0	92	Strong C_2H_5CN
497	$40_{21,19} - 39_{21,18}$	219465.183	14	522	99.4	92	Strong C_2H_5CN
498	$40_{21,20} - 39_{21,19}$	219465.523	100	522	99.4	92	Strong C_2H_5CN
499	$40_{20,20} - 39_{20,19}$	219469.782	10	493	102.9	92	Strong NH_2CN
500	$40_{20,21} - 39_{20,20}$	219469.912	100	493	102.9	92	Strong NH_2CN
501	$40_{19,21} - 39_{19,20}{}^\star$	219476.588	7	465	106.3	92	Strong NH_2CN
503	$40_{18,22} - 39_{18,21}$	219486.155	6	438	109.4	92	Strong HC_3N, $\upsilon_6=\upsilon_7=1$
504	$40_{18,23} - 39_{18,22}$	219486.310	100	438	109.4	92	Strong HC_3N, $\upsilon_6=\upsilon_7=1$
505	$40_{17,23} - 39_{17,22}$	219499.182	5	413	112.4	92	Strong C_2H_5CN
506	$40_{17,24} - 39_{17,23}$	219499.329	100	413	112.4	92	Strong C_2H_5CN
507	$40_{16,25} - 39_{16,24}{}^\star$	219516.573	5	390	115.3	92	Strong HC_3N, $\upsilon_6=\upsilon_7=1$
509	$40_{15,25} - 39_{15,24}{}^\star$	219539.521	5	367	117.9	92	Strong HNCO and HNCO, $\upsilon_5=1$
511	$40_{14,26} - 39_{14,25}{}^\star$	219569.648	5	346	120.4	92	Strong $C^{18}O$
513	$67_{4,63} - 67_{3,64}$	219571.157	30	609	13.4	92	Strong $C^{18}O$
514	$40_{13,27} - 39_{13,26}{}^\star$	219609.218	5	327	122.7	92	Strong C_2H_3CN, $\upsilon_{15}=1$ and $CH_2CH^{13}CN$
516	$40_{12,28} - 39_{12,27}$	219661.381	100	309	124.8	92	Strong HNCO and HC_3N, $\upsilon_7=2$
517	$40_{12,29} - 39_{12,28}$	219661.485	5	309	124.8	92	Strong HNCO and HC_3N, $\upsilon_7=2$
518	$40_{11,30} - 39_{11,29}{}^\star$	219731.290	4	293	126.8	92	Strong HNCO
520	$40_{7,34} - 39_{7,33}$	220431.537	100	241	133.0	98	Strong $CH_3{}^{13}CN$
521	$40_{7,33} - 39_{7,32}$	220446.964	100	241	133.0	98	Blend with U-line, uncertain baseline
522	$41_{7,35} - 40_{7,34}$	225996.244	100	252	136.5	278	Blend with CH_3CH_3CO, $\upsilon_t=1$, uncertain baseline
523	$41_{7,34} - 40_{7,33}$	226017.388	100	252	136.5	278	Blend with U-line?, uncertain baseline
524	$63_{3,60} - 63_{2,61}$	226393.597	33	530	10.0	278	Blend with CN in absorption, C_2H_3CN, and C_2H_5OH
525	$41_{6,36} - 40_{6,35}$	226400.096	100	243	137.6	278	Blend with CN in absorption and C_2H_5OH
526	$41_{5,37} - 40_{5,36}$	226540.631	4	235	138.5	278	Blend with CH_2NH
527	$41_{6,35} - 40_{6,34}$	226668.561	4	243	137.6	96	Strong CN absorption
528	$22_{4,18} - 21_{3,19}$	226986.056	11	67	3.0	96	Strong CN absorption
529	$42_{3,40} - 41_{3,39}$	227467.207	100	233	143.0	85	Blend with $CH_2(OH)CHO$, $CH_2CH^{13}CN$, and C_3H_7CN
530	$24_{4,21} - 23_{3,20}$	227801.331	12	80	3.2	85	Strong CH_3OH
531	$42_{9,34} - 41_{9,33}{}^\star$	231015.633	5	285	137.4	183	Blend with CH_3OCHO, $H_2{}^{13}CS$, and U-line
533	$42_{8,35} - 41_{8,34}$	231237.570	5	273	138.8	183	Strong $^{13}CH_2CHCN$ and C_2H_3CN, $\upsilon_{15}=1$
534	$42_{8,34} - 41_{8,33}$	231239.195	5	273	138.8	183	Strong $^{13}CH_2CHCN$ and C_2H_3CN, $\upsilon_{15}=1$
535	$25_{4,22} - 24_{3,21}$	231328.525	13	86	3.3	40	Blend with CH_3CHO and $^{13}CH_2CHCN$
536	$42_{7,36} - 41_{7,35}$	231564.827	4	262	140.1	40	Blend with C_2H_5OH
537	$42_{7,35} - 41_{7,34}$	231593.484	100	263	140.1	40	Blend with $CH_3{}^{13}CH_2CN$
538	$43_{3,41} - 42_{3,40}$	232661.017	5	243	146.4	19	Blend with C_2H_5CN, $\upsilon_{13}=1/\upsilon_{21}=1$
539	$42_{3,40} - 41_{2,39}$	232789.078	6	232	11.2	19	Strong CH_3OH, C_2H_5CN, and C_2H_3CN, $\upsilon_{11}=1$
540	$43_{26,17} - 42_{26,16}{}^\star$	235907.995	89	723	93.6	131	Blend with $HCC^{13}CN$, $\upsilon_6=1$
542	$43_{27,16} - 42_{27,15}{}^\star$	235908.172	120	761	89.3	131	Blend with $HCC^{13}CN$, $\upsilon_6=1$

Table 1. continued.

N^a	Transition^b	Frequency	Unc.^{c}	$E_l{}^d$	$S\mu^2$	σ^e	Comments
		(MHz)	(kHz)	(K)	(D^2)	(mK)	
(1)	(2)	(3)	(4)	(5)	(6)	(7)	(8)
544	$43_{25,18} - 42_{25,17}{}^\star$	235908.220	65	687	97.6	131	Blend with HCC^{13}CN, v_6=1
546	$43_{24,19} - 42_{24,18}{}^\star$	235909.130	46	652	101.6	131	Blend with HCC^{13}CN, v_6=1
548	$43_{23,20} - 42_{23,19}{}^\star$	235911.029	32	618	105.3	131	Blend with HCC^{13}CN, v_6=1
550	$43_{22,22} - 42_{22,21}{}^\star$	235914.238	100	586	108.9	131	Strong CH_3OCHO
552	$43_{21,22} - 42_{21,21}{}^\star$	235919.208	15	555	112.3	131	Strong CH_3OCHO
554	$43_{20,23} - 42_{20,22}$	235926.335	10	525	115.6	131	Strong CH_3OCHO, C_2H_3CN, v_{15}=1, and $^{13}CH_3OH$
555	$43_{20,24} - 42_{20,23}$	235926.477	100	525	115.6	131	Strong CH_3OCHO, C_2H_3CN, v_{15}=1, and $^{13}CH_3OH$
556	$43_{19,24} - 42_{19,23}{}^\star$	235936.190	8	497	118.7	131	Strong CH_3OCHO, C_2H_3CN, v_{15}=1, and $^{13}CH_3OH$
558	$43_{18,25} - 42_{18,24}{}^\star$	235949.452	6	471	121.6	131	Strong C_2H_3CN, v_{15}=1, $^{13}CH_3OH$, and $C_2H_5{}^{13}CN$
560	$43_{17,26} - 42_{17,25}{}^\star$	235966.980	6	446	124.4	131	Strong $^{13}CH_3OH$ and SiS
562	$43_{16,27} - 42_{16,26}{}^\star$	235989.879	100	422	127.1	131	Strong $^{13}CH_3OH$
564	$43_{13,31} - 42_{13,30}{}^\star$	236108.561	100	359	134.0	37	Blend with C_2H_5CN, v_{13}=1/v_{21}=1 and NH_2CH_2CN
566	$43_{12,31} - 42_{12,30}{}^\star$	236174.724	5	342	136.0	37	Blend with $^{13}CH_3CH_2CN$ and $CH_2{}^{13}CHCN$
568	$43_{11,32} - 42_{11,31}{}^\star$	236262.562	100	325	137.9	37	Blend with C_2H_5CN, v_{13}=1/v_{21}=1 and NH_2CH_2CN
570	$13_{6,8} - 12_{5,7}{}^\star$	236300.957	13	39	3.1	37	Strong $CH_2{}^{13}CHCN$ and C_2H_5OH
572	$65_{4,62} - 65_{3,63}$	236306.402	38	563	10.0	37	Strong $^{13}CH_3CH_2CN$
573	$43_{10,33} - 42_{10,32}{}^\star$	236381.716	100	310	139.5	37	Blend with $CH_2{}^{13}CHCN$
575	$43_{9,35} - 42_{9,34}$	236547.689	5	296	141.0	37	Blend with $^{13}CH_3CH_2CN$
576	$43_{9,34} - 42_{9,33}$	236547.789	5	296	141.0	37	Blend with $^{13}CH_3CH_2CN$
577	$20_{5,16} - 19_{4,15}$	244080.041	12	62	3.4	46	Blend with CH_3CH_3CO, v_t=1
578	$20_{5,15} - 19_{4,16}$	244307.468	12	62	3.4	46	Blend with CH_3OH and $C_2H_5{}^{13}CN$
579	$9_{7,2} - 8_{6,3}{}^\star$	244368.037	13	35	3.2	46	Blend with C_2H_5CN
581	$47_{0,47} - 46_{1,46}$	244480.036	7	272	21.2	91	Blend with $^{34}SO_2$
582	$47_{1,47} - 46_{1,46}$	244482.013	7	272	161.0	91	Blend with $^{34}SO_2$
583	$47_{0,47} - 46_{0,46}$	244482.600	7	272	161.0	91	Blend with $^{34}SO_2$
584	$47_{1,47} - 46_{0,46}$	244484.577	7	272	21.2	91	Blend with $^{34}SO_2$
585	$44_{3,41} - 43_{3,40}$	244500.437	5	260	149.8	91	Blend with CH_3OCH_3
586	$30_{4,27} - 29_{3,26}$	245163.234	16	123	3.8	72	Strong HCC^{13}CN, v_7=1
587	$25_{4,21} - 24_{3,22}$	245723.730	11	86	3.0	53	Blend with $CH_2{}^{13}CHCN$
588	$45_{17,28} - 44_{17,27}{}^\star$	246946.103	100	469	132.3	68	Strong C_2H_3CN
590	$45_{16,29} - 44_{16,28}{}^\star$	246973.216	6	445	134.8	68	Blend with C_2H_5CN and CH_3COOH
592	$45_{15,30} - 44_{15,29}{}^\star$	247008.106	100	423	137.2	68	Strong C_2H_3CN
594	$45_{14,31} - 44_{14,30}{}^\star$	247053.206	100	402	139.4	68	Strong CH_3OCHO
596	$45_{13,33} - 44_{13,32}{}^\star$	247111.643	100	382	141.5	68	Strong HC_3N, v_7=2 and CH_3OCHO
598	$45_{12,34} - 44_{12,33}{}^\star$	247188.187	5	364	143.4	68	Blend with C_2H_3CN, CH_3CH_3CO, v_t=1 and CH_3COOH
600	$15_{6,10} - 14_{5,9}$	247242.428	12	46	3.3	68	Strong C_2H_3CN, v_{15}=1 and $CH_3{}^{13}CH_2CN$
601	$15_{6,9} - 14_{5,10}$	247242.754	12	46	3.3	68	Strong C_2H_3CN, v_{15}=1 and $CH_3{}^{13}CH_2CN$
602	$31_{4,28} - 30_{3,27}$	247248.744	16	131	3.9	68	Strong C_2H_3CN, v_{15}=1 and $CH_3{}^{13}CH_2CN$
603	$45_{11,35} - 44_{11,34}{}^\star$	247289.755	5	348	145.1	68	Blend with C_2H_3CN, v_{15}=1
605	$56_{9,48} - 56_{8,49}$	247291.902	12	468	15.2	68	Blend with C_2H_3CN, v_{15}=1
606	$45_{10,36} - 44_{10,35}{}^\star$	247427.317	5	333	146.7	68	Blend with H^{13}CCCN, v_6=1 and t-HCOOH
608	$46_{4,43} - 45_{4,42}$	251970.749	5	285	156.4	42	Blend with CH_3OCH_3 and CH_3OH
609	$45_{5,40} - 44_{5,39}$	252031.184	100	281	152.5	42	Blend with C_2H_5CN, v_{13}=1/v_{21}=1
610	$46_{21,25} - 45_{21,24}$	252371.919	16	590	124.9	42	Strong $^{13}CH_3OH$
611	$46_{21,26} - 45_{21,25}$	252372.057	100	590	124.9	42	Strong $^{13}CH_3OH$
612	$46_{20,26} - 45_{20,25}$	252382.043	11	560	128.0	42	Blend with $^{13}CH_3CH_2CN$
613	$46_{20,27} - 45_{20,26}$	252382.165	100	560	128.0	42	Blend with $^{13}CH_3CH_2CN$
614	$46_{19,27} - 45_{19,26}$	252395.494	8	532	130.9	42	Strong NH_2CHO and C_2H_3CN, v_{11}=1
615	$46_{19,28} - 45_{19,27}$	252395.596	100	532	130.9	42	Strong NH_2CHO and C_2H_3CN, v_{11}=1
616	$26_{4,22} - 25_{3,23}$	252401.668	100	92	3.0	42	Strong NH_2CHO and C_2H_3CN, v_{11}=1
617	$46_{18,28} - 45_{18,27}{}^\star$	252413.093	7	506	133.6	42	Blend with C_2H_3CN, v_{11}=1 and U-line
619	$46_{17,30} - 45_{17,29}{}^\star$	252435.886	6	480	136.2	42	Strong C_2H_5CN, v_{13}=1/v_{21}=1
621	$46_{16,31} - 45_{16,30}$	252465.229	6	457	138.7	42	Strong U-line
622	$46_{16,30} - 45_{16,29}$	252465.379	100	457	138.7	42	Strong U-line
623	$93_{7,86} - 93_{6,87}$	252466.454	90	1191	24.1	42	Strong U-line
624	$34_{9,25} - 34_{8,26}$	253951.681	13	203	8.3	32	Strong C_2H_5CN and SO_2
625	$34_{9,26} - 34_{8,27}$	253951.859	13	203	8.3	32	Strong C_2H_5CN and SO_2
626	$46_{7,39} - 45_{7,38}$	253965.040	5	309	154.1	32	Strong NS
627	$48_{1,47} - 47_{2,46}$	254009.911	6	293	18.1	32	Strong CH_3OH in absorption
628	$35_{4,32} - 34_{3,31}$	254021.313	17	166	4.6	32	Strong CH_3OH in absorption
629	$46_{5,42} - 45_{5,41}$	254033.953	5	292	155.8	32	Blend with HC^{13}CCN, v_6=1 and C_2H_5OH
630	$33_{9,24} - 33_{8,25}$	254066.133	13	194	8.0	32	Blend with C_2H_5CN
631	$33_{9,25} - 33_{8,26}$	254066.244	13	194	8.0	32	Blend with C_2H_5CN

Table 1. continued.

N^a (1)	Transition^b (2)	Frequency (MHz) (3)	Unc.^{c} (kHz) (4)	$E_l{}^d$ (K) (5)	$S\mu^2$ (D^2) (6)	σ^e (mK) (7)	Comments (8)
632	$48_{2,47} - 47_{2,46}$	254081.225	6	293	163.9	32	Strong CH_3CH_3CO and C_2H_5CN
633	$86_{6,80} - 86_{5,81}$	254082.060	64	1013	20.4	32	Strong CH_3CH_3CO and C_2H_5CN
634	$48_{1,47} - 47_{1,46}$	254100.087	6	293	164.0	32	Blend with SiS
635	$32_{9,23} - 32_{8,24}{}^\star$	254170.380	13	185	7.7	32	Blend with $^{13}CH_3CH_2CN$
637	$48_{2,47} - 47_{1,46}$	254171.401	6	293	18.1	32	Blend with $^{13}CH_3CH_2CN$
638	$31_{9,22} - 31_{8,23}{}^\star$	254265.069	13	177	7.4	32	Strong $HCC^{13}CN$, υ_7=1 and SO_2
640	$46_{6,41} - 45_{6,40}$	254311.469	5	300	155.1	32	Strong C_2H_5CN and $^{13}CH_3CH_2CN$
641	$30_{9,21} - 30_{8,22}{}^\star$	254350.818	13	169	7.2	32	Strong $NH_2{}^{13}CHO$
643	$89_{8,82} - 89_{7,83}$	254352.623	46	1095	23.7	32	Strong $NH_2{}^{13}CHO$
644	$29_{9,20} - 29_{8,21}{}^\star$	254428.220	13	161	6.9	32	Strong CH_3OH
646	$11_{7,5} - 10_{6,4}{}^\star$	255337.696	13	40	3.4	217	Strong HC_3N, υ_7=1
648	$47_{3,45} - 46_{2,44}$	255440.594	6	289	13.8	217	Strong $CH_2CH^{13}CN$
649	$36_{4,33} - 35_{3,32}$	255457.676	18	175	4.9	217	Strong C_2H_5CN, υ_{13}=1/υ_{21}=1 and $CH_2{}^{13}CHCN$
650	$47_{18,29} - 46_{18,28}{}^\star$	257901.052	7	518	137.6	1127	Blend with CH_3CN, υ_8=1
652	$47_{17,30} - 46_{17,29}{}^\star$	257925.778	6	493	140.1	1127	Noisy, blend with C_2H_3CN, υ_{11}=1/υ_{15}=1 and CH_3OCHO
654	$46_{5,41} - 45_{5,40}$	257933.505	5	293	156.0	1127	Noisy, blend with C_2H_3CN, υ_{11}=1/υ_{15}=1 and CH_3OCHO
655	$47_{16,31} - 46_{16,30}{}^\star$	257957.480	6	469	142.5	1127	Blend with $C_2H_5{}^{13}CN$
657	$47_{15,32} - 46_{15,31}{}^\star$	257998.085	6	447	144.8	1127	Strong CH_3CN, υ_8=1 and CH_3OCHO
659	$47_{14,33} - 46_{14,32}{}^\star$	258050.228	6	426	146.9	1127	Strong CH_3CN, υ_8=1
661	$47_{13,34} - 46_{13,33}{}^\star$	258117.607	6	406	148.9	1127	Strong CH_3OCHO
663	$17_{6,12} - 16_{5,11}$	258162.597	12	54	3.5	1127	Strong $^{13}CH_3OH$ and $HC^{15}N$
664	$17_{6,11} - 16_{5,12}$	258163.845	12	54	3.5	1127	Strong $^{13}CH_3OH$ and $HC^{15}N$
665	$47_{12,35} - 46_{12,34}{}^\star$	258205.577	6	388	150.7	1127	Strong CH_3CN, υ_8=1
667	$38_{4,35} - 37_{3,34}$	258232.157	17	195	5.4	1127	Strong CH_3CN, υ_8=1
668	$47_{11,37} - 46_{11,36}{}^\star$	258322.177	6	372	152.4	1127	Strong CH_3CN, υ_8=1
670	$48_{2,46} - 47_{2,45}$	258838.876	6	302	163.6	1609	Noisy
671	$46_{4,42} - 45_{4,41}$	258951.138	5	288	156.6	1609	Strong CH_3CN, υ_8=2
672	$70_{4,67} - 70_{3,68}$	259007.596	58	650	10.0	1609	Blend with $H^{13}CN$ in absorption and CH_3CN, υ_8=2
673	$47_{8,40} - 46_{8,39}$	259016.319	6	331	156.5	1609	Blend with $H^{13}CN$ in absorption and CH_3CN, υ_8=2
674	$96_{11,85} - 96_{10,86}$	259022.243	75	1306	29.4	1609	Blend with $H^{13}CN$ in absorption, CH_3CN, υ_8=2, and $CH_3{}^{13}CH_2CN$
675	$47_{8,39} - 46_{8,38}$	259024.824	6	331	156.5	1609	Blend with $H^{13}CN$ in absorption, CH_3CN, υ_8=2, and $CH_3{}^{13}CH_2CN$
676	$94_{7,87} - 94_{6,88}$	259169.651	93	1215	24.0	1609	Noisy, blend with CH_3CH_3CO, υ_t=1 and C_2H_5CN, υ_{13}=1/υ_{21}=1
677	$49_{1,48} - 48_{2,47}$	259170.075	6	306	18.6	1609	Noisy, blend with CH_3CH_3CO, υ_t=1 and C_2H_5CN, υ_{13}=1/υ_{21}=1
678	$49_{2,48} - 48_{2,47}$	259226.397	6	306	167.4	1609	Strong $C_2H_5{}^{13}CN$, $^{13}CH_2CHCN$, and C_2H_5CN
679	$49_{1,48} - 48_{1,47}$	259241.389	6	306	167.4	1609	Strong $C_2H_5{}^{13}CN$, $^{13}CH_2CHCN$, and C_2H_5CN
680	$75_{4,71} - 75_{3,72}$	259244.206	58	756	13.4	1609	Strong $C_2H_5{}^{13}CN$, $^{13}CH_2CHCN$, and C_2H_5CN
681	$48_{3,46} - 47_{2,45}$	260229.609	6	302	14.3	413	Strong C_2H_5CN
682	$23_{5,18} - 22_{4,19}$	260510.203	11	78	3.6	413	Strong C_2H_5CN, υ_{13}=1/υ_{21}=1
683	$48_{20,28} - 47_{20,27}{}^\star$	263352.009	12	585	136.1	74	Blend with $HCC^{13}CN$, υ_7=1 and $^{13}CH_3CH_2CN$
685	$48_{19,29} - 47_{19,28}{}^\star$	263368.180	9	557	138.9	74	Blend with NH_2CH_2CN
687	$48_{18,30} - 47_{18,29}{}^\star$	263389.051	7	530	141.5	74	Strong HNCO, υ_4=1 and CH_3OCH_3
689	$48_{17,31} - 47_{17,30}{}^\star$	263415.803	7	505	144.0	74	Strong CH_3OCH_3
691	$48_{16,32} - 47_{16,31}{}^\star$	263449.974	6	481	146.4	74	Strong HNCO
693	$48_{15,33} - 47_{15,32}{}^\star$	263493.569	100	459	148.6	74	Blend with $C_2H_5{}^{13}CN$ and CH_3OCH_3
695	$48_{14,34} - 47_{14,33}{}^\star$	263549.541	100	438	150.6	74	Strong NH_2CHO, SO_2, and NH_2CHO, υ_{12}=1
697	$18_{6,13} - 17_{5,12}$	263612.153	12	58	3.6	74	Blend with NH_2CH_2CN and CH_3OCH_3
698	$18_{6,12} - 17_{5,13}$	263614.442	12	58	3.6	74	Blend with NH_2CH_2CN and CH_3OCH_3
699	$48_{13,35} - 47_{13,34}$	263621.701	6	419	152.5	74	Blend with CH_3OCH_3
700	$48_{13,36} - 47_{13,35}$	263621.895	100	419	152.5	74	Blend with CH_3OCH_3
701	$49_{3,47} - 48_{3,46}$	263687.072	100	314	167.0	108	Strong HNCO and $HN^{13}CO$
702	$48_{12,36} - 47_{12,35}{}^\star$	263715.805	6	401	154.4	108	Blend with $HCC^{13}CN$, υ_7=1 and HNCO, υ_6=1
704	$47_{5,42} - 46_{5,41}$	263828.012	6	305	159.5	108	Blend with HC_3N, υ_5=1/υ_7=3 and C_2H_5CN
705	$48_{11,38} - 47_{11,37}{}^\star$	263840.460	6	384	156.0	108	Blend with U-line and NH_2CHO
707	$49_{2,47} - 48_{2,46}$	263943.595	6	314	167.0	108	Blend with U-line and NH_2CHO
708	$76_{4,72} - 76_{3,73}$	264005.376	63	775	13.4	108	Strong $CH_3{}^{13}CH_2CN$ and C_2H_5CN
709	$48_{10,39} - 47_{10,38}{}^\star$	264009.192	6	369	157.5	108	Strong $CH_3{}^{13}CH_2CN$ and C_2H_5CN
711	$48_{6,42} - 47_{6,41}$	266696.771	100	324	162.1	91	Strong $CH_3{}^{13}CH_2CN$, C_2H_5CN, and CH_3OH

Notes: ^{a} Numbering of the observed transitions associated with a modeled line stronger than 20 mK. ^{b} Transitions marked with a * are double with a frequency difference less than 0.1 MHz. The quantum numbers of the second one are not shown. ^{c} Frequency uncertainty. ^{d} Lower energy level in temperature units (E_l/k_B). ^{e} Calculated rms noise level in T_{mb} scale.

Table 2. Transitions of the *gauche*-conformer of ethyl formate observed with the IRAM 30 m telescope toward Sgr B2(N). The horizontal lines mark discontinuities in the observed frequency coverage. Only the transitions associated with a modeled line stronger than 20 mK are listed.

N[a] (1)	Transition[b] (2)	Frequency (MHz) (3)	Unc.[c] (kHz) (4)	E_l[d] (K) (5)	$S\mu^2$ (D^2) (6)	σ[e] (mK) (7)	Comments (8)
1	$14_{7,8} - 13_{7,7}$	99252.267	9	140	43.9	19	Blend with a$(CH_2OH)_2$ and C_2H_5CN
2	$14_{7,7} - 13_{7,6}$	99252.460	9	140	43.9	19	Blend with a$(CH_2OH)_2$ and C_2H_5CN
3	$16_{1,16} - 15_{1,15}$	104834.473	10	132	66.3	25	Blend with C_2H_5CN, $\upsilon_{13}=1/\upsilon_{21}=1$ and U-line
4	$16_{0,16} - 15_{0,15}$	104848.839	10	132	66.3	25	Blend with C_2H_3CN, $\upsilon_{11}=1/\upsilon_{15}=1$
5	$15_{9,7} - 14_{9,6}{}^{\star}$	106216.238	9	154	40.2	25	Blend with C_2H_3CN, $\upsilon_{11}=1/\upsilon_{15}=1$
7	$15_{8,8} - 14_{8,7}{}^{\star}$	106286.532	9	149	44.9	25	Blend with U-line
9	$15_{7,9} - 14_{7,8}$	106400.093	9	144	49.1	25	Blend with U-line
10	$15_{7,8} - 14_{7,7}$	106400.593	9	144	49.1	25	Blend with U-line
11	$15_{2,13} - 14_{2,12}$	107933.484	100	131	60.9	46	Blend with C_2H_5CN, $\upsilon_{13}=1/\upsilon_{21}=1$, C_3H_7CN, and U-line
12	$15_{4,11} - 14_{4,10}$	108497.732	10	134	58.3	20	Blend with C_2H_5CN and U-line
13	$16_{2,15} - 15_{2,14}$	108858.373	9	135	65.2	20	Blend with ^{13}CN in absorption, CH_3CH_3CO, $\upsilon_t=1$, and U-line
14	$16_{1,15} - 15_{1,14}$	109206.256	100	135	65.3	29	Blend with C_2H_5CN, $\upsilon_{13}=1/\upsilon_{21}=1$ and U-line
15	$15_{3,12} - 14_{3,11}$	110117.142	10	133	60.4	24	Blend with U-lines
16	$17_{1,17} - 16_{1,16}$	111255.183	100	137	70.5	35	Blend with CH_3OH
17	$17_{0,17} - 16_{0,16}$	111263.830	100	137	70.5	35	Blend with C_2H_3CN, $\upsilon_{11}=1/\upsilon_{15}=1$ and $^{13}CH_3CH_2CN$
18	$16_{3,14} - 15_{3,13}$	112186.512	8	137	64.2	42	Blend with $CH_2{}^{13}CHCN$
19	$16_{10,6} - 15_{10,5}{}^{\star}$	113276.855	9	165	40.8	28	Blend with CH_3OCH_3
21	$16_{9,8} - 15_{9,7}{}^{\star}$	113332.031	9	159	45.8	28	Blend with C_2H_5CN, $\upsilon_{13}=1/\upsilon_{21}=1$ and $CH_2{}^{13}CHCN$
23	$16_{8,9} - 15_{8,8}{}^{\star}$	113419.845	9	154	50.2	28	Blend with C_2H_3CN, $\upsilon_{11}=1$
25	$46_{10,37} - 46_{9,38}$	113560.008	23	488	62.8	28	Strong CN in absorption
26	$16_{7,10} - 15_{7,9}$	113560.122	9	150	54.1	28	Strong CN in absorption
27	$16_{7,9} - 15_{7,8}$	113561.324	9	150	54.1	28	Strong CN in absorption
28	$16_{6,11} - 15_{6,10}$	113783.618	9	146	57.5	34	Blend with U-line
29	$16_{6,10} - 15_{6,9}$	113810.530	9	146	57.5	34	Blend with C_2H_3CN, $\upsilon_{15}=1$
30	$16_{4,13} - 15_{4,12}$	113866.411	9	139	62.7	34	Blend with a-C_2H_5OCHO and U-line
31	$16_{5,12} - 15_{5,11}$	114054.354	9	142	60.4	33	Blend with C_2H_3CN, $\upsilon_{15}=1$
32	$16_{2,14} - 15_{2,13}$	114356.265	100	137	64.9	33	Blend with CH_3CH_3CO and U-line
33	$16_{5,11} - 15_{5,10}$	114420.852	100	142	60.4	37	Blend with C_2H_3CN, $\upsilon_{11}=1/\upsilon_{15}=1$
34	$42_{6,36} - 42_{5,37}$	115318.413	41	411	44.6	60	Strong CO
35	$17_{2,16} - 16_{2,15}$	115319.089	9	140	69.4	60	Strong CO
36	$17_{1,16} - 16_{1,15}$	115551.954	100	140	69.4	60	Blend with C_2H_3CN
37	$22_{1,21} - 21_{2,20}$	147415.492	100	171	37.3	31	Blend with CH_3CH_3CO, $\upsilon_t=1$ and $CH_3{}^{13}CN$, $\upsilon_8=1$
38	$9_{7,3} - 8_{6,2}{}^{\star}$	147431.313	18	117	14.5	31	Blend with C_2H_5OH and CH_3CN, $\upsilon_8=1$
40	$9_{7,3} - 8_{6,3}{}^{\star}$	147431.321	18	117	0.9	31	Blend with C_2H_5OH and CH_3CN, $\upsilon_8=1$
42	$22_{2,21} - 21_{2,20}$	147454.440	100	171	90.3	31	Blend with a$(CH_2OH)_2$, $CH_3{}^{13}CN$, $\upsilon_8=1$, and CH_3OCH_3
43	$22_{1,21} - 21_{1,20}$	147479.064	100	171	90.3	31	Blend with CH_3CN, $\upsilon_8=1$ and $^{13}CH_3CH_2CN$
44	$22_{2,21} - 21_{1,20}$	147517.966	100	171	37.3	31	Blend with $CH_3{}^{13}CN$, $\upsilon_8=1$ and CH_3CN, $\upsilon_8=1$
45	$10_{7,4} - 9_{6,3}{}^{\star}$	154495.310	18	120	14.6	112	Blend with C_2H_5CN
47	$10_{7,4} - 9_{6,4}{}^{\star}$	154495.348	18	120	0.9	112	Blend with C_2H_5CN
49	$23_{9,15} - 22_{9,14}$	163354.580	7	205	81.5	38	Group possibly detected, partial blend with c-C_2H_4O, uncertain baseline
50	$23_{9,14} - 22_{9,13}$	163355.083	7	205	81.5	38	Group possibly detected, partial blend with c-C_2H_4O, uncertain baseline
51	$23_{3,20} - 22_{3,19}$	163550.748	100	184	93.0	38	Blend with CH_3OCHO, $\upsilon_t=1$ and $CH_2CH^{13}CN$
52	$23_{8,16} - 22_{8,15}$	163648.730	7	199	84.6	38	Blend with C_3H_7CN and $NH_2{}^{13}CHO$
53	$23_{8,15} - 22_{8,14}$	163658.516	7	199	84.6	38	Blend with C_3H_7CN, uncertain baseline
54	$24_{5,19} - 23_{5,18}$	176014.876	9	196	96.4	365	Blend with CH_3OCHO, $CH_2CH^{13}CN$, and HNCO, $\upsilon_5=1$
55	$19_{6,14} - 18_{5,13}$	202061.374	15	160	13.8	138	Blend with $CH_3{}^{13}CN$
56	$15_{8,8} - 14_{7,7}{}^{\star}$	202643.074	17	144	17.5	108	Blend with CH_3CN, $\upsilon_8=1$ and $CH_3{}^{13}CN$, $\upsilon_8=1$
58	$15_{8,8} - 14_{7,8}{}^{\star}$	202643.365	17	144	1.1	108	Blend with CH_3CN, $\upsilon_8=1$ and $CH_3{}^{13}CN$, $\upsilon_8=1$
60	$30_{2,28} - 29_{3,27}$	202805.197	7	241	47.3	138	Blend with C_2H_5CN and $CH_3{}^{13}CN$, $\upsilon_8=1$
61	$30_{3,28} - 29_{3,27}$	202824.924	100	241	122.7	138	Strong CH_3CN, $\upsilon_8=1$
62	$30_{2,28} - 29_{2,27}$	202837.051	100	241	122.6	138	Strong CH_3CN, $\upsilon_8=1$
63	$45_{9,37} - 44_{10,34}$	202856.742	41	463	10.5	138	Blend with CH_3CN, $\upsilon_8=1$
64	$30_{3,28} - 29_{2,27}$	202856.967	7	241	47.3	138	Blend with CH_3CN, $\upsilon_8=1$
65	$65_{8,58} - 65_{7,59}$	202857.921	214	828	52.8	138	Blend with CH_3CN, $\upsilon_8=1$
66	$17_{7,11} - 16_{6,10}$	203524.096	16	151	15.9	161	Blend with CH_3CN, $\upsilon_8=2$
67	$17_{7,10} - 16_{6,10}$	203528.806	16	151	1.1	161	Blend with CH_3CN, $\upsilon_8=2$
68	$17_{7,11} - 16_{6,11}$	203574.259	16	151	1.1	161	Blend with CH_3CN, $\upsilon_8=2$
69	$17_{7,10} - 16_{6,11}$	203578.970	16	151	15.9	161	Blend with CH_3CN, $\upsilon_8=2$ and C_2H_5CN, $\upsilon_{20}=1$
70	$29_{5,25} - 28_{5,24}$	204412.101	7	240	116.8	316	Blend with $^{13}CH_3CH_2CN$ and U-lines
71	$19_{6,14} - 18_{5,14}$	204417.969	16	160	1.2	316	Blend with $^{13}CH_3CH_2CN$ and U-lines

Table 2. continued.

N^a (1)	Transition^b (2)	Frequency (MHz) (3)	Unc.^{c} (kHz) (4)	$E_l{}^d$ (K) (5)	$S\mu^2$ (D^2) (6)	σ^e (mK) (7)	Comments (8)
72	$59_{17,43} - 59_{16,44}$	205092.813	17	774	72.3	100	Strong C_2H_5CN, CH_3OCH_3, and $CH_3{}^{13}CH_2CN$
73	$28_{5,23} - 27_{5,22}$	205093.048	8	232	113.5	100	Strong C_2H_5CN, CH_3OCH_3, and $CH_3{}^{13}CH_2CN$
74	$31_{1,30} - 30_{2,29}$	205095.436	11	245	57.4	100	Strong $CH_3{}^{13}CH_2CN$ and CH_3OCH_3
75	$31_{2,30} - 30_{2,29}$	205095.823	11	245	127.9	100	Strong $CH_3{}^{13}CH_2CN$ and CH_3OCH_3
76	$31_{1,30} - 30_{1,29}$	205096.091	11	245	127.9	100	Strong $CH_3{}^{13}CH_2CN$ and CH_3OCH_3
77	$31_{2,30} - 30_{1,29}$	205096.478	11	245	57.4	100	Strong $CH_3{}^{13}CH_2CN$ and CH_3OCH_3
78	$29_{18,11} - 28_{18,10}{}^{\star}$	205308.386	8	332	74.6	100	Strong SO_2
80	$29_{17,12} - 28_{17,11}{}^{\star}$	205313.243	8	321	79.7	100	Strong SO_2 and U-line?
82	$54_{14,40} - 53_{15,39}{}^{\star}$	205317.032	22	650	15.2	100	Strong SO_2 and U-line?
84	$29_{19,11} - 28_{19,10}$	205317.035	9	343	69.3	100	Strong SO_2 and U-line?
85	$29_{16,13} - 28_{16,12}{}^{\star}$	205334.455	8	311	84.4	100	Strong $CH_3{}^{13}CH_2CN$
87	$29_{20,9} - 28_{20,8}{}^{\star}$	205337.037	9	355	63.6	100	Strong $CH_3{}^{13}CH_2CN$
89	$29_{21,8} - 28_{21,7}{}^{\star}$	205366.726	10	368	57.7	100	Blend with $C_2H_5{}^{13}CN$
91	$29_{15,14} - 28_{15,13}{}^{\star}$	205375.865	8	301	88.9	100	Strong C_2H_5CN
93	$29_{14,15} - 28_{14,14}{}^{\star}$	205442.791	7	292	93.1	100	Blend with $CH_3{}^{13}CH_2CN$ and $C_2H_5{}^{13}CN$
95	$29_{13,17} - 28_{13,16}{}^{\star}$	205542.814	7	284	97.0	271	Blend with U-line
97	$29_{12,18} - 28_{12,17}{}^{\star}$	205687.132	7	276	100.6	271	Blend with C_2H_3CN, $\upsilon_{11}=1$, uncertain baseline
99	$29_{27,2} - 28_{27,1}{}^{\star}$	205690.300	20	456	16.2	271	Blend with C_2H_3CN, $\upsilon_{11}=1$, uncertain baseline
101	$29_{11,19} - 28_{11,18}{}^{\star}$	205893.033	7	269	103.9	271	Blend with $C_2H_5{}^{13}CN$
103	$29_{10,20} - 28_{10,19}$	206188.338	7	263	106.9	280	Blend with SO and ${}^{13}CH_2CHCN$
104	$29_{10,19} - 28_{10,18}$	206190.002	7	263	106.9	280	Blend with SO and ${}^{13}CH_2CHCN$
105	$29_{4,25} - 28_{4,24}$	206280.705	100	240	117.1	280	Blend with C_2H_5CN and C_2H_5CN, $\upsilon_{20}=1$
106	$29_{9,21} - 28_{9,20}$	206614.666	7	257	109.6	106	Strong C_2H_5CN and CH_3OCHO
107	$29_{9,20} - 28_{9,19}$	206639.557	7	257	109.6	106	Blend with U-lines
108	$56_{17,40} - 56_{16,40}$	206650.461	14	715	2.7	106	Blend with C_2H_5CN
109	$56_{17,39} - 56_{16,40}$	206650.601	14	715	67.2	106	Blend with C_2H_5CN
110	$56_{17,40} - 56_{16,41}$	206652.471	14	715	67.2	106	Blend with C_2H_5CN
111	$56_{17,39} - 56_{16,41}$	206652.612	14	715	2.7	106	Blend with C_2H_5CN
112	$30_{3,27} - 29_{4,26}$	206654.482	7	246	38.8	106	Blend with C_2H_5CN
113	$29_{6,24} - 28_{6,23}$	206929.917	8	244	115.8	117	Strong C_2H_5CN, $\upsilon_{20}=1$ and C_2H_5CN
114	$30_{4,27} - 29_{4,26}$	206996.130	100	246	121.8	117	Blend with OCS, $\upsilon_2=1$ and $NH_2{}^{13}CHO$
115	$28_{5,24} - 27_{4,23}$	207002.205	100	230	24.1	117	Blend with OCS, $\upsilon_2=1$ and $NH_2{}^{13}CHO$
116	$30_{3,27} - 29_{3,26}$	207175.063	100	246	121.8	117	Blend with U-line
117	$29_{8,22} - 28_{8,21}$	207183.249	7	252	112.1	117	Blend with U-line
118	$12_{10,2} - 11_{9,3}{}^{\star}$	207240.583	16	141	21.0	117	Blend with CH_3OCHO and U-line
120	$12_{10,2} - 11_{9,2}{}^{\star}$	207240.583	16	141	1.2	117	Blend with CH_3OCHO and U-line
122	$32_{0,32} - 31_{0,31}{}^{\star}$	207408.086	100	249	133.2	282	Blend with C_2H_5CN, $\upsilon_{13}=1/\upsilon_{21}=1$
124	$32_{0,32} - 31_{1,31}{}^{\star}$	207408.141	17	249	67.2	282	Blend with C_2H_5CN, $\upsilon_{13}=1/\upsilon_{21}=1$
126	$29_{8,21} - 28_{8,20}$	207451.586	7	252	112.1	282	Blend with C_2H_5CN, $\upsilon_{13}=1/\upsilon_{21}=1$ and C_2H_5OH
127	$30_{4,27} - 29_{3,26}$	207516.619	7	246	38.8	282	Blend with CH_3CH_3CO, $\upsilon_t=1$ and U-line
128	$29_{7,23} - 28_{7,22}$	207601.807	8	247	114.2	282	Strong NH_2CHO, $\upsilon_{12}=1$ and C_2H_3CN
129	$20_{6,15} - 19_{5,14}$	207703.938	15	166	13.7	282	Blend with CH_3OCH_3
130	$14_{9,6} - 13_{8,5}{}^{\star}$	208513.304	16	144	19.3	168	Blend with C_2H_5OH and C_2H_3CN
132	$14_{9,5} - 13_{8,6}{}^{\star}$	208513.306	16	144	19.3	168	Blend with C_2H_5OH and C_2H_3CN
134	$31_{2,29} - 30_{3,28}$	209205.202	8	251	49.5	58	Strong H_2CS and C_2H_3CN, $\upsilon_{15}=1$
135	$31_{3,29} - 30_{3,28}$	209217.484	100	251	126.8	58	Strong C_2H_3CN, $\upsilon_{15}=1$, CH_3OCHO, and HC_3N
136	$31_{2,29} - 30_{2,28}$	209225.073	100	251	126.8	58	Strong CH_3OCHO and HC_3N
137	$31_{3,29} - 30_{2,28}$	209237.276	8	251	49.5	58	Strong HC_3N
138	$74_{18,56} - 74_{17,57}{}^{\star}$	209239.716	197	1125	97.1	58	Strong HC_3N
140	$29_{7,22} - 28_{7,21}$	209426.660	9	248	114.3	58	Strong CH_3OCH_3 and CH_3CH_3CO
141	$16_{8,9} - 15_{7,8}{}^{\star}$	209662.326	16	150	17.7	45	Strong C_2H_3CN, $\upsilon_{11}=1$, $HC^{13}CCN$, $\upsilon_7=2$, and $HCC^{13}CN$, $\upsilon_7=2$
143	$16_{8,9} - 15_{7,9}{}^{\star}$	209663.117	16	150	1.2	45	Strong C_2H_3CN, $\upsilon_{11}=1$, $HC^{13}CCN$, $\upsilon_7=2$, and $HCC^{13}CN$, $\upsilon_7=2$
145	$18_{7,12} - 17_{6,11}$	210394.041	16	157	16.0	64	Blend with C_2H_5OH and CH_3OCHO
146	$18_{7,11} - 17_{6,12}$	210507.031	16	157	16.0	64	Strong HC_3N, $\upsilon_7=2$
147	$41_{17,24} - 41_{16,25}{}^{\star}$	210945.438	10	465	43.1	37	Strong $NH_2{}^{13}CHO$ and C_2H_5CN, $\upsilon_{13}=1/\upsilon_{21}=1$
149	$41_{17,25} - 41_{16,26}{}^{\star}$	210945.438	10	465	43.1	37	Strong $NH_2{}^{13}CHO$ and C_2H_5CN, $\upsilon_{13}=1/\upsilon_{21}=1$
151	$30_{5,26} - 29_{5,25}$	210948.194	7	250	121.0	37	Strong $NH_2{}^{13}CHO$ and C_2H_5CN, $\upsilon_{13}=1/\upsilon_{21}=1$
152	$29_{5,25} - 28_{4,24}$	211213.126	100	240	26.6	33	Strong H_2CO in absorption
153	$32_{1,31} - 31_{2,30}$	211492.742	12	255	59.6	33	Strong CH_3OCH_3
154	$32_{2,31} - 31_{2,30}$	211492.971	12	255	132.0	33	Strong CH_3OCH_3
155	$32_{1,31} - 31_{1,30}$	211493.129	12	255	132.0	33	Strong CH_3OCH_3
156	$32_{2,31} - 31_{1,30}$	211493.358	12	255	59.6	33	Strong CH_3OCH_3
157	$29_{5,24} - 28_{5,23}$	211817.880	100	242	117.5	47	Blend with CH_3OH, $\upsilon_t=1$ and U-line

Table 2. continued.

N^a (1)	Transition^b (2)	Frequency (MHz) (3)	Unc.^{c} (kHz) (4)	$E_\mathrm{l}{}^d$ (K) (5)	$S\mu^2$ (D^2) (6)	σ^e (mK) (7)	Comments (8)
158	$18_{17,1}-18_{16,2}{}^\star$	211857.177	16	231	4.4	47	Blend with C_2H_3CN, υ_{15}=1 and U-line
160	$29_{17,12}-29_{16,13}{}^\star$	211859.692	10	320	24.2	47	Blend with C_2H_3CN, υ_{15}=1 and U-line
162	$29_{17,12}-29_{16,14}{}^\star$	211859.692	10	320	1.2	47	Blend with C_2H_3CN, υ_{15}=1 and U-line
164	$28_{17,11}-28_{16,12}{}^\star$	211880.904	10	311	22.6	47	Blend with $CH_2CH^{13}CN$
166	$28_{17,11}-28_{16,13}{}^\star$	211880.904	10	311	1.1	47	Blend with $CH_2CH^{13}CN$
168	$27_{17,10}-27_{16,11}{}^\star$	211896.387	11	301	20.9	47	Strong C_2H_3CN, υ_{11}=1 and C_2H_5OH
170	$27_{17,10}-27_{16,12}{}^\star$	211896.387	11	301	1.0	47	Strong C_2H_3CN, υ_{11}=1 and C_2H_5OH
172	$21_{17,4}-21_{16,5}{}^\star$	211896.595	13	251	10.4	47	Strong C_2H_3CN, υ_{11}=1 and C_2H_5OH
174	$21_{17,4}-21_{16,6}{}^\star$	211896.595	13	251	0.5	47	Strong C_2H_3CN, υ_{11}=1 and C_2H_5OH
176	$22_{17,5}-22_{16,6}{}^\star$	211905.280	13	259	12.2	47	Blend with CH_3CH_3CO, υ_t=1, C_2H_3CN, υ_{11}=1, and U-line
178	$22_{17,5}-22_{16,7}{}^\star$	211905.280	13	259	0.6	47	Blend with CH_3CH_3CO, υ_t=1, C_2H_3CN, υ_{11}=1, and U-line
180	$26_{17,10}-26_{16,11}{}^\star$	211906.656	11	292	19.2	47	Blend with CH_3CH_3CO, υ_t=1, C_2H_3CN, υ_{11}=1, and U-line
182	$26_{17,10}-26_{16,10}$	211906.656	11	292	0.9	47	Blend with CH_3CH_3CO, υ_t=1, C_2H_3CN, υ_{11}=1, and U-line
183	$26_{17,9}-26_{16,10}$	211906.776	100	292	19.2	47	Blend with CH_3CH_3CO, υ_t=1, C_2H_3CN, υ_{11}=1, and U-line
184	$23_{17,6}-23_{16,7}{}^\star$	211911.066	12	266	14.0	47	Blend with CH_3CH_3CO, υ_t=1, C_2H_3CN, υ_{11}=1, and U-line
186	$23_{17,6}-23_{16,8}{}^\star$	211911.066	12	266	0.7	47	Blend with CH_3CH_3CO, υ_t=1, C_2H_3CN, υ_{11}=1, and U-line
188	$25_{17,8}-25_{16,9}{}^\star$	211912.208	11	283	17.5	47	Blend with CH_3CH_3CO, υ_t=1, C_2H_3CN, υ_{11}=1, and U-line
190	$25_{17,8}-25_{16,10}{}^\star$	211912.208	11	283	0.9	47	Blend with CH_3CH_3CO, υ_t=1, C_2H_3CN, υ_{11}=1, and U-line
192	$24_{17,8}-24_{16,9}{}^\star$	211913.523	12	275	15.8	47	Blend with CH_3CH_3CO, υ_t=1, C_2H_3CN, υ_{11}=1, and U-line
194	$24_{17,8}-24_{16,8}$	211913.523	12	275	0.8	47	Blend with CH_3CH_3CO, υ_t=1, C_2H_3CN, υ_{11}=1, and U-line
195	$24_{17,7}-24_{16,8}$	211913.626	100	275	15.8	47	Blend with CH_3CH_3CO, υ_t=1, C_2H_3CN, υ_{11}=1, and U-line
196	$20_{6,14}-19_{5,15}$	212146.465	17	166	13.4	36	Strong NH_2CHO, υ_{12}=1
197	$30_{4,26}-29_{4,25}$	212369.981	100	249	121.2	36	Blend with U-line, $NH_2{}^{13}CHO$, υ_{12}=1, and C_3H_7CN, uncertain baseline
198	$30_{18,12}-29_{18,11}{}^\star$	212385.195	8	341	80.3	36	Strong NH_2CHO, υ_{12}=1
200	$71_{18,54}-71_{17,55}$	212386.233	123	1051	91.5	36	Strong NH_2CHO, υ_{12}=1
201	$30_{19,11}-29_{19,10}{}^\star$	212390.341	8	353	75.2	36	Strong NH_2CHO, υ_{12}=1
203	$30_{17,13}-29_{17,12}{}^\star$	212394.782	8	331	85.2	36	Strong NH_2CHO, υ_{12}=1
205	$30_{20,11}-29_{20,10}{}^\star$	212407.836	9	365	69.7	36	Blend with $NH_2{}^{13}CHO$, υ_{12}=1 and CH_3CH_3CO, υ_t=1
207	$30_{16,14}-29_{16,13}{}^\star$	212422.256	8	320	89.8	36	Strong NH_2CHO
209	$30_{21,9}-29_{21,8}{}^\star$	212435.843	9	377	64.0	36	Strong NH_2CHO
211	$30_{15,15}-29_{15,14}{}^\star$	212471.882	8	311	94.1	99	Blend with C_2H_5OH, CH_3OCHO, and C_3H_7CN
213	$30_{22,8}-29_{22,7}{}^\star$	212472.920	10	391	58.0	99	Blend with C_2H_5OH, CH_3OCHO, and C_3H_7CN
215	$30_{14,17}-29_{14,16}{}^\star$	212549.578	7	302	98.2	99	Blend with $NH_2{}^{13}CHO$ and U-line
217	$29_{6,23}-28_{6,22}$	212550.033	10	244	116.6	99	Blend with $NH_2{}^{13}CHO$ and U-line
218	$30_{13,17}-29_{13,16}{}^\star$	212663.809	7	294	102.0	99	Blend with C_2H_5OH and $^{13}CH_2CHCN$
220	$30_{12,19}-29_{12,18}{}^\star$	212827.135	7	286	105.4	99	Strong $^{13}CH_2CHCN$ and NH_2CHO
222	$30_{28,3}-29_{28,2}{}^\star$	212834.203	100	482	16.2	99	Strong $^{13}CH_2CHCN$ and NH_2CHO
224	$21_{6,16}-20_{5,15}$	212845.604	15	173	13.7	99	Blend with $^{13}CH_2CHCN$, uncertain baseline
225	$11_{11,1}-10_{10,0}{}^\star$	212997.517	100	143	23.2	99	Blend with C_2H_5CN
227	$11_{11,0}-10_{10,0}{}^\star$	212997.572	16	143	1.3	99	Blend with C_2H_5CN
229	$30_{11,20}-29_{11,19}$	213059.055	7	279	108.7	48	Strong SO_2
230	$30_{11,19}-29_{11,18}$	213059.228	7	279	108.7	48	Strong SO_2
231	$31_{3,28}-30_{4,27}$	213169.983	7	255	41.1	48	Strong C_2H_3CN, υ_{11}=1
232	$30_{10,21}-29_{10,20}$	213390.877	7	273	111.6	48	Blend with CH_3CH_3CO, υ_t=1, uncertain baseline
233	$31_{4,28}-30_{4,27}$	213392.357	7	255	125.9	48	Blend with CH_3CH_3CO, υ_t=1, uncertain baseline
234	$30_{10,20}-29_{10,19}$	213394.012	7	273	111.6	48	Blend with CH_3CH_3CO, υ_t=1, uncertain baseline
235	$16_{4,13}-15_{1,14}$	213509.497	41	135	0.8	48	Blend with C_2H_5CN, υ_{13}=1/υ_{21}=1 and U-line
236	$31_{3,28}-30_{3,27}$	213511.580	100	255	125.9	48	Blend with C_2H_5CN, υ_{13}=1/υ_{21}=1 and U-line
237	$31_{4,28}-30_{3,27}$	213733.932	7	255	41.1	48	Blend with C_2H_5CN, υ_{13}=1/υ_{21}=1
238	$30_{6,25}-29_{6,24}$	213791.953	100	253	120.1	48	Blend with CH_3CH_3CO, υ_t=1, C_2H_3CN, υ_{15}=1, and U-line
239	$33_{0,33}-32_{1,32}{}^\star$	213807.575	17	259	69.4	48	Blend with C_2H_5CN
241	$33_{0,33}-32_{0,32}{}^\star$	213807.621	100	259	137.4	48	Blend with C_2H_5CN
243	$30_{9,22}-29_{9,21}$	213865.943	7	267	114.2	48	Blend with C_2H_5OH and $C_2H_5{}^{13}CN$
244	$30_{9,21}-29_{9,20}$	213909.016	7	267	114.2	48	Blend with C_3H_7CN and $^{13}CH_3OH$
245	$13_{10,3}-12_{9,4}{}^\star$	214314.472	16	145	21.1	75	Strong $^{13}CH_3CN$ and $C_2H_5{}^{13}CN$
247	$13_{10,3}-12_{9,3}{}^\star$	214314.472	16	145	1.2	75	Strong $^{13}CH_3CN$ and $C_2H_5{}^{13}CN$
249	$30_{8,23}-29_{8,22}$	214467.553	8	262	116.6	75	Blend with CH_3OCH_3
250	$30_{7,24}-29_{7,23}$	214783.566	8	257	118.6	75	Strong CH_3OCHO
251	$30_{8,22}-29_{8,21}$	214889.514	8	262	116.6	74	Blend with $^{13}CH_2CHCN$
252	$31_{4,27}-30_{5,26}$	214982.375	100	260	31.4	74	Strong $C_2H_5{}^{13}CN$ and $^{13}CH_3CN$, υ_8=1
253	$15_{9,7}-14_{8,6}{}^\star$	215567.674	16	149	19.5	74	Strong C_2H_5CN, υ_{20}=1 and C_2H_5CN, υ_{13}=1/υ_{21}=1
255	$15_{9,7}-14_{8,7}{}^\star$	215567.680	16	149	1.2	74	Strong C_2H_5CN, υ_{20}=1 and C_2H_5CN, υ_{13}=1/υ_{21}=1

Table 2. continued.

N^a (1)	Transition^b (2)	Frequency (MHz) (3)	Unc.^{c} (kHz) (4)	$E_l{}^d$ (K) (5)	$S\mu^2$ (D^2) (6)	σ^e (mK) (7)	Comments (8)
257	$32_{2,30} - 31_{3,29}$	215600.637	8	261	51.8	74	Strong C_2H_5CN
258	$32_{3,30} - 31_{3,29}$	215608.230	100	261	131.0	74	Strong C_2H_5CN
259	$32_{2,30} - 31_{2,29}$	215612.952	100	261	131.0	74	Strong C_2H_5CN
260	$32_{3,30} - 31_{2,29}$	215620.426	8	261	51.8	74	Strong C_2H_5CN
261	$36_{9,27} - 36_{6,30}$	215623.049	44	336	2.1	74	Strong C_2H_5CN
262	$30_{5,26} - 29_{4,25}$	215880.577	100	249	29.1	55	Strong $^{13}CH_3OH$
263	$17_{8,10} - 16_{7,9}$	216663.426	16	155	17.9	55	Blend with C_2H_5OH, C_3H_7CN, and U-line
264	$17_{8,9} - 16_{7,9}$	216663.574	16	155	1.2	55	Blend with C_2H_5OH, C_3H_7CN, and U-line
265	$17_{8,10} - 16_{7,10}$	216665.420	16	155	1.2	55	Blend with C_2H_5OH, C_3H_7CN, and U-line
266	$17_{8,9} - 16_{7,10}$	216665.567	16	155	17.9	55	Blend with C_2H_5OH, C_3H_7CN, and U-line
267	$61_{4,57} - 61_{4,58}{}^\star$	216666.695	128	715	4.3	55	Blend with C_2H_5OH, C_3H_7CN, and U-line
269	$61_{5,57} - 61_{4,58}{}^\star$	216666.699	128	715	29.9	55	Blend with C_2H_5OH, C_3H_7CN, and U-line
271	$19_{7,13} - 18_{6,12}$	217192.379	16	163	16.1	50	Strong CH_3OCH_3
272	$30_{7,23} - 29_{7,22}$	217285.278	10	258	118.8	50	Blend with ^{13}CN, $CH_2{}^{13}CHCN$, and U-line
273	$22_{6,17} - 21_{5,16}$	217407.902	17	181	13.6	50	Strong $HC^{13}CCN$, $^{13}CH_3OH$, $HCC^{13}CN$, and ^{13}CN in absorption
274	$21_{2,20} - 20_{1,20}$	217409.248	52	160	0.3	50	Strong $HC^{13}CCN$, $^{13}CH_3OH$, $HCC^{13}CN$, and ^{13}CN in absorption
275	$19_{7,12} - 18_{6,13}$	217414.071	16	163	16.1	50	Strong $HCC^{13}CN$ and ^{13}CN in absorption
276	$31_{5,27} - 30_{5,26}$	217441.193	100	260	125.2	50	Strong ^{13}CN in absorption, $CH_2{}^{13}CHCN$, and $CH_2CH^{13}CN$
277	$31_{18,13} - 30_{18,12}{}^\star$	219461.424	8	352	86.0	92	Strong C_2H_5CN
279	$31_{19,12} - 30_{19,11}{}^\star$	219462.695	8	363	81.0	92	Strong C_2H_5CN
281	$31_{17,14} - 30_{17,13}{}^\star$	219476.189	8	341	90.7	92	Strong NH_2CN
283	$31_{20,11} - 30_{20,10}{}^\star$	219477.375	9	375	75.7	92	Strong NH_2CN
285	$31_{21,10} - 30_{21,9}{}^\star$	219503.439	9	388	70.2	92	Strong C_2H_5CN
287	$31_{16,15} - 30_{16,14}{}^\star$	219510.475	8	331	95.1	92	Strong C_2H_5CN
289	$31_{22,9} - 30_{22,8}{}^\star$	219539.304	9	401	64.4	92	Strong HNCO, υ_5=1 and HNCO
291	$31_{15,16} - 30_{15,15}{}^\star$	219569.004	8	321	99.3	92	Strong $C^{18}O$
293	$62_{17,46} - 61_{18,43}$	219569.366	161	836	17.0	92	Strong $C^{18}O$
294	$62_{17,45} - 61_{18,44}$	219572.725	161	836	17.0	92	Strong $C^{18}O$
295	$31_{24,7} - 30_{24,6}{}^\star$	219635.627	11	429	52.0	92	Blend with C_2H_5CN, υ_{20}=1 and CH_3CN, υ_4=1
297	$32_{3,29} - 31_{4,28}$	219637.655	7	266	43.4	92	Blend with C_2H_5CN, υ_{20}=1 and CH_3CN, υ_4=1
298	$31_{14,17} - 30_{14,16}{}^\star$	219658.346	7	312	103.2	92	Strong NH_2CN and HNCO
300	$32_{4,29} - 31_{4,28}$	219781.349	100	266	130.1	92	Strong HNCO, υ_6=1 and HNCO
301	$31_{13,19} - 30_{13,18}{}^\star$	219787.930	7	304	106.9	92	Strong HNCO
303	$21_{6,15} - 20_{5,16}$	219793.028	100	173	13.1	92	Strong HNCO
304	$34_{1,34} - 33_{0,33}{}^\star$	220205.386	100	270	71.6	98	Strong HNCO, υ_5=1 and C_2H_5CN, υ_{13}=1/υ_{21}=1
306	$34_{1,34} - 33_{1,33}{}^\star$	220205.400	17	270	141.6	98	Strong HNCO, υ_5=1 and C_2H_5CN, υ_{13}=1/υ_{21}=1
308	$58_{18,41} - 58_{17,41}{}^\star$	220209.432	15	764	2.8	98	Strong HNCO, υ_5=1 and C_2H_5CN, υ_{13}=1/υ_{21}=1
310	$58_{18,41} - 58_{17,42}{}^\star$	220209.852	15	764	68.8	98	Strong HNCO, υ_5=1 and C_2H_5CN, υ_{13}=1/υ_{21}=1
312	$31_{11,21} - 30_{11,20}$	220231.977	7	289	113.4	98	Blend with CH_3CN and U-line
313	$31_{11,20} - 30_{11,19}$	220232.321	7	289	113.4	98	Blend with CH_3CN and U-line
314	$31_{6,26} - 30_{6,25}$	220580.985	100	264	124.3	98	Strong $CH_3{}^{13}CN$ and HNCO
315	$31_{10,22} - 30_{10,21}$	220603.352	7	283	116.2	98	Strong CH_3CN, $CH_3{}^{13}CN$, and C_2H_5OH
316	$62_{4,58} - 62_{3,59}{}^\star$	220606.847	154	735	30.0	98	Strong $CH_3{}^{13}CN$ and C_2H_5OH
318	$62_{5,58} - 62_{4,59}{}^\star$	220606.849	154	735	30.0	98	Strong $CH_3{}^{13}CN$ and C_2H_5OH
320	$31_{10,21} - 30_{10,20}$	220609.106	7	283	116.2	98	Strong $CH_3{}^{13}CN$ and C_2H_5OH
321	$33_{3,30} - 32_{4,29}$	226072.922	7	276	45.7	278	Blend with c-C_2H_4O and $^{13}CH_3OH$
322	$33_{4,30} - 32_{4,29}$	226165.300	7	276	134.3	278	Blend with CN in absorption and CH_3CH_3CO, υ_t=1
323	$33_{3,30} - 32_{3,29}$	226216.618	100	276	134.3	278	Blend with CH_3CH_3CO and CN in absorption
324	$33_{4,30} - 32_{3,29}$	226309.069	7	276	45.8	278	Strong CN in absorption
325	$32_{5,28} - 31_{4,27}$	226357.720	9	270	34.1	278	Strong CN in absorption
326	$32_{19,13} - 31_{19,12}{}^\star$	226534.021	8	373	86.7	278	Blend with CH_2NH
328	$32_{18,15} - 31_{18,14}{}^\star$	226537.002	100	362	91.5	278	Blend with CH_2NH
330	$32_{20,13} - 31_{20,12}{}^\star$	226545.568	8	385	81.6	278	Blend with CH_2NH
332	$32_{17,15} - 31_{17,14}{}^\star$	226557.411	8	351	96.1	278	Blend with C_2H_5CN, υ_{13}=1/υ_{21}=1
334	$32_{21,11} - 31_{21,10}{}^\star$	226569.424	9	398	76.2	278	Blend with CH_3COOH, C_2H_5OH, and CN in absorption
336	$32_{16,16} - 31_{16,15}{}^\star$	226599.078	8	341	100.4	278	Blend with $C_2H_5{}^{13}CN$
338	$35_{0,35} - 34_{1,34}{}^\star$	226601.560	18	280	73.8	278	Blend with $C_2H_5{}^{13}CN$
340	$35_{0,35} - 34_{0,34}{}^\star$	226601.561	18	280	145.8	278	Blend with $C_2H_5{}^{13}CN$
342	$32_{22,10} - 31_{22,9}{}^\star$	226603.850	9	411	70.6	278	Blend with $C_2H_5{}^{13}CN$
344	$32_{15,17} - 31_{15,16}{}^\star$	226667.222	8	332	104.5	96	Strong CN in absorption and C_2H_5OH
346	$32_{14,18} - 31_{14,17}{}^\star$	226769.121	8	323	108.3	96	Strong CN in absorption
348	$32_{13,20} - 31_{13,19}{}^\star$	226915.261	8	314	111.8	96	Strong CN in absorption
350	$32_{12,21} - 31_{12,20}{}^\star$	227121.372	7	307	115.1	96	Blend with C_2H_5CN, uncertain baseline

Table 2. continued.

N^a (1)	Transition^b (2)	Frequency (MHz) (3)	Unc.^{c} (kHz) (4)	$E_l{}^d$ (K) (5)	$S\mu^2$ (D^2) (6)	σ^e (mK) (7)	Comments (8)
352	$32_{11,22} - 31_{11,21}$	227412.121	7	300	118.1	85	Strong HC_3N
353	$32_{11,21} - 31_{11,20}$	227412.786	7	300	118.1	85	Strong HC_3N
354	$31_{6,25} - 30_{6,24}$	227600.701	10	265	125.4	85	Strong C_2H_5OH and NH_2CHO
355	$32_{10,23} - 31_{10,22}$	227826.118	8	293	120.8	85	Blend with CH_3OH
356	$32_{10,22} - 31_{10,21}$	227836.414	8	293	120.8	85	Blend with CH_3CH_3CO
357	$22_{6,16} - 21_{5,17}$	227855.315	20	180	12.7	85	Blend with $HC^{13}CCN$, $v_7=2$, $HCC^{13}CN$, $v_7=2$, and U-line
358	$81_{10,71} - 81_{9,72}{}^\star$	231205.772	1715	1244	77.8	183	Strong ^{13}CS and U-line
360	$34_{3,31} - 33_{4,30}$	232486.365	7	287	48.0	19	Strong $C_2H_5{}^{13}CN$ and C_2H_5OH
361	$34_{4,31} - 33_{4,30}$	232545.336	50	287	138.4	19	Blend uith C_2H_5CN and C_2H_5OH
362	$34_{3,31} - 33_{3,30}$	232578.686	50	287	138.4	19	Blend with $CH_3{}^{13}CH_2CN$ and $^{13}CH_2CHCN$
363	$34_{4,31} - 33_{3,30}$	232637.775	8	287	48.0	19	Blend with CH_3OH, $v_t=1$, CH_3CH_3CO, and $^{13}CH_2CO$
364	$12_{12,0} - 11_{11,1}{}^\star$	232895.717	15	153	25.4	19	Blend with C_2H_5CN and $^{13}CH_3CN$, $v_8=1$
366	$12_{12,0} - 11_{11,0}{}^\star$	232895.717	15	153	1.4	19	Blend with C_2H_5CN and $^{13}CH_3CN$, $v_8=1$
368	$33_{10,24} - 32_{10,23}$	235059.537	50	304	125.4	131	Strong CH_3OCHO and C_2H_5CN
369	$33_{10,23} - 32_{10,22}$	235077.408	8	304	125.4	131	Strong CH_3CH_3CO and C_2H_5OH
370	$16_{10,7} - 15_{9,6}{}^\star$	235511.949	15	159	21.6	131	Strong $HC^{13}CCN$
372	$16_{10,6} - 15_{9,7}{}^\star$	235511.949	15	159	21.6	131	Strong $HC^{13}CCN$
374	$33_{9,25} - 32_{9,24}$	235683.207	50	299	127.8	131	Blend with $HCC^{13}CN$, $v_5=1/v_7=3$
375	$33_{9,24} - 32_{9,23}$	235875.700	8	299	127.8	131	Strong $^{13}CH_3OH$ and CH_3OCHO
376	$34_{4,30} - 33_{5,29}$	235952.121	100	292	39.0	131	Strong $C_2H_5{}^{13}CN$, $^{13}CH_3OH$, and SiS
377	$33_{7,27} - 32_{7,26}$	236011.028	50	289	131.6	131	Strong $^{13}CH_3OH$
378	$66_{4,62} - 66_{3,63}{}^\star$	236269.468	357	816	30.1	37	Blend with NH_2CH_2CN and $H_2C^{34}S$
380	$66_{5,62} - 66_{4,63}{}^\star$	236269.469	357	816	30.1	37	Blend with NH_2CH_2CN and $H_2C^{34}S$
382	$33_{8,26} - 32_{8,25}$	236274.518	50	294	130.0	37	Blend with NH_2CH_2CN and $H_2C^{34}S$
383	$23_{6,17} - 22_{5,18}$	236483.115	100	188	12.0	37	Blend with NH_2CH_2CN and $CH_2{}^{13}CHCN$
384	$34_{23,11} - 33_{23,10}{}^\star$	240768.473	9	447	77.2	216	Strong $CH_3{}^{13}CH_2CN$, CH_3CH_3CO, and C_2H_5OH
386	$34_{16,18} - 33_{16,17}{}^\star$	240777.277	8	363	110.8	216	Strong $CH_3{}^{13}CH_2CN$, CH_3CH_3CO, and C_2H_5OH
388	$34_{15,19} - 33_{15,18}{}^\star$	240866.895	8	354	114.6	216	Strong C_2H_5CN and HNCO
390	$34_{14,21} - 33_{14,20}{}^\star$	240996.801	8	345	118.2	216	Strong $C_2H_5{}^{13}CN$, CH_3CH_3CO, and $C^{34}S$
392	$33_{7,26} - 32_{7,25}$	241104.938	12	290	132.3	216	Blend with $CH_3{}^{13}CH_2CN$ and U-line
393	$36_{2,34} - 35_{3,33}$	241154.165	10	304	60.8	216	Strong CH_3OH, $v_t=1$
394	$36_{3,34} - 35_{3,33}$	241155.214	10	304	147.7	216	Strong CH_3OH, $v_t=1$
395	$36_{2,34} - 35_{2,33}$	241155.889	10	304	147.7	216	Strong CH_3OH, $v_t=1$
396	$36_{3,34} - 35_{2,33}$	241156.938	10	304	60.8	216	Strong CH_3OH, $v_t=1$
397	$34_{29,5} - 33_{29,4}{}^\star$	241179.811	17	543	38.8	216	Strong CH_3OH, $v_t=1$
399	$34_{13,22} - 33_{13,21}{}^\star$	241179.912	8	337	121.5	216	Strong CH_3OH, $v_t=1$
401	$65_{3,62} - 65_{2,63}{}^\star$	241187.055	355	784	22.6	216	Strong CH_3OH, $v_t=1$
403	$65_{3,62} - 65_{3,63}{}^\star$	241187.055	355	784	3.4	216	Strong CH_3OH, $v_t=1$
405	$21_{8,14} - 20_{7,13}$	244391.993	15	180	18.5	46	Strong $^{13}CH_3CH_2CN$ and C_2H_5CN
406	$21_{8,13} - 20_{7,13}$	244396.589	15	180	1.4	46	Strong $^{13}CH_3CH_2CN$ and C_2H_5CN
407	$23_{5,18} - 22_{4,19}$	244399.583	45	185	5.5	46	Strong $^{13}CH_3CH_2CN$ and C_2H_5CN
408	$21_{8,14} - 20_{7,14}$	244437.241	15	180	1.4	46	Blend with C_2H_5CN, C_2H_5OH, and U-line
409	$21_{8,13} - 20_{7,14}$	244441.837	15	180	18.5	46	Blend with C_2H_5CN, C_2H_5OH, and U-line
410	$23_{7,16} - 22_{6,17}$	245129.808	16	191	16.1	72	Strong CH_2NH
411	$36_{3,33} - 35_{4,32}$	245273.854	100	310	52.6	72	Strong HC_3N, $v_4=1$ and $C_2H_5{}^{13}CN$
412	$36_{4,33} - 35_{4,32}$	245297.601	100	310	146.7	72	Blend with CH_3CH_3CO and $^{34}SO_2$
413	$36_{3,33} - 35_{3,32}$	245311.367	100	310	146.7	72	Blend with C_2H_5OH and SO_2
414	$36_{4,33} - 35_{3,32}$	245335.158	100	310	52.6	72	Strong SO_2
415	$34_{8,26} - 33_{8,25}$	245447.840	11	305	134.4	72	Strong C_2H_5OH, C_2H_5CN, $v_{13}=1/v_{21}=1$, and $^{13}CH_3CH_2CN$
416	$38_{0,38} - 37_{0,37}{}^\star$	245779.482	100	314	158.3	53	Strong $CH_2{}^{13}CHCN$ and C_2H_5CN, $v_{13}=1/v_{21}=1$
418	$38_{0,38} - 37_{1,37}{}^\star$	245779.550	18	314	80.5	53	Strong $CH_2{}^{13}CHCN$ and C_2H_5CN, $v_{13}=1/v_{21}=1$
420	$24_{6,18} - 23_{5,19}$	245842.016	26	196	11.2	53	Blend with C_2H_3CN, $v_{11}=1/v_{15}=1$
421	$14_{12,2} - 13_{11,3}{}^\star$	247059.416	14	162	25.4	68	Strong CH_3OCHO
423	$14_{12,2} - 13_{11,2}{}^\star$	247059.416	14	162	1.5	68	Strong CH_3OCHO
425	$35_{6,30} - 34_{6,29}$	247073.069	100	308	141.1	68	Strong C_2H_3CN and $CH_2{}^{13}CHCN$
426	$39_{0,39} - 38_{0,38}{}^\star$	252168.489	100	326	162.5	42	Blend with C_2H_5CN, $v_{13}=1/v_{21}=1$
428	$39_{0,39} - 38_{1,38}{}^\star$	252168.541	18	326	82.7	42	Blend with C_2H_5CN, $v_{13}=1/v_{21}=1$
430	$24_{7,17} - 23_{6,18}$	252254.714	16	199	16.0	42	Strong CH_3OH
431	$25_{7,19} - 24_{6,18}$	254026.124	15	207	16.1	32	Strong CH_3OH in absorption, C_2H_5CN, $v_{13}=1/v_{21}=1$, and $HC^{13}CCN$, $v_6=1$
432	$15_{12,3} - 14_{11,4}{}^\star$	254139.046	14	167	25.5	32	Strong C_2H_3CN
434	$15_{12,3} - 14_{11,3}{}^\star$	254139.046	14	167	1.5	32	Strong C_2H_3CN

Table 2. continued.

N^a (1)	Transition^b (2)	Frequency (MHz) (3)	Unc.^{c} (kHz) (4)	$E_l{}^d$ (K) (5)	$S\mu^2$ (D^2) (6)	σ^e (mK) (7)	Comments (8)
436	$36_{14,23} - 35_{14,22}{}^{\star}$	255232.834	8	368	127.8	217	Strong CH_3OH
438	$17_{11,6} - 16_{10,7}{}^{\star}$	255442.928	14	171	23.8	217	Strong $CH_2CH^{13}CN$
440	$17_{11,6} - 16_{10,6}{}^{\star}$	255442.928	14	171	1.4	217	Strong $CH_2CH^{13}CN$
442	$36_{13,24} - 35_{13,23}{}^{\star}$	255458.533	8	360	131.0	217	Strong C_2H_5CN, $\upsilon_{13}=1/\upsilon_{21}=1$ and $CH_2{}^{13}CHCN$
444	$37_{4,33} - 36_{5,32}$	255646.981	8	327	46.2	217	Strong $H^{13}CCCN$ and NH_2CHO, $\upsilon_{12}=1$
445	$23_{8,16} - 22_{7,15}$	257978.249	15	195	18.7	1127	Strong CH_3CN, $\upsilon_8=1$
446	$56_{11,46} - 55_{12,43}$	258029.375	88	664	12.8	1127	Strong CH_3CN, $\upsilon_8=1$
447	$38_{3,35} - 37_{4,34}$	258032.591	9	334	57.1	1127	Strong CH_3CN, $\upsilon_8=1$
448	$38_{4,35} - 37_{4,34}$	258042.009	9	334	155.1	1127	Strong CH_3CN, $\upsilon_8=1$
449	$38_{3,35} - 37_{3,34}$	258047.578	9	334	155.1	1127	Strong CH_3CN, $\upsilon_8=1$
450	$38_{4,35} - 37_{3,34}$	258056.996	9	334	57.1	1127	Strong CH_3CN, $\upsilon_8=1$
451	$23_{8,15} - 22_{7,16}$	258162.637	15	195	18.7	1127	Strong $^{13}CH_3OH$ and $HC^{15}N$
452	$36_{9,27} - 35_{9,26}$	258237.747	10	334	141.2	1127	Strong CH_3CN, $\upsilon_8=1$ and SO
453	$36_{6,31} - 35_{5,30}$	258252.184	13	320	33.8	1127	Strong CH_3CN, $\upsilon_8=1$ and SO
454	$26_{7,20} - 25_{6,19}$	258801.772	16	216	15.9	1609	Strong $CH_3{}^{13}CH_2CN$
455	$37_{6,32} - 36_{6,31}$	260009.847	8	332	149.4	413	Strong C_2H_5OH, $CH_2{}^{13}CHCN$, and CH_3OCH_3
456	$39_{2,37} - 38_{3,36}$	260297.586	10	340	67.4	413	Strong C_2H_5CN, $\upsilon_{13}=1/\upsilon_{21}=1$
457	$39_{3,37} - 38_{3,36}$	260297.819	10	340	160.2	413	Strong C_2H_5CN, $\upsilon_{13}=1/\upsilon_{21}=1$
458	$39_{2,37} - 38_{2,36}$	260297.972	10	340	160.2	413	Strong C_2H_5CN, $\upsilon_{13}=1/\upsilon_{21}=1$
459	$39_{3,37} - 38_{2,36}$	260298.205	10	340	67.4	413	Strong C_2H_5CN, $\upsilon_{13}=1/\upsilon_{21}=1$
460	$37_{7,31} - 36_{7,30}$	263345.617	9	337	148.6	74	Blend with $HCC^{13}CN$, $\upsilon_7=1$
461	$37_{6,32} - 36_{5,31}$	263354.897	11	332	36.3	74	Blend with NH_2CH_2CN
462	$37_{11,27} - 36_{11,26}$	263432.848	8	358	141.1	74	Strong HNCO, $\upsilon_5=1$ and HNCO
463	$37_{11,26} - 36_{11,25}$	263445.456	8	358	141.2	74	Strong HNCO, $\upsilon_5=1$ and HNCO
464	$20_{10,11} - 19_{9,10}{}^{\star}$	263669.118	14	183	22.4	108	Strong CH_3OCH_3, HNCO, and $HC^{13}CCN$, $\upsilon_7=1$
466	$20_{10,11} - 19_{9,11}{}^{\star}$	263669.145	14	183	1.4	108	Strong CH_3OCH_3, HNCO, and $HC^{13}CCN$, $\upsilon_7=1$
468	$36_{7,29} - 35_{7,28}$	264087.850	11	326	145.6	108	Blend with $H_2{}^{13}CS$ and U-line
469	$37_{10,28} - 36_{10,27}$	264094.028	9	351	143.5	108	Blend with $H_2{}^{13}CS$ and U-line
470	$40_{2,38} - 39_{3,37}$	266674.808	10	352	69.7	91	Blend with $O^{13}CS$ and $C_2H_5{}^{13}CN$
471	$40_{3,38} - 39_{3,37}{}^{\star}$	266674.948	10	352	164.4	91	Blend with $O^{13}CS$ and $C_2H_5{}^{13}CN$
473	$40_{3,38} - 39_{2,37}$	266675.181	10	352	69.7	91	Blend with $O^{13}CS$ and $C_2H_5{}^{13}CN$
474	$15_{13,2} - 14_{12,3}{}^{\star}$	266949.479	14	174	27.6	91	Blend with SO_2 and U-line
476	$15_{13,2} - 14_{12,2}{}^{\star}$	266949.479	14	174	1.6	91	Blend with SO_2 and U-line
478	$38_{5,33} - 37_{5,32}$	267143.852	100	344	153.6	91	Strong $NH_2{}^{13}CHO$, CH_3CH_3CO, and C_2H_5CN, $\upsilon_{13}=1/\upsilon_{21}=1$

Notes: [a] Numbering of the observed transitions associated with a modeled line stronger than 20 mK. [b] Transitions marked with a * are double with a frequency difference less than 0.1 MHz. The quantum numbers of the second one are not shown. [c] Frequency uncertainty. [d] Lower energy level in temperature units (E_l/k_B). [e] Calculated rms noise level in T_{mb} scale.

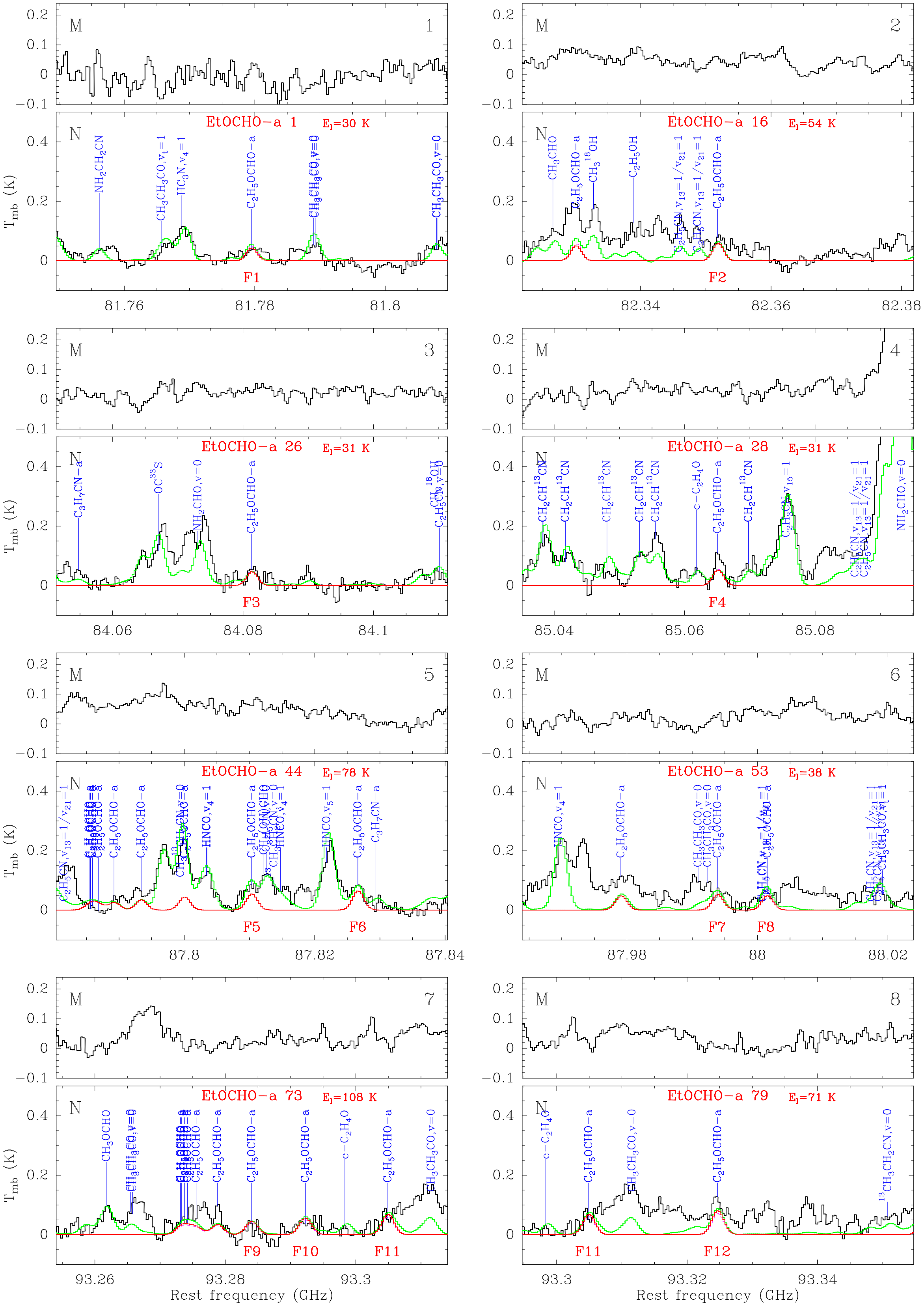

Fig. 1. Transitions of the *anti*-conformer of ethyl formate (EtOCHO-a) detected with the IRAM 30 m telescope. Each panel consists of two plots and is labeled in black in the upper right corner. The lower plot shows in black the spectrum obtained toward Sgr B2(N) in main-beam brightness temperature scale (K), while the upper plot shows the spectrum toward Sgr B2(M). The rest frequency axis is labeled in GHz. The systemic velocities assumed for Sgr B2(N) and (M) are 64 and 62 km s^{-1}, respectively. The lines identified in the Sgr B2(N) spectrum are labeled in blue. The top red label indicates the EtOCHO-a transition centered in each plot (numbered like in Col. 1 of Table 3), along with the energy of its lower level in K (E_l/k_B). The other EtOCHO-a lines are labeled in blue only. The bottom red label is the feature number (see Col. 8 of Table 3). The green spectrum shows our LTE model containing all identified molecules, including EtOCHO-a. The LTE synthetic spectrum of EtOCHO-a alone is overlaid in red, and its opacity in dashed violet. All observed lines which have no counterpart in the green spectrum are still unidentified in Sgr B2(N).

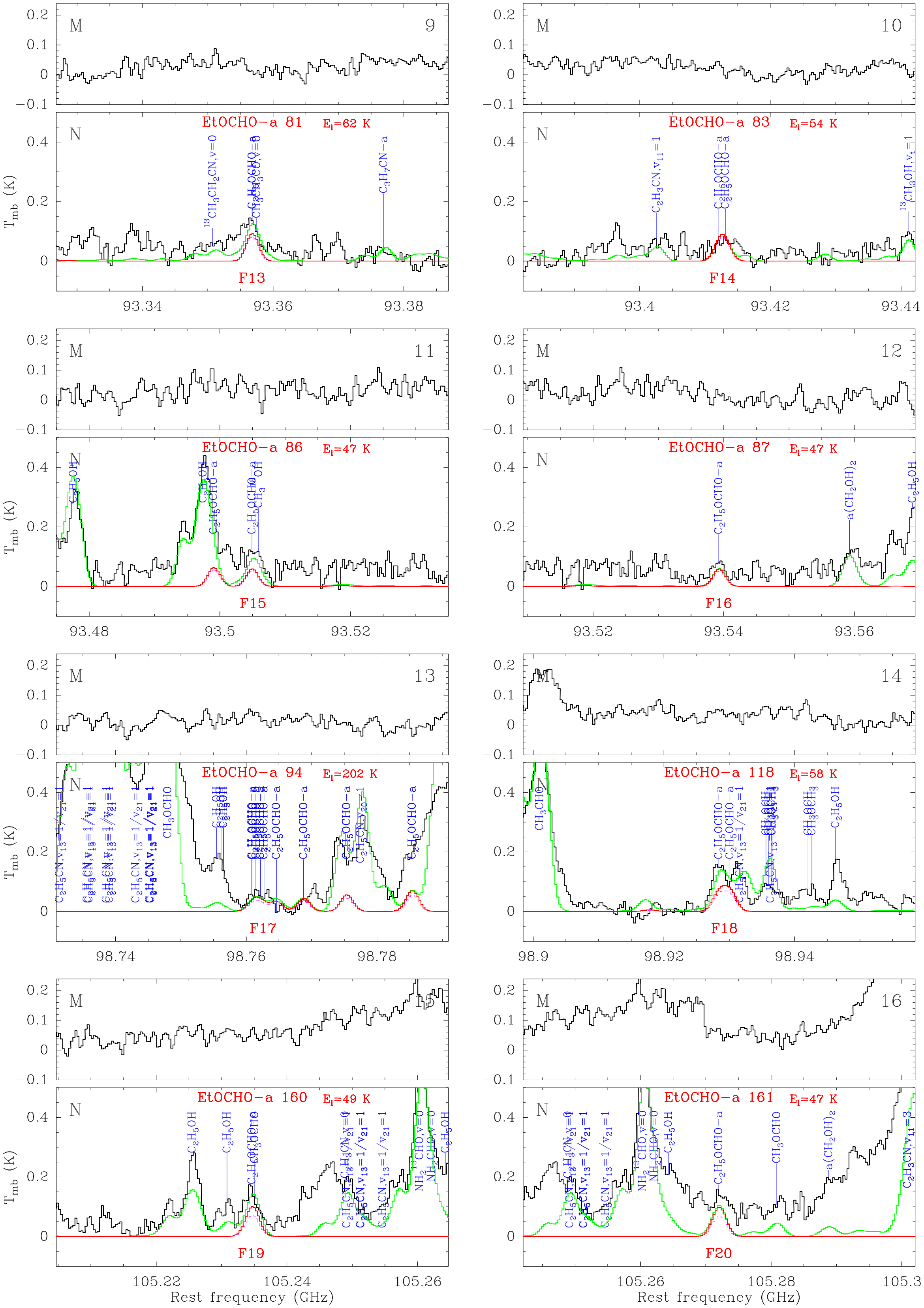

Fig. 1. (continued)

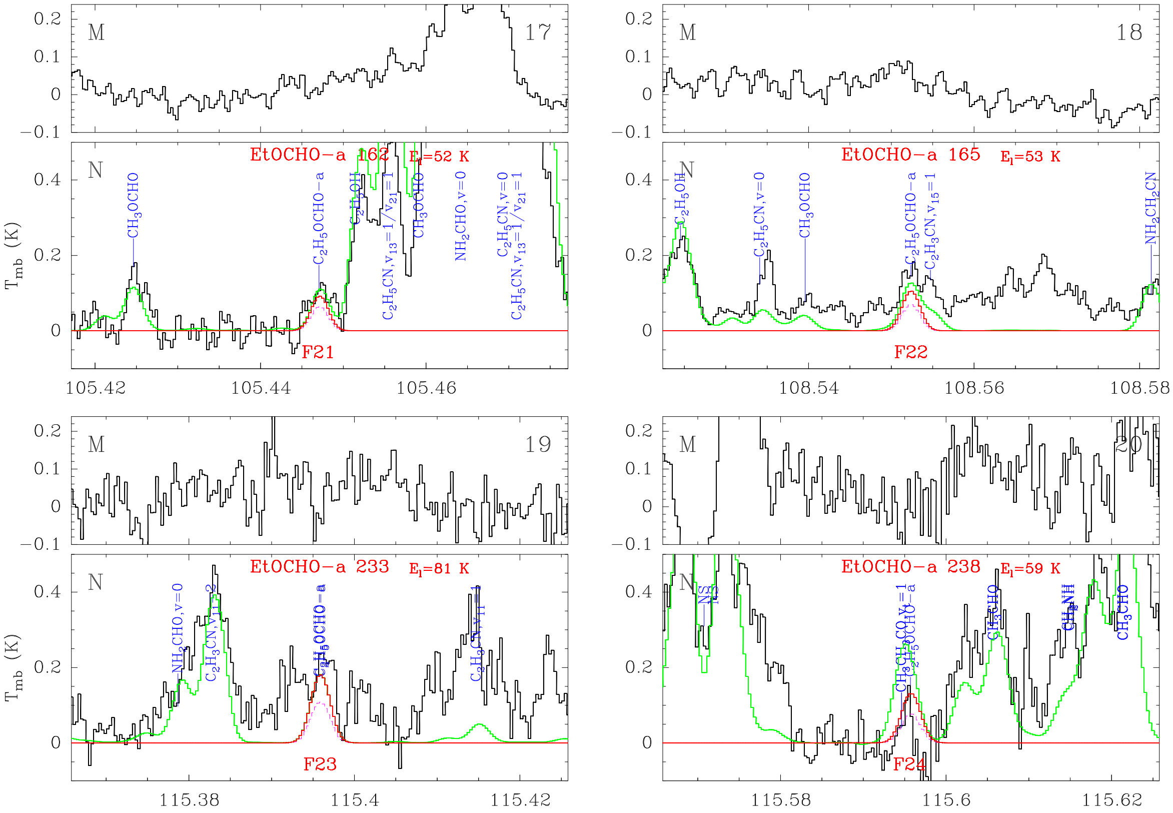

Fig. 1. (continued)

Table 9. Transitions of the *anti*-conformer of *n*-propyl cyanide observed with the IRAM 30 m telescope toward Sgr B2(N). The horizontal lines mark discontinuities in the observed frequency coverage. Only the transitions associated with a modeled line stronger than 20 mK are listed.

N^a (1)	Transition^b (2)	Frequency (MHz) (3)	Unc.^{c} (kHz) (4)	$E_l{}^d$ (K) (5)	$S\mu^2$ (D^2) (6)	σ^e (mK) (7)	Comments (8)
1	$18_{1,17} - 17_{1,16}$	80486.371	5	34	232.1	24	Blend with C_2H_5CN, $\upsilon_{13}=1/\upsilon_{21}=1$ and U-line
2	$19_{1,19} - 18_{1,18}$	82778.264	4	37	245.1	17	Blend with HC_3N, $\upsilon_5=1/\upsilon_7=3$ and C_2H_5CN
3	$19_{0,19} - 18_{0,18}$	83487.658	4	36	245.7	17	Blend with C_2H_3CN and U-line
4	$19_{2,18} - 18_{2,17}$	83906.011	5	40	243.1	16	Weak, blend with U-lines
5	$19_{6,14} - 18_{6,13}{}^\star$	84021.555	4	73	221.3	19	**Group detected**, partial blend with C_2H_5CN
7	$19_{7,12} - 18_{7,11}{}^\star$	84022.819	5	87	212.5	19	**Group detected**, partial blend with C_2H_5CN
9	$19_{5,15} - 18_{5,14}{}^\star$	84023.956	4	62	228.8	19	**Group detected**, partial blend with C_2H_5CN
11	$19_{8,11} - 18_{8,10}{}^\star$	84026.382	5	102	202.2	19	**Group detected**, partial blend with C_2H_5CN
13	$19_{9,10} - 18_{9,9}{}^\star$	84031.619	5	120	190.6	19	Blend with C_2H_5CN
15	$19_{4,16} - 18_{4,15}$	84033.299	4	53	234.9	19	Blend with C_2H_5CN
16	$19_{4,15} - 18_{4,14}$	84033.712	4	53	234.9	19	Blend with C_2H_5CN
17	$19_{10,9} - 18_{10,8}{}^\star$	84038.206	5	139	177.7	19	Blend with C_2H_5CN
19	$19_{11,8} - 18_{11,7}{}^\star$	84045.967	5	161	163.4	19	Blend with U-line
21	$19_{3,17} - 18_{3,16}$	84050.001	4	46	239.7	19	Blend with CH_3CH_3CO
22	$57_{3,54} - 57_{2,55}{}^\star$	84073.432	63	358	44.1	19	Blend with NH_2CHO
24	$19_{14,5} - 18_{14,4}{}^\star$	84075.429	7	238	112.4	19	Blend with NH_2CHO
26	$19_{2,17} - 18_{2,16}$	84408.080	4	40	243.1	19	Blend with ^{34}SO
27	$19_{1,18} - 18_{1,17}$	84940.688	5	38	245.1	22	Blend with C_2H_3CN
28	$20_{1,20} - 19_{1,19}$	87121.605	4	41	258.1	16	Blend with $HN^{13}C$ in absorption
29	$40_{1,39} - 40_{1,40}$	87829.125	82	172	0.8	17	Weak, partial blend with C_2H_5OCHO
30	$20_{0,20} - 19_{0,19}$	87829.384	5	40	258.6	17	Weak, partial blend with C_2H_5OCHO
31	$20_{2,19} - 19_{2,18}$	88310.935	5	44	256.2	17	Blend with $H^{13}CCCN$, $\upsilon_6=1$ and CH_3CH_3CO
32	$20_{6,14} - 19_{6,13}{}^\star$	88444.212	5	77	235.5	17	**Group detected**, partial blend with CH_3CH_3CO, C_2H_5OH, and U-line?
34	$20_{7,13} - 19_{7,12}{}^\star$	88445.075	5	91	227.0	17	**Group detected**, partial blend with CH_3CH_3CO, C_2H_5OH, and U-line?
36	$20_{5,16} - 19_{5,15}{}^\star$	88447.526	5	66	242.6	17	**Group detected**, partial blend with CH_3CH_3CO, C_2H_5OH, and U-line?
38	$20_{8,12} - 19_{8,11}{}^\star$	88448.528	5	106	217.4	17	**Group detected**, partial blend with CH_3CH_3CO, C_2H_5OH, and U-line?
40	$20_{9,11} - 19_{9,10}{}^\star$	88453.836	5	124	206.4	17	**Group detected**, partial blend with $C_2H_5{}^{13}CN$, $^{13}CH_3CH_2CN$, and $CH_2(OH)CHO$
42	$20_{4,17} - 19_{4,16}$	88458.794	5	57	248.4	17	**Group detected**, partial blend with $C_2H_5{}^{13}CN$, $^{13}CH_3CH_2CN$, and $CH_2(OH)CHO$
43	$20_{4,16} - 19_{4,15}$	88459.387	5	57	248.4	17	**Group detected**, partial blend with $C_2H_5{}^{13}CN$, $^{13}CH_3CH_2CN$, and $CH_2(OH)CHO$
44	$20_{10,10} - 19_{10,9}{}^\star$	88460.625	5	143	194.1	17	**Group detected**, partial blend with $C_2H_5{}^{13}CN$, $^{13}CH_3CH_2CN$, and $CH_2(OH)CHO$
46	$20_{11,9} - 19_{11,8}{}^\star$	88468.687	5	165	180.5	17	Weak
48	$20_{3,18} - 19_{3,17}$	88477.246	5	50	252.9	17	Blend with HNCO, $\upsilon_4=1$ and C_2H_5CN
49	$20_{12,8} - 19_{12,7}{}^\star$	88477.898	6	188	165.6	17	Blend with HNCO, $\upsilon_4=1$ and C_2H_5CN
51	$20_{3,17} - 19_{3,16}$	88507.586	5	50	252.9	17	Blend with C_2H_5CN, $\upsilon_{13}=1/\upsilon_{21}=1$ and $H^{13}CCCN$, $\upsilon_7=1$
52	$20_{2,18} - 19_{2,17}$	88890.385	5	45	256.2	21	Blend with $CH_2(OH)CHO$ and U-line
53	$20_{1,19} - 19_{1,18}$	89391.938	5	42	258.1	16	**Detected**, blend with CH_3OCHO, $\upsilon_t=1$
54	$21_{1,21} - 20_{1,20}$	91463.179	5	45	271.1	24	Blend with HC_3N, $\upsilon_6=\upsilon_7=1$ and U-line
55	$21_{0,21} - 20_{0,20}$	92164.912	5	44	271.6	27	**Detected**, blend with $CH_3{}^{13}CN$, $\upsilon_8=1$ and U-line?
56	$21_{2,20} - 20_{2,19}$	92714.159	5	49	269.2	28	Blend with CH_3OCH_3 and CH_3CH_3CO, $\upsilon_t=1$
57	$21_{6,16} - 20_{6,15}{}^\star$	92866.939	5	82	249.5	28	**Group detected**, uncertain baseline
59	$21_{7,14} - 20_{7,13}{}^\star$	92867.332	5	95	241.5	28	**Group detected**, uncertain baseline
61	$21_{8,13} - 20_{8,12}{}^\star$	92870.627	5	110	232.2	28	**Group detected**, uncertain baseline
63	$21_{5,17} - 20_{5,16}{}^\star$	92871.289	5	70	256.3	28	**Group detected**, uncertain baseline
65	$21_{9,12} - 20_{9,11}{}^\star$	92875.977	5	128	221.8	28	**Group detected**, uncertain baseline
67	$21_{10,11} - 20_{10,10}{}^\star$	92882.945	5	147	210.1	28	Blend with CH_3OCHO
69	$21_{4,18} - 20_{4,17}$	92884.684	5	61	261.8	28	Blend with CH_3OCHO
70	$21_{4,17} - 20_{4,16}$	92885.520	5	61	261.8	28	Blend with CH_3OCHO
71	$21_{11,10} - 20_{11,9}{}^\star$	92891.291	6	169	197.1	28	Noisy
73	$21_{12,9} - 20_{12,8}{}^\star$	92900.873	6	193	183.0	28	Blend with U-line
75	$21_{3,19} - 20_{3,18}$	92904.745	5	54	266.1	28	Blend with CH_3CH_3CO, $\upsilon_t=1$ and CH_3CH_3CO
76	$21_{3,18} - 20_{3,17}$	92943.421	5	54	266.2	28	Blend with CH_3OCHO
77	$21_{2,19} - 20_{2,18}$	93376.934	5	49	269.2	22	**Detected**
78	$21_{1,20} - 20_{1,19}$	93839.887	5	46	271.1	24	Blend with U-line
79	$22_{1,22} - 21_{1,21}$	95802.965	5	49	284.0	23	Blend with $^{13}CH_3CH_2CN$ and C_2H_5CN, $\upsilon_{13}=1/\upsilon_{21}=1$
80	$22_{0,22} - 21_{0,21}$	96494.470	5	49	284.5	32	Blend with CH_3OH, $\upsilon_t=1$ and CH_3CH_3CO

Table 9. continued.

N^a (1)	Transition^b (2)	Frequency (MHz) (3)	Unc.^{c} (kHz) (4)	$E_l{}^d$ (K) (5)	$S\mu^2$ (D^2) (6)	σ^e (mK) (7)	Comments (8)
81	$22_{2,21} - 21_{2,20}$	97115.607	5	53	282.3	21	Blend with U-line
82	$22_{7,15} - 21_{7,14}{}^\star$	97289.589	5	99	255.8	21	Blend with C_2H_3CN and OCS
84	$22_{6,17} - 21_{6,16}{}^\star$	97289.742	5	86	263.5	21	Blend with C_2H_3CN and OCS
86	$22_{8,14} - 21_{8,13}{}^\star$	97292.679	5	115	247.0	21	Blend with OCS
88	$22_{5,18} - 21_{5,17}{}^\star$	97295.253	5	75	269.9	21	Strong OCS
90	$22_{9,13} - 21_{9,12}{}^\star$	97298.036	5	132	237.0	21	Strong OCS
92	$22_{10,12} - 21_{10,11}{}^\star$	97305.160	5	152	225.8	21	Strong OCS
94	$22_{4,19} - 21_{4,18}$	97310.983	5	66	275.2	21	Blend with OCS and C_2H_3CN, $\upsilon_{11}=1$
95	$22_{4,18} - 21_{4,17}$	97312.143	5	66	275.2	21	Blend with OCS and C_2H_3CN, $\upsilon_{11}=1$
96	$22_{11,11} - 21_{11,10}{}^\star$	97313.773	6	173	213.5	21	Blend with OCS and C_2H_3CN, $\upsilon_{11}=1$
98	$22_{12,10} - 21_{12,9}{}^\star$	97323.712	6	197	199.9	21	Blend with CH_3OCHO
100	$22_{3,20} - 21_{3,19}$	97332.446	5	58	279.4	21	Blend with U-line
101	$22_{13,9} - 21_{13,8}{}^\star$	97334.877	7	223	185.2	21	Blend with U-line and CH_3OCHO
103	$22_{3,19} - 21_{3,18}$	97381.167	5	58	279.4	20	Blend with CH_3CH_3CO, $\upsilon_t=1$, uncertain baseline
104	$22_{2,20} - 21_{2,19}$	97867.394	5	53	282.3	20	**Detected**, uncertain baseline
105	$22_{1,21} - 21_{1,20}$	98284.291	5	51	284.0	18	Blend with CH_3OCH_3, CH_3OCHO, and U-line
106	$23_{1,23} - 22_{1,22}$	100140.951	5	54	296.9	14	Blend with CH_3OCHO, $\upsilon_t=1$ and HC_3N, $\upsilon_5=1/\upsilon_7=3$
107	$23_{0,23} - 22_{0,22}$	100818.358	5	53	297.4	20	Blend with $CH_3{}^{13}CH_2CN$ and U-line
108	$10_{4,6} - 11_{3,9}$	101512.348	5	23	1.2	16	**Detected**, small blend with CH_3CH_3CO, $\upsilon_t=1$
109	$23_{2,22} - 22_{2,21}$	101515.201	5	58	295.3	16	**Detected**, small blend with CH_3CH_3CO, $\upsilon_t=1$
110	$23_{7,16} - 22_{7,15}{}^\star$	101711.846	5	104	270.0	16	**Group detected**, partial blend with $^{13}CH_2CHCN$, uncertain baseline
112	$23_{6,18} - 22_{6,17}{}^\star$	101712.624	5	91	277.3	16	**Group detected**, partial blend with $^{13}CH_2CHCN$, uncertain baseline
114	$23_{8,15} - 22_{8,14}{}^\star$	101714.680	5	120	261.5	16	**Group detected**, uncertain baseline
116	$23_{5,19} - 22_{5,18}{}^\star$	101719.429	5	79	283.5	16	**Group detected**, small blend with $^{13}CH_2CHCN$
118	$23_{9,14} - 22_{9,13}{}^\star$	101720.011	5	137	252.0	16	**Group detected**, small blend with $^{13}CH_2CHCN$
120	$23_{10,13} - 22_{10,12}{}^\star$	101727.266	5	157	241.3	16	Blend with CH_3OCHO and U-line?
122	$23_{11,12} - 22_{11,11}{}^\star$	101736.128	6	178	229.5	16	Blend with CH_3OH
124	$23_{4,20} - 22_{4,19}$	101737.702	5	70	288.6	16	Blend with CH_3OH
125	$23_{4,19} - 22_{4,18}$	101739.288	5	70	288.6	16	Blend with CH_3OH
126	$23_{12,11} - 22_{12,10}{}^\star$	101746.410	6	202	216.6	16	Blend with U-line and C_2H_5CN, $\upsilon_{13}=1/\upsilon_{21}=1$
128	$23_{13,10} - 22_{13,9}{}^\star$	101757.997	7	227	202.5	16	Blend with U-line
130	$23_{3,21} - 22_{3,20}$	101760.286	5	63	292.5	16	Blend with U-line
131	$23_{17,6} - 22_{17,5}{}^\star$	101816.271	10	350	135.0	34	Blend with CH_3CH_3CO, $\upsilon_t=1$ and $\upsilon_t=0$, and U-line
133	$23_{3,20} - 22_{3,19}$	101820.997	5	63	292.5	34	Blend with CH_3CH_3CO, $\upsilon_t=1$ and $\upsilon_t=0$, and U-line
134	$25_{3,22} - 25_{2,23}$	102358.115	5	73	13.4	30	Blend with U-line
135	$23_{2,21} - 22_{2,20}$	102361.359	5	58	295.3	30	Blend with U-line
136	$23_{1,22} - 22_{1,21}$	102724.897	5	55	296.9	37	Noisy, baseline problem
137	$24_{1,24} - 23_{1,23}$	104477.131	5	59	309.9	48	Blend with U-line
138	$24_{0,24} - 23_{0,23}$	105136.938	5	58	310.3	28	Blend with U-line
139	$24_{2,23} - 23_{2,22}$	105912.868	5	63	308.3	43	Blend with $^{13}CH_3OH$
140	$24_{7,17} - 23_{7,16}{}^\star$	106134.103	5	109	284.1	25	Blend with NH_2CHO
142	$37_{2,36} - 37_{1,37}$	106135.161	50	148	12.1	25	Blend with NH_2CHO
143	$24_{6,19} - 23_{6,18}{}^\star$	106135.587	5	96	291.1	25	Blend with NH_2CHO
145	$24_{8,16} - 23_{8,15}{}^\star$	106136.628	5	124	276.0	25	Blend with NH_2CHO
147	$24_{9,15} - 23_{9,14}{}^\star$	106141.897	5	142	266.9	25	Blend with NH_2CHO
149	$24_{5,20} - 23_{5,19}{}^\star$	106143.824	5	84	297.0	25	Blend with NH_2CHO and C_2H_5CN, $\upsilon_{13}=1/\upsilon_{21}=1$
151	$24_{10,14} - 23_{10,13}{}^\star$	106149.258	5	161	256.6	25	Blend with C_2H_5CN, $\upsilon_{13}=1/\upsilon_{21}=1$
153	$24_{11,13} - 23_{11,12}{}^\star$	106158.350	6	183	245.3	25	Blend with CH_3CH_3CO and $CH_2CH^{13}CN$
155	$24_{4,21} - 23_{4,20}$	106164.853	5	75	301.9	25	Blend with $CH_2CH^{13}CN$ and C_2H_5CN, $\upsilon_{13}=1/\upsilon_{21}=1$
156	$24_{4,20} - 23_{4,19}$	106166.991	5	75	301.9	25	Blend with $CH_2CH^{13}CN$ and C_2H_5CN, $\upsilon_{13}=1/\upsilon_{21}=1$
157	$24_{12,12} - 23_{12,11}{}^\star$	106168.961	6	207	232.9	25	Blend with C_2H_5CN, $\upsilon_{13}=1/\upsilon_{21}=1$
159	$24_{13,11} - 23_{13,10}{}^\star$	106180.959	7	232	219.4	25	Blend with C_2H_5CN, $\upsilon_{13}=1/\upsilon_{21}=1$
161	$24_{3,22} - 23_{3,21}$	106188.197	5	68	305.7	25	**Detected**, noisy
162	$24_{14,10} - 23_{14,9}{}^\star$	106194.262	7	260	204.8	25	Blend with CH_3CH_3CO, $\upsilon_t=1$ and U-line
164	$24_{18,6} - 23_{18,5}{}^\star$	106259.676	12	391	135.8	25	Blend with $^{13}CH_3CH_2CN$
166	$24_{3,21} - 23_{3,20}$	106263.099	5	68	305.6	25	Blend with $^{13}CH_3CH_2CN$ and U-line
167	$24_{2,22} - 23_{2,21}$	106858.357	5	63	308.4	24	Blend with U-line, C_2H_5OH, and CH_3CH_3CO, $\upsilon_t=1$
168	$24_{1,23} - 23_{1,22}$	107161.444	5	60	309.9	24	Blend with CH_3OH and $^{13}CH_3CN$
169	$25_{1,25} - 24_{1,24}$	108811.506	5	64	322.9	20	Blend with ^{13}CN in absorption and C_2H_3CN
170	$25_{0,25} - 24_{0,24}$	109450.626	5	63	323.2	36	Blend with HC_3N, $\upsilon_7=1$ and OCS
171	$78_{4,74} - 78_{3,75}$	109452.759	321	668	59.9	36	Blend with HC_3N, $\upsilon_7=1$ and OCS
172	$25_{2,24} - 24_{2,23}$	110308.536	5	68	321.3	24	Strong $CH_3{}^{13}CN$

Table 9. continued.

N^a (1)	Transition^b (2)	Frequency (MHz) (3)	Unc.^{c} (kHz) (4)	$E_l{}^d$ (K) (5)	$S\mu^2$ (D^2) (6)	σ^e (mK) (7)	Comments (8)
173	$25_{7,18} - 24_{7,17}{}^{\star}$	110556.359	5	114	298.1	32	Blend with U-lines and CH_3OCHO
175	$25_{8,17} - 24_{8,16}{}^{\star}$	110558.521	5	130	290.3	32	Blend with U-lines and CH_3OCHO
177	$25_{6,20} - 24_{6,19}{}^{\star}$	110558.636	5	101	304.8	32	Blend with U-lines and CH_3OCHO
179	$25_{9,16} - 24_{9,15}{}^{\star}$	110563.690	5	147	281.5	32	Blend with U-line
181	$25_{5,21} - 24_{5,20}{}^{\star}$	110568.450	5	89	310.5	32	Blend with CH_3OCHO, $\upsilon_t=1$
183	$25_{10,15} - 24_{10,14}{}^{\star}$	110571.130	6	167	271.7	32	Blend with CH_3OCHO, $\upsilon_t=1$
185	$25_{11,14} - 24_{11,13}{}^{\star}$	110580.433	6	188	260.8	32	Blend with CH_3CH_3CO and U-line, uncertain baseline
187	$86_{6,80} - 85_{7,79}$	110581.350	563	826	15.9	32	Blend with CH_3CH_3CO and U-line, uncertain baseline
188	$25_{12,13} - 24_{12,12}{}^{\star}$	110591.357	6	212	248.9	32	Blend with U-line, $CH_3{}^{13}CN$, $\upsilon_8=1$, and HNCO, $\upsilon_4=1$
190	$25_{4,22} - 24_{4,21}$	110592.442	5	80	315.2	32	Blend with U-line, $CH_3{}^{13}CN$, $\upsilon_8=1$, and HNCO, $\upsilon_4=1$
191	$28_{3,26} - 28_{2,27}$	110593.409	5	90	14.3	32	Blend with U-line, $CH_3{}^{13}CN$, $\upsilon_8=1$, and HNCO, $\upsilon_4=1$
192	$25_{4,21} - 24_{4,20}$	110595.288	5	80	315.1	32	Blend with $CH_3{}^{13}CN$, $\upsilon_8=1$ and HNCO, $\upsilon_4=1$
193	$46_{1,45} - 46_{1,46}$	110603.457	123	227	0.8	32	Blend with CH_3CN, $\upsilon_8=1$ and U-line
194	$25_{13,12} - 24_{13,11}{}^{\star}$	110603.755	7	237	236.0	32	Blend with CH_3CN, $\upsilon_8=1$ and U-line
196	$25_{3,23} - 24_{3,22}$	110616.104	5	73	318.8	32	Blend with CH_3CN, $\upsilon_8=1$ and $CH_3{}^{13}CN$, $\upsilon_8=1$
197	$25_{14,11} - 24_{14,10}{}^{\star}$	110617.532	7	265	222.0	32	Blend with CH_3CN, $\upsilon_8=1$ and $CH_3{}^{13}CN$, $\upsilon_8=1$
199	$25_{15,10} - 24_{15,9}{}^{\star}$	110632.625	8	295	207.0	32	Blend with $CH_3{}^{13}CN$, $\upsilon_8=1$ and CH_3CN, $\upsilon_8=1$
201	$25_{19,6} - 24_{19,5}{}^{\star}$	110705.543	14	434	136.6	32	Strong CH_3CN, $\upsilon_8=1$
203	$25_{3,22} - 24_{3,21}$	110707.662	5	73	318.8	32	Strong CH_3CN, $\upsilon_8=1$
204	$25_{2,23} - 24_{2,22}$	111357.863	5	68	321.4	35	Noisy
205	$25_{1,24} - 24_{1,23}$	111593.662	5	65	322.9	29	**Detected**
206	$26_{1,26} - 25_{1,25}$	113144.084	5	69	335.9	40	Strong CN in absorption
207	$26_{0,26} - 25_{0,25}$	113759.873	5	69	336.1	34	Blend with CH_3OCHO and U-line
208	$26_{2,25} - 25_{2,24}$	114702.134	5	73	334.4	37	Blend with CH_3OCH_3
209	$26_{7,19} - 25_{7,18}{}^{\star}$	114978.615	5	119	312.0	59	Blend with C_2H_3CN, $\upsilon_{11}=3$ and $^{13}CH_3OH$
211	$26_{8,18} - 25_{8,17}{}^{\star}$	114980.356	5	135	304.5	59	Blend with C_2H_3CN, $\upsilon_{11}=3$ and $^{13}CH_3OH$
213	$26_{6,21} - 25_{6,20}{}^{\star}$	114981.774	5	106	318.5	59	Blend with C_2H_3CN, $\upsilon_{11}=3$, $^{13}CH_3OH$, and C_2H_3CN, $\upsilon_{11}=3$
215	$26_{9,17} - 25_{9,16}{}^{\star}$	114985.387	5	152	296.1	59	Blend with C_2H_3CN, $\upsilon_{11}=3$ and CH_3CH_3CO
217	$26_{10,16} - 25_{10,15}{}^{\star}$	114992.878	6	172	286.6	59	Blend with CH_3CH_3CO
219	$26_{5,22} - 25_{5,21}{}^{\star}$	114993.314	5	95	323.9	59	Blend with CH_3CH_3CO
221	$26_{11,15} - 25_{11,14}{}^{\star}$	115002.371	6	193	276.2	59	Blend with C_2H_5CN, $\upsilon_{13}=1/\upsilon_{21}=1$ and C_2H_3CN, $\upsilon_{11}=1$
223	$26_{12,14} - 25_{12,13}{}^{\star}$	115013.593	6	217	264.7	59	Blend with C_2H_5CN, $\upsilon_{13}=1/\upsilon_{21}=1$, $CH_2{}^{13}CHCN$, and U-line
225	$26_{4,23} - 25_{4,22}$	115020.476	5	85	328.4	59	Blend with U-line
226	$26_{4,22} - 25_{4,21}$	115024.221	5	85	328.4	59	Blend with U-line
227	$26_{13,13} - 25_{13,12}{}^{\star}$	115026.378	7	243	252.3	59	Blend with U-line and C_2H_5OH
229	$26_{14,12} - 25_{14,11}{}^{\star}$	115040.619	8	270	238.9	59	Blend with U-line
231	$26_{3,24} - 25_{3,23}$	115043.924	5	78	331.9	59	Blend with U-line
232	$26_{15,11} - 25_{15,10}{}^{\star}$	115056.245	8	300	224.4	59	Blend with $H^{13}CCCN$, $\upsilon_7=1$
234	$64_{4,60} - 64_{3,61}$	115150.722	157	453	43.9	59	Blend with C_2H_3CN, CH_3OCHO, $\upsilon_t=1$, NS, and CH_3CH_3CO, $\upsilon_t=1$
235	$26_{20,6} - 25_{20,5}{}^{\star}$	115154.006	17	479	137.3	59	Blend with CH_3OCHO, $\upsilon_t=1$, NS, and CH_3CH_3CO, $\upsilon_t=1$
237	$26_{3,23} - 25_{3,22}$	115154.885	5	78	331.9	59	Blend with CH_3OCHO, $\upsilon_t=1$, NS, and CH_3CH_3CO, $\upsilon_t=1$
238	$26_{2,24} - 25_{2,23}$	115859.309	5	73	334.4	79	Weak, blend with a$(CH_2OH)_2$ and C_2H_5OH
239	$33_{2,32} - 32_{2,31}$	145394.105	5	116	425.3	25	Blend with U-line and NH_2CH_2CN
240	$34_{1,34} - 33_{1,33}$	147742.893	6	118	439.5	31	Partial blend with C_2H_5CN and CH_3CN, $\upsilon_8=1$, uncertain baseline
241	$37_{8,29} - 36_{8,28}{}^{\star}$	163616.044	6	207	456.4	38	Blend with SO_2
243	$37_{9,28} - 36_{9,27}{}^{\star}$	163616.543	6	225	450.4	38	Blend with SO_2
245	$65_{4,62} - 65_{3,63}$	163620.536	185	464	33.9	38	Blend with SO_2
246	$37_{10,27} - 36_{10,26}{}^{\star}$	163622.456	6	244	443.8	38	Blend with U-line, uncertain baseline
248	$37_{7,31} - 36_{7,30}{}^{\star}$	163623.355	5	192	461.6	38	Blend with U-line, uncertain baseline
250	$37_{11,26} - 36_{11,25}{}^{\star}$	163632.454	7	266	436.4	38	Blend with NH_2CH_2CN, uncertain baseline
252	$37_{6,32} - 36_{6,31}{}^{\star}$	163643.143	5	178	466.1	38	Blend with NH_2CH_2CN, uncertain baseline
254	$37_{12,25} - 36_{12,24}{}^{\star}$	163645.748	7	289	428.3	38	Blend with NH_2CH_2CN, uncertain baseline
256	$37_{13,24} - 36_{13,23}{}^{\star}$	163661.850	8	315	419.6	38	Blend with C_2H_5OCHO, uncertain baseline
258	$37_{14,23} - 36_{14,22}{}^{\star}$	163680.443	8	343	410.2	38	Blend with C_2H_5CN, $\upsilon_{13}=1/\upsilon_{21}=1$ and $HC^{13}CCN$, $\upsilon_7=1$
260	$37_{5,33} - 36_{5,32}$	163684.984	5	167	470.0	38	Blend with $HC^{13}CCN$, $\upsilon_7=1$ and C_2H_5CN
261	$37_{5,32} - 36_{5,31}$	163686.545	5	167	470.0	38	Blend with $HC^{13}CCN$, $\upsilon_7=1$ and C_2H_5CN
262	$37_{15,22} - 36_{15,21}{}^{\star}$	163701.318	9	373	400.1	38	Blend with $HC^{13}CCN$, $\upsilon_7=1$
264	$37_{3,35} - 36_{3,34}$	163715.634	5	151	475.5	38	Blend with CH_3CH_3CO, $\upsilon_t=1$
265	$37_{16,21} - 36_{16,20}{}^{\star}$	163724.332	9	404	389.2	38	Blend with g-C_3H_7CN and U-line
267	$39_{9,30} - 38_{9,29}{}^{\star}$	172456.851	6	241	477.7	44	Strong C_2H_5CN and CH_3OCHO, $\upsilon_t=1$
269	$39_{8,31} - 38_{8,30}{}^{\star}$	172457.861	6	223	483.3	44	Strong C_2H_5CN and CH_3OCHO, $\upsilon_t=1$
271	$39_{10,29} - 38_{10,28}{}^{\star}$	172461.990	7	260	471.4	44	Strong C_2H_5CN and CH_3OCHO, $\upsilon_t=1$
273	$39_{7,33} - 38_{7,32}{}^{\star}$	172467.829	6	208	488.4	44	Strong CH_3OCHO, $\upsilon_t=1$ and C_2H_3CN

Table 9. continued.

N^a (1)	Transition^b (2)	Frequency (MHz) (3)	Unc.^{c} (kHz) (4)	$E_l{}^d$ (K) (5)	$S\mu^2$ (D^2) (6)	σ^e (mK) (7)	Comments (8)
275	$39_{11,28}-38_{11,27}{}^{\star}$	172471.720	7	282	464.4	44	Strong CH_3OCHO, $\upsilon_t=1$ and C_2H_3CN
277	$39_{12,27}-38_{12,26}{}^{\star}$	172485.116	8	305	456.8	44	Blend with C_2H_5CN
279	$39_{6,34}-38_{6,33}{}^{\star}$	172492.223	5	194	492.7	44	Blend with C_2H_5CN
281	$39_{13,26}-38_{13,25}{}^{\star}$	172501.606	8	331	448.5	44	Blend with C_2H_5CN, $\upsilon_{13}=1/\upsilon_{21}=1$
283	$52_{2,50}-51_{3,49}$	172516.550	77	291	14.0	44	Blend with C_2H_5CN, $\upsilon_{13}=1/\upsilon_{21}=1$ and CH_3OCHO, $\upsilon_t=1$
284	$39_{14,25}-38_{14,24}{}^{\star}$	172520.819	8	359	439.6	44	Blend with CH_3OCHO, $\upsilon_t=1$, $HC^{13}CCN$, $\upsilon_7=1$, and $HC^{13}CCN$, $\upsilon_6=1$
286	$39_{5,35}-38_{5,34}$	172542.025	5	183	496.3	44	Blend with NH_2CH_2CN and $HCC^{13}CN$, $\upsilon_6=1$
287	$39_{15,24}-38_{15,23}{}^{\star}$	172542.509	9	388	429.9	44	Blend with NH_2CH_2CN and $HCC^{13}CN$, $\upsilon_6=1$
289	$39_{5,34}-38_{5,33}$	172544.526	5	183	496.3	44	Blend with $HCC^{13}CN$, $\upsilon_6=1$ and $HCC^{13}CN$, $\upsilon_7=1$
290	$39_{3,37}-38_{3,36}$	172551.469	5	167	501.6	44	Blend with $HCC^{13}CN$, $\upsilon_6=1$ and $HCC^{13}CN$, $\upsilon_7=1$
291	$39_{16,23}-38_{16,22}{}^{\star}$	172566.508	9	420	419.6	44	Blend with NH_2CH_2CN
293	$39_{17,22}-38_{17,21}{}^{\star}$	172592.700	10	454	408.7	44	Blend with $CH_2(OH)CHO$ and U-line
295	$39_{18,21}-38_{18,20}{}^{\star}$	172621.005	11	490	397.1	44	Blend with NH_2CH_2CN, t-HCOOH, and U-line?
297	$39_{4,36}-38_{4,35}$	172622.501	5	174	499.2	44	Blend with NH_2CH_2CN, t-HCOOH, and U-line?
298	$39_{19,20}-38_{19,19}{}^{\star}$	172651.366	13	528	384.8	44	Blend with C_2H_5CN, $\upsilon_{20}=1$ and U-line
300	$39_{20,19}-38_{20,18}{}^{\star}$	172683.745	16	568	371.8	44	Strong $H^{13}CN$ in absorption and CH_3OCHO
302	$39_{4,35}-38_{4,34}$	172684.518	5	174	499.2	44	Strong $H^{13}CN$ in absorption and CH_3OCHO
303	$46_{2,45}-45_{2,44}$	202062.851	7	223	593.9	138	Blend with $CH_3{}^{13}CN$
304	$46_{1,45}-45_{1,44}$	203271.058	6	222	594.2	161	Strong $H^{13}CCCN$, $\upsilon_7=1$ and C_2H_3CN, $\upsilon_{11}=1$
305	$46_{9,37}-45_{9,36}{}^{\star}$	203392.918	7	303	572.3	161	Strong SO_2 and C_2H_5CN
307	$46_{10,36}-45_{10,35}{}^{\star}$	203393.942	8	323	567.0	161	Strong SO_2 and C_2H_5CN
309	$46_{8,39}-45_{8,38}{}^{\star}$	203401.192	7	286	577.1	161	Strong C_2H_5CN and CH_3OCH_3
311	$46_{11,35}-45_{11,34}{}^{\star}$	203401.696	8	344	561.1	161	Strong C_2H_5CN and CH_3OCH_3
313	$46_{12,34}-45_{12,33}{}^{\star}$	203414.661	9	368	554.6	161	Strong CH_3OCH_3 and $^{13}CH_2CHCN$
315	$46_{3,44}-45_{3,43}$	203419.779	6	229	592.5	161	Blend with $^{13}CH_2CHCN$
316	$46_{7,40}-45_{7,39}{}^{\star}$	203423.393	6	270	581.4	161	Blend with $^{13}CH_2CHCN$
318	$46_{13,33}-45_{13,32}{}^{\star}$	203431.894	9	393	547.6	161	Blend with CH_3CN, $\upsilon_8=2$
320	$46_{14,32}-45_{14,31}{}^{\star}$	203452.784	9	421	540.0	161	Blend with CH_3CN, $\upsilon_8=2$
322	$46_{6,41}-45_{6,40}$	203468.489	6	257	585.0	161	Blend with CH_3CN, $\upsilon_8=2$ and CH_3OCHO
323	$46_{6,40}-45_{6,39}$	203468.859	6	257	585.0	161	Blend with CH_3CN, $\upsilon_8=2$ and CH_3OCHO
324	$46_{15,31}-45_{15,30}{}^{\star}$	203476.924	9	451	531.9	161	Blend with CH_3OCHO and CH_3CN, $\upsilon_8=2$
326	$46_{16,30}-45_{16,29}{}^{\star}$	203504.034	9	483	523.1	161	Blend with $^{34}SO_2$ and CH_3CN, $\upsilon_8=2$
328	$46_{17,29}-45_{17,28}{}^{\star}$	203533.921	10	517	513.8	161	Blend with CH_3CN, $\upsilon_8=2$
330	$16_{7,9}-17_{6,12}{}^{\star}$	203535.308	25	70	1.6	161	Blend with CH_3CN, $\upsilon_8=2$ and C_2H_5OCHO
332	$46_{5,42}-45_{5,41}$	203552.152	6	245	588.1	161	Blend with CH_3CN, $\upsilon_8=2$ and $H^{13}CCCN$, $\upsilon_7=1$
333	$46_{5,41}-45_{5,40}$	203562.997	6	245	588.2	161	Strong CH_3CN, $\upsilon_8=2$, CH_3OCH_3, and $^{13}CH_2CHCN$
334	$46_{18,28}-45_{18,27}{}^{\star}$	203566.446	10	552	504.0	161	Strong CH_3CN, $\upsilon_8=2$, CH_3OCH_3, and $^{13}CH_2CHCN$
336	$46_{19,27}-45_{19,26}{}^{\star}$	203601.513	11	590	493.6	161	Blend with CH_3OCHO and CH_3CH_3CO
338	$46_{20,26}-45_{20,25}{}^{\star}$	203639.052	14	630	482.7	161	Blend with C_2H_5CN
340	$46_{4,43}-45_{4,42}$	203653.642	6	236	590.6	161	Blend with C_2H_5CN, C_2H_5OH, and U-line
341	$46_{21,25}-45_{21,24}{}^{\star}$	203679.015	17	672	471.1	161	Blend with CH_3CN, $\upsilon_8=2$
343	$46_{23,23}-45_{23,22}{}^{\star}$	203766.086	29	762	446.4	364	Blend with C_2H_5OCHO
345	$47_{1,47}-46_{1,46}$	203773.957	14	227	607.7	364	Blend with $^{13}CH_2CHCN$
346	$46_{4,42}-45_{4,41}$	203841.799	6	236	590.6	364	Blend with C_2H_5CN and CH_3OCHO
347	$47_{0,47}-46_{0,46}$	203894.538	14	227	607.7	364	Blend with U-line
348	$46_{2,44}-45_{2,43}$	205486.337	8	226	594.0	100	Blend with CH_3OCHO
349	$41_{2,40}-40_{1,39}$	205486.671	20	176	17.7	100	Blend with CH_3OCHO
350	$47_{2,46}-46_{2,45}$	206403.502	7	233	606.8	106	Strong C_2H_5CN
351	$47_{1,46}-46_{1,45}$	207565.934	6	232	607.1	282	Blend with C_2H_5OH and U-line?
352	$47_{9,38}-46_{9,37}{}^{\star}$	207811.666	7	313	585.8	173	Blend with $^{13}CH_3OH$ and C_2H_5CN
354	$47_{10,37}-46_{10,36}{}^{\star}$	207811.909	8	332	580.5	173	Blend with $^{13}CH_3OH$ and C_2H_5CN
356	$47_{11,36}-46_{11,35}{}^{\star}$	207819.239	8	354	574.7	173	Blend with C_2H_5CN and C_2H_5OCHO
358	$47_{3,45}-46_{3,44}$	207820.872	6	239	605.5	173	Blend with C_2H_5CN and C_2H_5OCHO
359	$47_{8,40}-46_{8,39}{}^{\star}$	207821.249	7	295	590.5	173	Blend with C_2H_5CN, C_2H_5OCHO, and C_2H_5OH
361	$47_{12,35}-46_{12,34}{}^{\star}$	207832.034	9	378	568.5	173	Strong NS, $CH_2{}^{13}CHCN$, and C_2H_5CN
363	$47_{7,41}-46_{7,40}{}^{\star}$	207845.603	7	280	594.7	173	Strong C_2H_5CN, $\upsilon_{13}=1/\upsilon_{21}=1$
365	$47_{13,34}-46_{13,33}{}^{\star}$	207849.289	9	403	561.6	173	Strong C_2H_5CN, $\upsilon_{13}=1/\upsilon_{21}=1$
367	$47_{14,33}-46_{14,32}{}^{\star}$	207870.351	9	431	554.2	173	Blend with C_2H_5OH, uncertain baseline
369	$47_{6,42}-46_{6,41}$	207894.282	6	267	598.2	173	Blend with C_2H_5OH and $CH_2{}^{13}CHCN$
370	$47_{6,41}-46_{6,40}{}^{\star}$	207894.750	6	267	598.2	173	Blend with C_2H_5OH and $CH_2{}^{13}CHCN$
372	$47_{15,33}-46_{15,32}$	207894.786	10	461	546.2	173	Blend with C_2H_5OH and $CH_2{}^{13}CHCN$
373	$47_{16,31}-46_{16,30}{}^{\star}$	207922.295	10	492	537.6	173	Blend with C_2H_3CN, $\upsilon_{15}=1$, $C_2H_5{}^{13}CN$, and CH_3CH_3CO, $\upsilon_t=1$
375	$47_{17,30}-46_{17,29}{}^{\star}$	207952.671	10	526	528.5	173	Blend with C_2H_5CN and $CH_2{}^{13}CHCN$

Table 9. continued.

N^a (1)	Transition^b (2)	Frequency (MHz) (3)	Unc.^{c} (kHz) (4)	$E_l{}^d$ (K) (5)	$S\mu^2$ (D^2) (6)	σ^e (mK) (7)	Comments (8)
377	$15_{7,8} - 16_{6,11}{}^{\star}$	207955.703	25	66	1.4	173	Blend with C_2H_5CN and $CH_2{}^{13}CHCN$
379	$47_{5,43} - 46_{5,42}$	207983.470	6	255	601.2	173	Blend with C_2H_5OH and $CH_2{}^{13}CHCN$
380	$47_{18,29} - 46_{18,28}{}^{\star}$	207985.767	10	562	518.9	173	Blend with C_2H_5OH and $CH_2{}^{13}CHCN$
382	$47_{5,42} - 46_{5,41}$	207996.582	6	255	601.2	173	Blend with C_2H_5CN, C_2H_5OH, and $CH_2CH^{13}CN$
383	$47_{19,28} - 46_{19,27}{}^{\star}$	208021.478	11	600	508.7	173	Blend with $CH_2{}^{13}CHCN$
385	$47_{20,27} - 46_{20,26}{}^{\star}$	208059.729	14	640	498.0	173	Blend with C_2H_5CN
387	$48_{1,48} - 47_{1,47}$	208076.611	16	236	620.6	173	Blend with C_2H_5CN and CH_3CH_3CO
388	$47_{4,44} - 46_{4,43}$	208085.930	6	246	603.7	173	Blend with CH_3CH_3CO and $CH_2CH^{13}CN$
389	$47_{21,26} - 46_{21,25}{}^{\star}$	208100.469	17	682	486.7	173	Blend with $CH_2CH^{13}CN$, C_2H_5CN, $v_{13}=1/v_{21}=1$, and $CH_2{}^{13}CHCN$
391	$48_{0,48} - 47_{0,47}$	208185.442	16	236	620.6	173	Blend with C_2H_5OH and $CH_2{}^{13}CHCN$
392	$47_{23,24} - 46_{23,23}{}^{\star}$	208189.277	29	771	462.5	173	Blend with C_2H_5OH and $CH_2{}^{13}CHCN$
394	$47_{25,22} - 46_{25,21}{}^{\star}$	208287.742	46	869	436.0	168	Blend with C_2H_5OH
396	$47_{4,43} - 46_{4,42}$	208302.740	7	246	603.7	168	Blend with C_2H_5CN
397	$47_{3,44} - 46_{3,43}$	209390.960	9	239	605.7	58	Blend with C_2H_5OH and C_2H_3CN, $v_{15}=1$
398	$47_{2,45} - 46_{2,44}$	209918.318	9	235	607.0	45	Strong $^{13}CH_3CH_2CN$, C_2H_5OH, and CH_3OCHO
399	$48_{2,47} - 47_{2,46}$	210741.480	50	243	619.6	37	Blend with C_2H_3CN, $v_{11}=3$ and C_2H_5CN, $v_{13}=1/v_{21}=1$, uncertain baseline
400	$48_{1,47} - 47_{1,46}$	211856.190	50	242	620.1	47	Blend with U-line
401	$48_{3,46} - 47_{3,45}$	212219.540	50	249	618.5	36	Blend with C_2H_5CN, $v_{20}=1$
402	$48_{10,38} - 47_{10,37}{}^{\star}$	212229.670	50	342	594.1	36	Strong C_2H_5CN, $v_{20}=1$ and NH_2CHO
404	$48_{9,39} - 47_{9,38}{}^{\star}$	212230.190	50	323	599.2	36	Strong C_2H_5CN, $v_{20}=1$ and NH_2CHO
406	$48_{11,37} - 47_{11,36}{}^{\star}$	212236.507	9	364	588.4	36	Strong C_2H_5CN, $v_{20}=1$ and NH_2CHO
408	$48_{8,40} - 47_{8,39}{}^{\star}$	212241.200	50	305	603.8	36	Strong NH_2CHO
410	$48_{12,36} - 47_{12,35}{}^{\star}$	212249.060	50	388	582.2	36	Strong NH_2CHO and NH_2CHO, $v_{12}=1$
412	$48_{13,35} - 47_{13,34}{}^{\star}$	212266.320	50	413	575.5	36	Strong C_2H_5OH, $NH_2{}^{13}CHO$, and NH_2CHO
414	$48_{7,41} - 47_{7,40}{}^{\star}$	212267.790	50	290	607.8	36	Strong C_2H_5OH, $NH_2{}^{13}CHO$, and NH_2CHO
416	$48_{14,34} - 47_{14,33}{}^{\star}$	212287.590	50	441	568.2	36	Blend with C_2H_5CN, $v_{13}=1/v_{21}=1$ and $v=0$, and U-line
418	$48_{15,33} - 47_{15,32}{}^{\star}$	212312.290	50	471	560.4	36	Strong C_2H_3CN, $v_{11}=1$ and NH_2CHO
420	$48_{6,43} - 47_{6,42}$	212320.280	50	276	611.3	36	Strong C_2H_3CN, $v_{11}=1$ and NH_2CHO
421	$48_{6,42} - 47_{6,41}$	212320.770	50	276	611.3	36	Strong C_2H_3CN, $v_{11}=1$ and NH_2CHO
422	$48_{16,32} - 47_{16,31}{}^{\star}$	212340.190	50	502	552.0	36	Strong C_2H_3CN
424	$48_{17,31} - 47_{17,30}{}^{\star}$	212371.060	50	536	543.1	36	Blend with $NH_2{}^{13}CHO$, $v_{12}=1$, uncertain baseline
426	$14_{7,7} - 15_{6,10}{}^{\star}$	212375.891	25	63	1.2	36	Blend with $NH_2{}^{13}CHO$, $v_{12}=1$, uncertain baseline
428	$49_{1,49} - 48_{1,48}$	212378.480	50	246	633.5	36	Blend with $NH_2{}^{13}CHO$, $v_{12}=1$, uncertain baseline
429	$48_{18,30} - 47_{18,29}{}^{\star}$	212404.720	50	572	533.7	36	Strong NH_2CHO, $v_{12}=1$ and $H^{13}CCCN$, $v_7=1$
431	$48_{5,44} - 47_{5,43}$	212415.060	50	265	614.2	36	Blend with NH_2CHO
432	$48_{5,43} - 47_{5,42}$	212430.890	50	265	614.3	36	Strong NH_2CHO
433	$48_{19,29} - 47_{19,28}{}^{\star}$	212441.110	50	610	523.7	99	Blend with NH_2CHO and CH_3OCHO
435	$49_{0,49} - 48_{0,48}$	212476.620	50	246	633.6	99	Blend with C_2H_5OH and CH_3OCHO
436	$48_{20,28} - 47_{20,27}{}^{\star}$	212480.030	50	650	513.3	99	Blend with $^{13}CH_3OH$, $v_t=1$ and CH_3CHO
438	$48_{4,45} - 47_{4,44}$	212517.790	50	256	616.8	99	Blend with C_2H_5CN and C_2H_5OH, uncertain baseline
439	$48_{21,27} - 47_{21,26}{}^{\star}$	212521.490	50	692	502.1	99	Blend with C_2H_5CN and C_2H_5OH, uncertain baseline
441	$48_{26,22} - 47_{26,21}{}^{\star}$	212766.374	57	931	438.8	99	Blend with $^{13}CH_3OH$ and C_2H_5CN, uncertain baseline
443	$48_{4,44} - 47_{4,43}$	212766.640	50	256	616.7	99	Blend with $^{13}CH_3OH$ and C_2H_5CN, uncertain baseline
444	$48_{3,45} - 47_{3,44}$	213912.029	10	249	618.6	48	Blend with $^{13}CH_3OH$
445	$48_{2,46} - 47_{2,45}$	214343.680	50	245	619.9	75	Strong $^{13}CH_3CN$ and $C_2H_5{}^{13}CN$
446	$49_{2,48} - 48_{2,47}$	215077.170	50	253	632.6	74	Strong C_2H_5CN
447	$49_{1,48} - 48_{1,47}$	216142.273	8	252	632.9	55	Blend with OCS and U-line
448	$49_{3,47} - 48_{3,46}$	216615.615	6	259	631.5	55	Blend with CH_3COOH and CH_3CHO
449	$49_{10,39} - 48_{10,38}{}^{\star}$	216647.130	8	352	607.5	55	Strong SO_2 and C_2H_5OH
451	$49_{9,40} - 48_{9,39}{}^{\star}$	216648.604	8	333	612.6	55	Strong SO_2 and C_2H_5OH
453	$49_{11,38} - 48_{11,37}{}^{\star}$	216653.496	9	374	602.0	55	Strong SO_2 and C_2H_5OH
455	$49_{8,42} - 48_{8,41}{}^{\star}$	216661.026	7	315	617.0	55	Strong SO_2 and C_2H_5OH
457	$49_{12,37} - 48_{12,36}{}^{\star}$	216665.865	9	398	596.0	55	Strong SO_2 and C_2H_5OH
459	$50_{1,50} - 49_{1,49}$	216679.385	20	257	646.5	55	Blend with H_2S
460	$49_{13,36} - 48_{13,35}{}^{\star}$	216683.096	10	423	589.3	55	Blend with H_2S
462	$49_{7,43} - 48_{7,42}{}^{\star}$	216690.012	7	300	621.0	55	Strong H_2S
464	$49_{14,35} - 48_{14,34}{}^{\star}$	216704.448	10	451	582.2	55	Strong H_2S
466	$49_{15,34} - 48_{15,33}{}^{\star}$	216729.429	10	481	574.6	50	Strong H_2S and C_2H_5CN, $v_{13}=1/v_{21}=1$
468	$49_{6,44} - 48_{6,43}$	216746.358	7	287	624.5	50	Strong C_2H_5CN
469	$49_{6,43} - 48_{6,42}$	216747.094	7	287	624.5	50	Strong C_2H_5CN
470	$49_{16,33} - 48_{16,32}{}^{\star}$	216757.710	50	513	566.3	50	Strong C_2H_5CN
472	$50_{0,50} - 49_{0,49}$	216767.700	50	256	646.5	50	Blend with C_2H_5CN and U-line

Table 9. continued.

N^a (1)	Transition^b (2)	Frequency (MHz) (3)	Unc.^{c} (kHz) (4)	E_l^d (K) (5)	$S\mu^2$ (D^2) (6)	σ^e (mK) (7)	Comments (8)
473	$49_{17,32} - 48_{17,31}{}^\star$	216789.070	50	546	557.7	50	Blend with CH_3CH_3CO, v_t=1
475	$13_{7,6} - 14_{6,9}{}^\star$	216795.931	26	59	1.0	50	Blend with CH_3CH_3CO, v_t=1
477	$49_{18,31} - 48_{18,30}{}^\star$	216823.235	10	582	548.3	50	Strong CH_3OCHO
479	$49_{5,45} - 48_{5,44}$	216847.000	7	275	627.3	50	Strong C_2H_5CN, v_{13}=1/v_{21}=1
480	$49_{19,30} - 48_{19,29}{}^\star$	216860.211	11	620	538.7	50	Blend with C_2H_5CN, v_{13}=1/v_{21}=1 and U-line
482	$49_{5,44} - 48_{5,43}$	216865.924	7	275	627.4	50	Blend with C_2H_5CN, v_{13}=1/v_{21}=1 and U-line
483	$49_{20,29} - 48_{20,28}{}^\star$	216899.870	50	660	528.3	50	Blend with U-line
485	$49_{21,28} - 48_{21,27}{}^\star$	216942.142	17	702	517.5	50	Strong CH_3OH
487	$49_{4,46} - 48_{4,45}$	216949.090	50	266	629.7	50	Strong CH_3OH
488	$42_{10,32} - 43_{9,35}{}^\star$	216956.684	77	284	6.3	50	Strong CH_3OH
490	$49_{4,45} - 48_{4,44}$	217233.695	7	266	629.8	50	Strong $CH_2{}^{13}CHCN$
491	$45_{2,44} - 44_{1,43}$	217511.675	25	213	21.1	50	Blend with ^{13}CN in absorption and U-line
492	$50_{1,50} - 49_{0,49}$	217512.520	22	256	41.1	50	Blend with ^{13}CN in absorption and U-line
493	$50_{2,49} - 49_{2,48}$	219410.228	10	263	645.7	92	Strong HC_3N, v_6=v_7=1
494	$6_{5,2} - 5_{4,1}{}^\star$	219563.799	11	20	4.4	92	Strong $C^{18}O$
496	$50_{1,49} - 49_{1,48}$	220424.730	8	262	645.9	98	Strong $CH_3{}^{13}CN$
497	$51_{4,47} - 50_{4,46}$	226177.852	9	287	655.8	278	Noisy
498	$51_{3,48} - 50_{3,47}$	227473.842	14	281	657.7	85	Blend with $CH_2CH^{13}CN$ and C_2H_5OCHO, uncertain baseline
499	$51_{2,49} - 50_{2,48}$	227577.811	11	277	658.7	85	Strong CH_3OCHO and C_2H_5OH
500	$29_{3,27} - 28_{2,26}$	227580.141	9	91	7.6	85	Strong CH_3OCHO and C_2H_5OH
501	$53_{2,52} - 52_{2,51}$	232395.004	14	295	684.5	19	Blend with C_2H_5OH
502	$9_{5,5} - 8_{4,4}{}^\star$	232831.850	11	24	4.9	19	Blend with CH_3CH_3CO, v_t=1 and U-line
504	$62_{6,57} - 62_{5,58}$	232836.738	28	440	32.6	19	Blend with CH_3CH_3CO, v_t=1 and U-line
505	$44_{6,39} - 44_{5,40}$	235131.269	9	236	22.2	131	Strong C_2H_5OH
506	$53_{4,49} - 52_{4,48}$	235136.432	11	309	681.8	131	Strong C_2H_5OH
507	$39_{6,33} - 39_{5,34}$	235437.401	9	191	19.4	131	Blend with $^{13}CH_3OH$, v_t=1
508	$38_{6,32} - 38_{5,33}$	235489.643	9	183	18.9	131	Blend with CH_3CH_3CO and $HC^{13}CCN$
509	$37_{6,31} - 37_{5,32}$	235537.303	9	175	18.4	131	Strong $HCC^{13}CN$
510	$37_{6,32} - 37_{5,33}$	235543.778	9	175	18.4	131	Strong $HCC^{13}CN$ and CH_3CH_3CO
511	$36_{6,30} - 36_{5,31}$	235580.671	9	167	17.8	131	Blend with C_2H_3CN, uncertain baseline
512	$36_{6,31} - 36_{5,32}$	235585.618	9	167	17.8	131	Blend with C_2H_3CN, uncertain baseline
513	$35_{6,29} - 35_{5,30}$	235620.022	9	159	17.3	131	Blend with C_2H_5CN, v_{13}=1/v_{21}=1
514	$35_{6,30} - 35_{5,31}$	235623.773	9	159	17.3	131	Blend with C_2H_5CN, v_{13}=1/v_{21}=1
515	$34_{6,28} - 34_{5,29}$	235655.616	9	152	16.7	131	Blend with C_2H_5CN, v_{13}=1/v_{21}=1, $HC^{13}CCN$, v_5=1/v_7=3, and C_2H_3CN, v_{11}=1
516	$34_{6,29} - 34_{5,30}$	235658.436	9	152	16.7	131	Blend with C_2H_5CN, v_{13}=1/v_{21}=1, $HC^{13}CCN$, v_5=1/v_7=3, and C_2H_3CN, v_{11}=1
517	$33_{6,27} - 33_{5,28}$	235687.700	10	145	16.2	131	Blend with $HCC^{13}CN$, v_5=1/v_7=3, uncertain baseline
518	$33_{6,28} - 33_{5,29}$	235689.803	10	145	16.2	131	Blend with $HCC^{13}CN$, v_5=1/v_7=3, uncertain baseline
519	$32_{6,26} - 32_{5,27}$	235716.510	10	138	15.7	131	Blend with CH_3OCH_3
520	$32_{6,27} - 32_{5,28}$	235718.063	10	138	15.7	131	Blend with CH_3OCH_3
521	$31_{6,25} - 31_{5,26}$	235742.268	10	131	15.1	131	Blend with U-line in absorption or baseline problem?
522	$31_{6,26} - 31_{5,27}$	235743.404	10	131	15.1	131	Blend with U-line in absorption or baseline problem?
523	$30_{6,24} - 30_{5,25}$	235765.188	10	124	14.6	131	Blend with U-line in absorption or baseline problem?
524	$30_{6,25} - 30_{5,26}$	235766.010	10	124	14.6	131	Blend with U-line in absorption or baseline problem?
525	$29_{6,23} - 29_{5,24}$	235785.473	10	118	14.1	131	Blend with CH_3OCH_3 and $^{13}CH_3CH_2CN$
526	$29_{6,24} - 29_{5,25}$	235786.062	10	118	14.1	131	Blend with CH_3OCH_3 and $^{13}CH_3CH_2CN$
527	$28_{6,22} - 28_{5,23}$	235803.318	11	112	13.6	131	Blend with CH_3CH_3CO, v_t=1
528	$28_{6,23} - 28_{5,24}$	235803.734	11	112	13.6	131	Blend with CH_3CH_3CO, v_t=1
529	$27_{6,21} - 27_{5,22}$	235818.908	11	106	13.0	131	Blend with CH_3CHO, uncertain baseline
530	$27_{6,22} - 27_{5,23}$	235819.199	11	106	13.0	131	Blend with CH_3CHO, uncertain baseline
531	$26_{6,20} - 26_{5,21}$	235832.420	11	100	12.5	131	Blend with CH_3OCHO
532	$26_{6,21} - 26_{5,22}$	235832.620	11	100	12.5	131	Blend with CH_3OCHO
533	$25_{6,19} - 25_{5,20}$	235844.025	11	95	12.0	131	Strong CH_3OCHO
534	$25_{6,20} - 25_{5,21}$	235844.161	11	95	12.0	131	Strong CH_3OCHO
535	$24_{6,18} - 24_{5,19}{}^\star$	235853.884	12	89	11.4	131	Blend with CH_3OCHO
537	$23_{6,17} - 23_{5,18}{}^\star$	235862.152	12	84	10.9	131	Strong CH_3OCHO and C_2H_5CN, v_{13}=1/v_{21}=1
539	$22_{6,16} - 22_{5,17}{}^\star$	235868.978	12	79	10.4	131	Strong CH_3OCHO and C_2H_5CN, v_{13}=1/v_{21}=1
541	$21_{6,15} - 21_{5,16}{}^\star$	235874.503	13	75	9.9	131	Strong $^{13}CH_3OH$, CH_3OCHO, and $HC^{13}CCN$, v_6=1
543	$6_{6,0} - 6_{5,1}{}^\star$	235877.922	15	30	0.9	131	Strong $^{13}CH_3OH$, CH_3OCHO, and $HC^{13}CCN$, v_6=1
545	$20_{6,14} - 20_{5,15}{}^\star$	235878.862	13	70	9.3	131	Strong $^{13}CH_3OH$, CH_3OCHO, and $HC^{13}CCN$, v_6=1
547	$7_{6,1} - 7_{5,2}{}^\star$	235879.246	15	32	1.7	131	Strong $^{13}CH_3OH$, CH_3OCHO, and $HC^{13}CCN$, v_6=1
549	$8_{6,2} - 8_{5,3}{}^\star$	235880.638	15	33	2.4	131	Strong $^{13}CH_3OH$, CH_3OCHO, and $HC^{13}CCN$, v_6=1
551	$9_{6,3} - 9_{5,4}{}^\star$	235882.048	15	35	3.1	131	Strong $^{13}CH_3OH$, CH_3OCHO, and $HC^{13}CCN$, v_6=1

Table 9. continued.

N^a	Transition^b	Frequency	Unc.^{c}	$E_l{}^d$	$S\mu^2$	σ^e	Comments
		(MHz)	(kHz)	(K)	(D^2)	(mK)	
(1)	(2)	(3)	(4)	(5)	(6)	(7)	(8)
553	$19_{6,13} - 19_{5,14}{}^\star$	235882.182	13	66	8.8	131	Strong $^{13}CH_3OH$, CH_3OCHO, and $HC^{13}CCN$, υ_6=1
555	$10_{6,4} - 10_{5,5}{}^\star$	235883.423	15	37	3.7	131	Strong $^{13}CH_3OH$, CH_3OCHO, and $HC^{13}CCN$, υ_6=1
557	$18_{6,12} - 18_{5,13}{}^\star$	235884.587	13	62	8.2	131	Strong $^{13}CH_3OH$, CH_3OCHO, and $HC^{13}CCN$, υ_6=1
559	$11_{6,5} - 11_{5,6}{}^\star$	235884.702	15	40	4.3	131	Strong $^{13}CH_3OH$, CH_3OCHO, and $HC^{13}CCN$, υ_6=1
561	$12_{6,6} - 12_{5,7}{}^\star$	235885.818	15	42	4.9	131	Strong $^{13}CH_3OH$, CH_3OCHO, and $HC^{13}CCN$, υ_6=1
563	$17_{6,11} - 17_{5,12}{}^\star$	235886.191	14	58	7.7	131	Strong $^{13}CH_3OH$, CH_3OCHO, and $HC^{13}CCN$, υ_6=1
565	$13_{6,7} - 13_{5,8}{}^\star$	235886.698	14	45	5.5	131	Strong $^{13}CH_3OH$, CH_3OCHO, and $HC^{13}CCN$, υ_6=1
567	$16_{6,10} - 16_{5,11}{}^\star$	235887.104	14	55	7.2	131	Strong $^{13}CH_3OH$, CH_3OCHO, and $HC^{13}CCN$, υ_6=1
569	$14_{6,8} - 14_{5,9}{}^\star$	235887.263	14	48	6.1	131	Strong $^{13}CH_3OH$, CH_3OCHO, and $HC^{13}CCN$, υ_6=1
571	$15_{6,9} - 15_{5,10}{}^\star$	235887.429	14	51	6.6	131	Strong $^{13}CH_3OH$, CH_3OCHO, and $HC^{13}CCN$, υ_6=1
573	$53_{2,51} - 52_{2,50}$	236363.740	13	299	684.6	37	Strong $CH_2CH^{13}CN$
574	$53_{3,50} - 52_{3,49}$	236507.754	18	303	683.6	37	Strong HC_3N
575	$54_{3,51} - 53_{3,50}$	241020.744	20	314	696.6	216	Strong $C^{34}S$
576	$55_{2,54} - 54_{2,53}$	241040.003	19	318	710.3	216	Strong C_2H_3CN, υ_{11}=2 and CH_3OH
577	$55_{4,51} - 54_{4,50}$	244110.418	14	332	707.8	46	Blend with CH_3CH_3CO, υ_t=1, C_2H_3CN, υ_{11}=1, and U-line
578	$55_{2,53} - 54_{2,52}$	245118.648	14	322	710.4	72	Blend with CH_2NH
579	$56_{2,55} - 55_{2,54}$	245359.219	21	329	723.3	72	Strong $^{13}CH_3CH_2CN$
580	$55_{3,52} - 54_{3,51}$	245530.359	22	326	709.6	72	Strong $HCC^{13}CN$, υ_7=1 and $^{13}CH_3CH_2CN$
581	$58_{1,57} - 57_{2,56}$	247309.555	23	353	33.7	68	Blend with C_2H_3CN, υ_{15}=1
582	$56_{3,54} - 55_{3,53}$	247311.322	10	336	722.3	68	Blend with C_2H_3CN, υ_{15}=1
583	$57_{10,47} - 56_{10,46}{}^\star$	251977.746	9	442	714.8	42	Strong CH_3OH
585	$57_{11,46} - 56_{11,45}{}^\star$	251978.622	9	463	709.9	42	Strong CH_3OH
587	$57_{12,45} - 56_{12,44}{}^\star$	251988.044	9	487	704.7	42	Strong CH_3OH
589	$57_{9,49} - 56_{9,48}{}^\star$	251988.316	8	422	719.0	42	Strong CH_3OH
591	$57_{13,44} - 56_{13,43}{}^\star$	252004.207	10	512	699.1	42	Strong C_2H_5CN
593	$57_{8,50} - 56_{8,49}{}^\star$	252015.263	9	405	722.9	42	Strong C_2H_5CN and $^{13}CH_2CO$
595	$57_{14,43} - 56_{14,42}{}^\star$	252025.947	10	540	692.9	42	Strong C_2H_5CN, υ_{13}=1/υ_{21}=1
597	$57_{15,42} - 56_{15,41}{}^\star$	252052.483	11	570	686.4	42	Blend with $CH_3{}^{13}CH_2CN$ and U-line
599	$57_{7,51} - 56_{7,50}$	252067.511	9	389	726.4	42	Blend with t-HCOOH
600	$57_{7,50} - 56_{7,49}$	252067.645	9	389	726.4	42	Blend with t-HCOOH
601	$57_{16,41} - 56_{16,40}{}^\star$	252083.278	11	602	679.4	42	Strong t-HCOOH and CH_3OH
603	$57_{17,40} - 56_{17,39}{}^\star$	252117.956	11	636	671.9	42	Blend with C_2H_5CN, υ_{13}=1/υ_{21}=1 and $CH_2(OH)CHO$
605	$57_{18,39} - 56_{18,38}{}^\star$	252156.248	12	671	664.0	42	Strong C_2H_5CN, υ_{13}=1/υ_{21}=1
607	$57_{6,52} - 56_{6,51}$	252161.456	10	376	729.2	42	Strong C_2H_5CN, υ_{13}=1/υ_{21}=1
608	$57_{6,51} - 56_{6,50}$	252165.248	10	376	729.2	42	Strong C_2H_5CN, υ_{13}=1/υ_{21}=1
609	$59_{1,58} - 58_{2,57}$	252195.854	23	365	34.8	42	Strong C_2H_5CN, υ_{13}=1/υ_{21}=1
610	$57_{19,38} - 56_{19,37}{}^\star$	252197.960	12	709	655.6	42	Strong C_2H_5CN, υ_{13}=1/υ_{21}=1
612	$57_{20,37} - 56_{20,36}{}^\star$	252242.951	14	749	646.7	42	Strong C_2H_5CN and CH_3OH
614	$57_{21,36} - 56_{21,35}{}^\star$	252291.118	17	791	637.4	42	Blend with U-line and CH_3CH_3CO, υ_t=1
616	$57_{5,53} - 56_{5,52}$	252310.240	11	365	731.8	42	Blend with CH_3CH_3CO, υ_t=1 and $^{13}CH_3CH_2CN$, uncertain baseline
617	$57_{4,54} - 56_{4,53}$	252367.776	11	355	733.8	42	Strong CH_3OCH_3 and $^{13}CH_3OH$
618	$57_{5,52} - 56_{5,51}$	252380.765	11	365	731.8	42	Blend with $^{13}CH_3CH_2CN$
619	$58_{2,57} - 57_{2,56}$	253991.392	28	353	749.1	32	Blend with NS and CH_3OH in absorption
620	$59_{1,59} - 58_{1,58}$	255355.480	56	358	762.9	217	Strong $^{13}CH_3OH$
621	$59_{0,59} - 58_{0,58}$	255388.370	56	358	762.8	217	Strong OCS, $CH_2{}^{13}CHCN$, and $CH_2CH^{13}CN$
622	$58_{2,56} - 57_{2,55}$	258190.922	16	358	749.2	1127	Strong CH_3CN, υ_8=1 and C_2H_3CN, υ_{15}=1
623	$59_{2,58} - 58_{2,57}$	258304.475	32	365	762.1	1127	Blend with CH_3CN, υ_8=1
624	$59_{1,58} - 58_{1,57}$	258877.691	30	365	762.2	1609	Noisy
625	$58_{3,55} - 57_{3,54}$	259034.024	30	362	748.4	1609	Strong $^{13}CH_3OH$ and $^{13}CH_2CHCN$
626	$59_{3,57} - 58_{3,56}$	260422.403	15	372	761.3	413	Strong CH_3OCHO and C_2H_5CN
627	$60_{1,59} - 59_{1,58}$	263146.854	35	377	775.1	74	Blend with $^{13}CH_3CH_2CN$, baseline problem
628	$59_{3,56} - 58_{3,55}$	263525.388	34	374	761.5	74	Strong CH_3OCH_3
629	$16_{5,12} - 15_{4,11}$	263780.394	11	42	6.3	108	Strong HC_3N and CH_3OH, υ_t=1
630	$16_{5,11} - 15_{4,12}$	263780.579	11	42	6.3	108	Strong HC_3N and CH_3OH, υ_t=1
631	$61_{1,61} - 60_{1,60}$	263943.020	70	382	788.7	108	Blend with C_2H_5CN and CH_3CH_3CO
632	$61_{0,61} - 60_{0,60}$	263969.205	70	382	788.7	108	Blend with HC_3N, υ_5=1/υ_7=3, C_2H_5CN, υ_{20}=1, and $CH_3{}^{13}CH_2CN$
633	$7_{6,1} - 6_{5,2}{}^\star$	266831.913	15	30	5.4	91	Strong CH_3OCHO, $CH_2{}^{13}CHCN$, and CH_3OH
635	$60_{2,58} - 59_{2,57}$	266865.326	17	383	775.0	91	Strong CH_3OH, υ_t=1
636	$61_{2,60} - 60_{2,59}$	266924.955	41	390	787.9	91	Blend with CH_3OCHO, C_2H_5CN, C_2H_3CN, SO_2, and U-line

Notes: ^{a} Numbering of the observed transitions associated with a modeled line stronger than 20 mK. ^{b} Transitions marked with a * are double with a frequency difference less than 0.1 MHz. The quantum numbers of the second one are not shown. ^{c} Frequency uncertainty. ^{d} Lower energy level in temperature units (E_l/k_B). ^{e} Calculated rms noise level in T_{mb} scale.

Table 10. Transitions of the *gauche*-conformer of *n*-propyl cyanide observed with the IRAM 30 m telescope toward Sgr B2(N). The horizontal lines mark discontinuities in the observed frequency coverage. Only the transitions associated with a modeled line stronger than 20 mK are listed.

N^a (1)	Transition^b (2)	Frequency (MHz) (3)	Unc.^{c} (kHz) (4)	$E_l{}^d$ (K) (5)	$S\mu^2$ (D^2) (6)	σ^e (mK) (7)	Comments (8)
1	$17_{9,9} - 16_{9,8}{}^{\star}$	101965.911	6	199	262.1	34	Blend with U-line
3	$17_{8,10} - 16_{8,9}{}^{\star}$	102048.097	6	193	283.5	34	Blend with NH_2CHO, $v_{12}=1$
5	$29_{2,27} - 29_{1,28}$	102048.362	6	253	66.0	34	Blend with NH_2CHO, $v_{12}=1$
6	$34_{5,30} - 34_{3,31}$	102175.037	5	308	17.0	30	Blend with C_2H_5CN, $v_{13}=1/v_{21}=1$, $^{13}CH_2CHCN$, and CH_3OCHO, $v_t=1$
7	$17_{7,11} - 16_{7,10}$	102176.110	6	188	302.4	30	Blend with C_2H_5CN, $v_{13}=1/v_{21}=1$, $^{13}CH_2CHCN$, and CH_3OCHO, $v_t=1$
8	$17_{7,10} - 16_{7,9}$	102176.872	6	188	302.3	30	Blend with C_2H_5CN, $v_{13}=1/v_{21}=1$, $^{13}CH_2CHCN$, and CH_3OCHO, $v_t=1$
9	$19_{0,19} - 18_{0,18}$	104811.610	6	179	403.9	25	Blend with C_2H_5CN, $v_{13}=1/v_{21}=1$ and C_2H_5OH
10	$20_{8,12} - 20_{7,13}$	104813.646	6	210	89.8	25	Blend with C_2H_5OH, C_2H_3CN, $v_{11}=1$, $CH_3{}^{13}CH_2CN$, and C_2H_5CN, $v_{13}=1/v_{21}=1$
11	$18_{10,8} - 17_{10,7}{}^{\star}$	107933.825	6	210	266.5	46	Blend with CH_3CH_3CO, $v_t=1$, C_2H_5CN, $v_{13}=1/v_{21}=1$, and U-line
13	$18_{9,10} - 17_{9,9}{}^{\star}$	107999.345	6	204	289.1	46	Blend with U-line
15	$18_{8,11} - 17_{8,10}{}^{\star}$	108098.501	6	198	309.4	48	Blend with U-line
17	$18_{7,12} - 17_{7,11}$	108252.103	6	193	327.2	48	Blend with U-line
18	$18_{7,11} - 17_{7,10}$	108253.743	6	193	327.2	48	Blend with U-line
19	$18_{4,15} - 17_{4,14}$	108520.203	7	182	365.9	20	Blend with C_2H_5OH
20	$18_{2,16} - 17_{2,15}$	108793.066	7	179	375.5	20	Blend with ^{13}CN in absorption and C_2H_5CN, $v_{13}=1/v_{21}=1$
21	$19_{2,18} - 18_{2,17}$	108827.746	7	182	399.0	20	Blend with ^{13}CN in absorption and U-line?
22	$19_{1,18} - 18_{1,17}$	109039.231	7	182	399.0	29	Blend with C_2H_3CN and U-line?
23	$20_{1,20} - 19_{1,19}$	110209.409	6	184	425.4	24	Blend with ^{13}CO and HC_3N, $v_5=1/v_7=3$
24	$20_{0,20} - 19_{0,19}$	110214.195	6	184	425.4	24	Blend with ^{13}CO and HC_3N, $v_5=1/v_7=3$
25	$18_{4,14} - 17_{4,13}$	111109.974	6	182	366.9	25	Blend with U-line
26	$18_{3,15} - 17_{3,14}$	112088.070	7	181	375.2	42	Blend with U-line
27	$19_{3,17} - 18_{3,16}$	112370.034	7	185	394.3	42	Blend with CH_3CH_3CO and CH_3OCH_3
28	$19_{15,4} - 18_{15,3}{}^{\star}$	113832.488	7	258	153.3	34	Blend with C_2H_3CN and U-line
30	$19_{16,3} - 18_{16,2}{}^{\star}$	113833.361	7	268	118.4	34	Blend with C_2H_3CN and U-line
32	$19_{12,7} - 18_{12,6}{}^{\star}$	113872.326	6	230	244.6	34	Blend with C_2H_5OH and U-line
34	$19_{11,8} - 18_{11,7}{}^{\star}$	113907.356	6	223	270.5	34	Strong C_2H_3CN
36	$19_{10,10} - 18_{10,9}{}^{\star}$	113960.196	6	216	294.2	33	Blend with C_2H_3CN
38	$19_{9,11} - 18_{9,10}{}^{\star}$	114038.886	6	209	315.7	33	Blend with U-line
40	$19_{2,17} - 18_{2,16}$	114077.162	7	184	396.3	33	Blend with C_2H_3CN, $v_{15}=1$ and U-line
41	$19_{8,12} - 18_{8,11}$	114157.197	6	203	334.8	33	Blend with U-line
42	$19_{8,11} - 18_{8,10}$	114157.321	6	203	334.8	33	Blend with U-line
43	$20_{2,19} - 19_{2,18}$	114255.098	6	187	420.4	33	Blend with C_2H_3CN, $v_{11}=1$
44	$19_{7,13} - 18_{7,12}$	114339.524	6	198	351.7	33	Blend with C_2H_3CN, $v_{11}=1$ and NH_2CHO
45	$20_{1,19} - 19_{1,18}$	114399.053	6	187	420.3	33	Blend with C_2H_5CN, $v_{13}=1/v_{21}=1$ and U-line?
46	$19_{4,16} - 18_{4,15}$	114451.328	7	187	388.1	37	Blend with C_2H_3CN, $v_{11}=1/v_{15}=1$ and c-C_2H_4O
47	$19_{6,14} - 18_{6,13}$	114615.647	6	194	366.3	37	Strong $H^{13}CCCN$ and C_2H_3CN
48	$19_{6,13} - 18_{6,12}$	114676.990	6	194	366.4	37	Blend with $H^{13}CCCN$, $v_5=1/v_7=3$ and U-line
49	$20_{2,19} - 19_{1,18}$	114679.259	7	187	130.0	37	Blend with $H^{13}CCCN$, $v_5=1/v_7=3$ and U-line
50	$19_{5,15} - 18_{5,14}$	114881.716	6	190	378.6	59	Blend with C_2H_3CN, $v_{11}=3$ and $CH_2(OH)CHO$
51	$19_{5,14} - 18_{5,13}$	115556.072	6	190	378.7	60	Blend with C_2H_3CN, NS, and CH_3OCHO, $v_t=1$
52	$21_{0,21} - 20_{1,20}$	115609.125	6	189	174.8	79	Blend with CH_2NH and U-line?
53	$21_{1,21} - 20_{1,20}$	115613.838	6	189	446.8	79	Blend with CH_2NH and CH_3CHO
54	$21_{0,21} - 20_{0,20}$	115616.804	6	189	446.8	79	Blend with CH_2NH and CH_3CHO
55	$24_{5,20} - 23_{5,19}$	145147.268	6	221	491.0	25	Strong C_2H_3CN
56	$25_{3,23} - 24_{3,22}$	145354.256	6	221	522.8	25	Blend with HC_3N, $v_4=1$
57	$24_{6,19} - 23_{6,18}$	145359.467	6	224	481.8	25	Blend with HC_3N, $v_4=1$
58	$26_{4,23} - 25_{4,22}$	154516.394	5	232	540.1	112	Blend with NH_2CH_2CN and C_2H_5CN, $v_{13}=1/v_{21}=1$
59	$27_{7,21} - 26_{7,20}$	163471.366	5	250	539.4	38	Blend with $HCC^{13}CN$, $v_7=1$ and NH_2CH_2CN
60	$12_{7,6} - 11_{6,5}$	163626.490	12	164	62.4	38	Blend with a-C_3H_7CN and U-line
61	$12_{7,5} - 11_{6,6}$	163626.670	12	164	62.4	38	Blend with a-C_3H_7CN and U-line
62	$27_{6,22} - 26_{6,21}$	163729.422	5	246	549.4	38	Blend with a-C_3H_7CN and U-line
63	$28_{3,25} - 27_{3,24}$	166501.674	5	247	583.3	66	Blend with C_2H_5CN, $v_{13}=1/v_{21}=1$ and CH_3CN, $v_8=2$
64	$30_{3,28} - 29_{2,27}$	172509.803	5	258	186.7	44	Strong C_2H_5CN, $v_{13}=1/v_{21}=1$
65	$24_{13,11} - 24_{12,12}{}^{\star}$	176027.815	8	268	88.7	365	Blend with HNCO, $v_5=1$ and $^{13}CH_2CO$
67	$23_{13,10} - 23_{12,11}{}^{\star}$	176085.591	8	261	82.2	365	Blend with CH_3OCH_3
69	$22_{13,9} - 22_{12,10}{}^{\star}$	176134.711	8	254	75.7	365	Blend with HNCO, $v_6=1$ and HNCO, $v_5=1$
71	$37_{0,37} - 36_{1,36}{}^{\star}$	201966.900	11	309	321.5	138	Blend with CH_3CN
73	$37_{0,37} - 36_{0,36}{}^{\star}$	201966.902	11	309	789.3	138	Blend with CH_3CN
75	$33_{5,29} - 32_{4,28}$	201985.474	6	293	131.9	138	Blend with CH_3OH

Table 10. continued.

N^a (1)	Transition^b (2)	Frequency (MHz) (3)	Unc.^{c} (kHz) (4)	$E_l{}^d$ (K) (5)	$S\mu^2$ (D^2) (6)	σ^e (mK) (7)	Comments (8)
76	$34_{5,30} - 33_{5,29}$	202090.888	6	303	707.1	138	Strong CH_2CO
77	$56_{3,53} - 56_{3,54}{}^{\star}$	202474.090	224	572	15.7	108	Blend with U-line and H_2CS
79	$56_{4,53} - 56_{3,54}{}^{\star}$	202474.109	224	572	100.1	108	Blend with U-line and H_2CS
81	$41_{15,26} - 41_{14,27}{}^{\star}$	202477.934	26	447	185.2	108	Blend with U-line and H_2CS
83	$40_{15,25} - 40_{14,26}{}^{\star}$	202689.659	25	435	178.9	108	Blend with C_2H_3CN, $\upsilon_{15}=1$ and NH_2CHO
85	$33_{7,26} - 32_{7,25}$	202881.421	5	302	675.4	138	Blend with C_2H_3CN, $\upsilon_{11}=1$
86	$39_{15,24} - 39_{14,25}{}^{\star}$	202883.694	24	423	172.6	138	Blend with C_2H_3CN, $\upsilon_{11}=1$
88	$38_{15,23} - 38_{14,24}{}^{\star}$	203061.073	23	412	166.3	138	Blend with $^{13}CH_3CH_2CN$ and C_2H_5OCHO
90	$34_{4,30} - 33_{4,29}$	203180.785	6	303	707.8	138	Blend with C_2H_3CN, $\upsilon_{11}=2$
91	$37_{15,22} - 37_{14,23}{}^{\star}$	203222.780	23	401	160.0	138	Blend with $^{34}SO_2$
93	$35_{3,32} - 34_{4,31}$	203290.077	6	308	195.3	161	Blend with C_2H_5OCHO, CH_3CN, $\upsilon_8=2$, and U-line
94	$36_{15,21} - 36_{14,22}{}^{\star}$	203369.755	22	390	153.7	161	Strong CH_3OCH_3
96	$35_{4,32} - 34_{4,31}$	203466.519	6	308	732.0	161	Blend with CH_3CN, $\upsilon_8=2$ and CH_3OCHO
97	$35_{15,20} - 35_{14,21}{}^{\star}$	203502.897	22	380	147.5	161	Blend with $^{34}SO_2$
99	$35_{3,32} - 34_{3,31}$	203552.465	6	308	732.0	161	Blend with CH_3CN, $\upsilon_8=2$ and $H^{13}CCCN$, $\upsilon_7=1$
100	$34_{15,19} - 34_{14,20}{}^{\star}$	203623.068	22	370	141.2	161	Blend with CH_3OCH_3
102	$35_{4,32} - 34_{3,31}$	203728.907	6	308	195.4	364	Blend with C_2H_5CN, $\upsilon_{13}=1/\upsilon_{21}=1$ and U-line
103	$33_{15,18} - 33_{14,19}{}^{\star}$	203731.092	21	360	135.0	364	Blend with C_2H_5CN, $\upsilon_{13}=1/\upsilon_{21}=1$ and U-line
105	$34_{20,14} - 33_{20,13}{}^{\star}$	203795.929	10	429	476.3	364	Strong C_2H_3CN
107	$34_{21,13} - 33_{21,12}{}^{\star}$	203796.393	10	443	450.5	364	Strong C_2H_3CN
109	$34_{22,12} - 33_{22,11}{}^{\star}$	203805.898	11	457	423.4	364	Strong C_2H_3CN
111	$34_{19,15} - 33_{19,14}{}^{\star}$	203805.992	10	416	500.8	364	Strong C_2H_3CN
113	$34_{23,11} - 33_{23,10}{}^{\star}$	203823.272	12	473	395.0	364	Blend with C_2H_3CN, $^{13}CH_3CH_2CN$, and C_2H_5CN
115	$32_{15,17} - 32_{14,18}{}^{\star}$	203827.761	21	351	128.7	364	Blend with C_2H_3CN, $^{13}CH_3CH_2CN$, and C_2H_5CN
117	$34_{18,16} - 33_{18,15}{}^{\star}$	203828.503	10	403	524.2	364	Blend with C_2H_3CN, $^{13}CH_3CH_2CN$, and C_2H_5CN
119	$14_{9,6} - 13_{8,5}{}^{\star}$	203835.897	12	180	80.1	364	Blend with C_2H_3CN, $^{13}CH_3CH_2CN$, and C_2H_5CN
121	$34_{24,10} - 33_{24,9}{}^{\star}$	203847.587	14	488	365.4	364	Blend with CH_3OCHO and C_2H_5OH
123	$65_{14,52} - 64_{15,49}$	203856.381	379	809	80.4	364	Blend with C_2H_5OH and CH_3OCHO
124	$34_{17,17} - 33_{17,16}{}^{\star}$	203865.981	10	392	546.2	364	Blend with CH_3OCHO
126	$34_{25,9} - 33_{25,8}{}^{\star}$	203878.090	15	505	334.5	364	Blend with CH_3CH_3CO and U-line
128	$31_{15,16} - 31_{14,17}{}^{\star}$	203913.834	21	342	122.4	364	Strong C_2H_5CN, $\upsilon_{13}=1/\upsilon_{21}=1$
130	$34_{26,8} - 33_{26,7}{}^{\star}$	203914.173	17	522	302.4	364	Strong C_2H_5CN, $\upsilon_{13}=1/\upsilon_{21}=1$
132	$34_{16,18} - 33_{16,17}{}^{\star}$	203921.785	10	380	567.0	364	Strong C_2H_5CN, $\upsilon_{13}=1/\upsilon_{21}=1$
134	$34_{27,7} - 33_{27,6}{}^{\star}$	203955.332	20	540	269.0	364	Blend with U-line
136	$33_{5,28} - 32_{5,27}$	203957.407	6	296	687.9	364	Blend with U-line
137	$30_{15,15} - 30_{14,16}{}^{\star}$	203990.040	20	333	116.1	364	Blend with C_2H_5CN and C_2H_3CN, $\upsilon_{11}=3$
139	$34_{15,19} - 33_{15,18}{}^{\star}$	204000.498	9	370	586.5	364	Strong C_2H_3CN, $\upsilon_{11}=3$ and C_2H_3CN, $\upsilon_{11}=2$
141	$34_{28,6} - 33_{28,5}{}^{\star}$	204001.151	22	558	234.3	364	Strong C_2H_3CN, $\upsilon_{11}=3$ and C_2H_3CN, $\upsilon_{11}=2$
143	$34_{29,5} - 33_{29,4}{}^{\star}$	204051.281	26	577	198.4	364	Blend with $H^{13}CCCN$, $\upsilon_7=2$ and U-line
145	$29_{15,14} - 29_{14,15}{}^{\star}$	204057.079	20	324	109.7	364	Blend with $H^{13}CCCN$, $\upsilon_7=2$ and U-line
147	$64_{6,58} - 64_{6,59}$	204063.746	316	734	27.7	364	Blend with $H^{13}CCCN$, $\upsilon_7=2$ and U-line
148	$64_{6,58} - 64_{5,59}$	204064.065	316	734	201.8	364	Blend with $H^{13}CCCN$, $\upsilon_7=2$ and U-line
149	$34_{30,4} - 33_{30,3}{}^{\star}$	204105.426	30	597	161.3	316	Blend with U-line
151	$34_{14,20} - 33_{14,19}{}^{\star}$	204108.522	9	360	604.7	316	Blend with U-line
153	$28_{15,13} - 28_{14,14}{}^{\star}$	204115.622	20	316	103.3	316	Blend with U-line
155	$34_{31,3} - 33_{31,2}{}^{\star}$	204163.336	36	618	122.8	316	Strong CH_3OCH_3, C_2H_3CN, $\upsilon_{11}=1$, and $^{13}CH_2CHCN$
157	$27_{15,12} - 27_{14,13}{}^{\star}$	204166.316	20	308	96.9	316	Strong CH_3OCH_3, C_2H_3CN, $\upsilon_{11}=1$, and $^{13}CH_2CHCN$
159	$22_{6,17} - 21_{5,16}$	204205.122	12	208	60.2	316	Blend with CH_3CH_3CO and U-line
160	$26_{15,11} - 26_{14,12}{}^{\star}$	204209.781	20	300	90.4	316	Blend with CH_3CH_3CO and U-line
162	$25_{15,10} - 25_{14,11}{}^{\star}$	204246.611	20	292	83.8	316	Strong SO_2
164	$34_{13,22} - 33_{13,21}{}^{\star}$	204255.076	8	351	621.9	316	Strong SO_2
166	$24_{15,9} - 24_{14,10}{}^{\star}$	204277.378	20	285	77.2	316	Blend with CH_3CH_3CO and U-line
168	$52_{1,51} - 52_{0,52}{}^{\star}$	204278.834	248	495	33.4	316	Blend with CH_3CH_3CO and U-line
170	$52_{2,51} - 52_{1,52}{}^{\star}$	204278.834	248	495	33.4	316	Blend with CH_3CH_3CO and U-line
172	$23_{15,8} - 23_{14,9}{}^{\star}$	204302.630	20	278	70.4	316	Strong C_2H_5CN
174	$22_{15,7} - 22_{14,8}{}^{\star}$	204322.890	20	272	63.5	316	Blend with C_2H_5CN and U-line
176	$21_{15,6} - 21_{14,7}{}^{\star}$	204338.662	20	265	56.5	316	Blend with C_2H_5CN, $\upsilon_{13}=1/\upsilon_{21}=1$ and U-line
178	$20_{15,5} - 20_{14,6}{}^{\star}$	204350.423	21	259	49.3	316	Blend with CH_3CH_3CO, $\upsilon_t=1$
180	$19_{15,4} - 19_{14,5}{}^{\star}$	204358.632	21	253	41.9	316	Blend with CH_3CH_3CO
182	$18_{15,3} - 18_{14,4}{}^{\star}$	204363.725	21	248	34.2	316	Blend with CH_3CH_3CO and C_2H_5OCHO
184	$15_{15,0} - 15_{14,1}{}^{\star}$	204364.340	22	233	9.2	316	Blend with CH_3CH_3CO and C_2H_5OCHO
186	$17_{15,2} - 17_{14,3}{}^{\star}$	204366.116	21	243	26.3	316	Blend with CH_3CH_3CO and C_2H_5OCHO
188	$16_{15,1} - 16_{14,2}{}^{\star}$	204366.197	22	238	18.0	316	Blend with CH_3CH_3CO and C_2H_5OCHO
190	$60_{12,49} - 59_{13,46}$	204450.542	260	701	72.3	316	Blend with CH_3CH_3CO and U-line

Table 10. continued.

N^a (1)	Transition^b (2)	Frequency (MHz) (3)	Unc.^{c} (kHz) (4)	$E_l{}^d$ (K) (5)	$S\mu^2$ (D^2) (6)	σ^e (mK) (7)	Comments (8)
191	$34_{12,23}-33_{12,22}{}^\star$	204453.939	8	343	637.5	316	Blend with CH_3CH_3CO and U-line
193	$34_{10,25}-33_{10,24}$	205107.534	6	328	665.3	100	Strong CH_3OCH_3, $C_2H_5{}^{13}CN$, and $CH_3{}^{13}CH_2CN$
194	$34_{10,24}-33_{10,23}$	205113.060	6	328	665.2	100	Strong CH_3OCH_3, $C_2H_5{}^{13}CN$, and $CH_3{}^{13}CH_2CN$
195	$34_{6,29}-33_{6,28}$	205176.196	6	307	703.2	100	Blend with CH_3CHO and $CH_3{}^{13}CH_2CN$
196	$35_{4,31}-34_{5,30}$	205501.651	7	313	152.2	100	Strong CH_3OCHO and c-C_2H_4O
197	$34_{9,26}-33_{9,25}$	205639.058	6	322	677.2	271	Strong $CH_3{}^{13}CH_2CN$ and C_2H_5CN
198	$34_{9,25}-33_{9,24}$	205708.710	6	322	677.2	271	Strong $C_2H_5{}^{13}CN$ and CH_3OCH_3
199	$33_{6,27}-32_{6,26}$	205773.682	6	299	685.9	271	Blend with U-line and CH_3OH in absorption
200	$12_{10,2}-11_{9,3}{}^\star$	205968.115	12	179	87.1	271	Blend with CH_3CH_3CO, $\upsilon_t=1$ and CH_3COOH
202	$37_{1,36}-36_{2,35}$	206014.847	7	315	287.3	280	Strong CH_3OH and C_2H_5CN, $\upsilon_{13}=1/\upsilon_{21}=1$
203	$37_{2,36}-36_{2,35}{}^\star$	206014.958	7	315	783.9	280	Strong CH_3OH and C_2H_5CN, $\upsilon_{13}=1/\upsilon_{21}=1$
205	$37_{2,36}-36_{1,35}$	206015.138	7	315	287.3	280	Strong CH_3OH and C_2H_5CN, $\upsilon_{13}=1/\upsilon_{21}=1$
206	$34_{5,30}-33_{4,29}$	206035.987	6	303	142.4	280	Strong C_2H_5CN, $\upsilon_{13}=1/\upsilon_{21}=1$ and C_2H_5CN
207	$34_{8,27}-33_{8,26}$	206266.954	6	316	687.9	280	Strong C_2H_5CN, $\upsilon_{20}=1$, C_2H_5CN, and CH_3OCHO
208	$34_{7,28}-33_{7,27}$	206461.559	6	312	696.8	106	Strong C_2H_5CN, $\upsilon_{13}=1/\upsilon_{21}=1$
209	$34_{8,26}-33_{8,25}$	206887.489	6	316	687.9	106	Blend with C_2H_5CN
210	$38_{0,38}-37_{1,37}{}^\star$	207355.545	13	318	330.6	117	Blend with $^{13}CH_2CHCN$ and CH_3COOH
212	$38_{0,38}-37_{0,37}{}^\star$	207355.546	13	318	810.7	117	Blend with $^{13}CH_2CHCN$ and CH_3COOH
214	$35_{5,31}-34_{5,30}$	207543.638	6	313	728.4	282	Blend with CH_3OCHO and U-line
215	$17_{8,10}-16_{7,9}$	207551.813	12	188	75.2	282	Blend with U-line
216	$17_{8,9}-16_{7,10}$	207552.401	12	188	75.2	282	Blend with U-line
217	$35_{4,31}-34_{4,30}$	208356.853	6	313	728.8	168	Strong $HC^{13}CCN$ and $HCC^{13}CN$
218	$36_{3,33}-35_{4,32}$	208729.722	6	318	204.9	160	Blend with CH_3OCHO and U-line
219	$36_{4,33}-35_{4,32}$	208847.713	6	318	753.3	160	Strong $HC^{13}CCN$, $\upsilon_6=1$
220	$36_{3,33}-35_{3,32}$	208906.164	6	318	753.4	160	Strong C_2H_3CN and CH_3OCHO
221	$36_{4,33}-35_{3,32}$	209024.156	6	318	204.9	160	Strong C_2H_3CN and CH_3OCHO
222	$34_{5,29}-33_{5,28}$	209279.146	6	306	708.3	58	Blend with NH_2CH_2CN and CH_3CH_3CO
223	$34_{7,27}-33_{7,26}$	209670.004	6	312	698.1	45	Blend with $HCC^{13}CN$, $\upsilon_7=2$ and C_2H_3CN, $\upsilon_{11}=1$
224	$35_{21,14}-34_{21,13}{}^\star$	209787.936	10	453	479.8	45	Blend with C_2H_3CN, $\upsilon_{11}=1/\upsilon_{15}=1$
226	$35_{20,15}-34_{20,14}{}^\star$	209790.453	10	439	504.9	45	Blend with C_2H_3CN, $\upsilon_{11}=1/\upsilon_{15}=1$
228	$35_{22,13}-34_{22,12}{}^\star$	209795.133	11	467	453.5	45	Blend with C_2H_3CN, $\upsilon_{11}=1/\upsilon_{15}=1$
230	$35_{19,16}-34_{19,15}{}^\star$	209804.307	10	426	528.7	45	Strong C_2H_3CN, $\upsilon_{11}=1$ and CH_3OCH_3
232	$15_{9,7}-14_{8,6}{}^\star$	209810.239	12	184	81.0	45	Strong C_2H_3CN, $\upsilon_{11}=1$ and CH_3OCH_3
234	$35_{23,12}-34_{23,11}{}^\star$	209810.767	12	482	425.9	45	Strong C_2H_3CN, $\upsilon_{11}=1$ and CH_3OCH_3
236	$35_{18,17}-34_{18,16}{}^\star$	209831.596	10	413	551.4	45	Blend with $^{13}CH_3CH_2CN$
238	$35_{24,11}-34_{24,10}{}^\star$	209833.824	13	498	397.2	45	Blend with $^{13}CH_3CH_2CN$
240	$35_{25,10}-34_{25,9}{}^\star$	209863.488	15	515	367.2	45	Strong C_2H_5OH, CH_3OCHO, and $^{13}CH_3CH_2CN$
242	$35_{17,18}-34_{17,17}{}^\star$	209875.072	10	401	572.9	45	Strong CH_3OCHO, $^{13}CH_3CH_2CN$, and C_2H_5CN
244	$35_{26,9}-34_{26,8}{}^\star$	209899.094	17	532	336.0	45	Blend with C_2H_3CN, $\upsilon_{11}=1$ and $^{13}CH_3CH_2CN$
246	$35_{16,19}-34_{16,18}{}^\star$	209938.416	10	390	593.0	45	Strong CH_3OCHO and SO_2
248	$35_{27,8}-34_{27,7}{}^\star$	209940.094	19	550	303.6	45	Strong CH_3OCHO and SO_2
250	$35_{15,20}-34_{15,19}{}^\star$	210026.654	10	380	612.0	45	Strong HC_3N, $\upsilon_7=1$
252	$37_{2,35}-36_{3,34}$	210086.448	6	322	251.9	45	Blend with C_2H_3CN, $\upsilon_{11}=2$
253	$37_{3,35}-36_{3,34}$	210090.303	6	322	779.0	45	Blend with C_2H_3CN, $\upsilon_{11}=2$
254	$35_{30,5}-34_{30,4}{}^\star$	210091.291	29	607	198.9	45	Blend with C_2H_3CN, $\upsilon_{11}=2$
256	$37_{2,35}-36_{2,34}$	210092.485	6	322	779.0	45	Blend with C_2H_3CN, $\upsilon_{11}=2$
257	$37_{3,35}-36_{2,34}$	210096.339	6	322	251.9	45	Blend with C_2H_3CN, $\upsilon_{11}=2$
258	$35_{14,22}-34_{14,21}{}^\star$	210146.825	9	370	629.7	64	Blend with $^{13}CH_3CH_2CN$
260	$35_{31,4}-34_{31,3}{}^\star$	210150.008	35	628	161.6	64	Blend with $^{13}CH_3CH_2CN$
262	$35_{13,23}-34_{13,22}{}^\star$	210309.100	9	361	646.3	64	Strong HC_3N, $\upsilon_6=\upsilon_7=1$ and C_2H_5CN, $\upsilon_{13}=1/\upsilon_{21}=1$
264	$35_{5,31}-34_{4,30}$	210398.840	6	313	152.8	64	Blend with C_2H_5OH and CH_3OCHO
265	$35_{12,24}-34_{12,23}{}^\star$	210528.754	8	353	661.6	64	Strong HC_3N, $\upsilon_7=2$ and C_2H_5OH
267	$20_{7,14}-19_{6,13}$	210694.282	12	199	69.5	37	Blend with C_2H_3CN, $\upsilon_{11}=2$
268	$35_{11,25}-34_{11,24}$	210829.766	7	345	675.7	37	Blend with $^{13}CH_3OH$ and NH_2CHO
269	$35_{11,24}-34_{11,23}$	210830.374	7	345	675.6	37	Blend with $^{13}CH_3OH$ and NH_2CHO
270	$20_{7,13}-19_{6,14}$	210837.991	12	199	69.5	37	Blend with $^{13}CH_3OH$ and NH_2CHO
271	$35_{6,30}-34_{6,29}$	210871.662	6	317	724.7	37	Blend with U-line and C_2H_5OH
272	$20_{5,15}-19_{3,16}$	210878.636	15	192	2.3	37	Blend with CH_3OCHO, $^{13}CH_3CH_2CN$, and U-line
273	$35_{10,26}-34_{10,25}$	211249.809	7	338	688.5	33	Strong CH_3OCHO
274	$35_{10,25}-34_{10,24}$	211259.223	7	338	688.5	33	Strong CH_3OCHO
275	$38_{1,37}-37_{2,36}{}^\star$	211401.390	50	325	296.5	33	Blend with C_2H_5CN and CH_3CH_3CO, $\upsilon_t=1$, uncertain baseline
277	$38_{1,37}-37_{1,36}{}^\star$	211401.444	9	325	805.2	33	Blend with C_2H_5CN and CH_3CH_3CO, $\upsilon_t=1$, uncertain baseline
279	$36_{4,32}-35_{5,31}$	211527.010	50	323	162.7	47	Blend with C_2H_3CN and CH_3OCHO
280	$35_{9,27}-34_{9,26}$	211828.060	50	332	700.1	47	Blend with U-line, C_2H_5OCHO, and $NH_2{}^{13}CHO$, $\upsilon_{12}=1$

Table 10. continued.

N^a (1)	Transition^b (2)	Frequency (MHz) (3)	Unc.^{c} (kHz) (4)	$E_l{}^d$ (K) (5)	$S\mu^2$ (D^2) (6)	σ^e (mK) (7)	Comments (8)
281	$35_{9,26} - 34_{9,25}$	211938.010	50	332	700.1	36	Strong $NH_2{}^{13}CHO$ and $NH_2{}^{13}CHO$, $v_{12}=1$
282	$13_{10,3} - 12_{9,4}{}^{\star}$	211955.981	12	182	87.6	36	Strong $NH_2{}^{13}CHO$, $v_{12}=1$ and $NH_2{}^{13}CHO$
284	$34_{6,28} - 33_{6,27}$	212120.060	50	309	708.0	36	Strong CH_3CHO and $NH_2{}^{13}CHO$
285	$35_{8,28} - 34_{8,27}$	212458.290	50	326	710.4	99	Blend with C_2H_3CN and C_2H_5OH
286	$35_{7,29} - 34_{7,28}$	212483.750	50	321	719.0	99	Blend with CH_3OCHO, a-C_3H_7CN, and $^{13}CH_3OH$, $v_t=1$
287	$39_{1,39} - 38_{1,38}{}^{\star}$	212743.017	15	328	832.1	99	Strong CH_3OCH_3 and C_2H_5OH
289	$39_{1,39} - 38_{0,38}{}^{\star}$	212743.018	15	328	339.8	99	Strong CH_3OCH_3 and C_2H_5OH
291	$36_{5,32} - 35_{5,31}$	212972.357	6	323	749.7	99	Blend with $^{13}CH_3CH_2CN$ and $^{34}SO_2$
292	$35_{8,27} - 34_{8,26}$	213353.646	6	326	710.6	48	Blend with $^{13}CH_2CHCN$, C_2H_5CN, and U-line
293	$18_{8,11} - 17_{7,10}$	213473.443	12	193	76.1	48	Blend with $C_2H_5{}^{13}CN$
294	$50_{11,40} - 50_{9,41}$	213474.581	160	532	6.1	48	Blend with $C_2H_5{}^{13}CN$
295	$18_{8,10} - 17_{7,11}$	213474.845	12	193	76.1	48	Blend with $C_2H_5{}^{13}CN$
296	$36_{4,32} - 35_{4,31}$	213568.985	6	323	749.9	48	Blend with C_2H_3CN, $v_{11}=1/v_{15}=1$ and $^{13}CH_2CHCN$
297	$11_{11,0} - 10_{10,1}{}^{\star}$	214056.089	12	182	95.9	48	Strong $^{13}CH_3CN$, $C_2H_5{}^{13}CN$, and $CH_3{}^{13}CH_2CN$
299	$37_{3,34} - 36_{4,33}$	214147.290	50	328	214.4	75	Strong $C_2H_5{}^{13}CN$ and $CH_3{}^{13}CH_2CN$
300	$37_{4,34} - 36_{4,33}$	214225.810	50	328	774.6	75	Strong CH_2NH, $^{13}CH_3CN$, and C_2H_5CN
301	$37_{3,34} - 36_{3,33}$	214265.300	50	328	774.6	75	Strong C_2H_5CN and C_2H_5OH
302	$37_{4,34} - 36_{3,33}$	214343.817	6	328	214.4	75	Strong $^{13}CH_3CN$ and $C_2H_5{}^{13}CN$
303	$35_{5,30} - 34_{5,29}$	214468.257	6	316	728.6	75	Blend with CH_3OCH_3
304	$51_{16,35} - 51_{15,36}$	214470.968	53	591	243.9	75	Blend with CH_3OCH_3
305	$51_{16,36} - 51_{15,37}$	214471.118	53	591	243.9	75	Blend with CH_3OCH_3
306	$36_{5,32} - 35_{4,31}$	215014.344	6	323	163.1	74	Blend with $^{13}CH_3CN$, $v_8=1$
307	$38_{2,36} - 37_{3,35}$	215469.850	50	332	261.1	74	Strong C_2H_5CN, $v_{13}=1/v_{21}=1$
308	$38_{3,36} - 37_{3,35}$	215472.342	7	332	800.3	74	Strong C_2H_5CN, $v_{13}=1/v_{21}=1$
309	$38_{2,36} - 37_{2,35}$	215473.742	7	332	800.3	74	Strong C_2H_5CN, $v_{13}=1/v_{21}=1$
310	$38_{3,36} - 37_{2,35}$	215476.230	50	332	261.1	74	Strong C_2H_5CN, $v_{13}=1/v_{21}=1$
311	$21_{5,16} - 20_{3,17}$	215480.099	15	198	2.7	74	Strong C_2H_5CN, $v_{13}=1/v_{21}=1$
312	$16_{9,8} - 15_{8,7}{}^{\star}$	215778.326	12	189	82.0	74	Blend with C_2H_5CN, $v_{20}=1$
314	$36_{21,15} - 35_{21,14}{}^{\star}$	215779.220	50	463	508.7	74	Blend with C_2H_5CN, $v_{20}=1$
316	$36_{22,14} - 35_{22,13}{}^{\star}$	215783.850	50	477	483.1	74	Blend with C_2H_5CN, $v_{20}=1$
318	$36_{20,16} - 35_{20,15}{}^{\star}$	215784.950	50	449	533.2	74	Blend with C_2H_5CN, $v_{20}=1$
320	$36_{23,13} - 35_{23,12}{}^{\star}$	215797.530	50	492	456.3	74	Blend with C_2H_5CN, $v_{13}=1/v_{21}=1$
322	$36_{19,17} - 35_{19,16}{}^{\star}$	215802.872	10	436	556.3	74	Blend with C_2H_5CN, $v_{13}=1/v_{21}=1$
324	$36_{24,12} - 35_{24,11}{}^{\star}$	215819.220	50	508	428.4	55	Strong C_2H_5CN, $v_{13}=1/v_{21}=1$
326	$36_{18,18} - 35_{18,17}{}^{\star}$	215835.300	50	423	578.4	55	Strong C_2H_5CN, $v_{13}=1/v_{21}=1$ and ^{34}SO
328	$36_{25,11} - 35_{25,10}{}^{\star}$	215847.810	50	525	399.2	55	Strong ^{34}SO
330	$36_{26,10} - 35_{26,9}{}^{\star}$	215882.850	50	542	368.9	55	Strong $^{13}CH_3OH$
332	$36_{17,19} - 35_{17,18}{}^{\star}$	215885.180	50	411	599.1	55	Strong $^{13}CH_3OH$ and C_2H_5OH
334	$36_{27,9} - 35_{27,8}{}^{\star}$	215923.600	50	560	337.4	55	Blend with C_2H_5OH, CH_3COOH, and U-line
336	$36_{16,20} - 35_{16,19}{}^{\star}$	215956.570	50	400	618.7	55	Strong C_2H_5CN
338	$36_{15,21} - 35_{15,20}{}^{\star}$	216055.006	10	390	637.2	55	Strong C_2H_5CN, $v_{13}=1/v_{21}=1$
340	$36_{14,22} - 35_{14,21}{}^{\star}$	216188.170	50	380	654.5	55	Blend with C_2H_5CN
342	$36_{32,4} - 35_{32,3}{}^{\star}$	216198.450	50	659	161.8	55	Blend with CH_3OCHO
344	$36_{13,23} - 35_{13,22}{}^{\star}$	216367.230	50	371	670.6	55	Strong CH_3OCHO and $^{13}CH_3OH$
346	$21_{7,15} - 20_{6,14}$	216386.644	12	205	70.1	55	Blend with U-line
347	$35_{7,28} - 34_{7,27}$	216489.383	6	322	720.8	55	Blend with C_2H_5CN, $v_{13}=1/v_{21}=1$ and U-line
348	$36_{6,31} - 35_{6,30}$	216511.289	7	327	746.2	55	Strong CH_3CH_3CO, $v_t=1$ and C_2H_5CN, $v_{13}=1/v_{21}=1$
349	$36_{12,24} - 35_{12,23}{}^{\star}$	216609.170	50	363	685.5	55	Blend with CH_3COOH
351	$21_{7,14} - 20_{6,15}$	216649.055	12	205	70.1	55	Strong SO_2
352	$39_{1,38} - 38_{2,37}{}^{\star}$	216786.652	10	335	305.7	50	Blend with U-line and CH_3CH_3CO, $v_t=1$
354	$39_{1,38} - 38_{1,37}{}^{\star}$	216786.721	10	335	826.7	50	Blend with U-line and CH_3CH_3CO, $v_t=1$
356	$42_{16,26} - 42_{15,27}{}^{\star}$	216853.893	37	469	186.2	50	Strong C_2H_5CN, $v_{13}=1/v_{21}=1$
358	$36_{11,26} - 35_{11,25}$	216940.590	50	355	699.1	50	Strong C_2H_3CN and CH_3OH
359	$36_{11,25} - 35_{11,24}$	216941.740	50	355	699.1	50	Strong C_2H_3CN and CH_3OH
360	$41_{16,25} - 41_{15,26}{}^{\star}$	217028.389	36	456	179.9	50	Blend with CH_3CH_3CO and ^{13}CN in absorption
362	$40_{16,24} - 40_{15,25}{}^{\star}$	217188.266	36	445	173.6	50	Strong CH_3OCH_3
364	$39_{16,23} - 39_{15,24}{}^{\star}$	217334.340	35	433	167.4	50	Blend with $CH_2{}^{13}CHCN$
366	$37_{4,33} - 36_{5,32}$	217368.200	8	333	173.0	50	Blend with ^{13}CN in absorption, $C_2H_5{}^{13}CN$, and U-line?
367	$36_{10,27} - 35_{10,26}$	217402.380	50	348	711.7	50	Strong $HC^{13}CCN$ and $^{13}CH_3OH$
368	$36_{10,26} - 35_{10,25}$	217418.120	50	348	711.6	50	Strong $HCC^{13}CN$
369	$38_{16,22} - 38_{15,23}{}^{\star}$	217467.396	35	422	161.1	50	Blend with ^{13}CN in absorption
371	$37_{16,21} - 37_{15,22}{}^{\star}$	217588.187	34	411	154.8	50	Blend with $(CH_2OH)_2$ and U-line
373	$36_{16,20} - 36_{15,21}{}^{\star}$	217697.439	34	400	148.6	50	Blend with $CH_2CH^{13}CN$ and U-line

Table 10. continued.

N^a (1)	Transition^b (2)	Frequency (MHz) (3)	Unc.^{c} (kHz) (4)	E_l^{d} (K) (5)	$S\mu^2$ (D^2) (6)	σ^e (mK) (7)	Comments (8)
375	$39_{8,31} - 39_{5,34}$	219371.585	37	370	11.6	92	Blend with C_2H_3CN, v_{11}=1/v_{15}=1
376	$19_{8,12} - 18_{7,11}$	219376.897	12	198	77.1	92	Blend with C_2H_3CN, v_{11}=1/v_{15}=1 and C_2H_5OH
377	$19_{8,11} - 18_{7,12}$	219380.063	12	198	77.1	92	Blend with C_2H_3CN, v_{11}=1/v_{15}=1 and C_2H_5OH
378	$38_{3,35} - 37_{4,34}$	219549.670	50	338	223.9	92	Strong $C^{18}O$
379	$36_{5,31} - 35_{5,30}$	219565.844	7	327	748.9	92	Strong $C^{18}O$
380	$38_{4,35} - 37_{4,34}$	219601.640	50	338	796.0	92	Blend with CH_3CN, v_4=1 and NH_2CN
381	$38_{3,35} - 37_{3,34}$	219628.210	50	338	796.0	92	Strong C_2H_5CN, v_{20}=1 and CH_3CN, v_4=1
382	$58_{2,56} - 58_{1,57}{}^\star$	219628.923	369	593	66.8	92	Strong C_2H_5CN, v_{20}=1 and CH_3CN, v_4=1
384	$58_{3,56} - 58_{2,57}{}^\star$	219628.923	369	593	66.8	92	Strong C_2H_5CN, v_{20}=1 and CH_3CN, v_4=1
386	$63_{11,53} - 62_{12,50}$	219678.339	347	748	53.1	92	Strong HC_3N, v_7=2
387	$38_{4,35} - 37_{3,34}$	219680.190	7	338	223.9	92	Strong HC_3N, v_7=2
388	$13_{11,2} - 12_{10,3}{}^\star$	226038.817	12	189	96.1	278	Blend with c-C_2H_4O
390	$40_{2,38} - 39_{3,37}$	226232.383	9	353	279.7	278	Noisy, blend with U-line?
391	$40_{3,38} - 39_{3,37}$	226233.371	9	353	843.2	278	Noisy, blend with U-line?
392	$40_{2,38} - 39_{2,37}$	226233.942	9	353	843.2	278	Noisy, blend with U-line?
393	$40_{3,38} - 39_{2,37}$	226234.930	9	353	279.6	278	Noisy, blend with U-line?
394	$59_{17,42} - 59_{16,43}$	226530.302	99	729	290.8	278	Blend with C_2H_5CN
395	$59_{17,43} - 59_{16,44}$	226530.999	99	729	290.8	278	Blend with C_2H_5CN
396	$37_{8,29} - 36_{8,28}$	226531.433	7	347	755.6	278	Blend with C_2H_5CN
397	$62_{3,59} - 62_{3,60}{}^\star$	226531.914	447	668	15.8	278	Blend with C_2H_5CN
399	$62_{4,59} - 62_{3,60}{}^\star$	226531.915	447	668	100.4	278	Blend with C_2H_5CN
401	$23_{7,17} - 22_{6,16}$	227460.224	12	218	70.9	85	Blend with CH_3COOH, $CH_2(OH)CHO$, and $CH_2CH^{13}CN$
402	$41_{1,40} - 40_{2,39}{}^\star$	227553.664	14	357	324.0	85	Strong C_2H_5CN and CH_3OCHO
404	$41_{1,40} - 40_{1,39}{}^\star$	227553.690	14	357	869.6	85	Strong C_2H_5CN and CH_3OCHO
406	$60_{2,58} - 60_{1,59}{}^\star$	227625.680	458	624	66.9	85	Strong C_2H_5CN, v_{13}=1/v_{21}=1
408	$60_{2,58} - 60_{2,59}{}^\star$	227625.680	458	624	10.9	85	Strong C_2H_5CN, v_{13}=1/v_{21}=1
410	$38_{6,33} - 37_{6,32}$	227639.839	9	348	788.8	85	Strong C_2H_5CN, v_{13}=1/v_{21}=1 and CH_3OCHO
411	$18_{9,10} - 17_{8,9}{}^\star$	227689.981	12	198	84.0	85	Blend with U-line
413	$23_{5,18} - 22_{3,19}$	227691.505	14	210	3.5	85	Blend with U-line
414	$38_{22,16} - 37_{22,15}{}^\star$	227759.604	11	498	541.1	85	Blend with $H_2{}^{13}CS$ and C_2H_5OH
416	$38_{21,17} - 37_{21,16}{}^\star$	227760.667	11	484	565.4	85	Blend with $H_2{}^{13}CS$ and C_2H_5OH
418	$38_{23,15} - 37_{23,14}{}^\star$	227768.859	12	513	515.7	85	Strong C_2H_5CN
420	$38_{20,18} - 37_{20,17}{}^\star$	227773.682	11	470	588.4	85	Strong C_2H_5CN
422	$38_{24,14} - 37_{24,13}{}^\star$	227787.136	12	529	489.3	85	Strong C_2H_5CN and HC_3N, v_6=1
424	$38_{19,19} - 37_{19,18}{}^\star$	227800.733	11	457	610.4	85	Strong $^{13}CH_3CH_2CN$ and CH_3OH
426	$38_{25,13} - 37_{25,12}{}^\star$	227813.392	14	546	461.7	85	Strong CH_3OH
428	$56_{17,39} - 56_{16,40}$	227818.866	80	679	270.6	85	Strong CH_3OH
429	$56_{17,40} - 56_{16,41}$	227819.010	80	679	270.6	85	Strong CH_3OH
430	$38_{18,20} - 37_{18,19}{}^\star$	227844.521	11	444	631.3	85	Blend with CH_3CH_3CO, $HC^{13}CCN$, v_7=2, and $HCC^{13}CN$, v_7=2
432	$38_{26,12} - 37_{26,11}{}^\star$	227846.781	15	563	432.9	85	Blend with CH_3CH_3CO, $HC^{13}CCN$, v_7=2, and $HCC^{13}CN$, v_7=2
434	$38_{27,11} - 37_{27,10}{}^\star$	227886.609	17	581	403.0	85	Strong C_2H_5OH
436	$38_{17,21} - 37_{17,20}{}^\star$	227908.603	11	432	651.0	85	Strong $CH_3{}^{13}CH_2CN$ and C_2H_3CN
438	$44_{17,27} - 44_{16,28}{}^\star$	231002.504	54	504	193.5	183	Noisy
440	$21_{8,14} - 20_{7,13}$	231114.753	12	210	78.8	183	Blend with C_2H_3CN, v_{11}=1, CH_3CHO, and U-line
441	$21_{8,13} - 20_{7,14}$	231128.746	12	210	78.8	183	Blend with U-line and $H_2{}^{13}CS$
442	$43_{17,26} - 43_{16,27}{}^\star$	231159.401	54	491	187.2	183	Strong $^{13}CH_2CHCN$
444	$42_{17,25} - 42_{16,26}{}^\star$	231303.368	53	479	180.9	40	Strong $^{13}CH_3CH_2CN$ and C_2H_5CN
446	$41_{17,24} - 41_{16,25}{}^\star$	231435.094	53	467	174.7	40	Blend with $^{13}CH_2CHCN$
448	$40_{17,23} - 40_{16,24}{}^\star$	231555.240	53	455	168.4	40	Blend with C_2H_5OH
450	$41_{2,39} - 40_{3,38}$	231611.663	10	364	288.9	40	Blend with HNCO, v_5=1, CH_3OCHO, $^{13}CH_3CN$, and U-line
451	$41_{3,39} - 40_{3,38}$	231612.288	10	364	864.4	40	Blend with HNCO, v_5=1, CH_3OCHO, $^{13}CH_3CN$, and U-line
452	$41_{2,39} - 40_{2,38}$	231612.651	10	364	864.6	40	Blend with HNCO, v_5=1, CH_3OCHO, $^{13}CH_3CN$, and U-line
453	$41_{3,39} - 40_{2,38}$	231613.276	10	364	288.9	40	Blend with HNCO, v_5=1, CH_3OCHO, $^{13}CH_3CN$, and U-line
454	$61_{2,59} - 61_{1,60}{}^\star$	231619.484	508	640	66.9	40	Blend with CH_3OCHO, $^{13}CH_3CN$, and U-line
456	$61_{3,59} - 61_{2,60}{}^\star$	231619.484	508	640	66.9	40	Blend with CH_3OCHO, $^{13}CH_3CN$, and U-line
458	$58_{11,47} - 57_{12,46}$	231619.899	325	659	71.0	40	Blend with CH_3OCHO, $^{13}CH_3CN$, and U-line
459	$39_{17,22} - 39_{16,23}{}^\star$	231664.446	53	444	162.2	40	Blend with $^{13}CH_3CH_2CN$ and C_2H_5OH
461	$37_{6,32} - 36_{5,31}$	232675.249	9	337	125.2	19	Blend with CH_3CH_3CO, v_t=1 and U-line
462	$24_{7,18} - 23_{6,17}$	232766.448	12	224	71.1	19	Blend with $^{13}CH_3CN$, v_8=1 and CH_3CH_3CO
463	$40_{5,36} - 39_{4,35}$	235023.563	9	365	203.0	131	Blend with CH_3OCHO
464	$39_{11,29} - 38_{11,28}$	235323.229	8	387	768.9	131	Blend with CH_3CHO and U-line
465	$23_{4,19} - 22_{3,20}$	235326.210	10	208	11.1	131	Blend with CH_3CHO and U-line
466	$39_{11,28} - 38_{11,27}$	235328.787	8	387	769.0	131	Blend with CH_3CHO and U-line

Table 10. continued.

N[a]	Transition[b]	Frequency (MHz)	Unc.[c] (kHz)	E_l[d] (K)	$S\mu^2$ (D^2)	σ[e] (mK)	Comments
(1)	(2)	(3)	(4)	(5)	(6)	(7)	(8)
467	$40_{5,35} - 39_{6,34}$	235342.332	14	370	156.8	131	Blend with U-line and CH_3CH_3CO
468	$62_{2,60} - 62_{1,61}{}^\star$	235610.226	562	656	67.0	131	Blend with CH_3CH_3CO, $^{13}CH_3OH$, $\upsilon_t=1$, and C_2H_5CN, $\upsilon_{13}=1/\upsilon_{21}=1$
470	$62_{2,60} - 62_{2,61}{}^\star$	235610.226	562	656	10.9	131	Blend with CH_3CH_3CO, $^{13}CH_3OH$, $\upsilon_t=1$, and C_2H_5CN, $\upsilon_{13}=1/\upsilon_{21}=1$
472	$38_{6,32} - 37_{6,31}$	235612.906	10	351	792.6	131	Blend with CH_3CH_3CO, $^{13}CH_3OH$, $\upsilon_t=1$, and C_2H_5CN, $\upsilon_{13}=1/\upsilon_{21}=1$
473	$38_{6,33} - 37_{5,32}$	235699.420	8	348	136.0	131	Blend with CH_3OCH_3, uncertain baseline
474	$41_{3,38} - 40_{4,37}$	235705.579	10	370	252.1	131	Blend with CH_3OCH_3, uncertain baseline
475	$41_{4,38} - 40_{4,37}$	235720.329	10	370	860.1	131	Blend with CH_3OCH_3, uncertain baseline
476	$41_{3,38} - 40_{3,37}$	235728.110	10	370	860.0	131	Blend with U-line, uncertain baseline
477	$67_{13,55} - 66_{14,52}$	235732.617	481	838	79.3	131	Blend with U-line, uncertain baseline
478	$41_{4,38} - 40_{3,37}$	235742.860	10	370	252.1	131	Baseline problem, or absorption line?
479	$17_{10,8} - 16_{9,7}{}^\star$	235876.754	12	199	90.8	131	Strong CH_3OCHO, C_2H_5CN, $\upsilon_{13}=1/\upsilon_{21}=1$, and $^{13}CH_3OH$
481	$39_{10,30} - 38_{10,29}$	235923.054	8	380	780.4	131	Blend with CH_3OCHO
482	$39_{10,29} - 38_{10,28}$	235988.744	8	380	780.5	131	Strong C_2H_5OH and $^{13}CH_3OH$
483	$68_{4,64} - 68_{3,65}{}^\star$	240990.966	671	784	134.4	216	Strong CH_3OCH_3, $C_2H_5{}^{13}CN$, and CH_3CH_3CO
485	$68_{5,64} - 68_{4,65}{}^\star$	240990.969	671	784	134.4	216	Strong CH_3OCH_3, $C_2H_5{}^{13}CN$, and CH_3CH_3CO
487	$40_{12,29} - 39_{12,28}$	240992.017	9	406	779.7	216	Strong CH_3OCH_3, $C_2H_5{}^{13}CN$, and CH_3CH_3CO
488	$40_{12,28} - 39_{12,27}$	240992.663	9	406	779.7	216	Strong CH_3OCH_3, $C_2H_5{}^{13}CN$, and CH_3CH_3CO
489	$39_{6,33} - 38_{6,32}$	241002.693	11	363	812.9	216	Strong $C_2H_5{}^{13}CN$, CH_3CH_3CO, and $C^{34}S$
490	$42_{3,39} - 41_{4,38}$	241081.365	11	382	261.4	216	Blend with $CH_3{}^{13}CH_2CN$ and U-line
491	$42_{4,39} - 41_{4,38}$	241090.991	11	382	881.3	216	Blend with $CH_3{}^{13}CH_2CN$ and U-line
492	$42_{3,39} - 41_{3,38}$	241096.116	11	382	881.3	216	Blend with $CH_3{}^{13}CH_2CN$ and U-line
493	$42_{4,39} - 41_{3,38}$	241105.742	11	382	261.4	216	Blend with U-line and C_2H_5CN
494	$16_{11,5} - 15_{10,6}{}^\star$	244001.794	12	201	97.9	46	Blend with C_2H_5OH
496	$41_{6,36} - 40_{6,35}$	244037.948	12	382	852.7	46	Strong H_2CS
497	$41_{5,36} - 40_{5,35}$	244944.066	12	382	853.1	39	Strong CS
498	$45_{0,45} - 44_{1,44}{}^\star$	245041.483	39	394	394.8	39	Blend with C_2H_5CN and $C_2H_5{}^{13}CN$
500	$45_{1,45} - 44_{1,44}{}^\star$	245041.483	39	394	960.6	39	Blend with C_2H_5CN and $C_2H_5{}^{13}CN$
502	$42_{4,38} - 41_{5,37}$	245115.653	12	388	222.4	72	Strong CH_2NH
503	$42_{5,38} - 41_{5,37}$	245270.702	12	388	877.3	72	Strong HC_3N, $\upsilon_4=1$ and $C_2H_5{}^{13}CN$
504	$45_{18,27} - 45_{17,28}{}^\star$	245277.970	79	528	194.5	72	Strong $C_2H_5{}^{13}CN$
506	$42_{4,38} - 41_{4,37}$	245344.019	12	388	877.3	72	Strong SO_2 and CH_3CH_3CO
507	$44_{18,26} - 44_{17,27}{}^\star$	245407.219	79	515	188.3	72	Blend with CH_3CH_3CO
509	$21_{9,13} - 20_{8,12}$	245470.669	12	215	86.9	72	Strong C_2H_5CN, $\upsilon_{13}=1/\upsilon_{21}=1$ and C_2H_3CN, $\upsilon_{11}=1$
510	$21_{9,12} - 20_{8,13}$	245471.188	12	215	86.9	72	Strong C_2H_5CN, $\upsilon_{13}=1/\upsilon_{21}=1$ and C_2H_3CN, $\upsilon_{11}=1$
511	$86_{10,76} - 86_{9,77}$	245475.958	1519	1239	344.4	72	Strong C_2H_5CN, $\upsilon_{13}=1/\upsilon_{21}=1$ and C_2H_3CN, $\upsilon_{11}=1$
512	$42_{5,38} - 41_{4,37}$	245499.068	12	388	222.4	72	Strong $HC^{13}CCN$, $\upsilon_7=1$
513	$43_{18,25} - 43_{17,26}{}^\star$	245525.550	78	502	182.0	72	Strong $HCC^{13}CN$, $\upsilon_7=1$
515	$42_{18,24} - 42_{17,25}{}^\star$	245633.528	78	490	175.7	53	Blend with $CH_2{}^{13}CHCN$ and C_2H_3CN, $\upsilon_{15}=2$
517	$77_{7,70} - 77_{7,71}{}^\star$	245718.043	974	998	32.3	53	Blend with $CH_2{}^{13}CHCN$ and HNCO, $\upsilon_5=1$
519	$77_{8,70} - 77_{7,71}{}^\star$	245718.533	974	998	237.4	53	Blend with $CH_2{}^{13}CHCN$ and HNCO, $\upsilon_5=1$
521	$41_{22,19} - 40_{22,18}{}^\star$	245718.666	11	532	625.3	53	Blend with $CH_2{}^{13}CHCN$ and HNCO, $\upsilon_5=1$
523	$41_{23,18} - 40_{23,17}{}^\star$	245719.705	12	547	601.8	53	Blend with $CH_2{}^{13}CHCN$ and HNCO, $\upsilon_5=1$
525	$41_{21,20} - 40_{21,19}{}^\star$	245730.112	12	517	647.8	53	Blend with HNCO, $\upsilon_5=1$
527	$41_{24,17} - 40_{24,16}{}^\star$	245731.600	12	563	577.2	53	Blend with HNCO, $\upsilon_5=1$
529	$41_{18,23} - 41_{17,24}{}^\star$	245731.700	78	478	169.5	53	Blend with HNCO, $\upsilon_5=1$
531	$42_{8,34} - 42_{5,37}$	245748.107	35	405	8.6	53	Strong $CH_2{}^{13}CHCN$ and CH_3OCHO
532	$41_{25,16} - 40_{25,15}{}^\star$	245753.043	13	579	551.6	53	Strong $CH_2{}^{13}CHCN$, CH_3OCHO, and HC_3N, $\upsilon_5=1/\upsilon_7=3$
534	$41_{20,21} - 40_{20,20}{}^\star$	245756.100	12	504	669.2	53	Strong CH_3OCHO and HC_3N, $\upsilon_5=1/\upsilon_7=3$
536	$41_{26,15} - 40_{26,14}{}^\star$	245782.976	14	597	525.1	53	Strong $CH_2{}^{13}CHCN$ and C_2H_5CN, $\upsilon_{13}=1/\upsilon_{21}=1$
538	$41_{19,22} - 40_{19,21}{}^\star$	245799.265	12	490	689.7	53	Blend with $CH_2CH^{13}CN$
540	$48_{8,40} - 47_{9,39}$	245812.073	103	487	81.9	53	Strong $CH_2CH^{13}CN$ and $CH_2{}^{13}CHCN$
541	$41_{27,14} - 40_{27,13}{}^\star$	245820.530	15	614	497.4	53	Strong $CH_2CH^{13}CN$ and $CH_2{}^{13}CHCN$
543	$40_{18,22} - 40_{17,23}{}^\star$	245820.595	78	466	163.2	53	Strong $CH_2CH^{13}CN$ and $CH_2{}^{13}CHCN$
545	$41_{18,23} - 40_{18,22}{}^\star$	245863.030	12	478	708.9	53	Blend with $CH_2CH^{13}CN$
547	$41_{28,13} - 40_{28,12}{}^\star$	245864.987	16	633	468.6	53	Blend with $CH_2CH^{13}CN$
549	$39_{18,21} - 39_{17,22}{}^\star$	245900.727	78	455	157.0	53	Strong CH_3OCHO and $CH_2CH^{13}CN$
551	$41_{29,12} - 40_{29,11}{}^\star$	245915.751	17	652	438.9	53	Strong $CH_2CH^{13}CN$ and $CH_2{}^{13}CHCN$
553	$26_{7,19} - 25_{6,20}$	245927.818	12	239	70.3	53	Blend with $CH_2CH^{13}CN$
554	$41_{17,24} - 40_{17,23}{}^\star$	245951.925	12	466	727.2	53	Blend with CH_3CH_3CO, $\upsilon_t=1$

Table 10. continued.

N^a (1)	Transition^b (2)	Frequency (MHz) (3)	Unc.^{c} (kHz) (4)	$E_l{}^d$ (K) (5)	$S\mu^2$ (D^2) (6)	σ^e (mK) (7)	Comments (8)
556	$41_{30,11} - 40_{30,10}{}^{\star}$	245972.316	19	672	408.0	53	Blend with C_2H_5CN, $v_{13}=1/v_{21}=1$ and $v=0$, and U-line
558	$38_{18,20} - 38_{17,21}{}^{\star}$	245972.593	78	443	150.7	53	Blend with C_2H_5CN, $v_{13}=1/v_{21}=1$ and $v=0$, and U-line
560	$41_{31,10} - 40_{31,9}{}^{\star}$	246034.256	22	692	376.2	53	Blend with C_2H_5CN, $v_{13}=1/v_{21}=1$ and CH_3OCHO
562	$37_{18,19} - 37_{17,20}{}^{\star}$	246036.674	78	432	144.4	53	Blend with C_2H_5CN, $v_{13}=1/v_{21}=1$ and CH_3OCHO
564	$27_{7,21} - 26_{6,20}$	247058.498	12	246	70.8	68	Strong CH_3OCHO
565	$63_{12,51} - 62_{13,50}$	247101.751	518	754	76.5	68	Blend with C_2H_3CN and HC_3N, $v_7=2$
566	$41_{12,30} - 40_{12,29}$	247104.436	10	418	803.0	68	Blend with C_2H_3CN and HC_3N, $v_7=2$
567	$41_{12,29} - 40_{12,28}$	247105.557	10	418	803.0	68	Blend with C_2H_3CN and HC_3N, $v_7=2$
568	$41_{6,36} - 40_{5,35}$	247299.045	10	382	168.3	68	Blend with C_2H_3CN, $v_{15}=1$
569	$41_{7,35} - 40_{7,34}$	247432.588	13	387	849.3	68	Blend with C_2H_5OCHO, t-HCOOH, and $^{34}SO_2$
570	$42_{17,25} - 41_{17,24}{}^{\star}$	251968.635	13	478	752.3	42	Blend with CH_3OCH_3
572	$27_{7,20} - 26_{6,21}$	252059.917	12	246	69.6	42	Blend with $CH_3{}^{13}CH_2CN$, C_2H_5CN, $v_{20}=1$, a-C_3H_7CN, and U-line
573	$42_{32,10} - 41_{32,9}{}^{\star}$	252075.949	25	725	377.4	42	Blend with a-C_3H_7CN and t-HCOOH
575	$15_{12,3} - 14_{11,4}{}^{\star}$	252090.157	12	204	105.6	42	Strong t-HCOOH and CH_3OH
577	$42_{16,27} - 41_{16,26}{}^{\star}$	252100.361	12	467	769.0	42	Strong CH_3OH and C_2H_5CN, $v_{13}=1/v_{21}=1$
579	$42_{15,28} - 41_{15,27}{}^{\star}$	252274.857	12	456	784.8	42	Strong C_2H_5CN, $v_{13}=1/v_{21}=1$
581	$64_{1,63} - 64_{0,64}{}^{\star}$	252277.352	860	678	33.6	42	Strong C_2H_5CN, $v_{13}=1/v_{21}=1$
583	$64_{1,63} - 64_{1,64}{}^{\star}$	252277.352	860	678	5.7	42	Strong C_2H_5CN, $v_{13}=1/v_{21}=1$
585	$25_{8,18} - 24_{7,17}$	254150.394	12	236	81.3	32	Blend with CH_3CH_3CO and U-line
586	$13_{13,0} - 12_{12,1}{}^{\star}$	254156.954	13	204	114.2	32	Blend with CH_3CH_3CO and U-line
588	$25_{8,17} - 24_{7,18}$	254324.253	12	236	81.3	32	Strong $^{13}CH_3OH$
589	$42_{9,34} - 41_{9,33}$	255230.622	14	409	858.3	217	Strong C_2H_5CN, $v_{20}=1$ and NH_2CHO
590	$43_{5,38} - 42_{5,37}$	255329.346	15	405	895.6	217	Strong C_2H_5CN, $v_{13}=1/v_{21}=1$ and HC_3N, $v_7=1$
591	$41_{7,34} - 40_{7,33}$	255562.496	16	389	855.2	217	Strong SO_2 and $CH_2CH^{13}CN$
592	$46_{7,39} - 45_{8,38}$	257971.741	60	454	112.3	1127	Strong t-HCOOH and CH_3CN, $v_8=1$
593	$43_{31,12} - 42_{31,11}{}^{\star}$	257980.769	18	716	442.3	1127	Strong t-HCOOH and CH_3CN, $v_8=1$
595	$43_{17,26} - 42_{17,25}{}^{\star}$	257986.516	13	490	777.1	1127	Strong t-HCOOH and CH_3CN, $v_8=1$
597	$55_{19,36} - 55_{18,37}{}^{\star}$	258045.723	118	685	252.3	1127	Strong CH_3CN, $v_8=1$
599	$43_{32,11} - 42_{32,10}{}^{\star}$	258048.624	22	737	410.9	1127	Strong CH_3CN, $v_8=1$
601	$16_{12,4} - 15_{11,5}{}^{\star}$	258080.161	12	208	106.2	1127	Strong CH_3OCHO, $CH_3{}^{13}CN$, $v_8=1$, and NH_2CN
603	$43_{33,10} - 42_{33,9}{}^{\star}$	258121.617	31	759	378.5	1127	Strong CH_3CN, $v_8=1$ and CH_3OCHO
605	$43_{16,28} - 42_{16,27}{}^{\star}$	258130.483	13	479	793.5	1127	Strong CH_3OCHO and CH_3CN, $v_8=1$
607	$43_{15,29} - 42_{15,28}{}^{\star}$	258320.451	13	469	809.0	1127	Strong CH_3CN, $v_8=1$
609	$43_{13,31} - 42_{13,30}$	258903.344	12	450	836.8	1609	Noisy, blend with $^{13}CH_2CHCN$
610	$43_{13,30} - 42_{13,29}$	258903.558	12	450	836.8	1609	Noisy, blend with $^{13}CH_2CHCN$
611	$43_{11,32} - 42_{11,31}$	260000.636	13	434	860.9	413	Strong CH_3OCH_3 and $CH_2{}^{13}CHCN$
612	$40_{19,21} - 40_{18,22}{}^{\star}$	260004.028	112	478	158.0	413	Strong CH_3OCH_3 and $CH_2{}^{13}CHCN$
614	$26_{8,18} - 25_{7,19}$	260060.358	12	243	81.7	413	Strong C_2H_5CN, $v_{20}=1$ and CH_3OH
615	$39_{19,20} - 39_{18,21}{}^{\star}$	260060.729	112	466	151.7	413	Strong C_2H_5CN, $v_{20}=1$ and CH_3OH
617	$38_{19,19} - 38_{18,20}{}^{\star}$	260110.774	112	455	145.4	413	Strong C_2H_5OH and C_2H_5CN, $v_{20}=1$
619	$14_{13,1} - 13_{12,2}{}^{\star}$	260151.979	13	207	114.1	413	Strong C_2H_5CN, $v_{20}=1$ and C_2H_5CN
621	$37_{19,18} - 37_{18,19}{}^{\star}$	260154.562	113	444	139.0	413	Strong C_2H_5CN, $v_{20}=1$ and C_2H_5CN
623	$36_{19,17} - 36_{18,18}{}^{\star}$	260192.478	113	434	132.7	413	Strong NH_2CHO and CH_2CO
625	$44_{6,39} - 43_{6,38}$	260216.245	17	418	916.5	413	Strong C_2H_5CN and C_2H_5CN, $v_{20}=1$
626	$35_{19,16} - 35_{18,17}{}^{\star}$	260224.898	113	423	126.2	413	Strong C_2H_5CN, $v_{20}=1$ and C_2H_5CN
628	$34_{19,15} - 34_{18,16}{}^{\star}$	260252.187	113	413	119.8	413	Strong C_2H_5OH, CH_3OCHO, $H^{13}CO^+$, and C_2H_5CN, $v_{13}=1/v_{21}=1$
630	$73_{14,60} - 72_{15,57}$	260255.958	771	968	86.0	413	Strong C_2H_5OH, CH_3OCHO, $H^{13}CO^+$, and C_2H_5CN, $v_{13}=1/v_{21}=1$
631	$19_{19,0} - 19_{18,1}{}^{\star}$	260262.738	117	297	9.3	413	Strong $H^{13}CO^+$ and C_2H_5CN, $v_{13}=1/v_{21}=1$
633	$33_{19,14} - 33_{18,15}{}^{\star}$	260274.699	113	403	113.3	413	Strong C_2H_5CN, $v_{13}=1/v_{21}=1$, C_2H_5CN, $v_{20}=1$, and $H_2{}^{13}CS$
635	$20_{19,1} - 20_{18,2}{}^{\star}$	260275.506	117	302	18.2	413	Strong C_2H_5CN, $v_{13}=1/v_{21}=1$, C_2H_5CN, $v_{20}=1$, and $H_2{}^{13}CS$
637	$21_{19,2} - 21_{18,3}{}^{\star}$	260287.415	116	309	26.7	413	Strong $H_2{}^{13}CS$ and C_2H_5CN, $v_{13}=1/v_{21}=1$
639	$32_{19,13} - 32_{18,14}{}^{\star}$	260292.777	113	394	106.7	413	Strong $H_2{}^{13}CS$ and C_2H_5CN, $v_{13}=1/v_{21}=1$
641	$22_{19,3} - 22_{18,4}{}^{\star}$	260298.247	116	315	34.9	413	Strong $H_2{}^{13}CS$ and C_2H_5CN, $v_{13}=1/v_{21}=1$
643	$31_{19,12} - 31_{18,13}{}^{\star}$	260306.755	113	385	100.0	413	Strong C_2H_5CN, $v_{13}=1/v_{21}=1$
645	$23_{19,4} - 23_{18,5}{}^{\star}$	260307.776	116	321	42.8	413	Strong C_2H_5CN, $v_{13}=1/v_{21}=1$
647	$24_{19,5} - 24_{18,6}{}^{\star}$	260315.766	115	328	50.5	413	Strong C_2H_5CN, $v_{13}=1/v_{21}=1$
649	$30_{19,11} - 30_{18,12}{}^{\star}$	260316.958	114	376	93.3	413	Strong C_2H_5CN, $v_{13}=1/v_{21}=1$, CH_3OCH_3, and C_2H_5CN
651	$25_{19,6} - 25_{18,7}{}^{\star}$	260321.972	115	336	58.0	413	Strong C_2H_5CN, $v_{13}=1/v_{21}=1$, CH_3OCH_3, and C_2H_5CN
653	$29_{19,10} - 29_{18,11}{}^{\star}$	260323.698	114	367	86.5	413	Strong C_2H_5CN, $v_{13}=1/v_{21}=1$, CH_3OCH_3, and C_2H_5CN
655	$26_{19,7} - 26_{18,8}{}^{\star}$	260326.138	115	343	65.4	413	Strong CH_3OCH_3 and C_2H_5CN

Table 10. continued.

N^a (1)	Transition^b (2)	Frequency (MHz) (3)	Unc.^{c} (kHz) (4)	$E_l{}^d$ (K) (5)	$S\mu^2$ (D^2) (6)	σ^e (mK) (7)	Comments (8)
657	$28_{19,9} - 28_{18,10}{}^\star$	260327.281	114	359	79.6	413	Strong CH_3OCH_3 and C_2H_5CN
659	$27_{19,8} - 27_{18,9}{}^\star$	260327.999	114	351	72.5	413	Strong CH_3OCH_3 and C_2H_5CN
661	$43_{9,34} - 42_{9,33}$	263500.082	18	422	881.1	74	Blend with $C_2H_5{}^{13}CN$ and CH_3OCH_3
662	$37_{7,31} - 36_{6,30}$	263656.862	14	340	85.0	108	Strong CH_3OCH_3
663	$44_{23,21} - 43_{23,20}{}^\star$	263662.413	12	583	684.9	108	Strong CH_3OCH_3, HNCO, and $HC^{13}CCN$, $v_7=1$
665	$44_{24,20} - 43_{24,19}{}^\star$	263666.216	12	599	662.1	108	Strong CH_3OCH_3, HNCO, and $HC^{13}CCN$, $v_7=1$
667	$44_{22,22} - 43_{22,21}{}^\star$	263671.555	13	568	706.8	108	Strong CH_3OCH_3, HNCO, and $HC^{13}CCN$, $v_7=1$
669	$44_{25,19} - 43_{25,18}{}^\star$	263681.350	13	616	638.2	108	Strong $HC^{13}CCN$, $v_7=1$, HNCO, and $HN^{13}CO$
671	$44_{21,23} - 43_{21,22}{}^\star$	263695.661	13	554	727.7	108	Strong $HCC^{13}CN$, $v_7=1$ and C_2H_5OH
673	$44_{26,18} - 43_{26,17}{}^\star$	263706.506	13	633	613.4	108	Strong $HCC^{13}CN$, $v_7=1$
675	$44_{20,24} - 43_{20,23}{}^\star$	263737.291	14	540	747.7	108	Strong HNCO
677	$44_{27,17} - 43_{27,16}{}^\star$	263740.615	14	651	587.6	108	Strong HNCO
679	$44_{28,16} - 43_{28,15}{}^\star$	263782.797	15	669	560.8	108	Strong HC_3N and CH_3OH, $v_t=1$
681	$44_{19,25} - 43_{19,24}{}^\star$	263799.727	14	527	766.8	108	Strong HC_3N, CH_3OH, $v_t=1$, and HC_3N, $v_5=1/v_7=3$
683	$44_{29,15} - 43_{29,14}{}^\star$	263832.314	16	688	533.0	108	Blend with NH_2CHO and U-line?
685	$38_{7,32} - 37_{6,31}$	263847.676	14	351	91.4	108	Blend with NH_2CHO
686	$47_{2,45} - 46_{3,44}{}^\star$	263860.484	28	434	344.1	108	Blend with C_2H_5OH and $C_2H_5{}^{13}CN$
688	$47_{2,45} - 46_{2,44}{}^\star$	263860.546	28	434	992.8	108	Blend with C_2H_5OH and $C_2H_5{}^{13}CN$
690	$44_{18,26} - 43_{18,25}{}^\star$	263887.257	14	514	784.7	108	Strong CH_3CH_3CO and HNCO, $v_4=1$
692	$44_{30,14} - 43_{30,13}{}^\star$	263888.552	16	708	504.4	108	Strong CH_3CH_3CO and HNCO, $v_4=1$
694	$44_{17,27} - 43_{17,26}{}^\star$	264005.588	14	502	801.8	108	Strong $CH_3{}^{13}CH_2CN$
696	$17_{12,5} - 16_{11,6}{}^\star$	264068.075	12	213	106.9	108	Blend with CH_3CH_3CO, $v_t=1$
698	$46_{4,42} - 45_{5,41}$	266675.648	20	436	260.6	91	Strong $O^{13}CS$ and $C_2H_5{}^{13}CN$
699	$46_{5,42} - 45_{5,41}$	266707.175	20	436	962.7	91	Strong CH_3OH
700	$29_{6,23} - 28_{5,24}$	266722.756	11	258	39.0	91	Blend with C_2H_5CN, $v_{13}=1/v_{21}=1$, CH_3CH_3CO, $v_t=1$, and U-line
701	$46_{4,42} - 45_{4,41}$	266722.874	20	436	962.6	91	Blend with C_2H_5CN, $v_{13}=1/v_{21}=1$, CH_3CH_3CO, $v_t=1$, and U-line
702	$46_{5,42} - 45_{4,41}$	266754.401	20	436	260.6	91	Blend with U-line
703	$44_{8,37} - 43_{8,36}$	266788.303	20	429	909.3	91	Blend with U-line
704	$44_{10,35} - 43_{10,34}$	266958.528	17	440	893.9	91	Blend with C_2H_5OH and U-line
705	$44_{10,34} - 44_{7,37}$	267152.855	100	440	8.9	91	Strong $NH_2{}^{13}CHO$, CH_3CH_3CO, and C_2H_5CN, $v_{13}=1/v_{21}=1$
706	$43_{7,36} - 42_{7,35}$	267157.130	20	414	897.1	91	Strong $NH_2{}^{13}CHO$, CH_3CH_3CO, and C_2H_5CN, $v_{13}=1/v_{21}=1$

Notes: [a] Numbering of the observed transitions associated with a modeled line stronger than 20 mK. [b] Transitions marked with a $\star$ are double with a frequency difference less than 0.1 MHz. The quantum numbers of the second one are not shown. [c] Frequency uncertainty. [d] Lower energy level in temperature units (E_l/k_B). [e] Calculated rms noise level in T_{mb} scale.

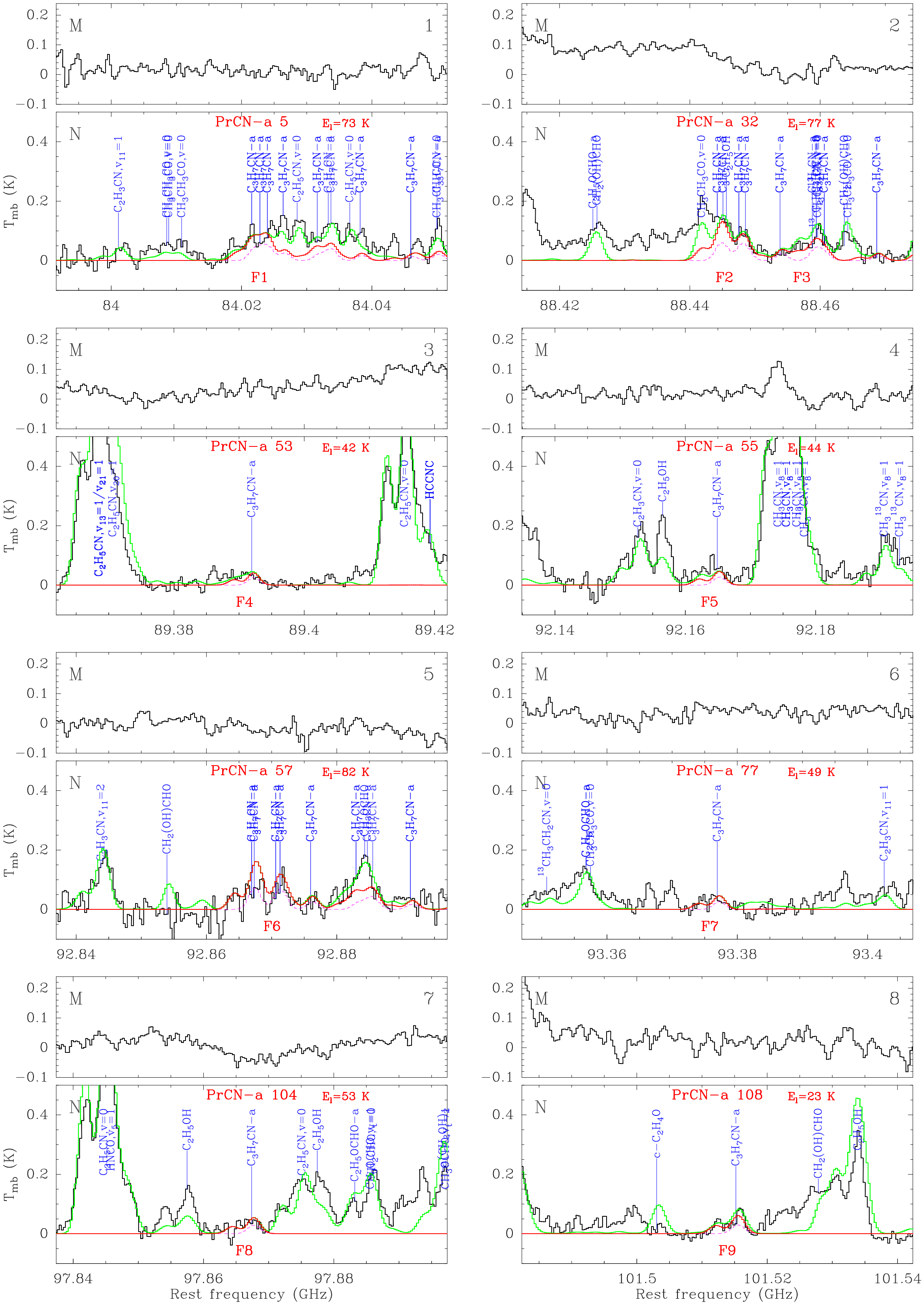

Fig. 3. Transitions of the *anti*-conformer of *n*-propyl cyanide (PrCN-a) detected with the IRAM 30 m telescope. Each panel consists of two plots and is labeled in black in the upper right corner. The lower plot shows in black the spectrum obtained toward Sgr B2(N) in main-beam brightness temperature scale (K), while the upper plot shows the spectrum toward Sgr B2(M). The rest frequency axis is labeled in GHz. The systemic velocities assumed for Sgr B2(N) and (M) are 64 and 62 km s^{-1}, respectively. The lines identified in the Sgr B2(N) spectrum are labeled in blue. The top red label indicates the PrCN-a transition centered in each plot (numbered like in Col. 1 of Table 11), along with the energy of its lower level in K (E_l/k_B). The other PrCN-a lines are labeled in blue only. The bottom red label is the feature number (see Col. 8 of Table 11). The green spectrum shows our LTE model containing all identified molecules, including PrCN-a. The LTE synthetic spectrum of PrCN-a alone is overlaid in red, and its opacity in dashed violet. All observed lines which have no counterpart in the green spectrum are still unidentified in Sgr B2(N).

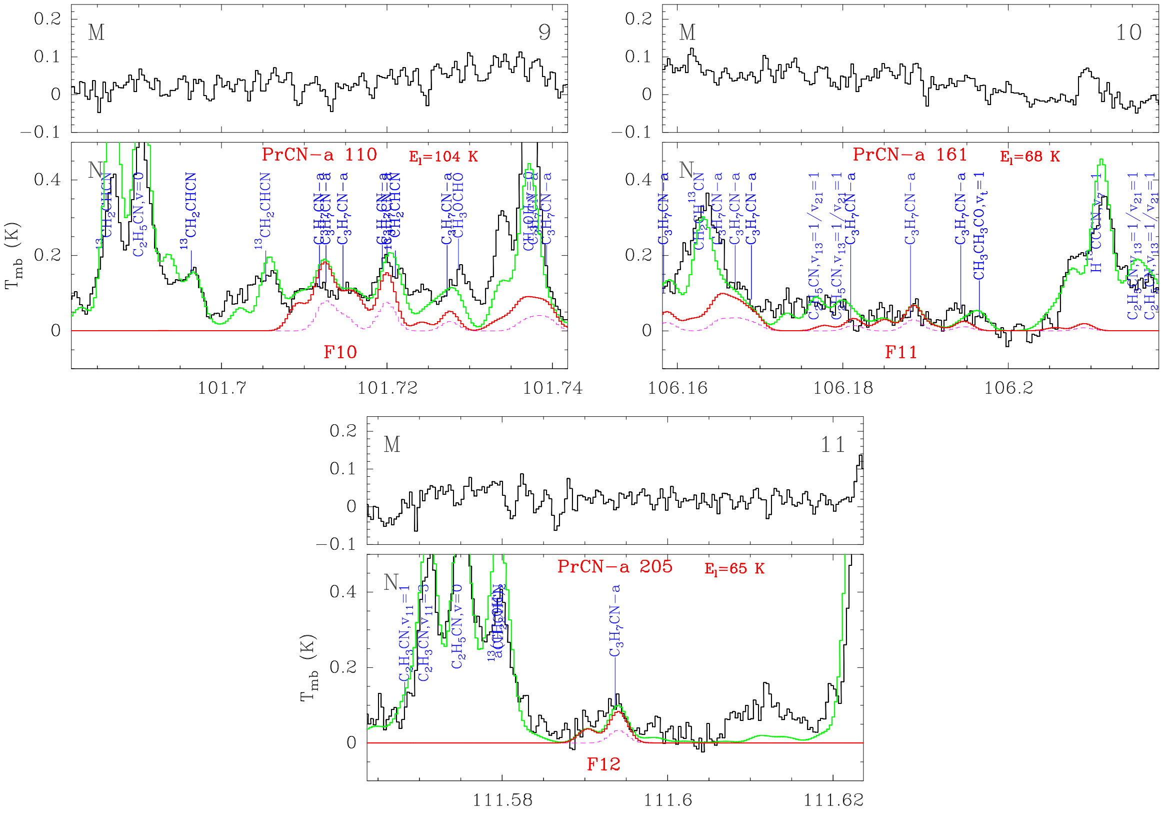

Fig. 3. (continued)

Table 6. Transitions of *anti*-*n*-propyl cyanide, employed in the present fits, their frequencies (MHz), uncertainties Unc. (kHz), and residuals O−C (kHz) between frequencies measured in the laboratory and those calculated from the final spectroscopic parameters. Unresolved asymmetry splitting (two transitions having the same K_a and the same transition frequency) has been treated as intensity-weighted average of the two lines.

J', K'_a, K'_c	–	J'', K''_a, K''_c	Frequency	Unc.	O−C
2, 1, 2	–	1, 1, 1	8727.068	10	−3
2, 0, 2	–	1, 0, 1	8841.749	10	4
2, 1, 1	–	1, 1, 0	8957.437	10	3
4, 1, 4	–	3, 1, 3	17453.162	10	12
3, 0, 3	–	2, 0, 2	13261.436	5	1
3, 1, 3	–	2, 1, 2	13090.304	5	8
3, 1, 2	–	2, 1, 1	13435.836	5	3
3, 2, 2	–	2, 2, 1	13263.547	5	−2
3, 2, 1	–	2, 2, 0	13265.404	5	−0
4, 2, 3	–	3, 2, 2	17684.317	5	−10
4, 3, 2	–	3, 3, 1	17686.050	5	2
4, 3, 1	–	3, 3, 0	17686.050	5	2
4, 2, 2	–	3, 2, 1	17688.965	5	2
5, 3, 3	–	4, 3, 2	22107.924	5	1
5, 3, 2	–	4, 3, 1	22107.924	5	1
5, 4, 2	–	4, 4, 1	22108.119	5	1
5, 4, 1	–	4, 4, 0	22108.119	5	1
9, 1, 8	–	9, 0, 9	24166.242	5	7
10, 1, 9	–	10, 0, 10	24799.350	5	3
11, 1, 10	–	11, 0, 11	25508.602	5	0
12, 1, 11	–	12, 0, 12	26297.469	5	−2
11, 2, 10	–	12, 1, 11	6897.938	5	−4
16, 1, 15	–	15, 2, 14	13992.090	5	−1
17, 1, 16	–	16, 2, 15	19339.460	5	1
19, 1, 19	–	18, 2, 16	6197.075	5	−1
17, 3, 15	–	18, 2, 16	26095.072	5	−3
18, 3, 16	–	19, 2, 17	21310.053	5	1
19, 3, 16	–	20, 2, 19	19831.330	5	5
20, 3, 18	–	21, 2, 19	11569.979	5	−1
21, 3, 19	–	22, 2, 20	6607.331	5	−0
22, 3, 19	–	23, 2, 22	7318.534	5	2
26, 2, 25	–	25, 3, 22	4813.248	5	−1
26, 2, 24	–	25, 3, 23	13932.516	5	−7
28, 2, 26	–	27, 3, 25	24644.757	5	−0
28, 2, 27	–	27, 3, 24	12629.848	5	4
29, 2, 28	–	28, 3, 25	16441.572	5	−1
30, 2, 29	–	29, 3, 26	20181.553	5	−0
31, 2, 30	–	30, 3, 27	23843.940	5	0
27, 4, 24	–	28, 3, 25	25160.533	5	3
27, 4, 23	–	28, 3, 26	26014.363	5	−8
28, 4, 25	–	29, 3, 26	20523.876	5	5
28, 4, 24	–	29, 3, 27	21572.582	5	−10
29, 4, 26	–	30, 3, 27	15856.700	5	6
29, 4, 25	–	30, 3, 28	17135.390	5	−4
30, 4, 27	–	31, 3, 28	11155.783	5	2
30, 4, 26	–	31, 3, 29	12704.192	5	−2
31, 4, 28	–	32, 3, 29	6417.726	5	3
31, 4, 27	–	32, 3, 30	8280.581	5	2
36, 3, 33	–	35, 4, 32	12979.624	5	4
36, 3, 34	–	35, 4, 31	9299.790	5	−2
37, 3, 35	–	36, 4, 32	13655.067	5	−4
38, 3, 35	–	37, 4, 34	22999.972	5	6
39, 3, 37	–	38, 4, 34	22299.091	5	3
37, 5, 32	–	38, 4, 35	24129.041	5	4
38, 5, 34	–	39, 4, 35	19274.638	5	−2
38, 5, 33	–	39, 4, 36	19621.858	5	1
39, 5, 34	–	40, 4, 37	15110.833	5	0
35, 0, 35	–	34, 0, 34	152420.07	50	10
35, 2, 33	–	34, 2, 32	156362.10	50	−19

Table 6. continued.

J', K'_a, K'_c	–	J'', K''_a, K''_c	Frequency	Unc.	O–C
35, 6, 29	–	34, 6, 28	154794.60	50	5
35, 6, 30	–	34, 6, 29	154794.60	50	5
35, 7, 28	–	34, 7, 27	154778.85	50	−24
35, 7, 29	–	34, 7, 28	154778.85	50	−24
35, 8, 27	–	34, 8, 26	154773.84	50	−40
35, 8, 28	–	34, 8, 27	154773.84	50	−40
35, 9, 26	–	34, 9, 25	154775.62	50	−38
35, 9, 27	–	34, 9, 26	154775.62	50	−38
35, 10, 26	–	34, 10, 25	154782.18	50	−3
35, 10, 25	–	34, 10, 24	154782.18	50	−3
35, 11, 25	–	34, 11, 24	154792.35	50	22
35, 11, 24	–	34, 11, 23	154792.35	50	22
35, 12, 24	–	34, 12, 23	154805.40	50	−28
35, 12, 23	–	34, 12, 22	154805.40	50	−28
36, 0, 36	–	35, 0, 35	156709.22	50	−7
36, 1, 36	–	35, 1, 35	156376.78	50	−9
36, 2, 34	–	35, 2, 33	160851.40	50	−55
36, 2, 35	–	35, 2, 34	158511.09	50	15
36, 3, 33	–	35, 3, 32	159816.09	50	−55
36, 3, 34	–	35, 3, 33	159295.56	50	−7
36, 4, 32	–	35, 4, 31	159360.35	50	−6
36, 4, 33	–	35, 4, 32	159324.49	50	−4
36, 5, 31	–	35, 5, 30	159258.14	50	−38
36, 5, 32	–	35, 5, 31	159256.97	50	14
36, 6, 31	–	35, 6, 30	159218.77	50	−44
36, 6, 30	–	35, 6, 29	159218.77	50	−44
36, 7, 30	–	35, 7, 29	159201.12	50	4
36, 7, 29	–	35, 7, 28	159201.12	50	4
36, 8, 29	–	35, 8, 28	159194.99	50	−15
36, 8, 28	–	35, 8, 27	159194.99	50	−15
36, 13, 24	–	35, 13, 23	159241.59	50	7
36, 13, 23	–	35, 13, 22	159241.59	50	7
36, 14, 23	–	35, 14, 22	159259.85	50	6
36, 14, 22	–	35, 14, 21	159259.85	50	6
36, 15, 22	–	35, 15, 21	159280.32	50	26
36, 15, 21	–	35, 15, 20	159280.32	50	26
36, 16, 21	–	35, 16, 20	159302.83	50	28
36, 16, 20	–	35, 16, 19	159302.83	50	28
36, 17, 20	–	35, 17, 19	159327.32	50	42
36, 17, 19	–	35, 17, 18	159327.32	50	42
36, 18, 19	–	35, 18, 18	159353.76	50	100
36, 18, 18	–	35, 18, 17	159353.76	50	100
37, 0, 37	–	36, 0, 36	160998.16	50	12
37, 1, 37	–	36, 1, 36	160691.64	50	25
48, 1, 47	–	47, 1, 46	211856.19	50	11
48, 2, 47	–	47, 2, 46	210741.48	50	−115
48, 2, 46	–	47, 2, 45	214343.68	50	15
48, 3, 46	–	47, 3, 45	212219.54	50	25
48, 4, 45	–	47, 4, 44	212517.79	50	5
48, 4, 44	–	47, 4, 43	212766.64	50	−12
48, 5, 44	–	47, 5, 43	212415.06	50	−32
48, 5, 43	–	47, 5, 42	212430.89	50	12
48, 6, 43	–	47, 6, 42	212320.28	50	40
48, 6, 42	–	47, 6, 41	212320.77	50	−59
48, 7, 42	–	47, 7, 41	212267.79	50	−29
48, 7, 41	–	47, 7, 40	212267.79	50	−29
48, 8, 41	–	47, 8, 40	212241.20	50	2
48, 8, 40	–	47, 8, 39	212241.20	50	2
48, 9, 40	–	47, 9, 39	212230.19	50	−42
48, 9, 39	–	47, 9, 38	212230.19	50	−42
48, 10, 39	–	47, 10, 38	212229.67	50	28

Table 6. continued.

J', K'_a, K'_c	–	J'', K''_a, K''_c	Frequency	Unc.	O–C
48, 10, 38	–	47, 10, 37	212229.67	50	28
48, 12, 37	–	47, 12, 36	212249.06	50	−46
48, 12, 36	–	47, 12, 35	212249.06	50	−46
48, 13, 36	–	47, 13, 35	212266.32	50	−39
48, 13, 35	–	47, 13, 34	212266.32	50	−39
48, 14, 35	–	47, 14, 34	212287.59	50	14
48, 14, 34	–	47, 14, 33	212287.59	50	14
48, 15, 34	–	47, 15, 33	212312.29	50	−1
48, 15, 33	–	47, 15, 32	212312.29	50	−1
48, 16, 33	–	47, 16, 32	212340.19	50	3
48, 16, 32	–	47, 16, 31	212340.19	50	3
48, 17, 32	–	47, 17, 31	212371.06	50	18
48, 17, 31	–	47, 17, 30	212371.06	50	18
48, 18, 31	–	47, 18, 30	212404.72	50	21
48, 18, 30	–	47, 18, 29	212404.72	50	21
48, 19, 30	–	47, 19, 29	212441.11	50	64
48, 19, 29	–	47, 19, 28	212441.11	50	64
48, 20, 29	–	47, 20, 28	212480.03	50	26
48, 20, 28	–	47, 20, 27	212480.03	50	26
48, 21, 28	–	47, 21, 27	212521.49	50	−24
48, 21, 27	–	47, 21, 26	212521.49	50	−24
48, 22, 27	–	47, 22, 26	212565.54	50	2
48, 22, 26	–	47, 22, 25	212565.54	50	2
48, 23, 26	–	47, 23, 25	212611.99	50	−58
48, 23, 25	–	47, 23, 24	212611.99	50	−58
49, 0, 49	–	48, 0, 48	212476.62	50	100
49, 1, 49	–	48, 1, 48	212378.48	50	62
49, 2, 48	–	48, 2, 47	215077.17	50	14
49, 4, 46	–	48, 4, 45	216949.09	50	−14
49, 16, 34	–	48, 16, 33	216757.71	50	9
49, 16, 33	–	48, 16, 32	216757.71	50	9
49, 17, 33	–	48, 17, 32	216789.07	50	45
49, 17, 32	–	48, 17, 31	216789.07	50	45
49, 20, 30	–	48, 20, 29	216899.87	50	3
49, 20, 29	–	48, 20, 28	216899.87	50	3
50, 0, 50	–	49, 0, 49	216767.70	50	−21
50, 3, 48	–	49, 3, 47	221009.11	50	7
50, 7, 44	–	49, 7, 43	221112.20	50	−26
50, 7, 43	–	49, 7, 42	221112.20	50	−26
50, 8, 43	–	49, 8, 42	221080.73	50	−13
50, 8, 42	–	49, 8, 41	221080.73	50	−13
50, 9, 42	–	49, 9, 41	221066.76	50	−28
50, 9, 41	–	49, 9, 40	221066.76	50	−28
50, 10, 41	–	49, 10, 40	221064.35	50	−25
50, 10, 40	–	49, 10, 39	221064.35	50	−25
50, 11, 40	–	49, 11, 39	221070.19	50	−11
50, 11, 39	–	49, 11, 38	221070.19	50	−11
50, 12, 39	–	49, 12, 38	221082.34	50	28
50, 12, 38	–	49, 12, 37	221082.34	50	28
50, 13, 38	–	49, 13, 37	221099.49	50	−5
50, 13, 37	–	49, 13, 36	221099.49	50	−5
50, 14, 37	–	49, 14, 36	221121.05	50	85
50, 14, 36	–	49, 14, 35	221121.05	50	85
50, 20, 31	–	49, 20, 30	221319.17	50	−141
50, 20, 30	–	49, 20, 29	221319.17	50	−141
51, 0, 51	–	50, 0, 50	221059.01	50	−5
51, 1, 51	–	50, 1, 50	220979.61	50	32
64, 6, 59	–	63, 6, 58	283158.51	50	−21
64, 6, 58	–	63, 6, 57	283171.68	50	33
64, 7, 58	–	63, 7, 57	283022.98	50	14
64, 7, 57	–	63, 7, 56	283022.98	50	14

Table 6. continued.

J', K_a', K_c'	–	J'', K_a'', K_c''	Frequency	Unc.	O–C
64, 8, 57	–	63, 8, 56	282943.15	50	24
64, 8, 56	–	63, 8, 55	282943.15	50	24
64, 9, 56	–	63, 9, 55	282898.81	50	1
64, 9, 55	–	63, 9, 54	282898.81	50	1
64, 10, 55	–	63, 10, 54	282877.00	50	−26
64, 10, 54	–	63, 10, 53	282877.00	50	−26
64, 11, 54	–	63, 11, 53	282870.71	50	−11
64, 11, 53	–	63, 11, 52	282870.71	50	−11
64, 12, 53	–	63, 12, 52	282875.72	50	−41
64, 12, 52	–	63, 12, 51	282875.72	50	−41
64, 13, 52	–	63, 13, 51	282889.55	50	−38
64, 13, 51	–	63, 13, 50	282889.55	50	−38
64, 14, 51	–	63, 14, 50	282910.51	50	−38
64, 14, 50	–	63, 14, 49	282910.51	50	−38
64, 15, 50	–	63, 15, 49	282937.54	50	6
64, 15, 49	–	63, 15, 48	282937.54	50	6
64, 16, 49	–	63, 16, 48	282969.81	50	25
64, 16, 48	–	63, 16, 47	282969.81	50	25
64, 17, 48	–	63, 17, 47	283006.76	50	−3
64, 17, 47	–	63, 17, 46	283006.76	50	−3
64, 18, 47	–	63, 18, 46	283048.15	50	64
64, 18, 46	–	63, 18, 45	283048.15	50	64
64, 19, 46	–	63, 19, 45	283093.46	50	−14
64, 19, 45	–	63, 19, 44	283093.46	50	−14
64, 20, 45	–	63, 20, 44	283142.77	50	47
64, 20, 44	–	63, 20, 43	283142.77	50	47
64, 21, 44	–	63, 21, 43	283195.66	50	−22
64, 21, 43	–	63, 21, 42	283195.66	50	−22

Table 7. Transitions of *gauche*-*n*-propyl cyanide, employed in the present fits, their frequencies (MHz), uncertainties Unc. (kHz), and residuals O−C (kHz) between frequencies measured in the laboratory and those calculated from the final spectroscopic parameters. Unresolved asymmetry splitting (two transitions having the same K_a and the same transition frequency) has been treated as intensity-weighted average of the two lines.

J', K'_a, K'_c	–	J'', K''_a, K''_c	Frequency	Unc.	O−C
2, 0, 2	–	1, 0, 1	11912.654	10	−18
2, 1, 2	–	1, 1, 1	11384.045	10	−0
2, 1, 1	–	1, 1, 0	12508.374	10	−10
3, 0, 3	–	2, 0, 2	17785.949	10	6
3, 1, 3	–	2, 1, 2	17055.610	5	1
2, 1, 2	–	1, 0, 1	18176.781	5	1
4, 1, 3	–	4, 0, 4	10286.601	5	0
5, 1, 4	–	5, 0, 5	12167.868	5	−3
6, 1, 5	–	6, 0, 6	14609.404	5	1
7, 1, 6	–	7, 0, 7	17634.822	5	1
2, 2, 1	–	2, 1, 2	22064.261	5	0
24, 3, 21	–	25, 2, 24	5073.952	5	0
10, 3, 7	–	9, 4, 6	12670.827	5	−2
11, 3, 9	–	10, 4, 6	16546.819	5	−3
28, 3, 26	–	27, 4, 23	19891.929	5	1
36, 4, 32	–	37, 3, 35	19547.899	5	1
13, 4, 10	–	12, 5, 7	15362.409	5	0
38, 4, 35	–	37, 5, 32	9991.617	5	0
39, 4, 36	–	38, 5, 33	5311.217	5	1
15, 5, 10	–	14, 6, 9	13597.769	5	1
12, 7, 6	–	13, 6, 7	13549.701	5	−1
12, 7, 5	–	13, 6, 8	13551.095	5	5
13, 7, 7	–	14, 6, 8	7398.401	5	−2
13, 7, 6	–	14, 6, 9	7401.855	5	4
15, 8, 8	–	16, 7, 9	9498.238	5	−4
15, 8, 7	–	16, 7, 10	9498.794	5	−5
19, 7, 12	–	18, 8, 11	9123.186	5	−1
19, 7, 13	–	18, 8, 10	9116.781	5	−1
20, 7, 14	–	19, 8, 11	15398.422	5	0
22, 8, 14	–	21, 9, 13	13221.090	5	−0
22, 8, 15	–	21, 9, 12	13218.792	5	−2
23, 8, 15	–	22, 9, 14	19511.211	5	2
23, 8, 16	–	22, 9, 13	19506.528	5	0
19, 10, 10	–	20, 9, 11	13681.725	5	−1
19, 10, 9	–	20, 9, 12	13681.725	5	−1
25, 9, 17	–	24, 10, 14	17310.401	5	−6
25, 9, 16	–	24, 10, 15	17311.214	5	2
26, 9, 18	–	25, 10, 15	23599.302	5	2
26, 9, 17	–	25, 10, 16	23600.945	5	11
28, 10, 19	–	27, 11, 16	21388.390	5	−9
28, 10, 18	–	27, 11, 17	21388.670	5	−6
26, 13, 14	–	27, 12, 15	13813.369	5	−3
26, 13, 13	–	27, 12, 16	13813.369	5	−3
22, 4, 18	–	22, 4, 19	25543.715	5	−1
25, 5, 20	–	25, 5, 21	16254.957	5	2
26, 5, 21	–	26, 5, 22	21090.090	5	−1
30, 6, 24	–	30, 6, 25	16246.388	5	1
31, 6, 25	–	31, 6, 26	21145.902	5	1
34, 7, 27	–	34, 7, 28	11727.780	5	−2
36, 7, 29	–	36, 7, 30	20572.880	5	−2
37, 7, 30	–	37, 7, 31	26237.933	5	4
39, 8, 31	–	39, 8, 32	11013.037	5	−2
25, 5, 21	–	24, 4, 20	182990.23	50	19
26, 6, 21	–	25, 6, 20	157628.25	50	16
26, 7, 19	–	25, 7, 18	157477.90	50	8
26, 10, 17	–	25, 10, 16	156296.53	50	−59
26, 10, 16	–	25, 10, 15	156296.53	50	−59
26, 11, 16	–	25, 11, 15	156141.79	50	65
26, 11, 15	–	25, 11, 14	156141.79	50	65

Table 7. continued.

J', K_a', K_c'	–	J'', K_a'', K_c''	Frequency	Unc.	O–C
26, 12, 15	–	25, 12, 14	156032.20	50	−22
26, 12, 14	–	25, 12, 13	156032.20	50	−22
26, 13, 14	–	25, 13, 13	155954.49	50	−56
26, 13, 13	–	25, 13, 12	155954.49	50	−56
26, 14, 13	–	25, 14, 12	155900.13	50	−0
26, 14, 12	–	25, 14, 11	155900.13	50	−0
26, 15, 12	–	25, 15, 11	155863.29	50	−10
26, 15, 11	–	25, 15, 10	155863.29	50	−10
26, 17, 10	–	25, 17, 9	155827.91	50	−33
26, 17, 9	–	25, 17, 8	155827.91	50	−33
26, 18, 9	–	25, 18, 8	155824.64	50	−20
26, 18, 8	–	25, 18, 7	155824.64	50	−20
26, 19, 8	–	25, 19, 7	155828.81	50	−17
26, 19, 7	–	25, 19, 6	155828.81	50	−17
28, 1, 27	–	27, 1, 26	157495.25	50	−33
28, 2, 27	–	27, 1, 26	157503.23	50	−51
28, 1, 27	–	27, 2, 26	157482.64	50	46
28, 2, 27	–	27, 2, 26	157490.60	50	8
29, 5, 25	–	28, 4, 24	189805.28	50	48
30, 4, 27	–	29, 3, 26	178167.69	50	31
30, 4, 26	–	29, 4, 25	182703.13	50	−23
30, 5, 26	–	29, 4, 25	192210.43	50	32
30, 7, 23	–	29, 7, 22	182961.27	50	−29
31, 2, 29	–	30, 2, 28	177803.90	50	−13
31, 3, 29	–	30, 2, 28	177857.94	50	−1
31, 2, 29	–	30, 3, 28	177721.22	50	6
31, 3, 29	–	30, 3, 28	177775.23	50	−12
31, 3, 28	–	30, 3, 27	182248.22	50	−22
31, 4, 28	–	30, 3, 27	183077.55	50	26
31, 3, 28	–	30, 4, 27	181050.65	50	36
31, 4, 27	–	30, 5, 26	178318.43	50	156
31, 5, 26	–	30, 5, 25	192803.61	50	6
31, 7, 25	–	30, 7, 24	188156.51	50	−20
31, 7, 24	–	30, 7, 23	189515.12	50	−74
31, 8, 23	–	30, 8, 22	187858.13	50	9
32, 2, 30	–	31, 2, 29	183183.36	50	18
32, 3, 30	–	31, 2, 29	183218.50	50	28
32, 2, 30	–	31, 3, 29	183129.35	50	37
32, 3, 30	–	31, 3, 29	183164.45	50	6
32, 4, 29	–	31, 3, 28	188119.54	50	−5
32, 4, 28	–	31, 4, 27	192927.96	50	−13
32, 4, 28	–	31, 5, 27	185714.09	50	6
32, 10, 23	–	31, 10, 22	192852.63	50	−4
32, 10, 22	–	31, 10, 21	192854.42	50	−4
32, 12, 21	–	31, 12, 20	192320.23	50	5
32, 12, 20	–	31, 12, 19	192320.23	50	5
32, 13, 20	–	31, 13, 19	192158.76	50	−19
32, 13, 19	–	31, 13, 18	192158.76	50	−19
32, 14, 19	–	31, 14, 18	192040.62	50	14
32, 14, 18	–	31, 14, 17	192040.62	50	14
33, 2, 31	–	32, 2, 30	188564.34	50	−33
33, 3, 31	–	32, 2, 30	188587.13	50	13
33, 2, 31	–	32, 3, 30	188529.24	50	−2
33, 3, 31	–	32, 3, 30	188551.94	50	−47
33, 3, 30	–	32, 3, 29	192871.17	50	−3
33, 4, 30	–	32, 3, 29	193259.00	50	18
33, 3, 30	–	32, 4, 29	192301.88	50	−16
33, 4, 30	–	32, 4, 29	192689.70	50	−5
33, 4, 29	–	32, 5, 28	192663.51	50	12
34, 2, 32	–	33, 2, 31	193946.21	50	−59
34, 3, 32	–	33, 2, 31	193960.95	50	14

Table 7. continued.

J', K_a', K_c'	–	J'', K_a'', K_c''	Frequency	Unc.	O–C
34, 2, 32	–	33, 3, 31	193923.55	50	26
34, 3, 32	–	33, 3, 31	193938.16	50	−32
34, 6, 28	–	33, 6, 27	212120.06	50	3
35, 6, 29	–	34, 6, 28	218287.17	50	−26
35, 7, 29	–	34, 7, 28	212483.75	50	16
35, 8, 28	–	34, 8, 27	212458.29	50	−13
35, 9, 27	–	34, 9, 26	211828.06	50	142
35, 9, 26	–	34, 9, 25	211938.01	50	7
36, 4, 32	–	35, 5, 31	211527.01	50	14
36, 10, 27	–	35, 10, 26	217402.38	50	−15
36, 10, 26	–	35, 10, 25	217418.12	50	−2
36, 11, 26	–	35, 11, 25	216940.59	50	−30
36, 11, 25	–	35, 11, 24	216941.74	50	33
36, 12, 25	–	35, 12, 24	216609.17	50	−33
36, 12, 24	–	35, 12, 23	216609.17	50	−33
36, 13, 24	–	35, 13, 23	216367.23	50	−1
36, 13, 23	–	35, 13, 22	216367.23	50	−1
36, 14, 23	–	35, 14, 22	216188.17	50	23
36, 14, 22	–	35, 14, 21	216188.17	50	23
36, 16, 21	–	35, 16, 20	215956.57	50	−26
36, 16, 20	–	35, 16, 19	215956.57	50	−26
36, 17, 20	–	35, 17, 19	215885.18	50	−12
36, 17, 19	–	35, 17, 18	215885.18	50	−12
36, 18, 19	–	35, 18, 18	215835.30	50	9
36, 18, 18	–	35, 18, 17	215835.30	50	9
36, 20, 17	–	35, 20, 16	215784.95	50	23
36, 20, 16	–	35, 20, 15	215784.95	50	23
36, 21, 16	–	35, 21, 15	215779.22	50	45
36, 21, 15	–	35, 21, 14	215779.22	50	45
36, 22, 15	–	35, 22, 14	215783.85	50	5
36, 22, 14	–	35, 22, 13	215783.85	50	5
36, 23, 14	–	35, 23, 13	215797.53	50	−19
36, 23, 13	–	35, 23, 12	215797.53	50	−19
36, 24, 13	–	35, 24, 12	215819.22	50	36
36, 24, 12	–	35, 24, 11	215819.22	50	36
36, 25, 12	–	35, 25, 11	215847.81	50	−52
36, 25, 11	–	35, 25, 10	215847.81	50	−52
36, 26, 11	–	35, 26, 10	215882.85	50	−12
36, 26, 10	–	35, 26, 9	215882.85	50	−12
36, 27, 10	–	35, 27, 9	215923.60	50	10
36, 27, 9	–	35, 27, 8	215923.60	50	10
36, 28, 9	–	35, 28, 8	215969.54	50	−15
36, 28, 8	–	35, 28, 7	215969.54	50	−15
36, 32, 5	–	35, 32, 4	216198.45	50	4
36, 32, 4	–	35, 32, 3	216198.45	50	4
37, 3, 34	–	36, 3, 33	214265.30	50	−8
37, 3, 34	–	36, 4, 33	214147.29	50	−26
37, 4, 34	–	36, 4, 33	214225.81	50	−13
38, 1, 37	–	37, 2, 36	211401.39	50	59
38, 3, 36	–	37, 2, 35	215476.23	50	36
38, 2, 36	–	37, 3, 35	215469.85	50	−35
38, 3, 35	–	37, 3, 34	219628.21	50	19
38, 3, 35	–	37, 4, 34	219549.67	50	−13
38, 4, 35	–	37, 4, 34	219601.64	50	−40
39, 0, 39	–	38, 1, 38	212743.02	50	6
39, 2, 37	–	38, 2, 36	220854.26	50	−8
39, 3, 37	–	38, 2, 36	220855.81	50	−18
39, 2, 37	–	38, 3, 36	220851.79	50	−24
39, 3, 37	–	38, 3, 36	220853.34	50	−33
40, 0, 40	–	39, 1, 39	218129.30	50	18
47, 14, 34	–	46, 14, 33	282874.18	50	42

Table 7. continued.

J', K_a', K_c'	–	J'', K_a'', K_c''	Frequency	Unc.	O–C
47, 17, 31	–	46, 17, 30	282070.21	50	4
47, 17, 30	–	46, 17, 29	282070.21	50	4
47, 19, 29	–	46, 19, 28	281801.94	50	20
47, 19, 28	–	46, 19, 27	281801.94	50	20
47, 20, 28	–	46, 20, 27	281716.83	50	33
47, 20, 27	–	46, 20, 26	281716.83	50	33
47, 21, 27	–	46, 21, 26	281656.67	50	10
47, 21, 26	–	46, 21, 25	281656.67	50	10
47, 22, 26	–	46, 22, 25	281617.41	50	−44
47, 22, 25	–	46, 22, 24	281617.41	50	−44
47, 23, 25	–	46, 23, 24	281596.02	50	−16
47, 23, 24	–	46, 23, 23	281596.02	50	−16
47, 24, 24	–	46, 24, 23	281589.94	50	8
47, 24, 23	–	46, 24, 22	281589.94	50	8
47, 25, 23	–	46, 25, 22	281597.15	50	−18
47, 25, 22	–	46, 25, 21	281597.15	50	−18
47, 26, 22	–	46, 26, 21	281616.14	50	−10
47, 26, 21	–	46, 26, 20	281616.14	50	−10
47, 27, 21	–	46, 27, 20	281645.57	50	−9
47, 27, 20	–	46, 27, 19	281645.57	50	−9
47, 28, 20	–	46, 28, 19	281684.43	50	48
47, 28, 19	–	46, 28, 18	281684.43	50	48
47, 29, 19	–	46, 29, 18	281731.64	50	−30
47, 29, 18	–	46, 29, 17	281731.64	50	−30
47, 30, 18	–	46, 30, 17	281786.66	50	−36
47, 30, 17	–	46, 30, 16	281786.66	50	−36
47, 31, 17	–	46, 31, 16	281848.86	50	31
47, 31, 16	–	46, 31, 15	281848.86	50	31
47, 33, 15	–	46, 33, 14	281992.38	50	34
47, 33, 14	–	46, 33, 13	281992.38	50	34
47, 34, 14	–	46, 34, 13	282072.85	50	−22
47, 34, 13	–	46, 34, 12	282072.85	50	−22
48, 5, 43	–	47, 5, 42	281724.06	50	0
48, 6, 43	–	47, 6, 42	281635.78	50	−33